



HAL
open science

New activity-based probes to detect matrix metalloproteases

Monika Kaminska

► **To cite this version:**

Monika Kaminska. New activity-based probes to detect matrix metalloproteases. Biochemistry [q-bio.BM]. Université Paris-Saclay, 2018. English. NNT : 2018SACLS538 . tel-02157954

HAL Id: tel-02157954

<https://theses.hal.science/tel-02157954>

Submitted on 17 Jun 2019

HAL is a multi-disciplinary open access archive for the deposit and dissemination of scientific research documents, whether they are published or not. The documents may come from teaching and research institutions in France or abroad, or from public or private research centers.

L'archive ouverte pluridisciplinaire **HAL**, est destinée au dépôt et à la diffusion de documents scientifiques de niveau recherche, publiés ou non, émanant des établissements d'enseignement et de recherche français ou étrangers, des laboratoires publics ou privés.

New activity-based probes to detect matrix metalloproteases.

Thèse de doctorat de l'Université Paris-Saclay
préparée à l'Université Paris-Sud
au CEA Saclay

École doctorale n°569 : innovation thérapeutique,
du fondamental à l'appliqué (ITFA)

Spécialité de doctorat: chimie thérapeutique

Thèse présentée et soutenue à Gif-sur-Yvette, le 14 Décembre 2018, par

Monika Kaminska

Composition du Jury:

Pr. Erwan Poupon (Université Paris Saclay)	Présidente
Pr. Rebecca Deprez-Poulain (Université de Lille)	Rapporteur
Dr. Vincent Aucagne DR2 (Centre de Biophysique Moléculaire, Orléans, CNRS)	Rapporteur
Dr. Sonia Cantel, MC/HDR (Université de Montpellier)	Examineur
Dr. Laurent Devel, HDR (CEA Saclay)	Directeur de thèse

Acknowledgments

The thesis presented in this manuscript was completed at the The French Alternative Energies and Atomic Energy Commission (CEA Saclay) unit of the Molecular engineering of proteins (SIMOPRO) thanks to funding from Excellence in Research on Medication and Innovative Therapeutics (Labex Lermite).

Firstly, I would like to express my very profound gratitude to my family, my parents and brother who were always with me despite the distance, for their faith in me, their love, their invaluable support and for standing beside me throughout my studies and all of my life. This accomplishment would not have been possible without them. Dziękuję!

I would like to dedicate special thanks to my thesis supervisor Dr. Laurent Devel for his optimism, patience, motivation, and for sharing his immense knowledge. During the past three years I always could rely on his help and support whenever I encountered an obstacle or had a question relating to my research.

I would like to thank Pr. Rebecca Deprez-Poulain and Dr. Vincent Aucagne for having agreed to be the reviewers of this manuscript. I would like also thank Pr. Erwan Poupon and Dr. Sonia Cantel for having accepted to be part of the jury in my thesis' defense.

I am very grateful to everyone in the SIMOPRO unit, especially to the members that I had the pleasure of sharing my daily routine with; Bob, Steven, Carole, Mylene, Fabrice, Andrzej, Pavel, Evelyne. I really appreciate the warm welcome and kindness that they showed me. I could not have completed this work without their help. I am so thankful to Dr. Sarah Bregant for her scientific and emotional support, especially during the period in which I was writing this manuscript. I deeply appreciate the kindness and friendliness displayed by Livia, Alessia and Fabien. During every workday in the laboratory they were always encouraging towards me, willing to listen, and I could count on their help concerning every problem. I would also really like to thank Kiarach who offered me a large amount of support, especially during the last months of my PhD.

I could not imagine passing these last few years without my dear friends. I am extremely grateful that I have had the opportunity to meet such wonderful people who were motivated to build our CEA students/postdocs/researchers' crew and international family together. Thanks to: Ewa, Livia, Manu, Alessia, Oscar, Fabien, Martin, Malik, Aninda, Anshuman, Hector, Abdullah, Jorge, Liza, Vittore, Bianca, Mohcine, Anouar, Blake.

"Nothing in life is to be feared, it is only to be understood." - Marie Skłodowska-Curie

Abbreviations

ABP	Activity-Based probe
ACE	Angiotensin-converting enzyme
ACN	Acetonitrile
ADAM	A Disintegrin And Metalloproteinase
ADAMTS	A Disintegrin And Metalloproteinase with Thrombospondin Motifs
AfBP	Affinity-based probes
APS	ammonium persulfate
BIC	Bicarbonate
cDNA	Complementary DNA
ClHOBT	6-Chloro-1-Hydroxybenzotriazole di-hydrate
COPD	chronic obstructive pulmonary disease
DC	dendritic cell
DCM	Dichloromethane
DIC	Diisopropylcarbodiimide
DIEA	N,N-Diisopropylethylamine
DMAP	4-Dimethylaminopyridine
DMF	N,N-Dimethylformamide
DMF	Dimethylformamide
DSC	<i>N,N'</i> disuccinimidyl carbonate
ECM	Extracellular matrix
EDC. HCl	N-(3-Dimethylaminopropyl)-N'-ethylcarbodiimide hydrochloride
EDTA	Ethylenediaminetetraacetic acid
EGF	Epidermal growth factor
ESI-MS	Electrospray Mass spectrometry
FACS	Fluorescence-activated cell sorting
DIEA	N,N-Diisopropylethylamine
Fmoc	Fluorenylmethyloxycarbonyl
GM-CSF	Recombinant murine granulocyte-macrophage colony stimulating factor
GPI	Glycosylphosphatidyl inositol
hCA	Human Carbonic anhydrase
HCCA	4-hydroxycinnamic acid
HCCE	Alpha-cyano-4-hydroxycinnamic methyl ester

HEPES	4-(2-hydroxyethyl)-1-piperazineethanesulfonic acid
hMMP	Human matrix metalloproteinases
hsa	Human serum albumin
iDC	Immature dendritic cells
IFN- α	Favour interferon- α
IMDM	Iscoe's Modified Dulbecco's Medium
LC/MS	Liquid chromatography/Mass spectrometry
LDAI	The ligand-directed acyl imidazole
LDSP	Ligand-directed N-Sulfonyl pyridone
LDT	Ligand-directed tosyl
MALDI-TOF	Matrix-assisted laser desorption/ionization Time of Flight
MAP-Kinase	Mitogen activating protein kinase
Mca-MAT	Metoxycoumarin- Matrixine substrate
MME	Murine macrophage elastase
MMP	Matrix metalloproteinases
mRNA	Messenger RNA
MT-MMP	Membrane-type matrix metalloproteinases
NEP	Neutral endopeptidase
NHS	N-Hydroxysuccinimide
NMR	Nuclear magnetic resonance
PA	Activators of plasminogen
PCA	Principal Component Analysis
PDB	Protein data bank
PDGF	Platelet-derived growth factor
PEA3	Activator that enhances the expression of poliovirus genes
PEG	Polyethylene glycol
RP-HPLC	Reverse phase- high performance liquid chromatography
SDS	Sodium dodecyl sulphate
SDS-PAGE	Sodium dodecyl sulphate- Polyacrylamide gel electrophoresis
SP	spacer N-sulfonyl pyridone
TACE	Tumour necrosis factor-alpha converting enzyme belonging to ADAM family
TEMED	N, N, N', N'-tetramethylethylenediamine
TFA	Trifluoroacetic acid

TGF- β	Transforming growth factor
TIMP-2	Tissue inhibitors of metalloproteinases
TIMPS	Tissue inhibitors of metalloproteinases
TIS	Triisopropylsilane
TNF α	Tumour necrosis factor α
tPA	Tissue type activator
uPA	Urokinase
β -FGF	Fibroblast growth factor

TABLE OF CONTENTS

CHAPTER I: LITERATURE REVIEW	1
1. GENERAL CONSIDERATIONS ON PROTEASES	3
2. MATRIX METALLOPROTEINASES	5
2.1. Discovery and MMPs classification.....	5
2.2. MMPs belong to the metzincin family.....	7
2.3. MMPs possess a modular structure.....	8
2.4. Regulation of MMPs activities	10
2.4.1. Transcription	11
2.4.2. Extracellular activation and cysteine switch concept	12
2.4.3. Intracellular activation	13
2.4.4. Cell Surface activation involving TIMP-2.....	13
2.4.5. Inactivation by endogenous inhibitors.....	14
3. BIOLOGICAL FUNCTIONS OF MMPS	15
3.1. The physiological function of MMPs.....	16
3.2. Pathological function of MMPs.....	16
3.3. The specific case of macrophage elastase (MMP12).....	17
4. INHIBITORS OF MMPS: CHEMICAL TOOLS TO INVESTIGATE MMPS BIOLOGICAL FUNCTION.	19
4.1. Structure-based design of MMP inhibitors: from broad-spectrum to selective inhibitors	19
4.1.1. RXP470.1 as a highly selective inhibitor of MMP12.....	22
4.1.2. RXP 470.1 as a chemical tool to study MMP12 in vivo	25
4.1.2.1. RXP470.1 target MMP12 within atherosclerotic plaques.....	25
4.1.2.2 RXP470.1 can target extracellular MMP12 during viral infection.....	26
5. CHEMICAL PROBES FOR DETECTING MMPS ACTIVATION IN COMPLEX PROTEOMES	28
5.1. Imaging of MMPs activity with substrate- and ligand-derived probes.....	28
5.2. Activity-based profiling of MMPs.....	30

5.2.1.	The concept of activity-based protein profiling.....	30
5.2.2.	Affinity-based probes (AfBP) directed to MMPs.....	32
5.2.3.	Targeting amino acids within metalloproteases active sites.	35
5.2.4.	Traceless affinity labelling of native proteins	38
5.2.5.	Comparison between LDT/LDAI and LDSP on hCA.....	40
BIBLIOGRAPHY CHAPTER I.....		43

CHAPTER II: RESULTS.....53

6. CONCEPTION AND IN VITRO EVALUATION OF ACYL IMIDAZOLE PROBES		
TARGETING RECOMBINANT HMMP12..... 55		
6.1.	Rational design of the probes	55
6.2.	Synthesis and characterisation of probes 9 and 10	59
6.3.	Choice of the labelling conditions.....	61
6.4.	Stability of Probes 9 and 10 in labelling buffer.	63
6.5.	Determination of Probe 9 and 10 affinity constants	64
6.6.	Labelling of recombinant hMMP12 catalytic domain by probe 9 and 10.....	64
6.7.	Determination of residue(s) identity covalently modified within hMMP-12 S ₃ ' region	69
6.8.	Impact of a labelling within hMMP12 S ₃ ' region on its proteolytic activity.....	72
7. LABELLING OF OTHERS MMPS..... 74		
7.1.	A favorable structural context for extending the ligand-directed acyl imidazole chemistry to other MMPs	74
7.2.	Evaluation of Probe 10 on a set of seven hMMPs	75
7.3.	Conception and validation of a broad-spectrum acyl imidazole probe directed towards hMMPs. 76	
7.4.	Attempts to determine labelled residues within the S ₃ ' region of hMMP-13.	81
8. TARGETING HMMP12 ACTIVE FORM IN COMPLEX PROTEOMES 82		
8.1.	Labelling of hMMP12 in presence of serum albumin.	82
8.2.	Labelling of hMMP12 in liver extract.....	83
9. LABELLING OF ENDOGENOUS MMP12..... 86		
9.1.	Labelling of human dendritic cells with acyl imidazole probe 10 and 11.	86
9.2.	Labelling of endogenous mMMP12	89

9.2.1.	Validation of mMMP12 labelling with acyl imidazole probe 10 and 11	89
9.2.2.	Labelling of endogenous mMMP12 secreted by dendritic cells	92
9.2.3.	Labelling of mMMP12 secreted by thioglycollate-stimulated mouse macrophages.....	94
10. COMPARISON BETWEEN LIGAND-DIRECTED TOSYL AND ACYL IMIDAZOLE CHEMISTRY.....		98
11. NEW ACTIVITY-BASED PROBES FOR MASS SPECTROMETRY PROFILING OF METALLOPROTEASES: PRELIMINARY DATA.		100
12. TOWARDS SUBSTRATE-DERIVED ACYL IMIDAZOLE PROBES?		103
BIBLIOGRAPHY CHAPTER II.....		105
CHAPTER III: GENERAL DISCUSSION.....		107
CHAPTER IV: MATERIALS AND METHODS.....		113
13. PROBES SYNTHESIS AND ANALYTICAL CHARACTERIZATION.....		115
13.1.	General information.....	115
13.1.1.	Materials	115
13.1.2.	Instrumentation	115
13.2.	Synthetic protocols and compounds characterisation	117
13.2.1.	Solid phase synthesis of pseudo peptides 1 and 2.....	117
13.2.2.	Incorporation of 4-Imidazole acetic acid and access to compounds 3 and 4.	122
13.2.3.	Synthesis of precursors 5, 6, 7, and 8	126
13.2.4.	Synthesis of ligand-derived acyl imidazole probes 9 to 14.	131
13.2.5.	Synthesis of substrate-derived acyl imidazole probes 15, 16, 17, and 18	139
13.2.6.	Synthesis of Tosyl probe 19.....	149
13.3.	Stability of probe 9 and 10.....	151
14. MMPS PRODUCTION AND CHARACTERIZATION		152
14.1.	Production of mMMP12 catalytic domain.....	152
14.2.	MMPs UV dosing.....	154

14.3.	MMPs catalytic activity	155
14.3.1.	General principle of the enzymatic assay with fluorogenic substrate	155
14.3.2.	MMPs activity.....	156
14.3.3.	MMPs Titration	157
14.4.	Analysis of MMP catalytic domain by SDS-PAGE	161
14.4.1.	Principle of one-dimensional electrophoresis in denaturing conditions	161
15.	INHIBITORY POTENCY OF PROBES VS MMPS.	165
16.	LABELLING OF MMPS WITH PROBES	167
16.1.	Production of complex proteomes	168
16.1.1.	Murine sources of complex proteomes	168
16.1.2.	Human sources of complex proteomes	174
16.2.	Procedures of labelling.....	175
16.3.	RP-HPLC samples analysis and labelling yield determination.....	179
16.4.	Samples analysis by SDS-Page followed by In gel fluorescence imaging and western blot....	182
17.	PROTEOMICS.....	185
17.1.	Determination of the position of MMP12 labelling by RXP 470.1 derived probes.....	185
17.2.	Digestion by chymotrypsin and MALDI analysis	189
	BIBLIOGRAPHY CHAPTER IV.....	192
	I. FIGURES.....	193
	II. TABLES.....	197
	III. SCHEMES.....	198
	IV. ANNEXES.....	199
	A. LIST OF COMPOUNDS.....	201
	B. ARTICLE.....	205
	ABSTRACTS.....	215

CHAPTER I

LITERATURE REVIEW

1. General considerations on proteases

By cleaving peptides bonds, proteases (proteinases, peptidases or proteolytic enzymes) play many vital roles in living organisms like apoptosis, autophagy, digestion and activation/deactivation of many different biological processes. So far, more than 500 proteolytic enzymes have been identified in the human proteome, corresponding to 2% of all genes. Proteolytic enzymes are a subclass of hydrolase class and are identified by the EC 3.4 code.

Proteases differentiate according to four different criteria: I) the position along the peptide sequence on which they intervene, II) the optimal pH at which they work, III) their cell compartmentalization and IV) their mechanism of hydrolysis.

The proteases that hydrolyse peptide bonds in the middle of protein sequence are named endopeptidases (e.g. elastase, trypsin, pepsin, chymotrypsin, papain). Those that detach the terminal amino acids from the protein chain are exopeptidases and can be further distinguished between aminopeptidases and carboxypeptidase processing the N-terminal and C-terminal side of peptides sequence respectively (Figure 1A).

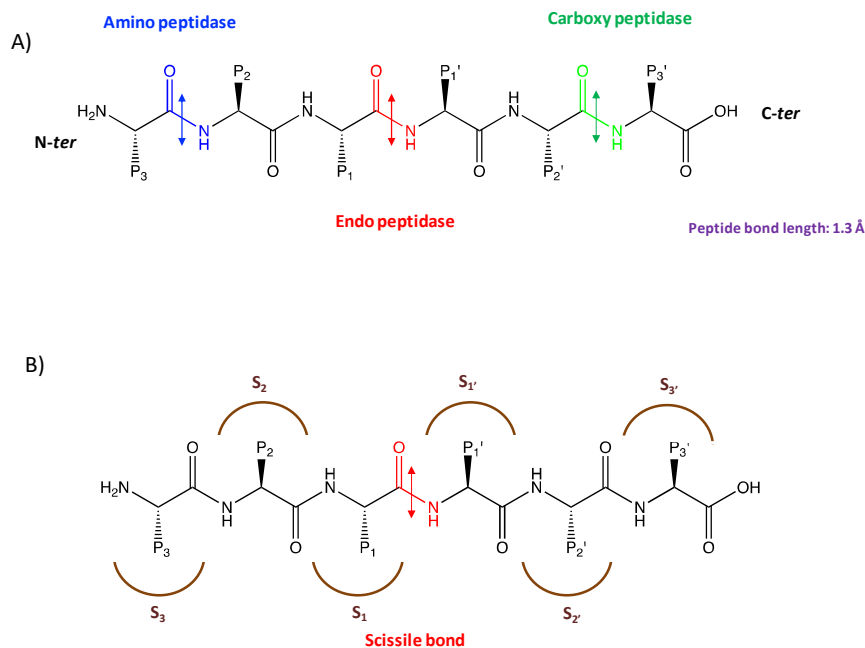


Figure 1. Proteases standard nomenclature. A) distinction between Amino peptidase, Endo peptidase and Carboxypeptidase as function to the position of cleavage along peptide sequence. B) Enzyme Subsite (S₃-S₂-S₁-S₁'-S₂'-S₃') binds to a corresponding residue in the substrate sequence (P₃-P₂-P₁-P₁'-P₂'-P₃'). The numbering is defined as function to the position of the scissile bond.

The active site residues in protease are composed of contiguous pockets termed subsites ¹. Each subsite pocket binds to a corresponding residue in the substrate sequence. According to this definition, amino acid residues from substrate sequence are numbered from either side of scissile bond: ...-P₃-P₂-P₁-P₁'-P₂'-P₃'-

... while the corresponding subsites within the protease active site are labelled as ...-S3-S2-S1-S1'-S2'-S3'-... (Figure 1B).

Based on the pH in which proteases show maximum activity, basic (or alkaline), neutral and acid proteases can be distinguished. Further, depending on their compartment in which they are located three groups are identified: extracellular, intracellular and transmembrane proteases.

Considering their catalytic mechanism seven groups of proteases are identified: aspartic- (first described in 1993), cysteine- (1993), serine (1993) metallo- (1993), threonine- (1997), glutamic- (2004) and asparagine peptidase (2010). The cysteine, serine and threonine proteases possess a nucleophilic residue within their active site (thiol or alcohol function) that directly participates in peptide bond hydrolysis. In the case of aspartic and glutamic proteases, these enzymes benefit from the presence of acid residues (glutamic or aspartic acid) that activates a molecule of water participating in hydrolysis. In addition to a similar residue (Glutamic acid), Metalloproteases possess a zinc ion that acts as a Lewis acid. For each class of proteases, their environment in active site amino acids rules their catalytic mechanism (Figure 2).

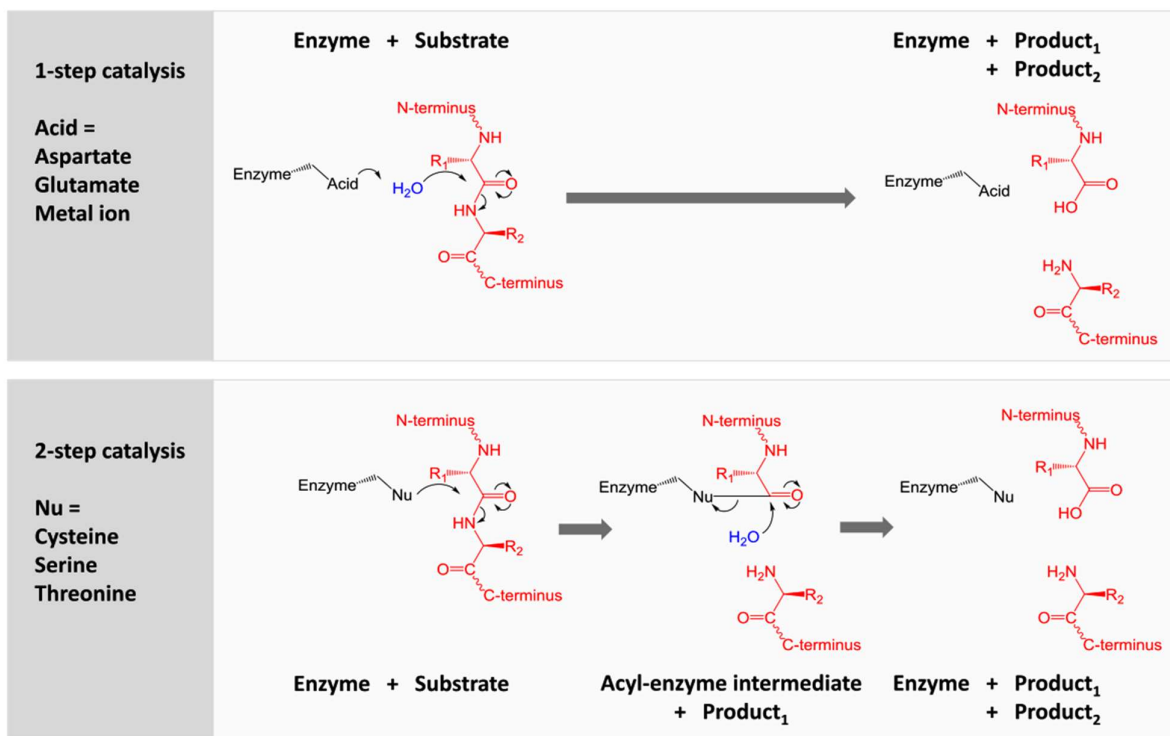


Figure 2. One or two-step mechanism as function to environment in amino acids within protease active site.

In the case of cysteine, serine and threonine proteases a two-step mechanism takes place. Thus, the nucleophilic residue (thiol or alcohol group) performs a nucleophilic attack onto the carbonyl function, which results in the formation of a covalent adduct between the protease and the substrate protein (acyl-

enzyme intermediate). Noteworthy, two other residues within the active site (acid and basic residues) form a charge-relay network to polarize and activate the nucleophile: catalytic triad. The acyl-enzyme intermediate is then hydrolysed by an activated molecule of water.

In a one-step mechanism, a water molecule is activated by an acid residue that acts as a general base. Concomitantly, the activated water molecule proceeds to a nucleophilic attack on peptide bond carbonyl function leading to its hydrolysis. In the case of metalloprotease, a zinc ion (catalytic ion) binds to the oxygen carbonyl function thus increasing the electrophilic character of this latter.

The case of asparagine peptidase is very specific as they cleave themselves by an autoproteolytic reaction involving a glutamine residue.

2. Matrix Metalloproteinases

2.1. Discovery and MMPs classification.

In 1962, Gross and Lapiere described an enzyme responsible for the degradation of extracellular matrix proteins (ECM). Particularly, this enzyme displayed a collagenolytic activity during metamorphosis of tadpole tail fin tissue explants ². The identification of this protease named collagenase and matrix metalloprotease 1 (MMP-1) later on, constituted the first milestone into a field that grew exponentially in the following years, resulting notably in the characterisation of 23 MMPs in human. This name MMPs was based on the initial assumption that these proteases only cleaved the protein components of the extracellular matrix.

Since the pioneered works of Gross and Lapiere, researches on MMPs have focused on various aspects such as biochemistry (purification, activation, inhibition, structure), molecular biology (cloning of MMPs and regulation of gene expression) and MMP biology in normal and pathological process ³. Among the most significant steps, one can mention I) the first isolation of human collagenase from rheumatoid synovium ⁴, II) the identification, isolation and sequencing of MMP-2 (gelatinase A) and MMP-3 in the 1970s ⁵, III) the identification and characterisation of TIMP-1 (Tissue Inhibitor of metalloproteinase) as endogenous metalloproteases inhibitors ⁶, IV) the emergence in the early 1990s of cysteine switch concept associated to MMP activation ⁷ and V) the first crystal structure of collagenase catalytic domain in 1994 ⁸, that paved the way for the rational design of MMPs inhibitors.

Historically, the first members of the MMP family were named and classified according to several criteria: their sequence homology, the nature of the matrix extracellular components that they degraded *in vitro* and the number of years elapsed from the discovery of the first family member. In this respect, MMPs were initially divided into four subgroups: I) collagenases (MMP-1, 8 and 13), II) gelatinases (MMP-2 and 9), III)

stromelysins (MMP-3, 10 and 11) and IV) matrilysin (MMP-7). Over the years, this classification has largely evolved with the discovery of new family members and additional observations made regarding MMP substrates specificity. Further, these proteins show high variability at the level of their quaternary structure, with differences in the structure of their subunits.

To be classified as an MMP family member, the protease should meet the following requirements: I) cDNA has sequence homology to MMP-1, II) activation by proteinases or organomercurials, III) catalysis dependent on zinc at the active site, iv) processing of at least one ECM component, and v) inhibition by ethylenediaminetetraacetic acid (EDTA), 1,10 phenanthroline, and one of the TIMPS.

Due to the specificity of the substrate and the mechanism of action, MMPs is now divided into six groups:

- ❖ **Collagenases:** **MMP-1** (Collagenase I, interstitial, fibroblast); **MMP-8** (Collagenase II, neutrophilic) and **MMP-13** (Collagenase III) degrade type I, II, III, VII, VIII, X collagen, gelatine, IL-1b, L-selectin, proteoglycans, proMMP-2, proMMP-9 and fibronectin.
- ❖ **Gelatinases:** **MMP-2** (in other: Gelatinase A or neutrophilic) and **MMP-9** (Gelatinase B) degrade collagen type IV, V, VII, IX, fibronectin, proteoglycans, plasminogen, act synergistically with collagenases.
- ❖ **Stromelysins/ matrilysin:** **MMP-3** (Stromelysin-1, Transylin); **MMP-10** (Stromelysin-2) and **MMP-11** (Stromelysin-3) digest the base membrane collagen, proteoglycans and glycoproteins of the extracellular matrix; whereas **MMP-7** (Matrilysin-1, others PUMP-1) and **MMP-26** (Matrilysin-2) degrade type I and IV collagen, gelatine, laminin, elastin, fibronectin, proteoglycans, pro-MMP, pro-TNF α , E-cadherin.
- ❖ **Membrane type MT-MMP** (membrane-type matrix metalloproteinases) characterised by the presence of a C-terminal transmembrane domain that maintains the enzyme in the cell membrane structure. This group includes: **MT1-MMP** (MMP-14), which degrades type I, II III collagen, gelatine, fibronectin, laminin, vitronectin, proteoglycans, pro-MMP-2 and pro-MMP-13; **MT2-MMP** (MMP-15), **MT3-MMP** (MMP-16), **MT4-MMP** (MMP-17) and **MT5-MMP** (MMP-24) that activate pro-MMP-2; **MT6-MMP** (MMP-25), which degrades gelatine. Some of these enzymes (MT4- and MT6-MMPs) are membrane-anchored through glycosylphosphatidyl inositol (GPI).
- ❖ **Other metalloproteinases** not included in the above groups, **MMP-12** (macrophage elastase), **MMP-18** (Collagenase 4), **MMP-19**, **-21**, **-27** and epilisin **MMP-28** were classified as "other"^{9,10}.

In recent peptidase nomenclature, MMPs are included in the M10A subfamily described as a broad family of endopeptidases where enzymatic activity is determined by Ca²⁺ and Zn²⁺ ions.

Although these proteases were discovered more than 50 years ago, researches on MMPs remain particularly active as attested by the increasing number of publications in this field since the mid-1980s.

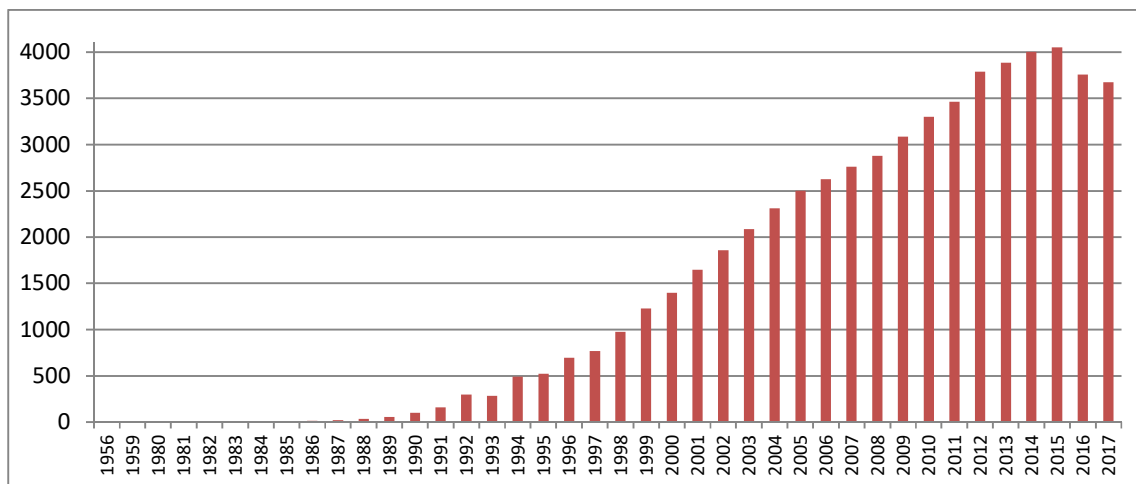


Figure 3 Timeline – the number of publications about matrix metalloproteinases over the years.

2.2. MMPs belong to the metzincin family

MMPs belong to the metzincin family which is part of vast family of zinc metalloproteases.

The metzincin superfamily is composed of five groups:

- **Astacins:** subdivided into Meprin and BMP1 enzymes. They were originally named from the prototypical proteinases astacin which functions as a major collagenolytic enzyme in the digestive tract of the crayfish *Astacus astacus* L. ^{11,12}.
- **Adamalysins** subdivided into ADAM (A Disintegrin and Metalloproteinase) and ADAMTS (A Disintegrin and Metalloproteinase with Thrombospondin Motifs), in the past called the snake venom zinc endopeptidases.
- **Serralysins:** proteolytic enzymes secreted into their environment by various pathogenic bacteria of the genera *Serratia* ¹³, *Pseudomonas* ¹⁴, and *Erwinia* ¹⁵.
- **Pappalysins.**
- **MMPs or Matrixines** ^{16–18}.

In the family of metzincines all members are characterised by the presence within their active site of a catalytic zinc atom and a C-terminal consensus sequence HEXXHXXGXXH/D. This sequence contains I) three zinc-binding residues: two conserved Histidine and a third one that can be either a Histidine or an Aspartate, II) a catalytic glutamate, and III) a strictly conserved glycine. Moreover, all metzincines share a conserved methionine residue below the active site metal as part of a “Met-turn” ^{19,20}.

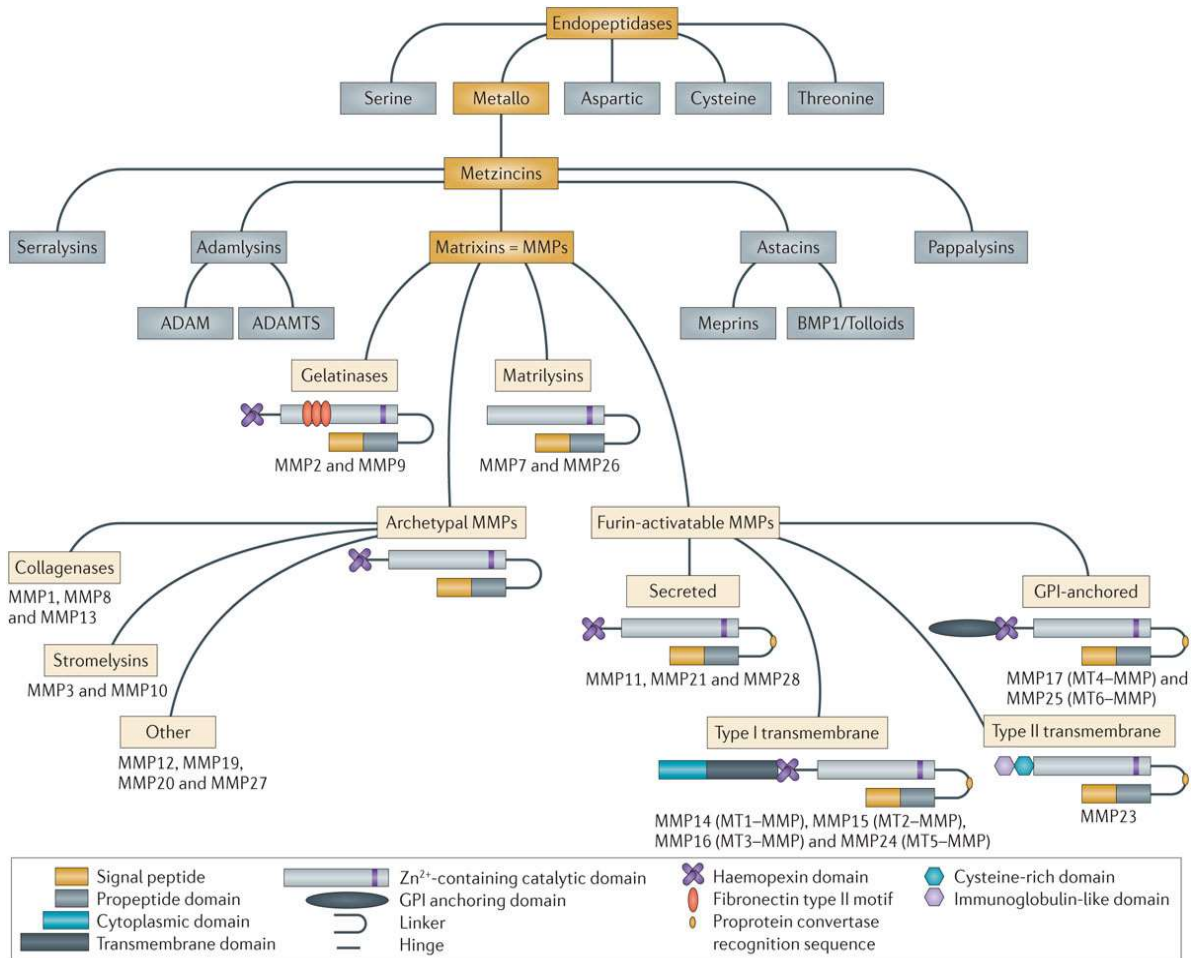


Figure 4. Metzincin superfamily members and structure of Matrixins family ²¹.

Each individual family distinguished by the residue following the third histidine zinc ligand in the motif, and the residues surrounding the methionine in the Met-turn.

2.3. MMPs possess a modular structure

In humans, 23 different MMPs and 24 encoding them genes have been identified. MMP-23 is encoded by two identical genes located on chromosome 1. As extracellular or membrane endopeptidases, metalloproteinases are multi-domain enzymes. All MMPs share a minimal structure composed of a signal peptide (S), a pro peptide domain (Pro) and a catalytic domain containing Zinc ion (Cat Zn).

In addition, subfamilies are categorized by other domains such as fibronectin-like repeats, C-terminal hemopexin-like domains, Ig-like domain and transmembrane domains.

Signal peptide directs MMPs to the secretory pathway.

Catalytic domain composed of approximately 170 acids, two zinc ions (one catalytic and one structural) and usually three structural calcium ions. As mentioned for all the proteases belonging to the metzincines

family, the catalytic domain contains a highly conserved HEXGHXXGXXH motif in a conserved AXMX sequence ("Met-turn") located below the active site. This methionine residue appears at the beginning of a loop and is responsible for the proper structure around the catalytic zinc ion ²²

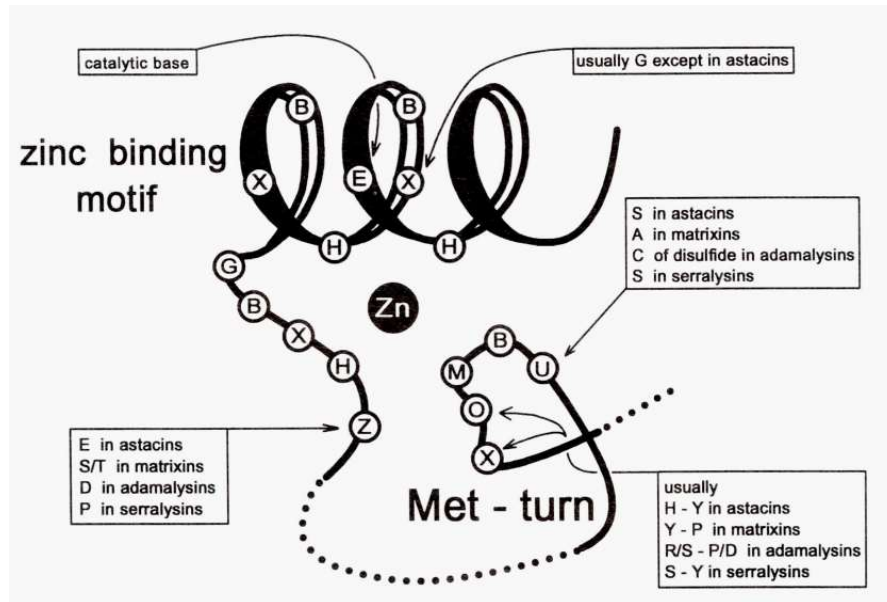


Figure 5. Scheme of the zinc-binding motif and the Met-turn showing the common sequence motifs of the metzincins. Variable segments are shown as dotted lines ²⁰.

Pro-peptide domain is 80 amino acids long. It contains in its C-terminal part a conservative PRCGVDP motif with a cysteine residue, behaving like a fourth zinc ligand, preventing activation of the water molecule. MMPs activation requires to abolish the interaction between cysteine residue and catalytic zinc ion. This process is called the "cysteine switch" and takes place in two stages (see below 2.4.2).

Hemopexin domain possesses approximately 200 amino acids structured in four-blended β -sheet. This domain plays a significant roles in substrate recognition, interaction with tissue inhibitors of metalloproteinases (TIMPs), binding to the ECM or cell surface, MMPs internalization and degradation ²².

Linker region rich in proline, links the hemopexin domain (C terminal) to the catalytic domain. This flexible linkage helps to maintain the stable structure of the enzyme, and may also be important in recognition of some MMPs substrates.

Fibronectin domain insert in triplicate within the sequence of MMP-2 and 9 catalytic domains and mediates binding to gelatin substrate.

Transmembrane domain (type I or II) that can be prolonged by a very short cytoplasmic domain (Cyt) or by a signal domain allows the anchoring to cell membrane (MMP-14/16/23 and 24). MMP-17 and 25 anchors the cell membrane with a **glycosylphosphatidylinositol domain** ^{10,23,24}.

Furin-like domain as a domain recognized by serine proteases allows the intracellular activation of MMPs. This motif is located between the prodomain and the catalytic domain.

Immunoglobulin-like motif, cysteine-rich domain and pro peptide domain without cysteine switch-motif are characteristic of MMP-23.

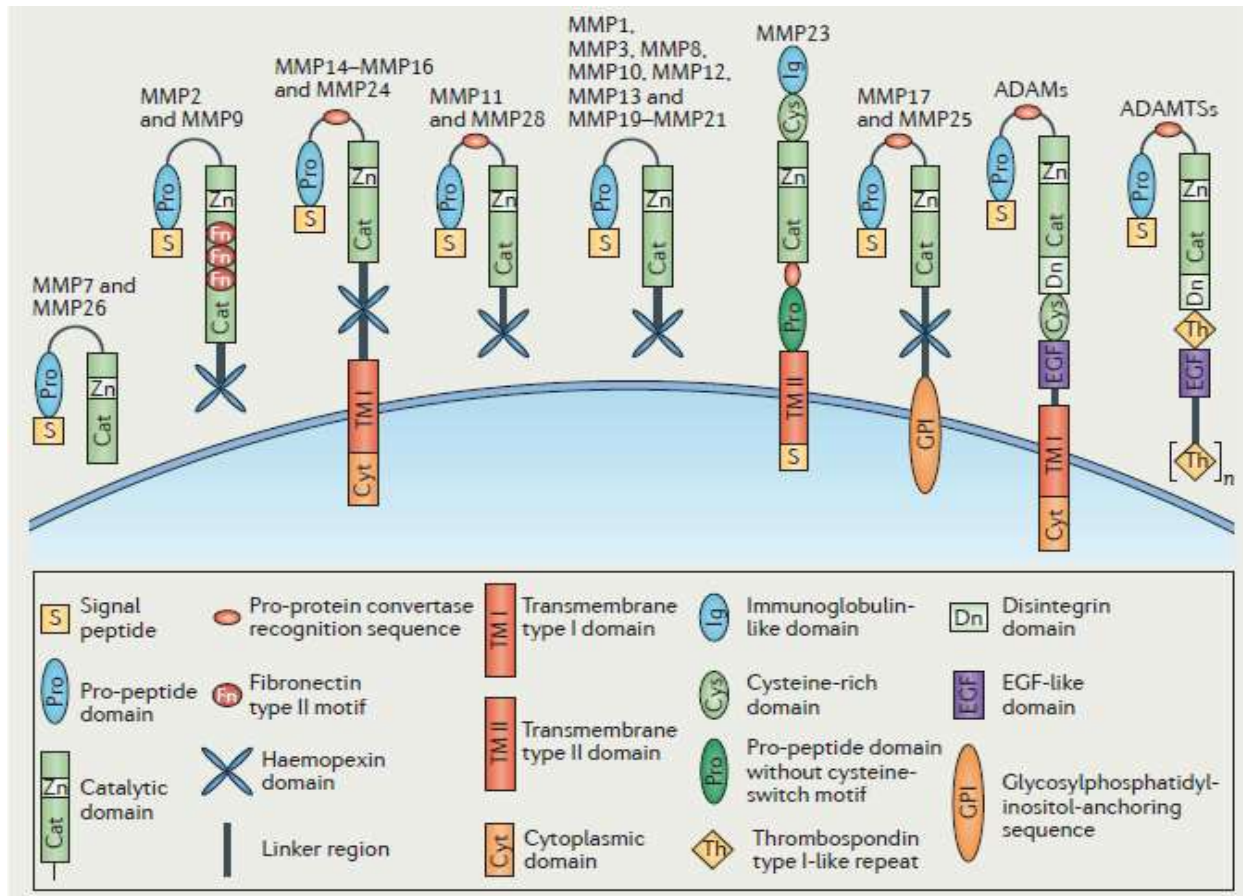


Figure 6. Domain structure of matrix metalloproteinases family ²³.

2.4. Regulation of MMPs activities

Since MMPs are able collectively to degrade all the protein constituents within extracellular matrix, their proteolytic activity has to be tightly controlled under normal conditions to prevent tissue destruction. Like other enzymes, the functioning of MMPs is regulated at different levels: from transcription and secretion to activation, inhibition and degradation (Figure 7).

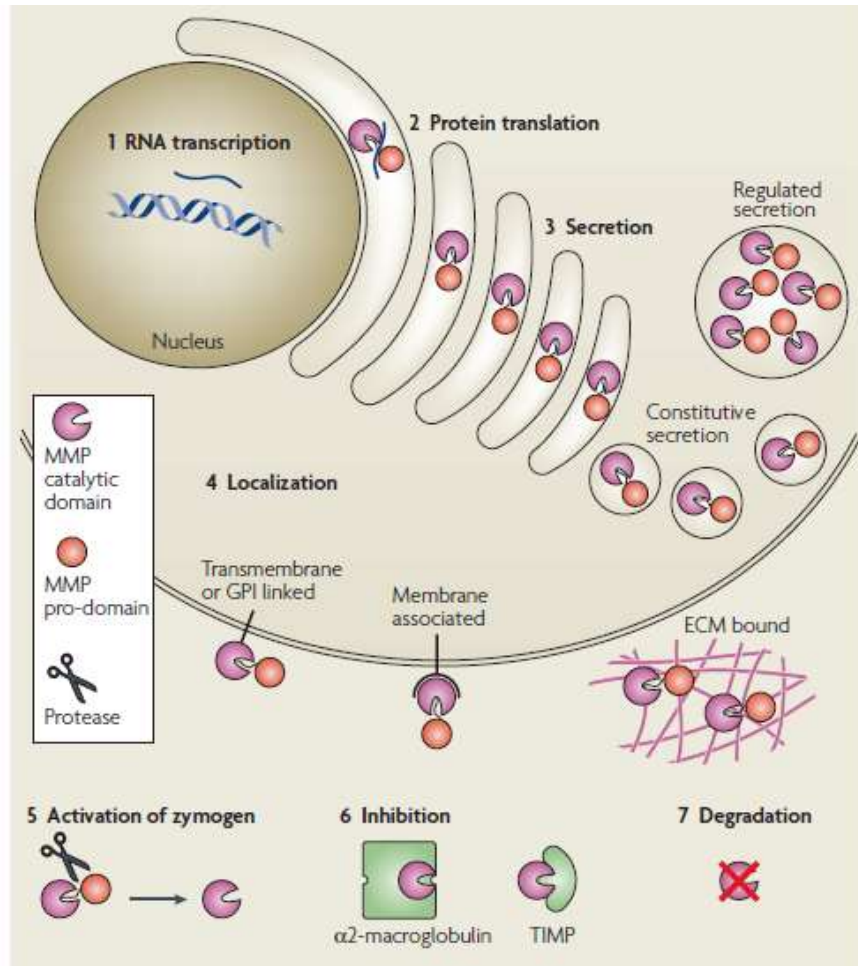


Figure 7. Regulation of extracellular proteolysis ²⁵.

2.4.1. Transcription

The first level of regulation of MMP activity is during translation and transcription of RNAs. This regulation is modulated by very specific signals which themselves are subjected to precise spatial and temporal control. Transcription of genes encoding MMPs is induced by growth factors: transforming growth factor (TGF- β), epidermal growth factor (EGF), platelet-derived growth factor (PDGF) and fibroblast growth factor (β -FGF), hormones, inflammatory cytokines (interleukin-1, interleukin-6, tumour necrosis factor α TNF- α) and others. Most of them interact with protein activators of transcription AP-1 (protein transcription activator 1) and PEA3 (activator that enhances the expression of poliovirus genes) that lead to the initiation of transcription. Activation via these factors takes place through the phosphorylation cascade, dependent on the mitogen activating protein kinase (MAP-Kinase).

The activity of genes encoding some MMPs is also influenced by epigenetic factors such as DNA methylation and histone modifications. The expression level of MMP genes is also controlled by post-transcriptional

processes. TGF- β has been shown to increase the levels of MMP-2 and MMP-9 mainly by prolonging the half-life of these metalloproteinases in prostate cancer cells and human fibroblasts, and signals from $\alpha 3\beta 1$ integrin stabilise MMP-9 mRNA. Similarly, cortisol enhances the stability of MMP-13 mRNA in rat osteoblasts^{26–28}.

2.4.2. Extracellular activation and cysteine switch concept

Most of the MMPs are extracellularly secreted as inactive zymogen also called pro-MMPs that needs to be subsequently activated. Within the extracellular space, zymogens are activated through different mechanisms involving proteolytic enzyme (e.g. MMPs and serine proteases) and action of active forms of oxygen.

The N-terminal segment of zymogens possess a pro peptide with a molecular weight of 9-20 kD, depending on the type of metalloproteinases. This pro domain consists of three α helices connected by flexible loops. Contiguous to the third helix, a sequence with a cysteine residue (PRCGXPD) has been preserved in evolution, except in the case of MMP-23. As illustrated by Figure 8, the thiol group of the cysteine residue interacts with the catalytic zinc ion (Zn^{2+}), maintaining the pro enzyme in its inactive state.

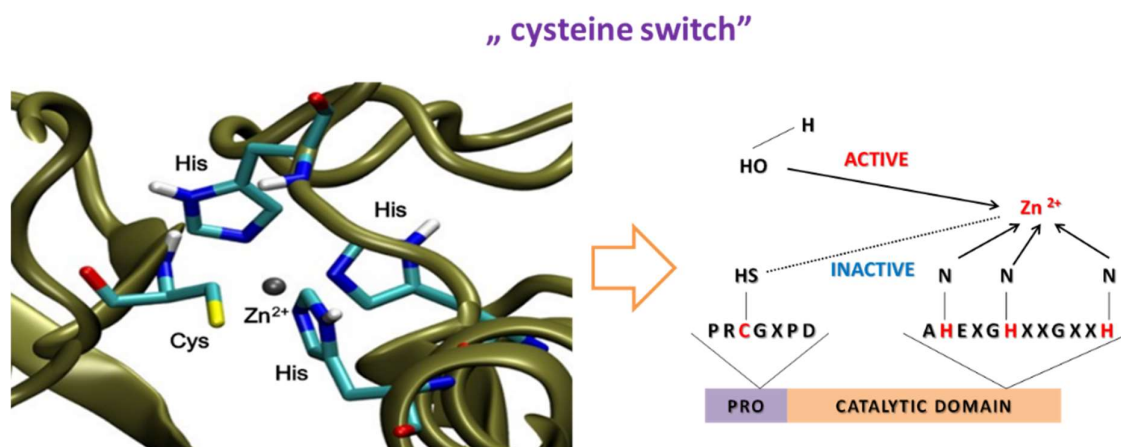


Figure 8. Activation of MMPs, the interaction of cysteine residue from the pro peptide with the catalytic zinc ion of the catalytic domain²⁹.

The activation process is a two step-process that requires abolishing interactions between cysteine and zinc ion followed by pro domain removal upon proteolysis, resulting in active site unveiling. Various mechanisms can lead to such an activation:

- 1) Allosteric perturbation or posttranslational modifications that induces pro-MMP conformational changes that lead to the exposure of pro domain flexible loops to proteolysis³⁰.

2) Modification of the thiol function integrity by physiological agents or non-physiological agents leading to destabilizing interaction between cysteine and zinc ion. This is often accompanied by an autolysis.

3) Direct cleavage of the pro domain by a other proteolytic activity.

The proteases responsible for pro domain processing are serine proteases (trypsin, chymotrypsin, plasmin) as well as other MMPs (-1, -2, -8, -9). In the case of activation by plasmin, the plasminogen Activator System (PAS) is required. The system consists of two activators of plasminogen (PA), urokinase (uPA) and a tissue type activator (tPA), that are membrane-associated. They both activate plasminogen into plasmin, that subsequently process proMMP at the cell surface. This mechanism is likely involved in the activation of proMMP-3, proMMP-12 and proMMP-13³¹⁻³⁴.

The prodomain removal is commonly called in the literature the "cysteine switch"^{35,36}.

2.4.3. Intracellular activation

Most of MMPs are activated outside the cell, although it has been shown that for some members this activation can be carried out intracellularly in the Golgi apparatus. In this respect, It was demonstrated that proMMP-11 (stromelysin 3) is processed intracellularly by furin that specifically recognizes a RXKR or RRKR sequence within the pro domain sequence³⁷. Besides MMP-11, MT-MMPs, MMP-23 and MMP-28 also possesses a furin-like proprotein convertase recognition sequence³⁸. Once activated, MMPs are extracellularly secreted.

2.4.4. Cell Surface activation involving TIMP-2

Contrary to what has been long considered, endogenous TIMP can also participate to MMPs activation. In the respect, the activation proMMP-2 by the combined action of MT-1 MMP and TIMP-2 constitutes one of the most characteristic examples. As illustrated by Figure 9, the proposed mechanism of activation is a multistep process.

First, MT1-MMP (blue) is activated intracellularly by furin and localizes to the cell surface through the transmembrane domain. A MT1-MMP dimers is formed through hemopexin-domain interactions. The amino-terminal domain of TIMP-2 (red) binds to the active catalytic domain of MT1-MMP. The MT1-MMP-TIMP-2 complex recruits proMMP-2 (green) by interactions of the carboxy-terminal domain of TIMP-2 with the hemopexin domain of proMMP-2. The 'receptor' MT1-MMP thereby brings proMMP-2 close to the 'catalytic' MT1-MMP, which cleaves the pro-domain of MMP-2 and activates the enzyme³.

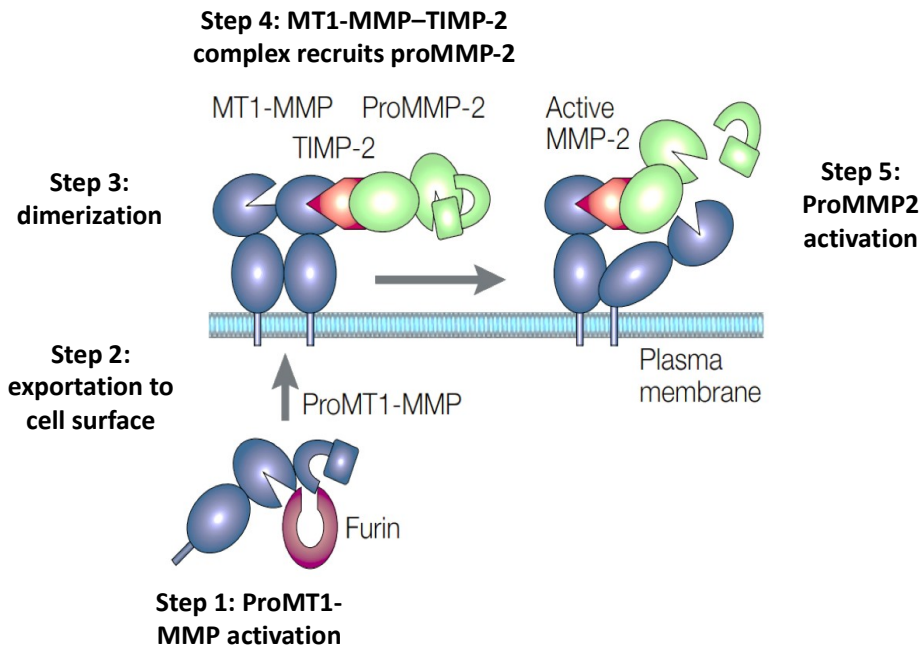


Figure 9. Schematic representation of two-step ProMMP-2 activation process by the combined action of MT1-MMP (MMP-14) and TIMP-2³.

2.4.5. Inactivation by endogenous inhibitors

The regulation of MMPs activity takes place not only through the mechanisms of their activation, but also in the processes of enzymes inhibition by protease inhibitors. Non-specific metalloproteinase inhibitors like α -2-macroglobulin and α -antiprotease are mainly responsible for the regulation of MMPs activity in plasma. Human α 2-macroglobulin is a broad-spectrum proteinase inhibitor of tissue fluids and blood. It is a homo tetrameric macromolecule of 725 kDa which is able to inhibit almost all classes of endopeptidases by entrapping the whole enzyme. During the inactivation of MMPs by α macroglobulin, the first step of proteolysis leads to the formation of a covalent complex between these two partners, this complex is subsequently removed from circulation by endocytosis. Noteworthy, MMPs/ α -macroglobulin complex is no longer able to degrade MMPs endogenous substrates but can always degrade synthetic substrates or interact with small ligands.

Natural and specific inhibitors of MMPs are proteins belonging to the group of tissue inhibitors of metalloproteinases (TIMPs). TIMP proteins are a family of 4 glycoproteins: TIMP-1, TIMP-2, TIMP-3 and TIMP-4. They are characterized by a molecular weight ranging from 21 to 29 kD³⁹. TIMP 1, 2 and 4 forms are soluble and they are detected in the blood serum, whereas TIMP-3 is insoluble and anchored in the ECM⁴⁰. All TIMPs have similar folding with a N-terminal domain containing six cysteine residues assembled in three disulphide bridges. Despite their structural similarity, TIMPs differ in their selectivity profile. TIMP1

inhibits all MMPs, particularly MMP-9, with the exception of membrane metalloproteases MT1-MMP, MT3-MMPs, MT5-MMPs and MMP-19⁴¹. In contrast, TIMP-3 specifically inhibits MMP-2, -3, -7 and -9.

As illustrated by Figure 10, the N-terminal segment of TIMP-1 structured around two disulphide bridges between Cys¹-Cys⁷⁰ and Cys³-Cys⁹⁹ interacts within the active MMP site through a hydrogen bonding network and catalytic zinc atom chelation. Coordination of TIMP to the catalytic zinc displaces a zinc-bound water molecule present at the MMP active site, removing the nucleophile essential for peptide bond hydrolysis.

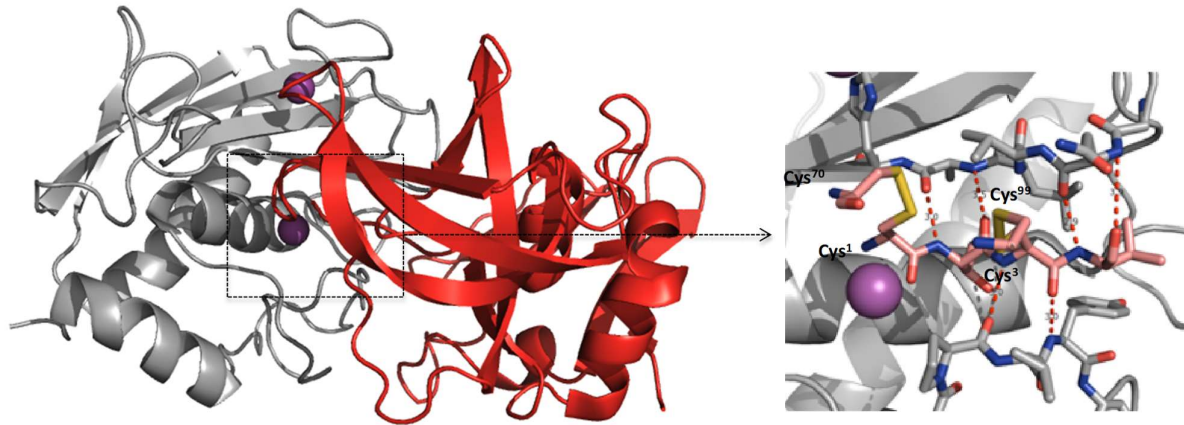


Figure 10. Crystallographic structure of MMP-3 catalytic domain (in grey) interacting with TIMP-1 (in red), (PDB code: 1UEA). Zoom of the N-terminal part of TIMP-1-Cys1 interacting within the catalytic domain of MMP-3, hydrogen bonds are shown in hatched form.

In vitro, this interaction is described of high affinity but remains reversible. Similar to MMPs, expression of TIMP genes is regulated by vasoconstrictor stimulators such as haemodynamic stimuli, oxidative stress, pro- and anti-inflammatory factors (cytokines or vasoactive agents). Disturbing the balance between MMPs and TIMPs is systematically associated with progressive pathological changes⁴².

3. Biological functions of MMPs

Although latent forms of MMPs (pro-MMPs) have been shown to be involved in a few biological processes, a wide consensus in the literature attributes a functional role to MMPs under their active forms. MMPs have been originally described as proteases acting exclusively on extracellular matrix components with consequences on tissue remodelling. It is now clear that MMPs are capable to process a wide range of matrix and non-matrix substrates. Thus, MMPs degrade adhesion proteins, apoptosis mediators, receptors, chemokines, cytokines, growth factors, and cell-to-cell linkage proteins. As a consequence, these proteases are involved in numerous biological processes that go far beyond the simple remodelling of the extracellular matrix and should no longer be perceived as simple molecular scissors. To add another level of complexity to MMP biology, each MMPs does not present strict specificity for one single substrate. Accordingly, collagen

can be degraded by collagenases but also by MMP-14 (MT-MMP) and MMP-9. Another difficulty relies on compensation phenomenon, very common in this group of enzymes⁴³. Further, MMPs are integrated into a network of proteases. Thus, a single MMP can play a direct or indirect function during the evolution of biological process.

3.1. The physiological function of MMPs.

MMP are characterized by a broad spectrum of activity and are involved in various many different biological events including embryonic implantation, tissue morphogenesis, mechanisms of healing, control of the immune response and cell death^{25,44,45}.

As already mentioned, MMPs are able collectively to transform and degrade many components of the extracellular matrix (ECM) e.g. collagen, elastin, fibronectin, laminin, fibronectin, entactin, aggrecan, osteonectin, vitronectin and tenascin⁴⁶. Degradation of ECM by MMPs can lead to the destruction of adhesive interactions between the cell and the matrix, preventing the cell to receive signals from the environment and, consequently, introducing it into apoptosis. Since ECM is a reservoir of numerous growth factors, MMPs also participate in signals transfer from the ECM to the cells. MMPs regulate bioavailability of VEGF (Vascular Endothelial Growth Factor) by cleaving matrix-bound isoforms of VEGF, a critical mediator for specification, morphogenesis, differentiation, and homeostasis of vessels⁴⁷. Cutting off some ECM proteins can also reveal inaccessible cryptic sites that can transmit signals or lead to products with completely new biological activity. For example, the migration of endothelium cells is triggered by a MMP- 14-processed form of laminin 5^{48,49}.

3.2. Pathological function of MMPs

In the late 1960s MMPs overexpression was demonstrated in various pathological states such as cancer and rheumatoid arthritis^{3,50,51}. Since these pioneered studies and beside their involvement in tumour progression and metastasis^{52,53}, MMPs have been shown to play critical roles in pathologies with inflammatory components including emphysema, asthma^{54,55} and atherosclerosis⁵⁶⁻⁵⁸, in cardiovascular diseases⁵⁶⁻⁵⁸, and in diseases of central nervous system⁵⁹.

Originally, MMPs were considered as solely overexpressed by cancer cells to support tumour growth and metastasis. However, in 1990 Paul Basset showed that Stromelysin-3 (MMP-11) activity could be also found in stromal host cells surrounding the tumour, drastically upset this paradigm⁶⁰. Thus, MMP secretion is not exclusively limited to cancer cells and host cells can also produce MMPs in response to changes in their environment. From such a study but also from those on MMPs knock out (KO) mice for which MMP genes have been invalidated, emerged the concept that MMPs could indeed support disease progress but could also play opposite functions^{61,62}. Thus, in a given pathological process, some MMPs are considered as

targets while other are anti-targets. To add another degree of complexity, for one given MMP divergent functions can be observed depending on pathological stage. Retrospectively, these observations largely explain the failure of clinical assays with broad-spectrum MMP inhibitors in cancer patients ⁶³.

3.3. The specific case of macrophage elastase (MMP12)

In 1975, Z. Werb reported for the first time a proteolytic activity associated to murine macrophage. Under thioglycolate-stimulation, murine macrophages secreted a proteinase able to degrade insoluble elastin ⁶⁴. A few years later, the same group isolated a protein that showed characteristic properties of zinc metalloproteases, with inhibition by EDTA and TIMP-1⁶⁵. This enzyme was initially named murine macrophage elastase (MME). In 1992 Shapiro's group was able to isolate and identify MME cDNA and definitely confirmed its membership to MMPs family⁶⁶. As expected for MMPs, this enzyme of 54 kDa possesses a pro domain, a catalytic domain with the characteristic sequence signature HEXXHXXGXXH and a haemopexin domain. Interestingly in solution, the pro domain turned out instable and only an active form of 22 kDa corresponding to haemopexin domain removal was observed ⁶⁶. Macrophage elastase was further named MMP12.

The murine and human forms of MMP12 only possess 64% sequence identity. This is a rather surprising observation considering that percentages of identity between human and murine MMPs are usually around 95%. Similarly, percentages of identity between MMP12 and other MMPs vary between 33% and 49%, which is, again, a fairly low percentage. However, MMP12 coding sequence is located on 11q22 human chromosome, a location shared with many other MMPs.

As it is mainly expressed by macrophages, MMP-12 overexpression has been associated to inflammatory pathologies such as abdominal aortic aneurysm, atherosclerosis, rheumatoid arthritis, asthma, emphysema or bronchitis, and chronic obstructive pulmonary disease (COPD) ^{54-56,58,67-70}.

Like other MMPs, MMP12 can adopt ambivalent function depending on pathological context. As a consequence, MMP12 cannot be systematically considered as valuable therapeutic target. For instance, MMP12 expression in mouse melanoma cells resulted in reduction in early-stage tumour growth and a reduction in blood vessel formation, effects that seemed to be mediated by the ability of MMP12 to generate angiostatin through cleavage of plasminogen ⁷¹. In patients with primary colorectal carcinomas, MMP12 expression was associated with increased survival times ⁷². In those cases, MMP12 is clearly a candidate anti-target.

Conversely, MMP-12 overexpression was associated to atherosclerotic plaque development and rupture. In murine model of atherosclerosis, MMP-12-KO mice showed more stable plaques ⁶¹. MMP-12 seems to favour the recruitment of macrophages within the plaque and facilitating the migration of smooth muscle

cells ⁷³. In human, the existence of a unique relationship between expression of MMP-12 and atherosclerosis development remains to be established. However, the presence of MMP-12 has been linked to instable atherosclerotic plaque ^{74,75}

Shapiro's group also demonstrated an antimicrobial activity for MMP12. Surprisingly in this case, the antimicrobial properties of MMP12 do not reside within its catalytic domain, but rather within the heamopexin domain ⁷⁶. More recently, the participation of MMP-12 in defence processes against viral infections was also demonstrated⁷⁷. Thus, during viral infection, active forms of MMP-12 secreted by macrophages can translocate to the nucleus of virus-infected cells while a portion of these active forms remains outside of the cell (Figure 11).

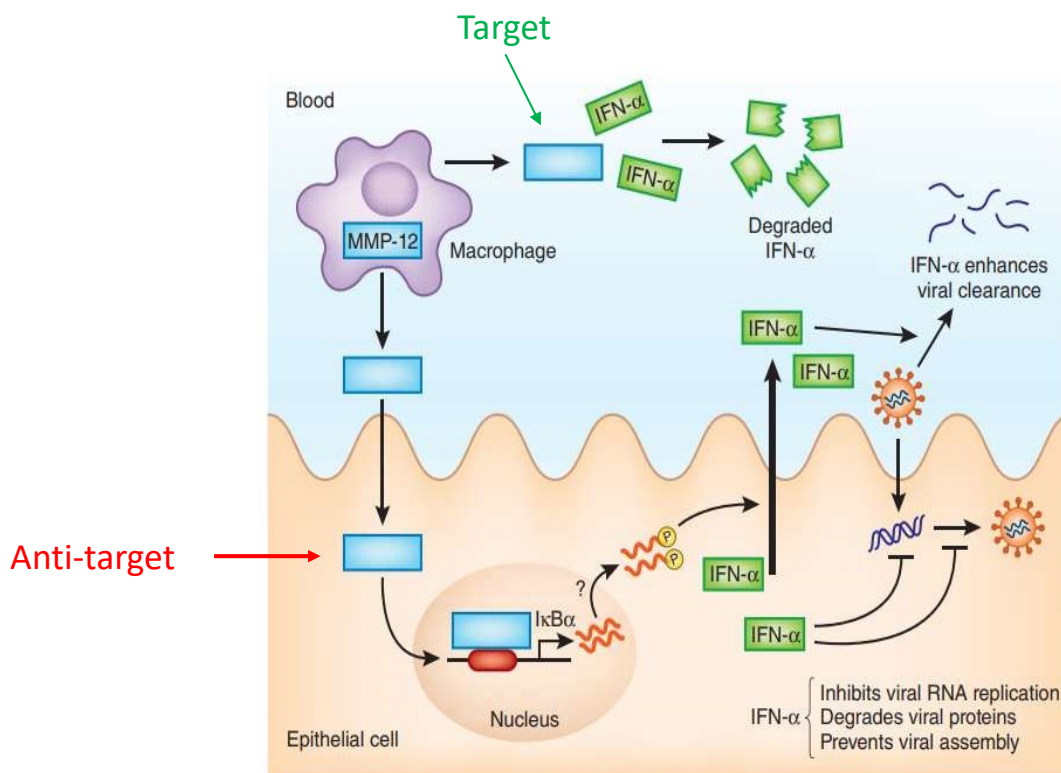


Figure 11. In antiviral immunity, MMP12 can adopt a dual localisation associated to opposite functions ⁷⁸.

Interestingly, this ubiquitous localisation is associated to opposite functions. Whereas nuclear MMP-12 active forms favour interferon- α (IFN- α) secretion essential for host protection, extracellular active forms cleave off the IFN- α preventing an unchecked immune response. In this regard, a therapeutic intervention aiming to elevate systemic IFN- α level for improving antiviral response, should have to target selectively the extracellular active form of MMP-12 while sparing the intracellular one. Very recently, MMP12 was also shown to downregulate INF- γ activity with consequences on resolution of acute inflammation ⁷⁹.

The case of MMP-12 is particularly enlightening and illustrates well the difficulty to unambiguously attribute to one given MMP a clear function during a pathological process, with an enzyme that potentially processes a wide diversity of substrates and can adopt opposite functions depending on its cell compartmentalization.

This stresses the need to develop selective methods and chemical tools to document MMP spatial and temporal activation in various biological contexts. In other words, during the evolution of a pathological process it is critical to unambiguously determine which MMP(s) are present in their active form and which of them actually support disease development. Only these latter must be subjected to therapeutic intervention. This last point strongly suggests that highly selective MMPs inhibitor is the most favourable therapeutic option ⁶⁷.

4. Inhibitors of MMPs: chemical tools to investigate MMPs biological function.

Originally, MMPs inhibitors (MMPIs) were developed without knowledge on MMP 3D-structure and directly derived from substrate sequences on which a zinc chelating moiety was conjugated. The first structure of MMP-1 catalytic domain in complex with a synthetic inhibitor ⁸, allowed to take a step towards structure-based design of synthetic inhibitors. Since this pioneered study, more than 200 MMPs structures (RX and NMR) have been deposited in the protein data bank (PDB) and several generations of inhibitors with improved selectivity profile have emerged within this well-defined structural context.

4.1. Structure-based design of MMP inhibitors: from broad-spectrum to selective inhibitors

All the MMP catalytic domains share a marked sequence similarity, where the percentage of identical residues ranges from a minimum of 33% between MMP-21 and MMP-23, to a maximum of 86% between MMP-3 and MMP-10. The catalytic domain contains two zinc and three calcium atoms which are involved in the stabilization of the three-dimensional structure. Interestingly, no disulphide bridges are present. The second zinc atom (catalytic zinc) is located in the middle of the catalytic cleft crossing the protein from west to east (zinc ion in magenta, Figure 12).

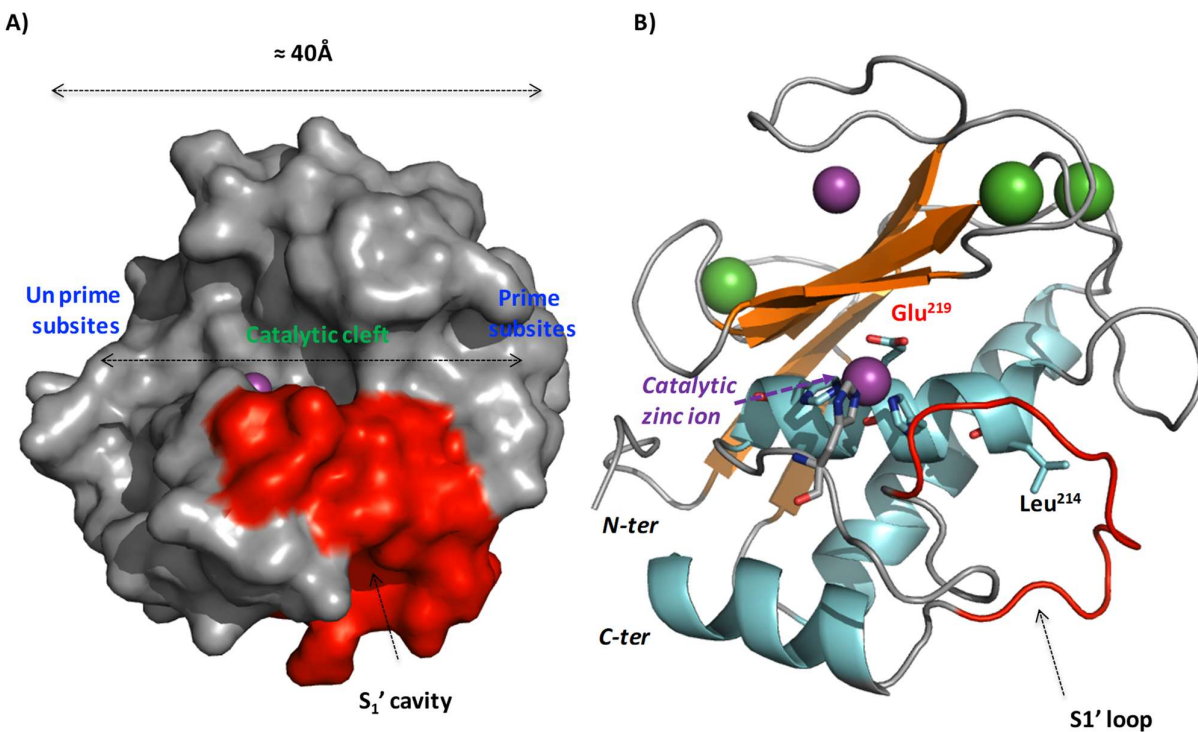


Figure 12. Catalytic domain of hMMP12. A) In surface representation with S_1' cavity highlighted in red. B) In ribbon representation with β -sheets in orange, α -helix in cyan and S_1' loop in red.

In this standard orientation, peptide substrates of at least 6 residues bind on either side of the catalytic zinc ion in a conformation extending from the left (un prime subsites) to the right (prime subsites). The zinc ion, whose degree of oxidation is 2+ is in interaction with three histidine residues (Figure 12B). The α -helix that carries two of the three chelating histidine also contains the catalytic glutamate (Glu²¹⁹ in the case of MMP12). At the bottom of the catalytic zinc ion, a rather hydrophobic cavity open to the solvent on both sides is present. This S_1' cavity constitutes an important element of variability between different MMPs with outer wall of this cavity defined by a flexible S_1' loop (in red in Figure 12B). Depending on MMPs, this loop also called specificity loop varies in amino acid composition (number and nature of residues)⁸⁰. Thus, the length of this loop can range from 9 (MMP-1, 9, 11 and 23) to 13 residues (MMP-17 and 25) resulting in S_1' cavity varying in volume. The volume of S_1' cavity volume is also influenced by the nature of the residue at position 214 (with reference to MMP-1) on the α -helix defining the rear wall of the S_1' cavity. When this residue is a leucine, which is the case for most MMPs, the S_1' cavity is relatively wide and deep. In the case of MMP-1 and MMP-7, the presence in this position of an arginine (MMP-1) or a Tyrosine residue (MMP-7) pointing to the interior of the S_1' cavity significantly reduces its internal volume. In an equivalent position, a methionine and a glutamine residue also clog S_1' cavity of MMP-16 and MMP-11 respectively. Moreover, superposition of three-dimensional structures of MMP catalytic domains coupled with the use of in silico

comparison tools such as Principal Component Analysis (PCA) also revealed small topological differences within S_2 and S_3 sub sites ⁸¹.

The particular topology of MMP active site has greatly influenced the design of synthetic inhibitors. Particularly, most synthetic MMPs inhibitors are competitive inhibitors that contain I) a zinc-binding group, II) a P_1' hydrophobic side chain inserting within S_1' cavity, III) a peptide or pseudo peptide backbone interacting within the catalytic cleft through hydrogen bonds network and IV) additional residues to bind further sub sites (Figure 13A).

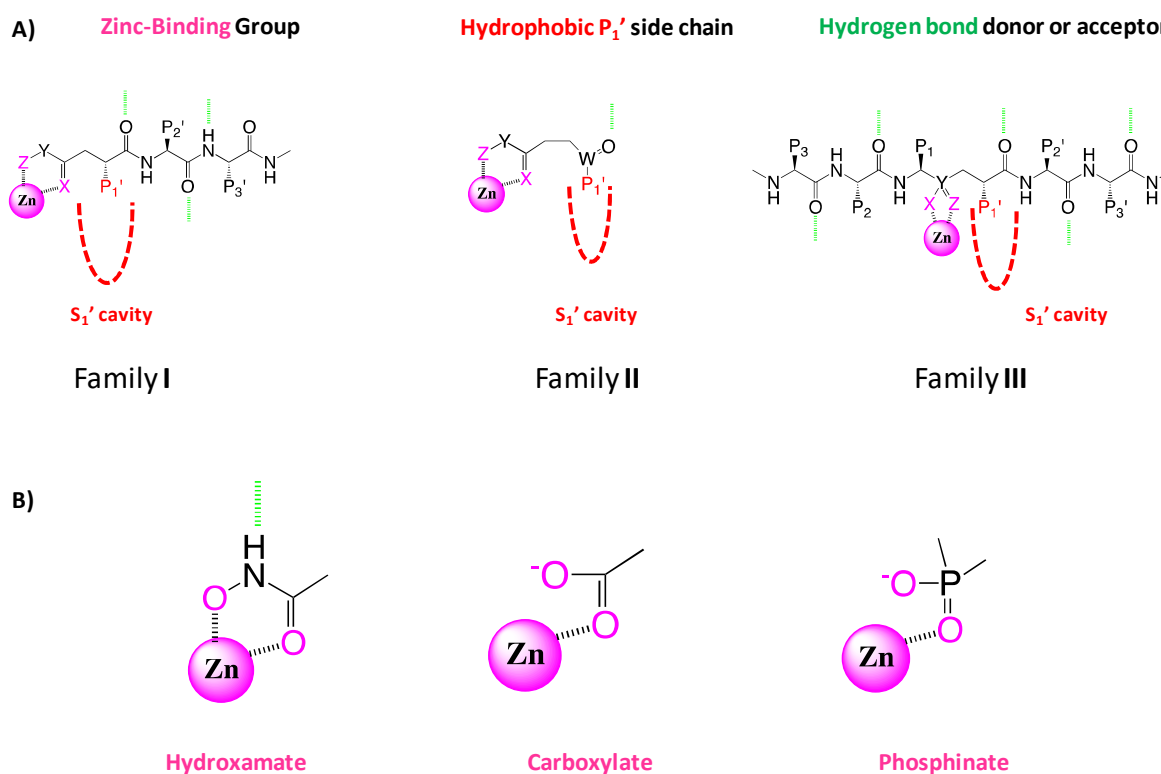


Figure 13. A) Generic structure of the most representative families of MMPs inhibitors sharing a common zinc-binding moiety (magenta), a hydrophobic P_1' side chain (red) and a peptide or pseudo peptide backbone to make hydrogen bonds within catalytic site. B) Schematic representation of most standard zinc-chelating moieties found in structure of MMPs inhibitors.

Since the first generation of MMPs inhibitors whose structure was inspired from collagen sequence, several successive generations of inhibitors have emerged and can be divided in three big families. These families mainly differ in their binding within MMPs catalytic domains. The first family (Family I) comprises inhibitors interacting with the catalytic zinc atom and exploring only the prime subsites. The second family (Family II) clusters synthetic inhibitors whose structure was largely simplified with only a zinc-binding moiety and a long P_1' hydrophobic chain inserting into the S_1' cavity. The third family (Family III) is mainly constituted by phosphinic pseudo peptides with a phosphinate function as zinc-binding group ⁸². By comparison with

compounds from the two other series, phosphinic derivatives can probe the whole enzyme active site across prime and unprime subsites.

Among the factor that can modulate MMPs selectivity, the chemical nature of the zinc-chelating moiety is critical. In this respect, the hydroxamate function as a bidentate ligand can be considered as a strong zinc chelator while the carboxylate or phosphinate functions as monodentate binder display lower avidity for the zinc ion (Figure 13B)⁸³. Thus, inhibitors incorporating a hydroxamate function are very potent but non-selective for MMPs. In this series of compounds, GM6001 (see annex A for structure) is even capable to bind to zinc metalloproteases that do not possess any structural analogies with MMPs⁸⁴.

The incorporation of a weak binder such as carboxylate function within the structure of family II compounds, combined with variation on P₁' side chain (variation in length and flexibility) resulted in the identification of more selective MMPs⁸². Based on this approach, MMP-12⁸⁵ and MMP-13⁸⁶ selective inhibitors were developed. Thus, by tuning the strength of interaction with the zinc ion, it was possible to increase the contribution of P₁' side chain that could generate more specific interaction within S₁' pocket. This concept has been pushed further through the development of MMPs inhibitors that do not possess any zinc binding-group and only interacted within the S₁' cavity. In this series highly selective MMP8 and MMP-13 inhibitors were identified^{87,88}.

The phosphinic pseudo peptides also possess a weak zinc-chelating moiety and through its unique capacity to interact within the entire catalytic cleft offer further opportunities for selective interactions compared to inhibitors with a hydroxamate or carboxylate zinc-binding group. In this respect, phosphinic pseudo peptides were considered as a good starting point for the development of MMPs selective inhibitors^{80,89}.

4.1.1. RXP470.1 as a highly selective inhibitor of MMP-12

Through the screening of focused libraries, RXP470.1, a pseudo tetra peptide was identified by our group as the first potent and highly selective inhibitor of MMP-12 (Figure 14)⁹⁰.

This phosphinic pseudo peptide, incorporates a bulky side chain in its P₁' position and two glutamate residues in P₂' and P₃' positions. *In vitro*, this molecule was characterised by a high potency toward hMMP12 catalytic domain (K_i = 0.19 nM) and was 2-3 orders of magnitude less potent toward other examined MMPs. Further, RXP470.1 behaves as a very weak binder toward other metalloproteases such as TACE (Tumour necrosis factor-Alpha Converting Enzyme belonging to ADAM family), NEP (neutral endopeptidase) and ACE (Angiotensin-Converting Enzyme).

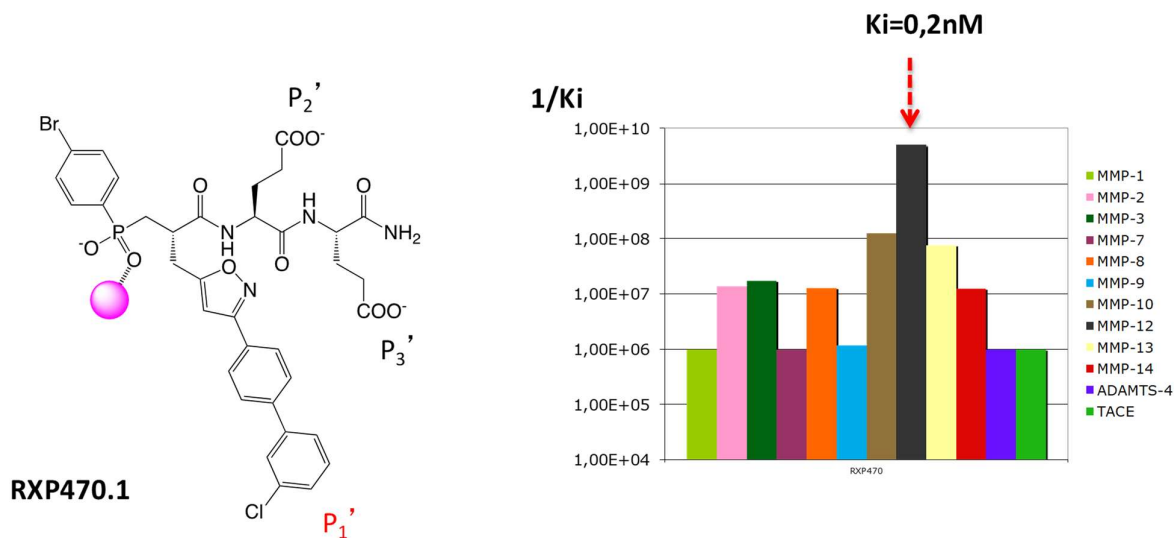


Figure 14. RXP470.1 structure and its selectivity profile towards a set of human metalloproteases. The $1/K_i$ (M) values are reported in logarithm scale. The higher is the bar the higher is the inhibitor potency. Each MMP is identified with a colour code and hMMP12 is represented by a black bar.

Our group recently reported a study combining crystallography and isothermal titration calorimetry in order to clarify the role of P_1' , P_2' , P_3' positions in the excellent affinity and selectivity of RXP470.1 for MMP-12⁹¹. Through the resolution of RXP470.1/hMMP12 complex crystal structure, RXP470.1 binding mode was first confirmed.

As illustrated by Figure 15, the phosphinate function interacts in a monodentate manner with catalytic zinc ion. The P_1' isoxazol side chain inserts deeply into the S_1' cavity, potentially generating several Van der Waals contacts with side chains of S_1' loop. Further, distance measurements between RXP470.1 and protein backbones were compatible with hydrogen bonds. Surprisingly, no evident interactions involving the two glutamate residues were observed within S_2' and S_3' regions.

Despite a multitude of interactions potentially generated upon RXP470.1 binding to hMMP12, calorimetric studies revealed that RXP470.1 binding is not characterized by a large enthalpy component. Indeed, the formation of RXP470.1/hMMP-12 complex is mostly entropically driven, which was ascribed to hydrophobic effects associated with the burial of RXP470.1 P_1' side chain into the hydrophobic MMP12 S_1' cavity.

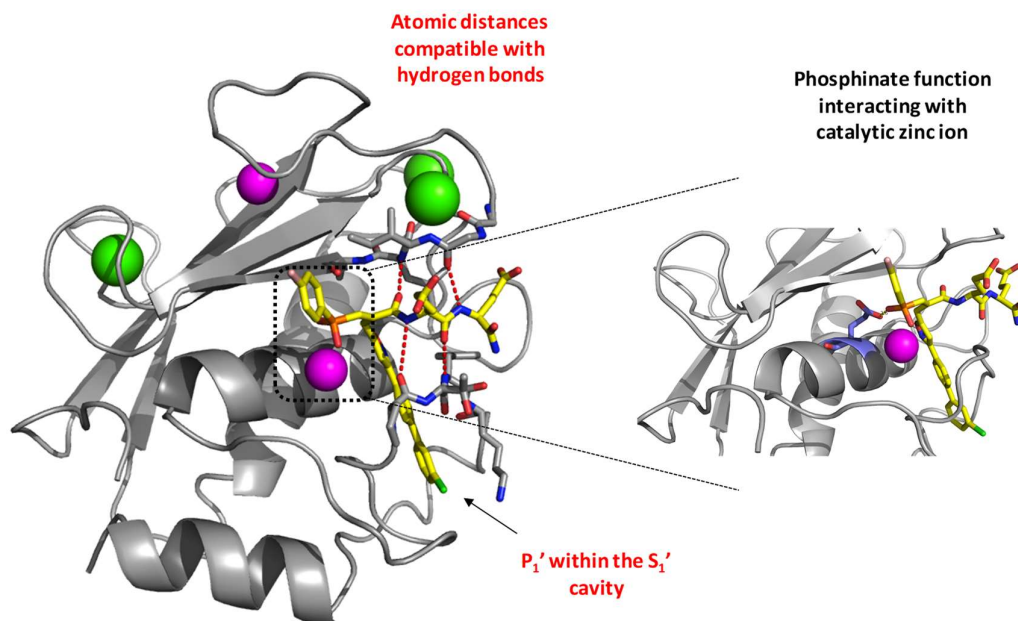


Figure 15. Crystal structure of RXP470.1 in interaction with hMMP12 catalytic domain (PDB: 4GQL, 1.15 Å). hMMP-12 is represented in grey (cartoon representation), RXP470.1 in yellow stick, calcium and zinc ions are in green and magenta spheres respectively. Distances compatible with potential hydrogen bonds are highlighted with red dot lines. Catalytic glutamate is blue stick.

This study has also revealed a pH dependence upon RXP470.1 binding, with a marked shift in association constant value (K_a) when pH raised from 6 to 7 (Figure 16A). This pH dependence was associated with a proton uptake from the buffer upon inhibitor binding (Figure 16B). This proton linkage was postulated to be necessary for neutralizing the two negative charges of ionized phosphinate ($pK_a = 1.5$) and catalytic glutamate 219 ($pK_a = 4$).

The analysis of crystallographic structure showed a very short distance separating one oxygen from the phosphinate (PO ext) and one from Glu219 (Figure 16C), a distance compatible with hydrogen bonding. Furthermore, calorimetric titration measurements were carried out on MMP-12 E219Q mutant and confirmed the involvement of Glu219 in the protonation phenomenon induced by RXP470.1 binding.

The importance of zinc-chelating moiety in selectivity profile was very recently discussed through the development of RXP470.1 analogues within which the phosphinate function was replaced by a hydroxamate or a carboxylate zinc-binding moiety⁹². This study first showed that parent RXP470.1 remained the most selective compound towards MMP12 while its hydroxamate version was more potent but not selective. Furthermore, modifying the nature of the zinc-binding group seems to impact inhibitor positioning and dynamics within the active site, with potential impacts on its selectivity profile.

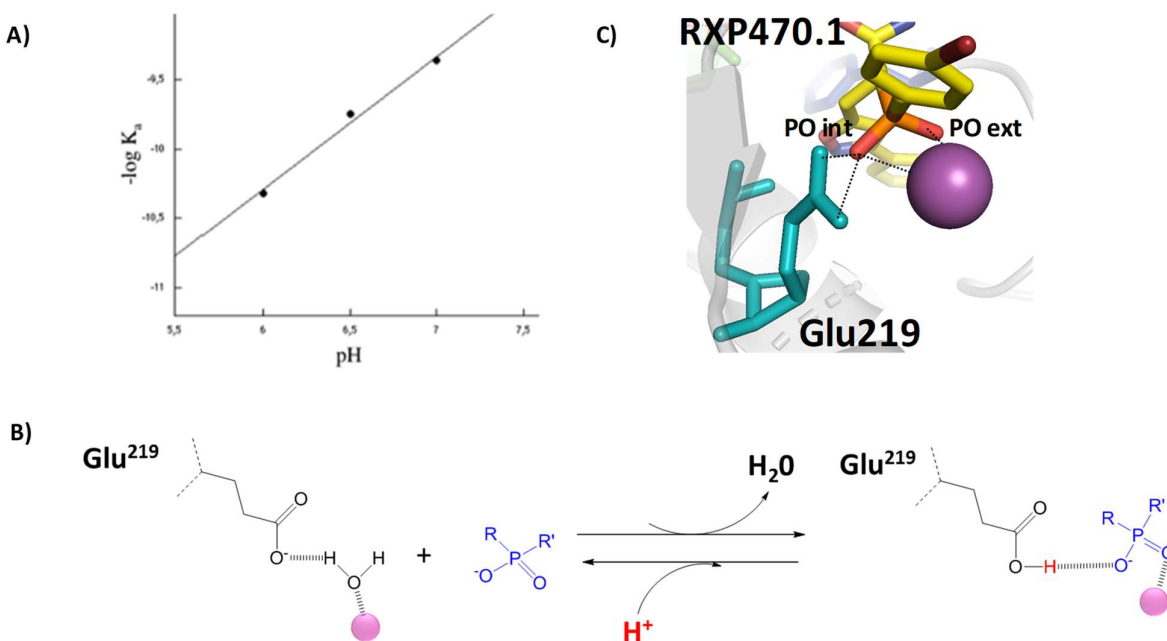


Figure 16. A) Change in RXP470.1 affinity toward MMP12 as function to pH, Association constant (K_a) is in logarithm scale and binding measurements were performed in single buffer (20 mM ACES). **B)** Schematic representation of proton uptake upon phosphinic inhibitor binding, **C)** Zoom on the catalytic zinc ion region catalytic, zinc is in magenta; RXP470.1 in yellow stick and glutamate 219 in cyan⁹¹.

Overall, these two recent studies suggest that at least two main parameters govern the excellent selectivity of RXP470.1 toward MMP12: the nature of its zinc binding group and its long P₁' side chain interacting within S₁' cavity. Importantly, these studies also stressed that it was possible to modulate RXP470.1 potency as function to pH without affecting its selectivity profile.

4.1.2. RXP 470.1 as a chemical tool to study MMP-12 in vivo

Considering its excellent selectivity profile, RXP470.1 appeared as an ideal tool to study MMP-12 in preclinical models in which this protease was susceptible to play a critical role. In addition, it was previously demonstrated in the lab that phosphinic pseudo peptides were particularly stable *in vivo* with no apparent toxicity⁹³⁻⁹⁵.

4.1.2.1. RXP470.1 target MMP-12 within atherosclerotic plaques.

As mentioned above, certain MMPs are overexpressed within atherosclerotic plaques and can contribute to their destabilization through ECM degradation. However, the link between MMP activity and plaque rupture is not so easy to establish. Thus, it has been shown in hypercholesterolemic mice that MMP-3 and

MMP-9 had a plaque stabilizing effect while MMP-12 a detrimental one ⁶¹. In this context, RXP470.1 was assessed in a mice models of atherosclerosis and its effect on plaques progression and morphology was investigated ⁹⁶.

To evaluate the effect of RXP470.1 an intervention protocol was chosen. In this respect, mice were fed a high-fat rodent diet for 8 weeks to develop mature atherosclerotic plaques. At this stage, RXP470.1 was administrated by using osmotic pumps over a period of four weeks. This mode of administration allowed circumventing rapid blood clearance of RXP470.1 while maintaining a constant plasmatic concentration of 200 nM.

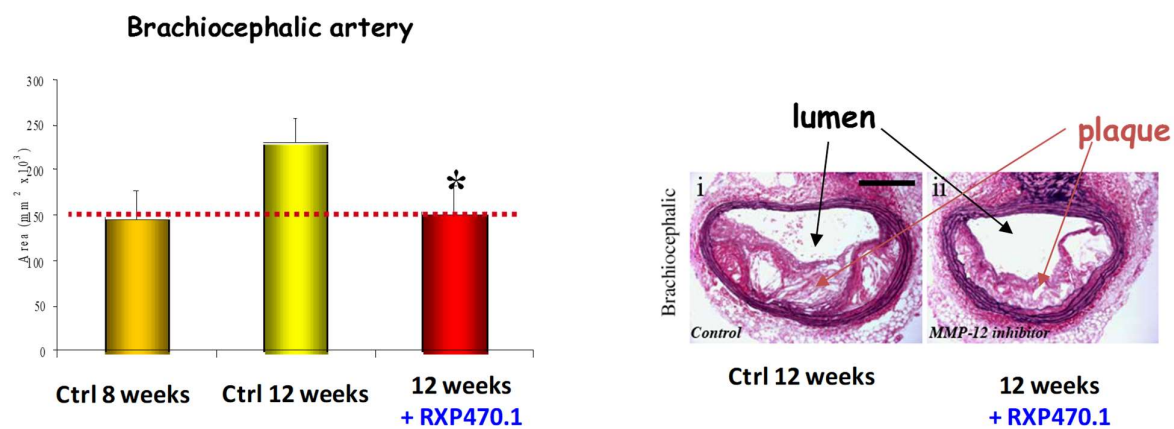


Figure 17. Effect of RXP470.1 treatment on atheroma plaque size ⁹⁶.

Within their brachiocephalic arteries, animals treated with RXP470.1 showed similar plaque sizes to those in control group after 8 weeks (Figure 17). Conversely, untreated animal (Ctrl 12 week) presented plaques of larger size. Thus, RXP470.1 was able to block plaques progression. In addition, RXP470.1 was also capable to modify plaques composition by decreasing their content in marker of instability (necrotic core, foam cells), thus inducing a stable phenotype. Within atherosclerotic plaque, RXP470.1 also significantly reduced elastolytic activity. Importantly, effects of this inhibitor on plaque development and composition were comparable to those observed in MMP-12 KO mice.

Taken together, these data strongly suggested that RXP470.1 was able to target MMP12 *in vivo* and confirmed the detrimental role of MMP12 in plaque development and rupture.

4.1.2.2. RXP470.1 can target extracellular MMP12 during viral infection.

Recently, RXP470.1 was also shown to be able to block MMP-12 activity in model of viral infection ⁷⁷. In such a pathological context, active forms of MMP-12 (catalytic domain) can penetrate virus-infected cells

and further translocate to the nucleus where it activates interferon- α transcription. Remarkably, a part of MMP-12 remains outside at the cell surface to process circulating interferon- α , thus modulating antiviral response. In the perspective of antiviral therapy, RXP470.1 was evaluated for boosting systemic IFN- α level. Infected mice by coxsackievirus type B3 were exposed on continuous infusion of RXP470.1 using minipumps over 7 days.

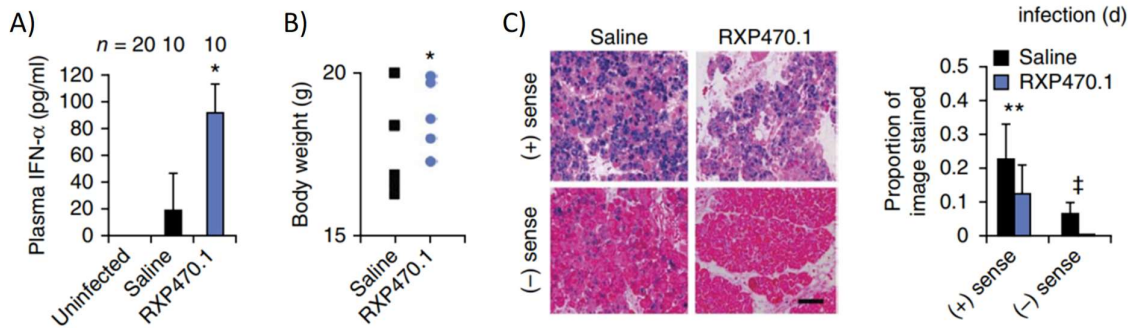


Figure 18. A) J mice infected with coxsackievirus type B3 were treated with MMP-12 inhibitor RXP470.1 or saline by continuous minipump infusion for 7 d. ELISA detected plasma IFN- α levels after 96 h of virus infection. Uninfected control animals B) Effect of extracellular MMP-12 inhibition on body weight during coxsackievirus type B3 infection. C) Coxsackievirus replication, as detected by in situ hybridization of the viral RNA genome (+ sense stained blue) and replication intermediates (- sense) in pancreas from infected mice ⁷⁷.

This treatment resulted in highly elevated plasma IFN- α levels (Figure 18A), and reduced morbidity. Moreover, viral replication was also abolished on day 7, resulting in approximately 50% reduction in viral load (Figure 18C).

These data further validated the RXP470.1 capacity to target MMP12 *in vivo*. More importantly maybe, they also suggested a marked preference of this inhibitor for the extracellular portion of MMP-12, a property that can be explained by RXP470.1 global negative charge preventing its cellular internalisation.

The MMP12 targeting capacity of RXP470.1 was also demonstrated I) in a mouse model of rheumatoid arthritis ⁹⁷, II) in a model of cardiac dysfunction in which the critical role of MMP12 in inflammation resolution was demonstrated ⁹⁸, III) during lung tumor propagation ⁹⁹ and IV) in an acute model of inflammation ⁷⁹.

In all these preclinical studies, RXP470.1 can be considered as a valuable chemical probe able to indirectly document the presence of MMP12 active form *in vivo*. By combining its use with models in which its privileged target has been invalidated (KO), it allows better deciphering the role of MMP12 in different pathological contexts.

More generally, selective MMPs inhibitors are particularly useful for validating or not MMPs as relevant target for therapeutic intervention. However, they cannot inform precisely about spatial and temporal activation of these proteases. Considering the MMPs ambivalent function during disease progress, this aspect may turn out critical to define the most appropriate therapeutic window for treating diseases. In this respect, imaging strategies as well as proteomic and chemical biology approaches allow to take a step in this direction.

5. Chemical probes for detecting MMPs activation in complex proteomes

Existing methods to detect MMPs within complex tissues include genomic techniques to measure mRNA, immunoassays, gelatin zymography and in situ zymography. Although largely explored, these methods present evident limits since they cannot differentiate between TIMP-complexed MMPs (inactive) and active MMPs. To solve these limitations, several chemical probes has been developed. Based on their chemical structures they can be divided into two main categories: the ligand-derived and substrate-derived probes.

5.1. Imaging of MMPs activity with substrate- and ligand-derived probes

Substrate-derived probes are composed of characteristic sequence recognized by targeted protease. Most of them are quenched near-infrared fluorescent probes possessing a fluorophore whose fluorescent signal is abolished by a second fluorophore in close proximity (auto quenching) or by a quencher (Figure 19). The intact probe is optically silent and becomes highly fluorescent upon protease-mediated activation.

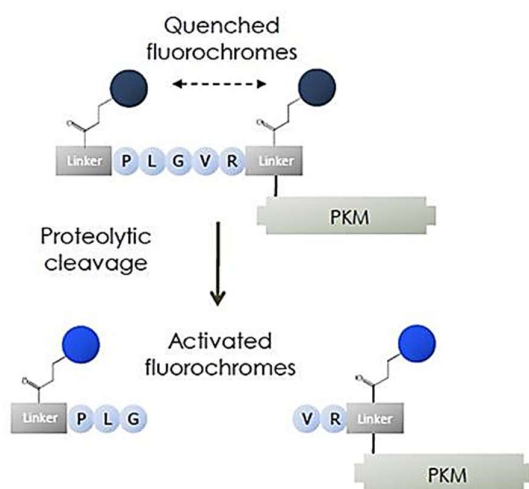


Figure 19. Schematic representation of MMPsense agents. Two quenched fluorophores are separated by a cleavable linker in the native state. MMPs recognize the cleavable linker and once the agent is cleaved, the fluorophores

produce signal. The agents also contain a pharmacokinetic modifier (PKM) selected to provide optimal attributes for in vivo imaging.

By nature, these probes can detect protease in very low amount due to signal amplification by enzyme turnover. Among the most representative substrate-derived probes developed in the literature, activatable optical probes MMPsense™ 680 allowed a real-time monitoring of MMPs activity in tumour¹⁰⁰ and within atherosclerotic plaques¹⁰¹.

Despite their high sensitivity and low background noise *in vivo*, these probes suffered from some disadvantages including long-time imaging and signal attenuation due to diffusion within the tissues. This last point has been partly overcome through the development of probes connected to cell-penetrating peptides that induce their cell internalisation, thus limiting their tissue diffusion¹⁰².

More questionable is their ability to selectively target MMPs *in vivo*¹⁰³. Indeed, such substrate-derived probes can be processed by other proteases present locally at much higher concentration than that of MMP, yielding a signal that cannot be attributed unambiguously to targeted protease. In principle, the combined use of activatable probes with MMPs inhibitors may address this limitation. Nevertheless, considering the small repertoire of highly selective inhibitors, this strategy is not fully suitable for the unambiguous detection of MMPs. Finally, in pathological contexts where circulating MMP activity has been evidenced^{104–106}, substrate-derived probes may turn out unstable within the blood stream leading to poor target/non-target contrast when imaging diseased tissues.

These stability issues can be overcome, at least in part, by probes possessing an inhibitor-derived scaffold. Such ligand-derived probes are composed of a MMP-targeting moiety conjugated to a reporter group for imaging modalities (Figure 20A). Among the most successful candidates, RP805 as a SPECT tracer is able to selectively accumulate within tissues overexpressing MMPs under their active form¹⁰⁷.

Similarly, our group has recently developed a selective RXP470.1-derived tracer able to target MMP12 (Figure 20B) in a mouse model of aneurysm (manuscript in preparation).

Overall, although capable of visualizing *in vivo* MMPs activity, these probes do not provide any direct evidences as to the presence of MMPs under their active form. This can be only achieved through functional proteomic strategies, with activity-based protein profiling as the most effective one.

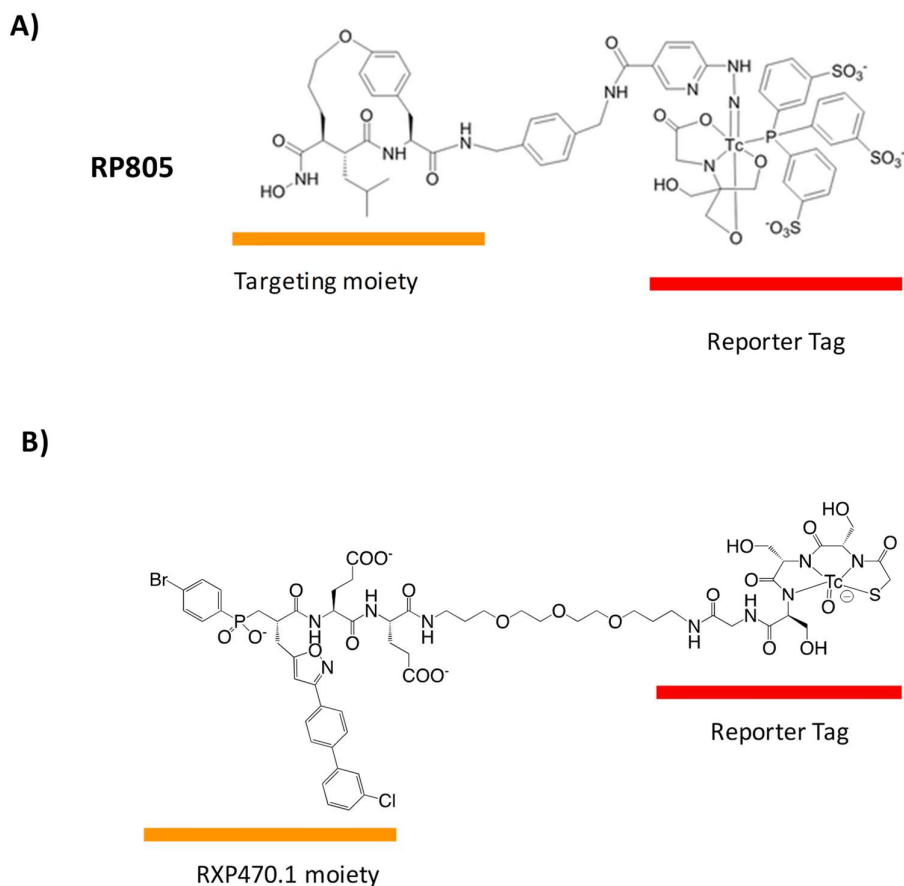


Figure 20. Structure of SPECT contrast agents targeting MMPs. A) Structure of RP805 composed of a broad-spectrum targeting moiety and a reporter tag B) RXP470.1-derived probes conjugated to a reporter Tag.

5.2. Activity-based profiling of MMPs

5.2.1. The concept of activity-based protein profiling

Activity-based protein profiling (ABPP) aim to analyse the functional state of proteins within complex biological samples. In the late 1990s, the Cravatt's group was the first to report a proteomic method using chemical probes able react in a mechanism-based manner with enzyme under their functional state within complex proteomes ¹⁰⁹. A typical Activity-Based probe (ABP) is composed of I) a reactive warhead, which reacts in a covalent manner with residues (electrophilic or nucleophilic residues) within enzyme active site, II) a targeting moiety that imposes selectivity upon the reactive group for a specific subset of enzymes and III) a detectable group for subsequent analyses (Figure 21).

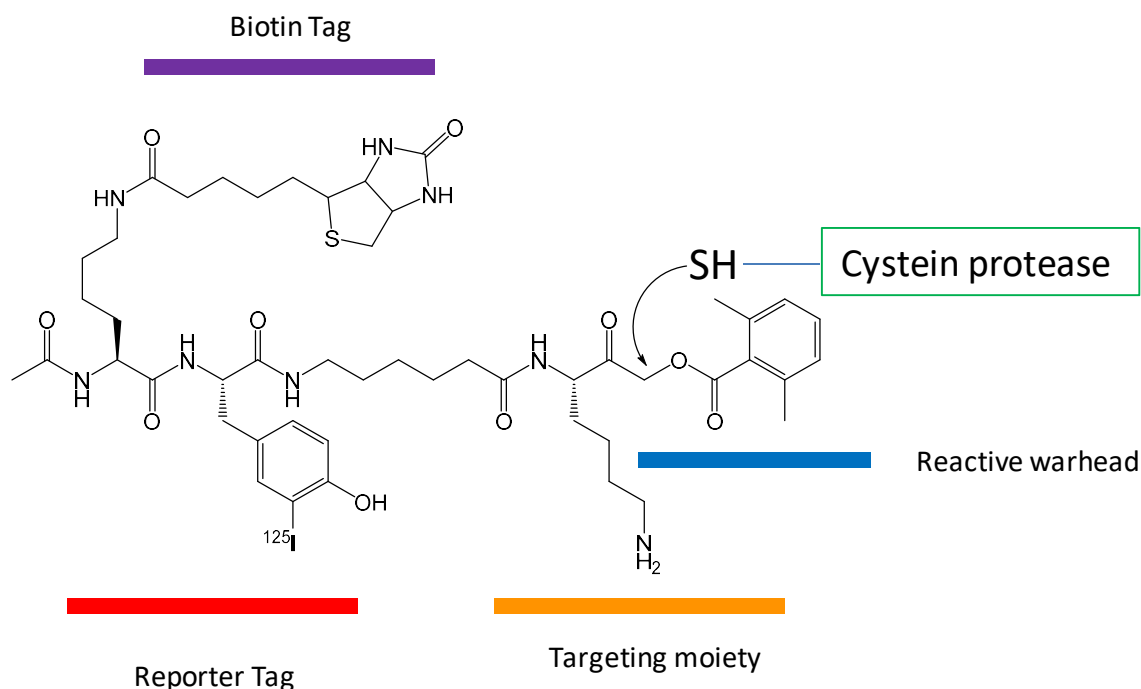


Figure 21. Structure of a representative ABPs targeting cysteine proteases ¹¹⁰.

In addition, a linker between the reactive group and reporter tag is incorporated to avoid steric hindrance upon binding. The resulting covalent complex between ABP and targeted enzyme can be further distinguished from the unmodified inactive and inhibitor-bound fractions, but also from other proteins, through various analytical techniques. The analytical moiety conjugated to the enzyme enables target visualization, identification and quantitation. In this respect, it can be of different chemical nature: I) a fluorophore (rhodamine, fluorescein or cyanine) or a radioactive moiety for in-gel fluorescence visualization of labelled enzyme or II) an affinity tags such as biotin for affinity capture followed by mass spectrometry analysis. ABPs can also incorporate the two tags simultaneously (Figure 21). Very recent generations of ABPs only possess a small reactive group (azido or alkyne motif) that can subsequently modify by an analytical tag through a biorthogonal reaction (Dipolar cycloaddition also called Click reaction). The aim here is to limit steric hindrance that may prevent probe binding while reducing non-specific components.

Since the pioneered works of Cravatt, activity-based protein profiling has been also used to I) investigate inhibitor efficiency in vivo, and II) to identify and localize the privileged target of various class of compounds ^{111,112}.

In the protease field, ABPP has been largely explored to target cysteine, threonine and serine proteases. As mentioned above, all these proteases possess a catalytic triad (acid-base-nucleophile triad) within their active site. Particularly, cysteine and serine proteases, contain a reactive nucleophile: cysteine and serine

respectively which are specifically targeted by ABPs (see Figure 21 for a representative structure of APBs target cysteine proteases). ABPP turned out successful to report on protease activities in very different biological systems including cells, preclinical animal models and human samples ^{113–115}.

Conversely to serine or cysteine proteases, no conserved nucleophiles are present within the MMPs active site and a water molecule, activated by a zinc ion, attacks the substrate scissile bond. As a consequence, MMP are beyond the scope of standard ABPP and alternative strategies have been implemented to overcome this limitation.

5.2.2. Affinity-based probes (AfBP) directed to MMPs

In the case of MMPs, photo affinity-labelling approach appeared as the most appropriate alternative. This strategy, first reported in the early 1960s for the labelling of antibody and enzyme ¹¹⁶, relies on the use of targeting ligand to which a reactive group (photoactivatable group) was attached (Figure 22A).

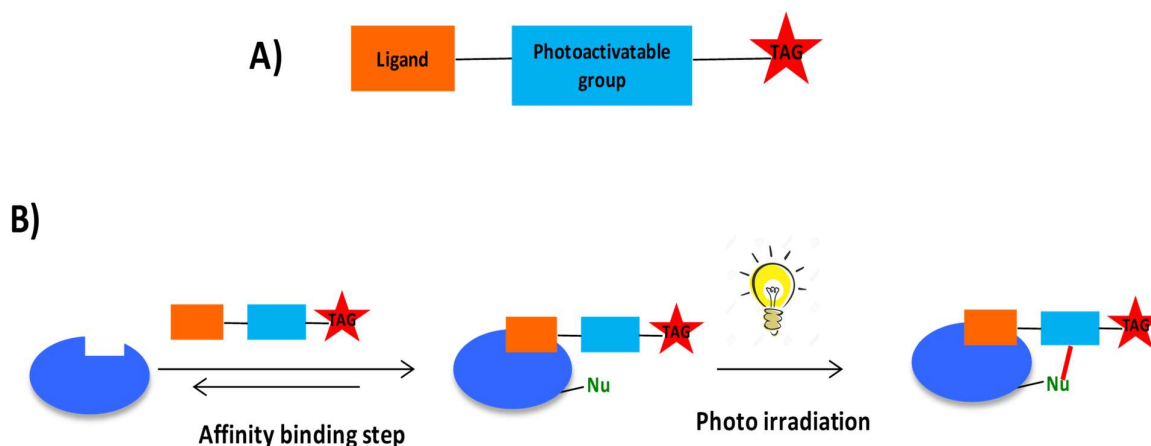


Figure 22. A) Schematic representation of a photoaffinity probe B) Two- step process of labelling by a photo affinity probe.

The labelling with a photoactivatable probe is a two-steps process. First, the photoactivatable inhibitor forms an affinity complex with its target. Once this complex is generated, UV irradiation induces the formation of a highly reactive specie that reacts in a covalent manner with protein residues in close proximity.

Particularly, photo labelling reactions have been carried out using several photoactivatable groups: benzophenone, azido and diazirine motif (Figure 23). Upon UV irradiation (300-350 nm), these photoactivatable groups generate highly reactive species (radical, nitrene, and carbene respectively) of very short lifetime that are capable to form covalent bonds with atoms in their close environment.

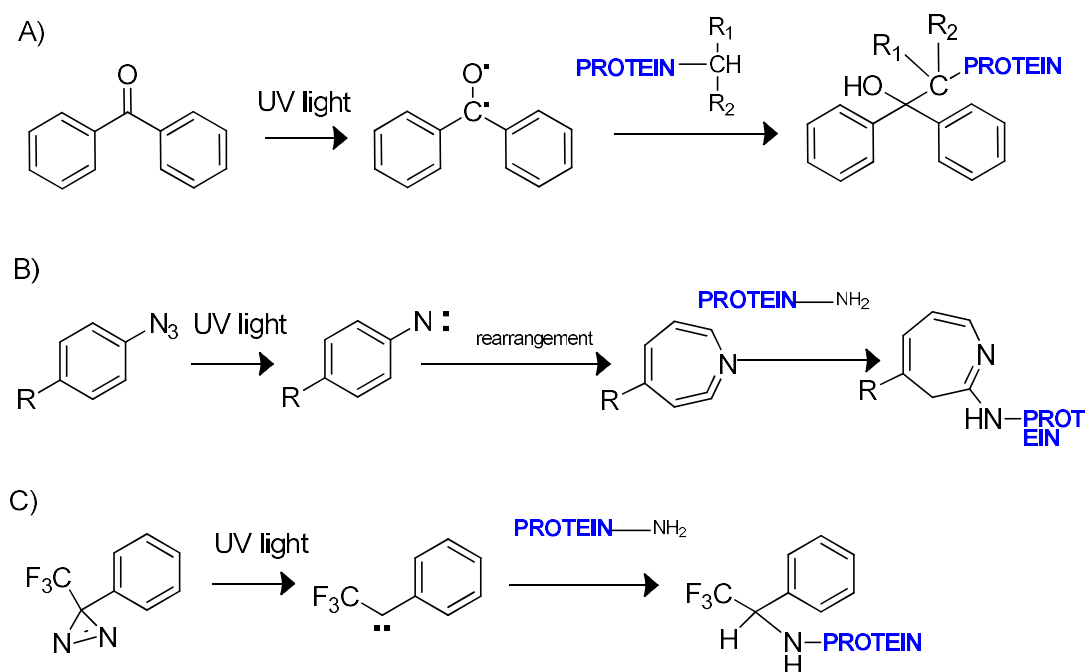


Figure 23. Photoreactive crosslinking reactions employing A) a benzophenone B) an aryl azide, and C) trifluoromethylphenyldiazirine group ¹¹⁷.

Photoactivatable probes must comply with several criteria: I) they must be stable in biological media, II) their temporal activation upon photoirradiation should occur at specific wavelengths that do not damage the target protein ($\lambda > 300$ nm), III) the resulting covalent adduct must be stable during subsequent analysis and IV) the size and position of the photoactivated group must not disturb the inhibitor interaction with its target.

Following this principle, Cravatt's team was the first to report an AfBPs directed toward MMPs ⁸⁴. This photoactivatable probe (hydroxamate HxBP-Rh probe) contains a targeting moiety derived from ilomastat scaffold with a hydroxamate group as a broad spectrum MMP inhibitor, a photoactivatable benzophenone and a fluorescent rhodamine (Figure 24).

HxBP-Rh probe was able to label spiked recombinant MMPs into complex proteomes but not their zymogen or inhibited fractions. Moreover, competitive experiments in presence of TIMP-1 or a broad spectrum MMP-inhibitor GM6001 (see annex I for the structure), showed a labelling specificity for MMP active site (Figure 24B). In addition, the probe does not label the hMMP-2 pro form. A few years later, the same group produced optimized analogues of this probe carrying an alkyne group. In this case the probe/MMPs complex was detectable after coupling with a Rhodamine-azide derivatives through a click reaction ^{118,119}. Following these founding studies, other groups have developed pan-AfBPs with hydroxamate scaffolds incorporating trifluoromethylphenyldiazirine-type photoactivatable group ¹²⁰⁻¹²³. Importantly, none of these probes were able to target endogenous MMPs.

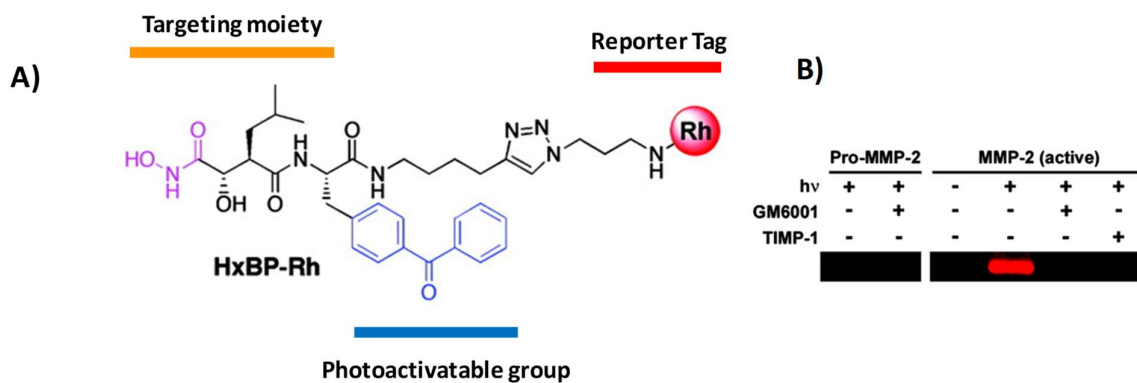


Figure 24. A) HxBO-Rh MMP-directed active probe composed of targeting moiety, a benzophenone photoactivatable group and a Rhodamine (Rh) as reporter tag B) In-gel fluorescence imaging of MMP2 labelled by HxBP-Rh⁸⁴

In the mid-2000s, our group described the first photoaffinity probe whose structure was derived from a phosphinic peptide scaffold (Figure 25)¹²⁴. In a unique way, this AfBP incorporated an azido phenyl photoactivatable moiety in its P₁' side chain and a radioactive tag to reach high sensitivity of detection.

In this respect, the presence of a radioisotope (tritium) allows achieving very low level of detection, down to 2,5 fmol for MMP12, with an exclusive covalent modification of Lys²⁴¹ within the S₁' cavity¹²⁵. Competitions experiments confirmed that the labelling was driven by a ligand-protein recognition. Despite a great affinity for MMPs, this probe did not modify MMPs homogeneously. Thus, the labelling yields towards MMP12 and MMP3 were around 40%, while a rather low yield was observed in the case of other MMPs (only 1% for MMP-8). This difference in labelling has been explained by the limited number of nucleophiles present within MMPs S₁' cavity, with only MMP12 and MMP3 possessing a reactive Lysine and Histidine respectively.

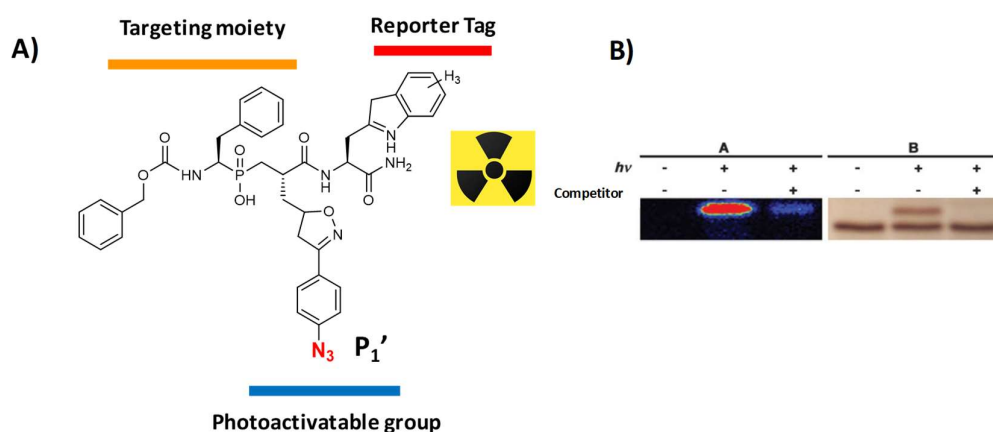


Figure 25. A) Chemical structure of photoactivatable probe derived from phosphinic peptide B) In-gel visualisation of MMP12 labelling by β -imager¹²⁴.

To overcome these limitations, a new generation of photoactivatable AfBP containing a trifluoromethylphenyldiazirine group was designed (Figure 26A). In this case, light excitation of the diazirine moiety generates a reactive intermediate potentially able to crosslink a wide range of protein residues in close proximity.

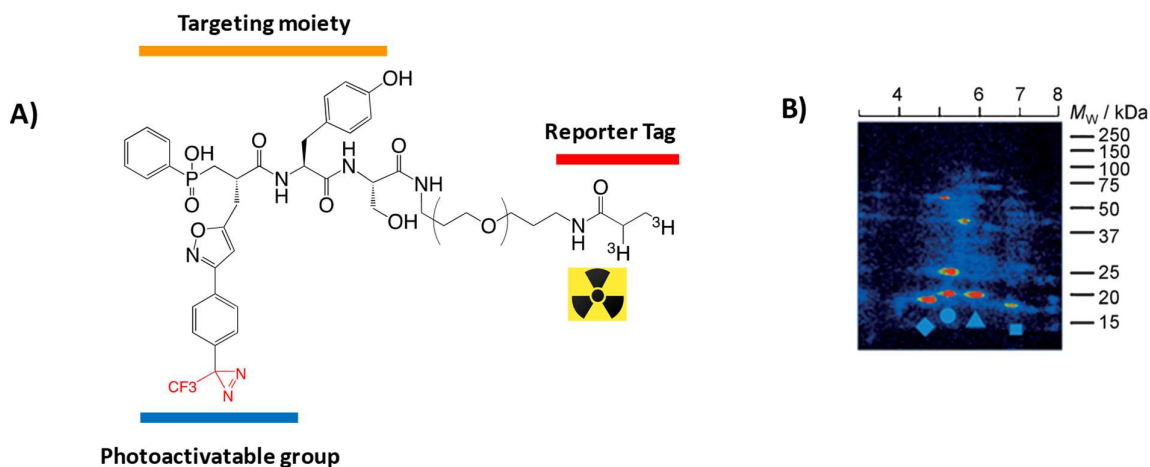


Figure 26. A) Chemical structure of phosphinic peptide-derived probe with a diazirine function B) In-gel visualization of recombinant MMP2, MMP-9, MMP-12 and MMP-13 catalytic domain labelled in complex proteome ¹²⁶.

This pan-AfBP demonstrated its capacity to covalently label several MMP2, 9, 12 and 13 in mixture spiked into complex proteomes (Figure 26 B).

Overall, most of photoactivatable AfBP have demonstrated their ability to selectively label and detect active forms of matrix metalloproteases with a very high sensitivity. However, due to irradiation conditions incompatible with *in vivo* context, the scope of these ABPs remains restricted to *ex vivo* use.

5.2.3. Targeting amino acids within metalloproteases active sites.

Among the very few approaches proposed to target amino acids within metalloproteases active sites, substrate-derived activatable probes generating a highly reactive motif upon cleavage have been effective in targeting active-site nucleophiles of different protease classes including metalloproteases ¹²⁷.

In this case, the recognition head was linked to a p-aminomandelic acid moiety *via* an amide bond which mimics the scissile bond in a protease substrate. A fluorescent group (Cyanine 3) was attached to the other end of the probe. Upon protease cleavage, a reactive moiety (quinolimine methide) is transiently generated and can further reacts with a nucleophile in close proximity within proteases active site. Although very effective to label a wide variety of proteases, the use of these probes remained *ex vivo* restricted mainly due to their lack of selectivity. Further, such a probe has never been validated on MMPs.

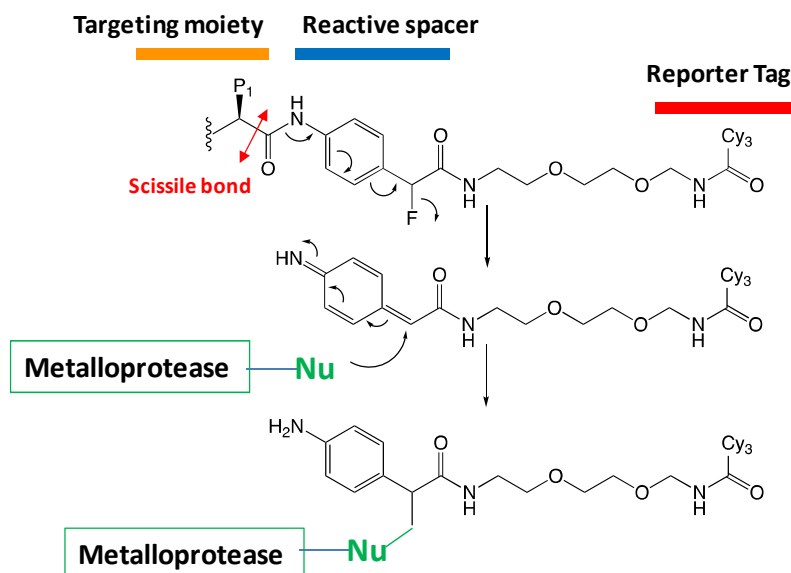


Figure 27. The activity-based labeling mechanism of protease by quinolimine methide probes.

Thiirane-based inhibitors were also proposed to target the conserved catalytic glutamate present within the active site of all metalloproteases (Figure 28) ¹²⁸.

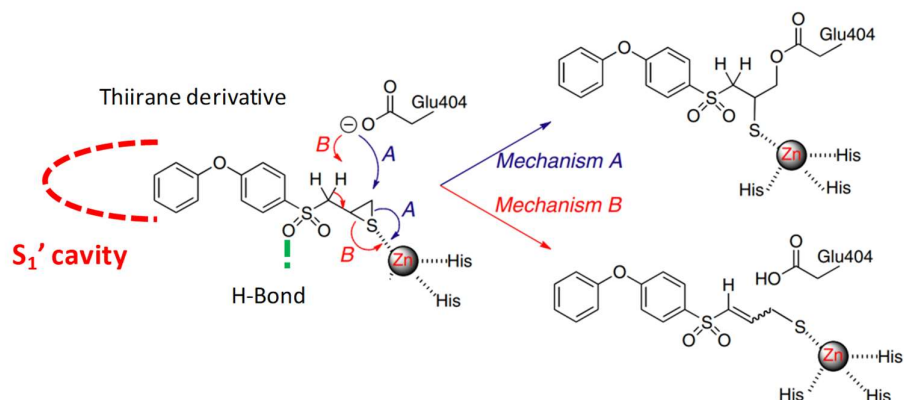


Figure 28. Two possible mechanisms of metalloprotease inhibition by a Thiirane derivative: Enzyme inhibition can occur by direct alkylation of the catalytic glutamate (Mechanism A) or through deprotonation at the methylene adjacent to the sulfone, initiating ring opening of the thiirane and formation of a stable zinc–thiolate complex (Mechanism B) ¹²⁸.

A representative thiirane inhibitor was composed of three complementary structural components: a hydrophobic phenoxyphenyl moiety inserting within MMP S_1' cavity, a sulfone that makes a hydrogen bond at the cavity entrance and a thiirane moiety that binds to the catalytic zinc ion. The interaction between zinc ion and sulphur atom destabilises the thiirane ring initiating its opening according to two possible mechanisms (Figure 28). In mechanism A, the catalytic glutamate would act as a nucleophile leading to the inhibitor covalent attachment while in mechanism B this glutamate would behave as

a general base deprotonating a proton adjacent to thiirane ring, thus inducing its opening by β -elimination reaction. In the case of MMPs, it was clearly demonstrated that only mechanism B occurred. Conversely, in the case of metallocarboxypeptidases a thiirane-based inhibitor was able to perform a chemical reaction within the active site leading to the catalytic glutamate covalent modification (Mechanism A). This covalent linkage was confirmed by crystallography with electron density and distance compatible with an ester bond between the catalytic glutamate and the thiolate derivative resulting from ring opening¹²⁹. This difference in behaviour between MMPs and metallocarboxypeptidase could be related to differences in glutamate environment that may modulate its reactivity. Overall, these data both suggest that in some specific conditions, metalloprotease catalytic glutamate can behave as a nucleophile and ABPs derived from the thiirane scaffold could be designed to target metallocarboxypeptidase in complex proteomes.

Recently, the Bogoy laboratory described an approach consisting in labelling engineered MMP14 and MMP12 on cells and *in vivo*¹³⁰. This method was based on the design of mutants where a cysteine residue has been introduced within the MMPs catalytic cleft. After demonstrating that such a mutation did not perturb catalytic activity, Bogoy's group showed that the cysteine residue as a latent nucleophile could react covalently with a suitably designed probe containing a reactive electrophile (Figure 29).

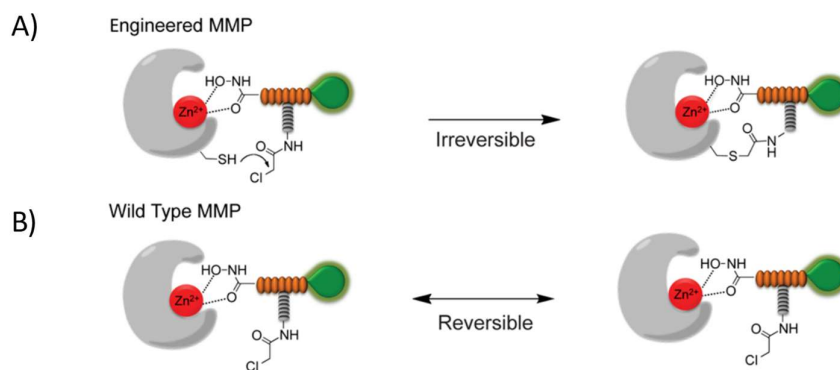


Figure 29. Binding reaction of a MMPs-directed reactive probes towards A) an engineered MMP and B) a wild type MMP. The reactive probe is composed of a peptide backbone responsible for specific MMPs targeting (in orange) a reactive warhead (α -chloroacetamide) and a fluorescent tag (green)¹³⁰.

A representative probe was composed of I) a reactive electrophile (α -chloroacetamide), II) a targeting moiety that imposed selectivity upon the reactive group and whose structure was derived from MMPs broad spectrum scaffold with a hydroxamate zinc-chelating, and III) a fluorescent tag. The reaction between the reactive probe and MMPs mutant resulted in permanent covalent labelling and inhibition. In the case of the WT-MMP, the probe binding did not yield any covalent linkage and was therefore reversible. Although this approach enables monitoring the activity of a single MMP on cells and in Zebrafish, it

possesses one evident limitation with the need for protein engineering, which definitely prevents its extension to native conditions.

As illustrated through the above examples, only a very small repertoire of approaches is suitable for the chemical modification of metalloprotease without any photo trigger. In the case of MMPs, this was only achieved by requiring a protein engineering. As a consequence, no ABPs enabling the *in vivo* covalent modification of MMPs under their functional state have been developed until now.

In this context, we considered that the recognition driven chemical modification of proteins¹³¹ constituted one of the most promising strategy that could be declined for the development of a new generation of MMPs-directed ABPs.

5.2.4. Traceless affinity labelling of native proteins

In the late 2000s, Hamachi and co-workers reported the first example of a traceless affinity-based chemical labelling strategy that allowed selective modification of endogenous target proteins in live cells without any artificial genetic manipulations¹³². In this pioneered approach, a key phenyl sulfonyl group (Tosyl) behaves as a reactive spacer between the ligand and a tag to be transferred to the target protein (Figure 30A).

Specifically, after an initial recognition step mainly governed by the ability of the ligand to selectively interact with its target, a TAG is transferred to the protein through a reaction between the reactive tosyl and a nucleophile in close proximity at the protein surface. This ligand-directed tosyl (LDT) chemistry proceeds *via* an SN₂ reaction with nucleophilic amino acids, such as His, Tyr, Glu, Cys and Asp. The ligand, which does not form any covalent linkage with the target, can be further released from the active site, making that this approach could be considered as a traceless labelling strategy. This LDT chemistry was successfully applied for the labelling of protein such as human Carbonic Anhydrase I and II, Congerin II, SH2 domain (Src homology 2) and FKBP12 (FK506-binding protein 12) in living cells and organisms. Although the LDT chemistry has been demonstrated to be applicable to a variety of endogenous proteins, it has not been that successful to label membrane proteins and suffered from a rather slow labelling rate.

In this context, a second next generation of probes exploiting the acyl imidazole chemistry has been developed (Figure 30B). The ligand-directed acyl imidazole (LDAI) chemistry displayed higher labelling rate and allowed the selective modification of Lys, Ser and Tyr residues exposed on membrane proteins on live cells and organisms¹³³⁻¹³⁵

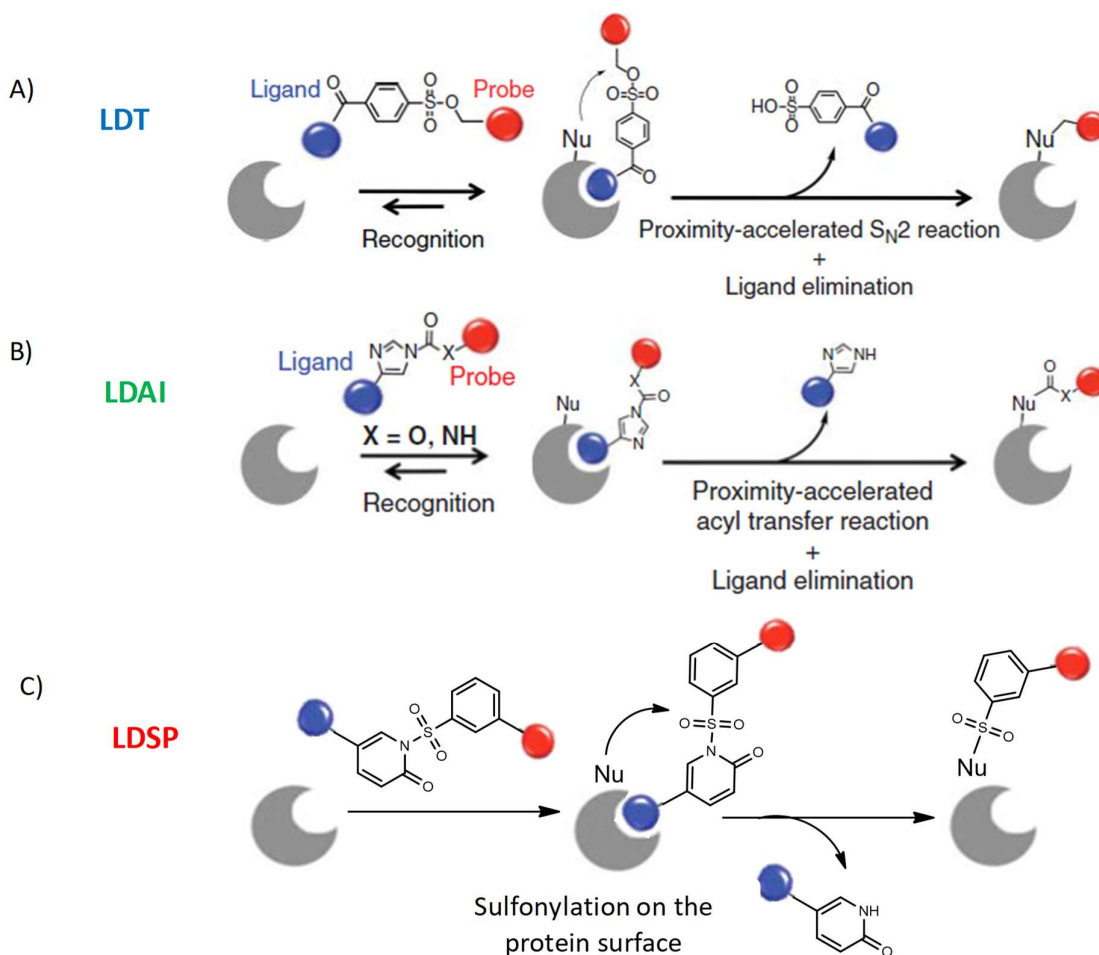


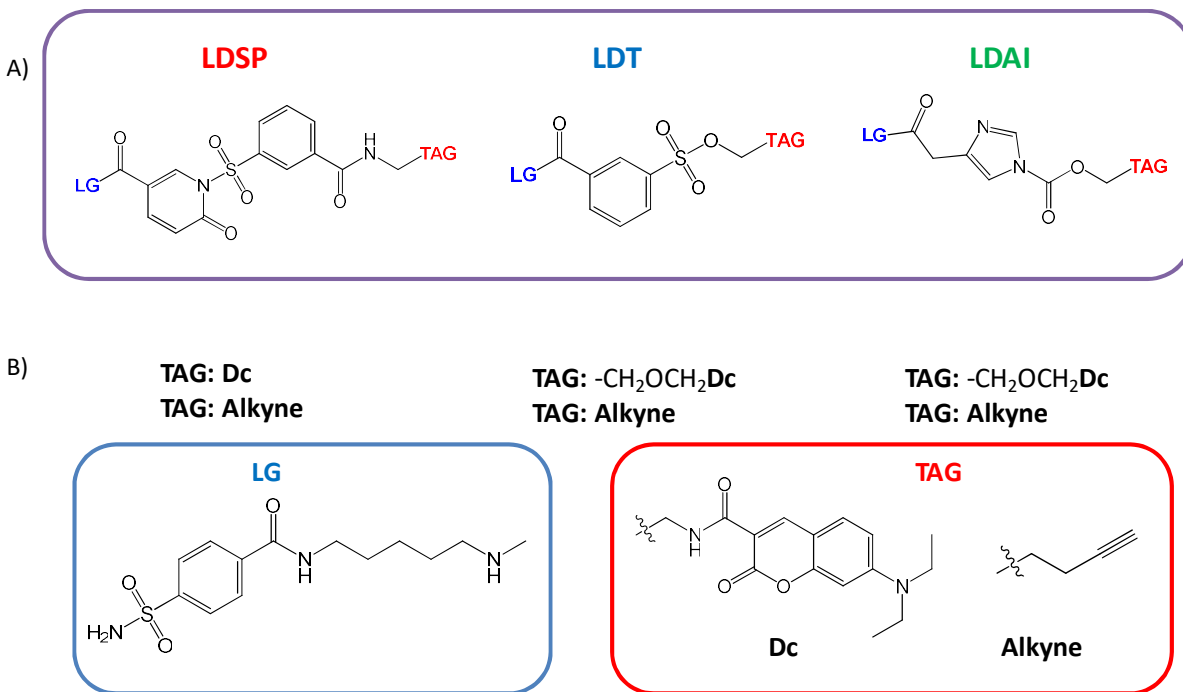
Figure 30. A) Mechanism of LDT chemistry B) mechanism of LDAI chemistry C) mechanism of LDSP chemistry.

The characteristics of LDT and LDAI chemistry demonstrated to date are I) a one-step labelling process driven by proximity effect, II) a sufficient stability of the resulting covalent linkage for subsequent analyses, III) no or minimum perturbations of the protein functions and IV) a high selectivity toward the target proteins in complex proteomes. Moreover, due to the versatility of the chemistry implemented, these techniques allowed the labelling of several proteins with various TAGs including fluorophore, biotin TAG and turn-on fluorescence biosensors .

Very recently, Hamachi and co-workers also reported a complementary strategy that exploits another type of chemistry termed Ligand-directed N-Sulfonyl pyridone Chemistry (LDSP, Figure 30C). In this case, the reactive spacer N-sulfonyl pyridone (SP) enables the labelling of both intracellular and cell surface membrane proteins with improved reaction kinetics when compared with those of the LDT and LDAI chemistries ¹³⁶.

5.2.5. Comparison between LDT/LDAI and LDSP on hCA.

hCA-II (human Carbonic anhydrase II) was used as a model protein to compare efficiency of the different ligand-directed labelling methods.



The probes varying in their reactive spacer (Figure 31A) possess a common ligand part (LG) and are able to transfer two types of Tag. The kinetics comparison of the three ligand-directed chemistry was performed through In-gel fluorescence imaging. As illustrated in Figure 31C, the initial rate (2.9 $\mu\text{M}/\text{h}$) of LDSP was about 5 fold greater than those of LDT (0.53 $\mu\text{M}/\text{h}$) and 2 fold greater LDAI (1.4 $\mu\text{M}/\text{h}$)¹³⁶. MALDI TOF MS analysis showed that CA II labelling (12h, 37°C) is related to the nature of the chemical spacer.

Proteolytic digestion and tandem mass spectroscopy analysis of labelled CA2 revealed that both a Tyr (67%) and a Lys (33%) located close to the entrance of ligand binding pocket were preferentially labelled by LDSP chemistry. On the same enzyme, it was previously shown that LDT chemistry solely modified the tyrosine residue while LDAI chemistry only the lysine one. This likely depends on the nature of the targeted proteins. Comparison between chemo selectivity and targeted proteins was summarized in a Table 1.

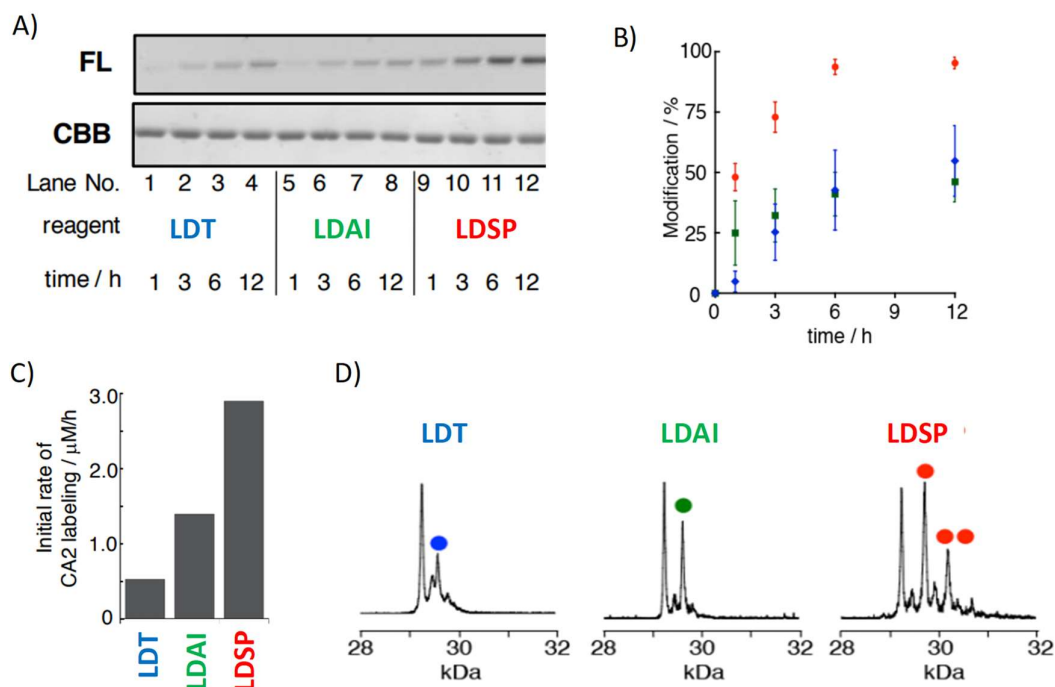


Figure 32. Analyses of the labelling reactivity of LDSP, LDAI and LDT chemistry in vitro on CA2 A) SDS PAGE and in-gel fluorescence analysis of hCA II labelling, B) Time plots of the modification yields by SDS PAGE analysis, Red circle the LDSP chemistry, blue diamond, the LDT chemistry, green square the LDAI chemistry, C) Initial velocity of in vitro CA2 labelling reactions, D) MALDI TOF MS analyses of CA2 labelling¹³⁶.

	LDT chemistry	LDAI chemistry	LDSP chemistry
Labeled amino acids	His, Tyr, Glu, Cys	Lys, Ser, Tyr	Tyr, Lys
Reaction mode	S_N2	Acylation	Sulfonylation
Applicable proteins	CA1, CA2, FKBP12, Cong II, 14-3-3- δ , Hsc70, eDHFR, HER2, SMP	CA1, CA2, CA12, eDHFR, FR, bradykinin B_2 receptor, NMDA receptor, AMPA receptor, GABA $_A$ receptor	CA1 (data not published), CA2, CA12, FR, HSP90, COX-2

Table 1. Comparison of LDT, LDAI and LDSP chemistry.

The labelling efficiency of LDSP, LDAI and LDT methods were also compared in living MCF cells (Figure 33). Surprisingly, LDAI reagent provided almost no labelling, most likely due to the low stability of acyl imidazole motif in complex proteomes. The LDT reagent gave a weak band together with a few nonspecific bands (> 50 kDa) while LDSP chemistry provided a clear and detectable labelling of intracellular CA2. This demonstrated that LDSP chemistry was the most effective for the rapid and specific labelling of this enzyme in complex proteomes¹³⁶.

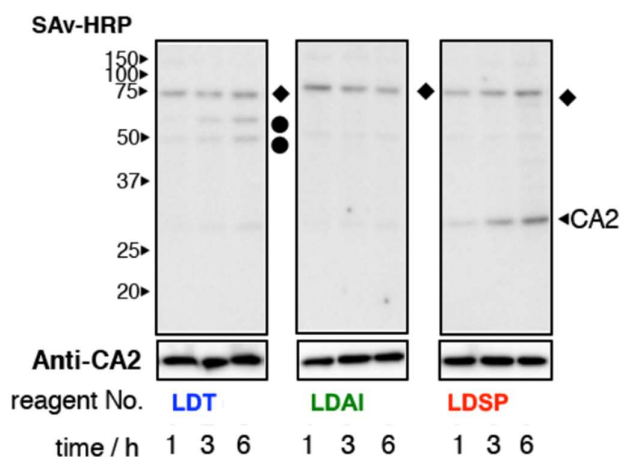


Figure 33. Intracellular CA2 labelling by LD chemistry, western blot analyses of the CA2 labelling process in living MCF7 cells. ◆ endogenously biotinylated protein, ● nonspecific bands ¹³⁶.

Aim of the project:

To our knowledge, the traceless affinity labelling of proteins has not yet been extended to the labelling of MMPs in their natural environment. In this purpose and as a proof of concept, we envisaged to assess the reactivity of nucleophiles within the MMPs catalytic cleft through a proximity-driven reaction. One of our main objectives was to develop a new generation of ABPs able to covalently modify active forms of MMPs without any photo-activation. By developing such probes the unresolved proteomic profiling of active MMPs could be further addressed *in vivo*. Please note that at the beginning of the project, the LDSP chemistry was not described yet.

BIBLIOGRAPHY I

1. Schechter, I. & Berger, A. On the size of the active site in proteases. I. Papain. *Biochem. Biophys. Res. Commun.* **27**, 157–162 (1967).
2. Gross, J. & Lapiere, C. M. COLLAGENOLYTIC ACTIVITY IN AMPHIBIAN TISSUES: A TISSUE CULTURE ASSAY*. *Proc Natl Acad Sci U S A* **48**, 1014–1022 (1962).
3. Brinckerhoff, C. E. & Matrisian, L. M. Matrix metalloproteinases: a tail of a frog that became a prince. *Nature Reviews Molecular Cell Biology* **3**, 207 (2002).
4. Woolley, D. E., Glanville, R. W., Crossley, M. J. & Evanson, J. M. Purification of Rheumatoid Synovial Collagenase and Its Action on Soluble and Insoluble Collagen. *European Journal of Biochemistry* **54**, 611–622
5. Woessner, J. F. & Nagase, H. *Matrix Metalloproteinases and TIMPs*. (Oxford University Press, 2000).
6. Bauer, E. A., Eisen, A. Z. & Jeffrey, J. J. Regulation of vertebrate collagenase activity in vivo and in vitro. *J. Invest. Dermatol.* **59**, 50–55 (1972).
7. Chen, L. C., Noelken, M. E. & Nagase, H. Disruption of the cysteine-75 and zinc ion coordination is not sufficient to activate the precursor of human matrix metalloproteinase 3 (stromelysin 1). *Biochemistry* **32**, 10289–10295 (1993).
8. Lovejoy, B. *et al.* Structure of the catalytic domain of fibroblast collagenase complexed with an inhibitor. *Science* **263**, 375–377 (1994).
9. Cauwe, B., Steen, P. E. V. den & Opdenakker, G. The Biochemical, Biological, and Pathological Kaleidoscope of Cell Surface Substrates Processed by Matrix Metalloproteinases. *Critical Reviews in Biochemistry and Molecular Biology* **42**, 113–185 (2007).
10. Visse, R. & Nagase, H. Matrix Metalloproteinases and Tissue Inhibitors of Metalloproteinases: Structure, Function, and Biochemistry. *Circulation Research* **92**, 827–839 (2003).
11. Bond, J. S. & Beynon, R. J. The astacin family of metalloendopeptidases. *Protein Sci* **4**, 1247–1261 (1995).
12. Gomis-Rüth, F. X., Trillo-Muyo, S. & Stöcker, W. Functional and structural insights into astacin metallopeptidases. *Biol. Chem.* **393**, 1027–1041 (2012).
13. Nakahama, K. *et al.* Cloning and sequencing of Serratia protease gene. *Nucleic Acids Res* **14**, 5843–5855 (1986).
14. Okuda, K. *et al.* Complete nucleotide sequence of the structural gene for alkaline proteinase from Pseudomonas aeruginosa IFO 3455. *Infect Immun* **58**, 4083–4088 (1990).
15. Delepelaire, P. & Wandersman, C. Protease secretion by Erwinia chrysanthemi. Proteases B and C are synthesized and secreted as zymogens without a signal peptide. *J. Biol. Chem.* **264**, 9083–9089 (1989).
16. Bode, W., Gomis-Rüth, F.-X. & Stöckler, W. Astacins, serralysins, snake venom and matrix metalloproteinases exhibit identical zinc-binding environments (HEXXHXXGXXH and Met-turn) and

- topologies and should be grouped into a common family, the 'metzincins'. *FEBS Letters* **331**, 134–140 (1993).
17. Gomis-Rüth, F. X. Catalytic Domain Architecture of Metzincin Metalloproteases. *J. Biol. Chem.* **284**, 15353–15357 (2009).
 18. Killar, L., White, J., Black, R. & Peschon, J. Adamalysins: A Family of Metzincins Including TNF- α Converting Enzyme (TACE). *Annals of the New York Academy of Sciences* **878**, 442–452 (1999).
 19. Gomis-Rüth, F. X. Structural aspects of the metzincin clan of metalloendopeptidases. *Mol Biotechnol* **24**, 157–202 (2003).
 20. Stöcker, W. *et al.* The metzincins--topological and sequential relations between the astacins, adamalysins, serralysins, and matrixins (collagenases) define a superfamily of zinc-peptidases. *Protein Sci* **4**, 823–840 (1995).
 21. Vandenbroucke, R. E. & Libert, C. Is there new hope for therapeutic matrix metalloproteinase inhibition? *Nature Reviews Drug Discovery* **13**, nrd4390 (2014).
 22. DeClerck, Y. A. Interactions between tumour cells and stromal cells and proteolytic modification of the extracellular matrix by metalloproteinases in cancer. *Eur. J. Cancer* **36**, 1258–1268 (2000).
 23. Khokha, R., Murthy, A. & Weiss, A. Metalloproteinases and their natural inhibitors in inflammation and immunity. *Nature Reviews Immunology* **13**, 649 (2013).
 24. Piccard, H., Van den Steen, P. E. & Opdenakker, G. Hemopexin domains as multifunctional liganding modules in matrix metalloproteinases and other proteins. *J. Leukoc. Biol.* **81**, 870–892 (2007).
 25. Page-McCaw, A., Ewald, A. J. & Werb, Z. Matrix metalloproteinases and the regulation of tissue remodelling. *Nature Reviews Molecular Cell Biology* **8**, 221 (2007).
 26. Overall, C. M., Wrana, J. L. & Sodek, J. Transcriptional and post-transcriptional regulation of 72-kDa gelatinase/type IV collagenase by transforming growth factor-beta 1 in human fibroblasts. Comparisons with collagenase and tissue inhibitor of matrix metalloproteinase gene expression. *J. Biol. Chem.* **266**, 14064–14071 (1991).
 27. Iyer, V., Pumiglia, K. & DiPersio, C. M. Alpha3beta1 integrin regulates MMP-9 mRNA stability in immortalized keratinocytes: a novel mechanism of integrin-mediated MMP gene expression. *J. Cell. Sci.* **118**, 1185–1195 (2005).
 28. Delany, A. M., Jeffrey, J. J., Rydziel, S. & Canalis, E. Cortisol increases interstitial collagenase expression in osteoblasts by post-transcriptional mechanisms. *J. Biol. Chem.* **270**, 26607–26612 (1995).
 29. Trojanek, J. Metaloproteinazy macierzy zewnątrzkomórkowej i ich tkankowe inhibitory. (2009).
 30. Ra, H.-J. & Parks, W. C. Control of Matrix Metalloproteinase Catalytic Activity. *Matrix Biol* **26**, 587–596 (2007).
 31. Baker, E. A. & Leaper, D. J. The plasminogen activator and matrix metalloproteinase systems in colorectal cancer: relationship to tumour pathology. *European Journal of Cancer* **39**, 981–988 (2003).

32. Carmeliet, P. *et al.* Urokinase-generated plasmin activates matrix metalloproteinases during aneurysm formation. *Nature Genetics* **17**, 439–444 (1997).
33. Monea, S., Lehti, K., Keski-Oja, J. & Mignatti, P. Plasmin activates pro-matrix metalloproteinase-2 with a membrane-type 1 matrix metalloproteinase-dependent mechanism. *Journal of Cellular Physiology* **192**, 160–170
34. Visse, R. & Nagase, H. Matrix Metalloproteinases and Tissue Inhibitors of Metalloproteinases: Structure, Function, and Biochemistry. *Circulation Research* **92**, 827–839 (2003).
35. Van Wart, H. E. & Birkedal-Hansen, H. The cysteine switch: a principle of regulation of metalloproteinase activity with potential applicability to the entire matrix metalloproteinase gene family. *Proc Natl Acad Sci U S A* **87**, 5578–5582 (1990).
36. Rosenblum, G. *et al.* Molecular Structures and Dynamics of the Stepwise Activation Mechanism of a Matrix Metalloproteinase Zymogen: Challenging the Cysteine Switch Dogma. *J. Am. Chem. Soc.* **129**, 13566–13574 (2007).
37. Pei, D. & Weiss, S. J. Furin-dependent intracellular activation of the human stromelysin-3 zymogen. *Nature* **375**, 244–247 (1995).
38. Nagase, H., Visse, R. & Murphy, G. Structure and function of matrix metalloproteinases and TIMPs. *Cardiovasc Res* **69**, 562–573 (2006).
39. Brew, K., Dinakarandian, D. & Nagase, H. Tissue inhibitors of metalloproteinases: evolution, structure and function. *Biochim. Biophys. Acta* **1477**, 267–283 (2000).
40. Palosaari, H. *et al.* Expression profile of matrix metalloproteinases (MMPs) and tissue inhibitors of MMPs in mature human odontoblasts and pulp tissue. *Eur. J. Oral Sci.* **111**, 117–127 (2003).
41. Giarnieri, E. *et al.* Tissue inhibitor of metalloproteinase 2 (TIMP-2) expression in adenocarcinoma pleural effusions. *Oncology Reports* **19**, 483–487 (2008).
42. Yaghooti, H., Firoozrai, M., Fallah, S. & Khorramizadeh, M. R. Angiotensin II Differentially Induces Matrix Metalloproteinase-9 and Tissue Inhibitor of Metalloproteinase-1 Production and Disturbs MMP/TIMP Balance. *Avicenna J Med Biotechnol* **2**, 79–85 (2010).
43. Rudolph-Owen, L. A., Hulboy, D. L., Wilson, C. L., Mudgett, J. & Matrisian, L. M. Coordinate expression of matrix metalloproteinase family members in the uterus of normal, matrilysin-deficient, and stromelysin-1-deficient mice. *Endocrinology* **138**, 4902–4911 (1997).
44. Egeblad, M. & Werb, Z. New functions for the matrix metalloproteinases in cancer progression. *Nature Reviews Cancer* **2**, 161 (2002).
45. Elkington, P. T., Green, J. A. & Friedland, J. S. Analysis of matrix metalloproteinase secretion by macrophages. *Methods Mol. Biol.* **531**, 253–265 (2009).
46. Sternlicht, M. D. & Werb, Z. HOW MATRIX METALLOPROTEINASES REGULATE CELL BEHAVIOR. *Annu Rev Cell Dev Biol* **17**, 463–516 (2001).
47. Lee, S., Jilani, S. M., Nikolova, G. V., Carpizo, D. & Iruela-Arispe, M. L. Processing of VEGF-A by matrix metalloproteinases regulates bioavailability and vascular patterning in tumors. *J. Cell Biol.* **169**, 681–691 (2005).

48. van Hinsbergh, V. W. M., Engelse, M. A. & Quax, P. H. A. Pericellular proteases in angiogenesis and vasculogenesis. *Arterioscler. Thromb. Vasc. Biol.* **26**, 716–728 (2006).
49. Streuli, C. Extracellular matrix remodelling and cellular differentiation. *Curr. Opin. Cell Biol.* **11**, 634–640 (1999).
50. Parks, W. C., Wilson, C. L. & López-Boado, Y. S. Matrix metalloproteinases as modulators of inflammation and innate immunity. *Nat Rev Immunol* **4**, 617–629 (2004).
51. Yong, V. W. Metalloproteinases: mediators of pathology and regeneration in the CNS. *Nat. Rev. Neurosci.* **6**, 931–944 (2005).
52. Gialeli, C., Theocharis, A. D. & Karamanos, N. K. Roles of matrix metalloproteinases in cancer progression and their pharmacological targeting. *The FEBS Journal* **278**, 16–27 (2011).
53. Kessenbrock, K., Plaks, V. & Werb, Z. Matrix metalloproteinases: regulators of the tumor microenvironment. *Cell* **141**, 52–67 (2010).
54. Lagente, V. & Boichot, E. Role of matrix metalloproteinases in the inflammatory process of respiratory diseases. *J. Mol. Cell. Cardiol.* **48**, 440–444 (2010).
55. Vandembroucke, R. E., Dejonckheere, E. & Libert, C. A therapeutic role for matrix metalloproteinase inhibitors in lung diseases? *European Respiratory Journal* **38**, 1200–1214 (2011).
56. Bäck, M., Ketelhuth, D. F. J. & Agewall, S. Matrix metalloproteinases in atherothrombosis. *Prog Cardiovasc Dis* **52**, 410–428 (2010).
57. Chow, A. K., Cena, J. & Schulz, R. Acute actions and novel targets of matrix metalloproteinases in the heart and vasculature. *Br. J. Pharmacol.* **152**, 189–205 (2007).
58. Newby, A. C. Matrix metalloproteinase inhibition therapy for vascular diseases. *Vascular Pharmacology* **56**, 232–244 (2012).
59. Huntley, G. W. Synaptic circuit remodelling by matrix metalloproteinases in health and disease. *Nature Reviews Neuroscience* **13**, 743–757 (2012).
60. Basset, P. *et al.* A novel metalloproteinase gene specifically expressed in stromal cells of breast carcinomas. *Nature* **348**, 699–704 (1990).
61. Johnson, J. L., George, S. J., Newby, A. C. & Jackson, C. L. Divergent effects of matrix metalloproteinases 3, 7, 9, and 12 on atherosclerotic plaque stability in mouse brachiocephalic arteries. *Proc. Natl. Acad. Sci. U.S.A.* **102**, 15575–15580 (2005).
62. Overall, C. M. & Kleinfeld, O. Tumour microenvironment - opinion: validating matrix metalloproteinases as drug targets and anti-targets for cancer therapy. *Nat. Rev. Cancer* **6**, 227–239 (2006).
63. Turk, B. Targeting proteases: successes, failures and future prospects. *Nat Rev Drug Discov* **5**, 785–799 (2006).
64. Werb, Z. & Gordon, S. Elastase secretion by stimulated macrophages. Characterization and regulation. *J. Exp. Med.* **142**, 361–377 (1975).

65. Banda, M. J. & Werb, Z. Mouse macrophage elastase. Purification and characterization as a metalloproteinase. *Biochem J* **193**, 589–605 (1981).
66. Shapiro, S. D. *et al.* Molecular cloning, chromosomal localization, and bacterial expression of a murine macrophage metalloelastase. *J. Biol. Chem.* **267**, 4664–4671 (1992).
67. Hu, J., Van den Steen, P. E., Sang, Q.-X. A. & Opdenakker, G. Matrix metalloproteinase inhibitors as therapy for inflammatory and vascular diseases. *Nat Rev Drug Discov* **6**, 480–498 (2007).
68. Lagente, V., Quement, C. L. & Boichot, E. Macrophage metalloelastase (MMP-12) as a target for inflammatory respiratory diseases. *Expert Opinion on Therapeutic Targets* **13**, 287–295 (2009).
69. Li, W. *et al.* A selective matrix metalloprotease 12 inhibitor for potential treatment of chronic obstructive pulmonary disease (COPD): discovery of (S)-2-(8-(methoxycarbonylamino)dibenzo[b,d]furan-3-sulfonamido)-3-methylbutanoic acid (MMP408). *J. Med. Chem.* **52**, 1799–1802 (2009).
70. Nuti, E. *et al.* Design, Synthesis, Biological Evaluation, and NMR Studies of a New Series of Arylsulfones As Selective and Potent Matrix Metalloproteinase-12 Inhibitors. *J. Med. Chem.* **52**, 6347–6361 (2009).
71. Gorrin Rivas, M. J. *et al.* Expression of human macrophage metalloelastase gene in hepatocellular carcinoma: correlation with angiostatin generation and its clinical significance. *Hepatology* **28**, 986–993 (1998).
72. Yang, W. *et al.* Human macrophage metalloelastase gene expression in colorectal carcinoma and its clinicopathologic significance. *Cancer* **91**, 1277–1283 (2001).
73. Liang, J. *et al.* Macrophage Metalloelastase Accelerates the Progression of Atherosclerosis in Transgenic Rabbits. *Circulation* **113**, 1993–2001 (2006).
74. Halpert, I. *et al.* Matrilysin is expressed by lipid-laden macrophages at sites of potential rupture in atherosclerotic lesions and localizes to areas of versican deposition, a proteoglycan substrate for the enzyme. *Proc. Natl. Acad. Sci. U.S.A.* **93**, 9748–9753 (1996).
75. Scholtes, V. P. W. *et al.* Carotid atherosclerotic plaque matrix metalloproteinase-12-positive macrophage subpopulation predicts adverse outcome after endarterectomy. *J Am Heart Assoc* **1**, e001040 (2012).
76. Houghton, A. M., Hartzell, W. O., Robbins, C. S., Gomis-Rüth, F. X. & Shapiro, S. D. Macrophage elastase kills bacteria within murine macrophages. *Nature* **460**, 637–641 (2009).
77. Marchant, D. J. *et al.* A new transcriptional role for matrix metalloproteinase-12 in antiviral immunity. *Nat. Med.* **20**, 493–502 (2014).
78. Dandachi, N. G. & Shapiro, S. D. A protean protease: MMP-12 fights viruses as a protease and a transcription factor. *Nat Med* **20**, 470–472 (2014).
79. Dufour, A. *et al.* C-terminal truncation of IFN- γ inhibits proinflammatory macrophage responses and is deficient in autoimmune disease. *Nature Communications* **9**, 2416 (2018).
80. Cuniasse, P. *et al.* Future challenges facing the development of specific active-site-directed synthetic inhibitors of MMPs. *Biochimie* **87**, 393–402 (2005).

81. Pirard, B. Insight into the structural determinants for selective inhibition of matrix metalloproteinases. *Drug Discov Today* **12**, 640–646 (2007).
82. Devel, L. *et al.* Insights from Selective Non-phosphinic Inhibitors of MMP-12 Tailored to Fit with an S1' Loop Canonical Conformation. *J Biol Chem* **285**, 35900–35909 (2010).
83. Sang, Q.-X. A. *et al.* Matrix metalloproteinase inhibitors as prospective agents for the prevention and treatment of cardiovascular and neoplastic diseases. *Curr Top Med Chem* **6**, 289–316 (2006).
84. Saghatelian, A., Jessani, N., Joseph, A., Humphrey, M. & Cravatt, B. F. Activity-based probes for the proteomic profiling of metalloproteases. *Proc Natl Acad Sci U S A* **101**, 10000–10005 (2004).
85. Devel, L. *et al.* Simple Pseudo-dipeptides with a P2' Glutamate. *J Biol Chem* **287**, 26647–26656 (2012).
86. Hu, Y. *et al.* Potent, selective, and orally bioavailable matrix metalloproteinase-13 inhibitors for the treatment of osteoarthritis. *Bioorg. Med. Chem.* **13**, 6629–6644 (2005).
87. Engel, C. K. *et al.* Structural basis for the highly selective inhibition of MMP-13. *Chem. Biol.* **12**, 181–189 (2005).
88. Pochetti, G. *et al.* Extra binding region induced by non-zinc chelating inhibitors into the S1' subsite of matrix metalloproteinase 8 (MMP-8). *J. Med. Chem.* **52**, 1040–1049 (2009).
89. Dive, V. *et al.* Phosphinic peptides as zinc metalloproteinase inhibitors. *CMLS, Cell. Mol. Life Sci.* **61**, 2010–2019 (2004).
90. Devel, L. *et al.* Development of Selective Inhibitors and Substrate of Matrix Metalloproteinase-12. *J. Biol. Chem.* **281**, 11152–11160 (2006).
91. Czarny, B. *et al.* Molecular Determinants of a Selective Matrix Metalloprotease-12 Inhibitor: Insights from Crystallography and Thermodynamic Studies. *J. Med. Chem.* **56**, 1149–1159 (2013).
92. Rouanet-Mehouas, C. *et al.* Zinc-Metalloproteinase Inhibitors: Evaluation of the Complex Role Played by the Zinc-Binding Group on Potency and Selectivity. *J. Med. Chem.* **60**, 403–414 (2017).
93. Defamie, V. *et al.* Matrix metalloproteinase inhibition protects rat livers from prolonged cold ischemia-warm reperfusion injury. *Hepatology* **47**, 177–185 (2008).
94. Dive, V. *et al.* RXP 407, a phosphinic peptide, is a potent inhibitor of angiotensin I converting enzyme able to differentiate between its two active sites. *Proc Natl Acad Sci U S A* **96**, 4330–4335 (1999).
95. Georgiadis, D. *et al.* Roles of the two active sites of somatic angiotensin-converting enzyme in the cleavage of angiotensin I and bradykinin: insights from selective inhibitors. *Circ. Res.* **93**, 148–154 (2003).
96. Johnson, J. L. *et al.* A Selective Matrix Metalloproteinase-12 Inhibitor Retards Atherosclerotic Plaque Development in Apolipoprotein E-Knockout Mice. *Arterioscler Thromb Vasc Biol* **31**, 528–535 (2011).
97. Lim, N. H. *et al.* In Vivo Imaging of Matrix Metalloproteinase 12 and Matrix Metalloproteinase 13 Activities in the Mouse Model of Collagen-Induced Arthritis. *Arthritis & Rheumatology* **66**, 589–598 (2014).

98. Iyer, R. P. *et al.* Early Matrix Metalloproteinase-12 Inhibition Worsens Post-Myocardial Infarction Cardiac Dysfunction by Delaying Inflammation Resolution. *Int J Cardiol* **185**, 198–208 (2015).
99. Ella, E. *et al.* Matrix metalloproteinase 12 promotes tumor propagation in the lung. *J. Thorac. Cardiovasc. Surg.* **155**, 2164–2175.e1 (2018).
100. Bremer, C., Tung, C. H. & Weissleder, R. In vivo molecular target assessment of matrix metalloproteinase inhibition. *Nat. Med.* **7**, 743–748 (2001).
101. Deguchi, J. *et al.* Inflammation in atherosclerosis: visualizing matrix metalloproteinase action in macrophages in vivo. *Circulation* **114**, 55–62 (2006).
102. Jiang, T. *et al.* Tumor imaging by means of proteolytic activation of cell-penetrating peptides. *Proc. Natl. Acad. Sci. U.S.A.* **101**, 17867–17872 (2004).
103. Lebel, R. & Lepage, M. A comprehensive review on controls in molecular imaging: lessons from MMP-2 imaging. *Contrast Media Mol Imaging* **9**, 187–210 (2014).
104. Goncalves, I. *et al.* Elevated Plasma Levels of MMP-12 Are Associated With Atherosclerotic Burden and Symptomatic Cardiovascular Disease in Subjects With Type 2 Diabetes. *Arterioscler. Thromb. Vasc. Biol.* **35**, 1723–1731 (2015).
105. Hadler-Olsen, E., Winberg, J.-O. & Uhlir-Hansen, L. Matrix metalloproteinases in cancer: their value as diagnostic and prognostic markers and therapeutic targets. *Tumour Biol.* **34**, 2041–2051 (2013).
106. Roy, R., Yang, J. & Moses, M. A. Matrix metalloproteinases as novel biomarkers and potential therapeutic targets in human cancer. *J. Clin. Oncol.* **27**, 5287–5297 (2009).
107. Ye, Y. *et al.* Novel Arginine-containing Macrocyclic MMP Inhibitors: Synthesis, ^{99m}Tc-labeling, and Evaluation. *Sci Rep* **8**, 11647 (2018).
108. Bordenave, T. *et al.* Synthesis, in vitro and in vivo evaluation of MMP-12 selective optical probes. *Bioconjug Chem* **27**, 2407–2417 (2016).
109. Evans, M. J. & Cravatt, B. F. Mechanism-Based Profiling of Enzyme Families. *Chem. Rev.* **106**, 3279–3301 (2006).
110. Kato, D. *et al.* Activity-based probes that target diverse cysteine protease families. *Nat. Chem. Biol.* **1**, 33–38 (2005).
111. Jin, Q. *et al.* A highly selective near-infrared fluorescent probe for carboxylesterase 2 and its bioimaging applications in living cells and animals. *Biosensors and Bioelectronics* **83**, 193–199 (2016).
112. Yang, P. & Liu, K. Activity-based protein profiling: recent advances in probe development and applications. *ChemBiochem* **16**, 712–724 (2015).
113. Garland, M., Yim, J. J. & Bogoy, M. A bright future for precision medicine: advances in fluorescent chemical probe design and their clinical application. *Cell Chem Biol* **23**, 122–136 (2016).
114. Nomura, D. K., Dix, M. M. & Cravatt, B. F. Activity-based protein profiling for biochemical pathway discovery in cancer. *Nat. Rev. Cancer* **10**, 630–638 (2010).

115. Verdoes, M. & Verhelst, S. H. L. Detection of protease activity in cells and animals. *Biochimica et Biophysica Acta (BBA) - Proteins and Proteomics* **1864**, 130–142 (2016).
116. Wofsy, L., Metzger, H. & Singer, S. J. Affinity Labeling—a General Method for Labeling the Active Sites of Antibody and Enzyme Molecules*. *Biochemistry* **1**, 1031–1039 (1962).
117. Sinz, A. Chemical Cross-Linking and Mass Spectrometry for Investigation of Protein–Protein Interactions. in *Mass Spectrometry of Protein Interactions* 83–107 (Wiley-Blackwell, 2006). doi:10.1002/9780470146330.ch5
118. Sieber, S. A., Niessen, S., Hoover, H. S. & Cravatt, B. F. Proteomic profiling of metalloprotease activities with cocktails of active-site probes. *Nature Chemical Biology* **2**, nchembio781 (2006).
119. Sieber, S. A. & Cravatt, B. F. Analytical platforms for activity-based protein profiling – exploiting the versatility of chemistry for functional proteomics. *Chem. Commun.* **0**, 2311–2319 (2006).
120. Geurink, P. P. *et al.* Design of Peptide Hydroxamate-Based Photoreactive Activity-Based Probes of Zinc-Dependent Metalloproteases. *European Journal of Organic Chemistry* 2100–2112 (2010). doi:10.1002/ejoc.200901385
121. Leeuwenburgh, M. A. *et al.* Solid-phase synthesis of succinylhydroxamate peptides: Functionalized matrix metalloproteinase inhibitors. *Org.Lett.* **8**, 1705–1708 (2006).
122. Qiu, W. *et al.* Design and Synthesis of Matrix Metalloprotease Photoaffinity Trimodular Probes. *Chinese Journal of Chemistry* **27**, 825–833 (2009).
123. Wang, J., Uttamchandani, M., Li, J., Hu, M. & Yao, S. Q. ‘Click’ synthesis of small molecule probes for activity-based fingerprinting of matrix metalloproteases. *Chem. Commun. (Camb.)* 3783–3785 (2006). doi:10.1039/b609446e
124. David, A. *et al.* Cross-Linking Yield Variation of a Potent Matrix Metalloproteinase Photoaffinity Probe and Consequences for Functional Proteomics. *Angewandte Chemie International Edition* **46**, 3275–3277 (2007).
125. Dabert-Gay, A.-S. *et al.* Molecular Determinants of Matrix Metalloproteinase-12 Covalent Modification by a Photoaffinity Probe. *J Biol Chem* **283**, 31058–31067 (2008).
126. Nury, C. *et al.* A Pan Photoaffinity Probe for Detecting Active Forms of Matrix Metalloproteinases. *ChemBioChem* **14**, 107–114 (2013).
127. Zhu, Q., Girish, A., Chattopadhyaya, S. & Yao, S. Q. Developing novel activity-based fluorescent probes that target different classes of proteases. *Chem. Commun.* **0**, 1512–1513 (2004).
128. Forbes, C. *et al.* Active Site Ring-Opening of a Thiirane Moiety and Picomolar Inhibition of Gelatinases. *Chemical Biology & Drug Design* **74**, 527–534 (2009).
129. Testero, S. A. *et al.* Discovery of Mechanism-Based Inactivators for Human Pancreatic Carboxypeptidase A from a Focused Synthetic Library. *ACS Med. Chem. Lett.* **8**, 1122–1127 (2017).
130. Morell, M. *et al.* Coupling Protein Engineering with Probe Design To Inhibit and Image Matrix Metalloproteinases with Controlled Specificity. *J. Am. Chem. Soc.* **135**, 9139–9148 (2013).

131. Sakamoto, S. & Hamachi, I. Recent progress in chemical modification of proteins. *Anal Sci* (2018). doi:10.2116/analsci.18R003
132. Tsukiji, S., Miyagawa, M., Takaoka, Y., Tamura, T. & Hamachi, I. Ligand-directed tosyl chemistry for protein labeling *in vivo*. *Nature Chemical Biology* **5**, nchembio.157 (2009).
133. Fujishima, S., Yasui, R., Miki, T., Ojida, A. & Hamachi, I. Ligand-Directed Acyl Imidazole Chemistry for Labeling of Membrane-Bound Proteins on Live Cells. *J. Am. Chem. Soc.* **134**, 3961–3964 (2012).
134. Matsuo, K. *et al.* One-step construction of caged carbonic anhydrase I using a ligand-directed acyl imidazole-based protein labeling method. *Chem. Sci.* **4**, 2573–2580 (2013).
135. Miki, T. *et al.* LDAI-Based Chemical Labeling of Intact Membrane Proteins and Its Pulse-Chase Analysis under Live Cell Conditions. *Chemistry & Biology* **21**, 1013–1022 (2014).
136. Matsuo, K., Nishikawa, Y., Masuda, M. & Hamachi, I. Live-Cell Protein Sulfonylation Based on Proximity-driven N-Sulfonyl Pyridone Chemistry. *Angew. Chem. Int. Ed. Engl.* **57**, 659–662 (2018).

CHAPTER II

RESULTS

6. Conception and in vitro evaluation of acyl imidazole probes targeting recombinant hMMP12

6.1. Rational design of the probes

We have seen in the previous chapter that metalloproteases activity-based probes developed so far came to limited use *in vivo*. Based on the recent concept of traceless labelling reported by Hamashi's group, a new generation of affinity probes able to label active forms of MMPs without any external stimuli has been envisaged.

A typical probe would be composed of a MMP targeting motif, a chemically sensitive spacer to react with nucleophile(s) from the protease, and a tag to be transferred for subsequent analyses (Figure 34A).

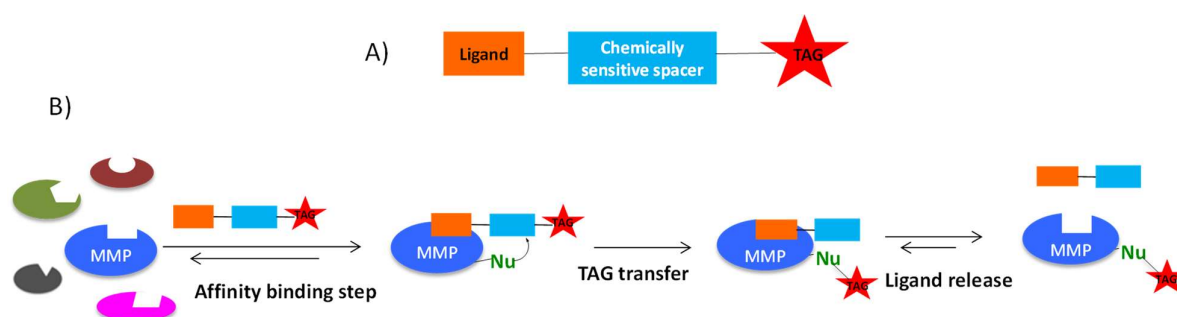


Figure 34: Schematic representation of MMPs labelling process using a new generation of affinity probes. A) MMP probes composed of ligand part, a chemically sensitive spacer a tag. B) Two steps labelling process of MMPs within a complex proteome.

After an initial affinity binding step mainly governed by the ability of the ligand to selectively interact with its target, a TAG would be transferred to the protein through a chemical reaction between the chemically sensitive spacer and a nucleophile in close proximity at the protein surface (Figure 34B). The ligand, which does not form any covalent linkage with the target, should be then released from the active site. In such an approach, the choice of the targeting moiety as well as that of the reactive spacer are critical to achieve both efficiency and selectivity.

Choice of the targeting motif:

The phosphinic pseudo peptide, RXP470.1, has been identified by our group as the first potent and highly selective inhibitor of MMP-12 (see introduction part 4.1.1) ¹. Remarkably, in a mouse model of atherosclerosis, RXP470.1 has proven its efficiency to inhibit atheroma plaque development and to promote a "stable" plaque phenotype by targeting MMP-12 *in vivo* ². This inhibitor is also able to block MMP-12 activity in a mouse model of rheumatoid arthritis ³, during viral infection ⁴ and during lung tumour propagation ⁵. On the basis of these results, we consider that RXP470.1 template may serve as a valuable

starting point for the development of a first generation of affinity probes that could selectively target MMP 12 in complex proteomes including cells, biological fluids and *in vivo*.

Choice and positioning of the chemically sensitive spacer in a well-defined structural context:

A detailed analysis of the crystal structure of RXP470.1 in interaction with hMMP-12 catalytic domain shows that RXP470.1 P₃' glutamate points towards three potential nucleophiles present within the protease S₃' region (Lys¹⁷⁷, Thr²¹⁰ and Tyr²⁴⁰, Figure 35).

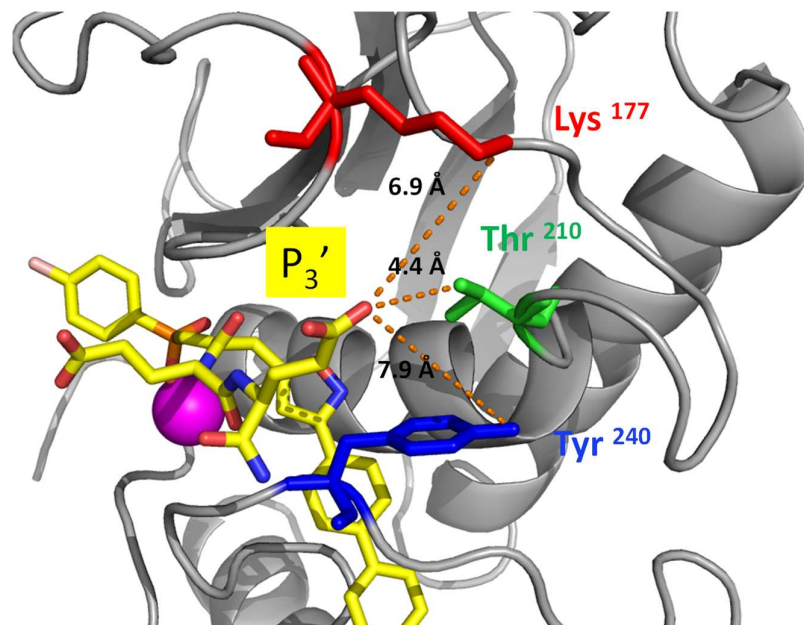


Figure 35. Crystal structure of hMMP12 in complex with RXP470.1, MMP12 catalytic domain is represented in cartoon mode and coloured in grey. Carbon atoms of RXP470.1 are shown as sticks coloured in yellow. Lys¹⁷⁷, Thr²¹⁰ and Tyr²⁴⁰ side chains are in stick representation coloured in red, green and blue respectively. Catalytic zinc ion is a magenta sphere. The distance measurements are indicated in orange dotted lines and the distances given in Ångstrom.

Considering their orientation and distance relative to that of RXP470.1 glutamate side chain, these three residues could be considered as potential anchoring points for chemical labelling. Based on these observations and having in mind that RXP470.1 P₃' glutamate was not essential to maintain a favourable affinity-selectivity profile towards hMMP-12^{1,6}, we chose conserving a part of the RXP470.1 scaffold (P₁' and P₂' side chain) and only modifying the P₃' residue.

With no *a priori* regarding the accessibility/reactivity of Lys¹⁷⁷, Thr²¹⁰ and Tyr²⁴⁰ in solution, we proposed to install the future chemically sensitive spacer onto a ϵ -amino group of a lysine side chain that can offer a sufficient flexibility for probing the whole S₃' region. In addition, preliminary studies in the lab have shown that replacing the RXP470.1 P₃' glutamate by a lysine harbouring a phenyl acyl moiety affected only

moderately the affinity/selectivity profile of the resulting compound **A**, thus confirming the minor impact of P₃' position on inhibitor binding properties (Figure 36A).

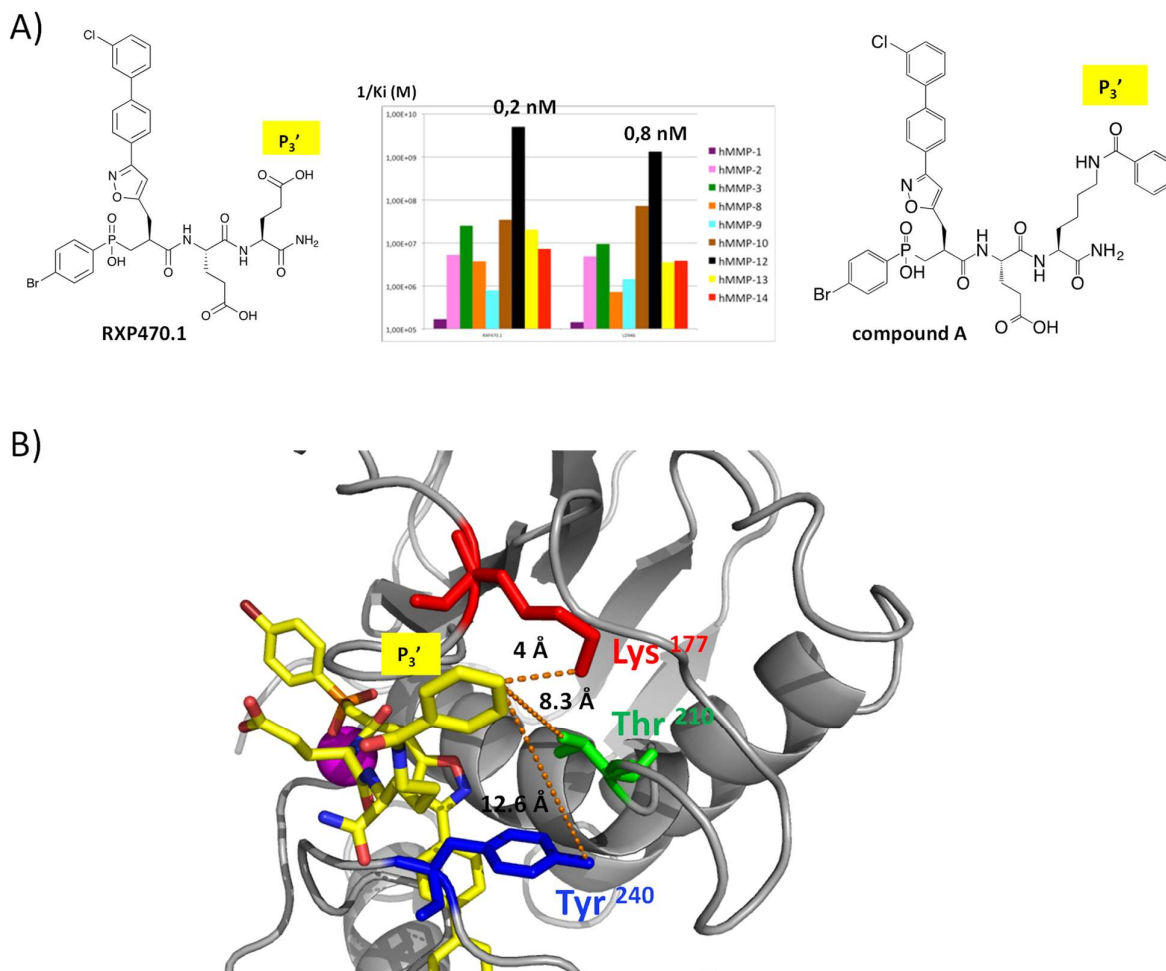


Figure 36 A) Comparison of affinity/selectivity profile between RXP470.1 and its P₃' modified analogues A towards a panel of ten human MMPs identified by the colour code on right of the figure. K_i (M) values were determined in 50 mM Tris-HCl buffer, pH 6.8 with 10 mM CaCl₂ at 25°C. 1/K_i values are reported in logarithm scale. B) Crystal structure of hMMP12 in complex with compound A, MMP12 catalytic domain is represented in cartoon mode and coloured in grey. Carbon atoms of A are shown as sticks coloured in yellow. Lys¹⁷⁷, Thr²¹⁰ and Tyr²⁴⁰ side chains are in stick representation coloured in red, green and blue respectively. Catalytic zinc ion is a magenta sphere. The distance measurements are indicated in orange dotted lines and the distances given in Ångstrom.

Moreover, crystal structure of **A**/hMMP12 complex showed a close proximity (4Å) between compound **A** P₃' phenyl ring and Lys¹⁷⁷ amino function (Figure 36B), suggesting that the installation of a chemically sensitive on a lysine linker might lead to a preferential targeting of Lys¹⁷⁷.

Regarding the chemical nature of the self-immolative spacer, it is worth mentioning that only two types of chemistry were described at the beginning of the project: ligand-directed tosyl and acyl imidazole chemistry (see introduction 5.2.4). In this context, we selected the acyl imidazole spacer since it was described to

exhibit faster kinetics and higher labelling efficiency than the tosyl group⁷. This reactive spacer was also chosen for its ability to preferentially target amino acids such as lysine, serine or tyrosine⁷⁻¹⁰.

Choice of the TAG:

Two fluorescent reporters were envisaged as tags for subsequent in-gel labelled-protein visualisation: a fluorescein and a cyanine 3 (Cy3) reporter.

Based on the different aspects discussed above, we designed two fluorescent acyl imidazole probes whose structure derived from RXP470.1 scaffold: probe **9** and **10** with a fluorescein and a Cy3 reporter respectively (Figure 37).

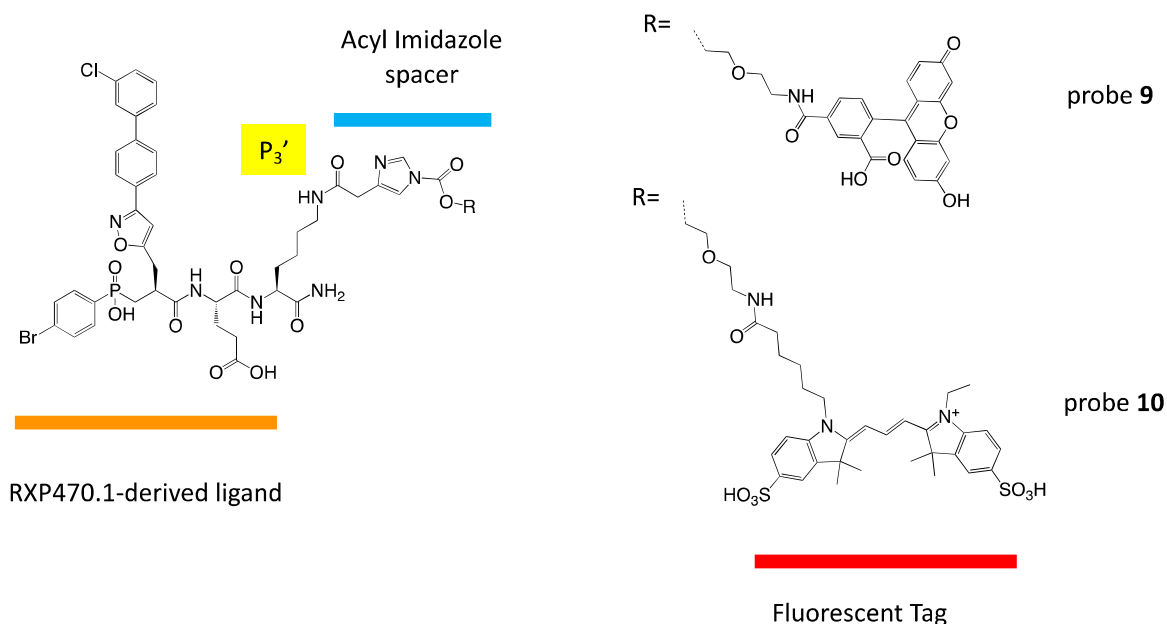


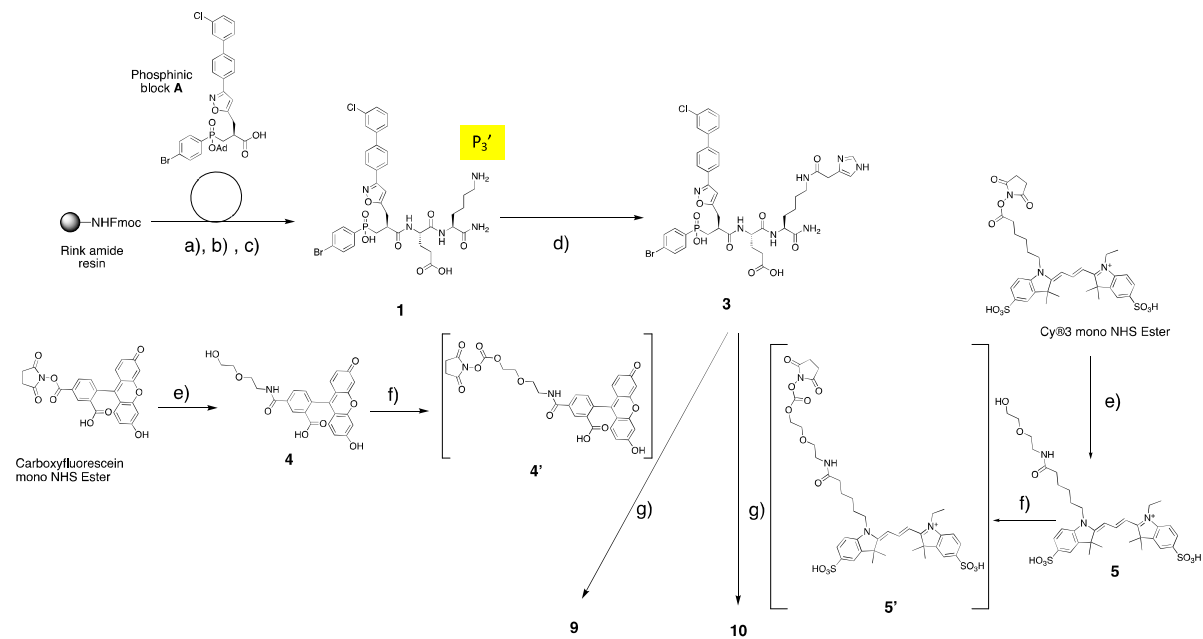
Figure 37. Chemical structure of probe 9 and 10.

A short peg linker was incorporated between the acyl imidazole moiety and the bulky fluorescent group to limit steric clashes during probes/MMP binding events.

In such a design, we also make the hypothesis that installation of a fluorescent tag within hMMP-12 S₃' region should modify only slightly the structural integrity of protease active site and therefore should not compromise its function.

6.2. Synthesis and characterisation of probes 9 and 10

Probes **9** and **10** were synthesised according to the following scheme 1.



Scheme 1. Chemical pathway to access to probe 9 and 10. Reaction conditions: (a) Fmoc solid phase synthesis, Fmoc-AA-OH (10 eq), ClHOBT/DIC in DMF, 60°C, MW, 10 min followed by Phosphinic block A (1.2 eq), ClHOBT/DIC, DMF, RT, overnight. (b) TFA cleavage, r.t., 2h (c) RP-HPLC separation, 34% yield (d) 4-Imidazole acetic acid hydrochloride (10 eq), EDC.HCl (3 eq), ClHOBT (3 eq), DIEA (30 eq) in DMF, r.t., overnight., 54 % yield. (e) Carboxyfluorescein (1 eq) or Cy³ (1 eq) mono NHS ester, 2-(2-aminoethoxy) ethan-1-ol (1 eq), DIEA (10 eq) in DMF, r.t., 1h, 54% and 47% yield for **4 and **5** respectively. f) Compound **4** or **5** (1 eq), DSC (1 eq), DIEA (9 eq) in DMF, r.t., 4h. g) **4'** or **5'** (1eq), pyridine (5 eq) in DMF, r.t., 2h, 16% and 39 % for probes **9** and **10** respectively.**

The two probes were obtained in five steps from a protected phosphinic building block **A** whose synthesis has been previously described^{1,11}. The amino acid sequence was first synthesised on a solid support using the standard Fmoc strategy. The protected phosphinic building block was then incorporated on a solid support under microwave irradiations in the presence of DIC/ClHOBT. After cleavage from the support, the two resulting diastereomers with a R or S configuration at the P₁' position (see experimental part 13.2.1 Figure 70) were separated and compound **1** with the “natural” configuration was isolated with 34% yield. The 4-Imidazole acetic acid was then incorporated onto the ε-amino group of lysine in P₃' to yield **3** (54%) after RP-HPLC purification. From the commercially available fluorescein mono NHS-ester and after a coupling step with 2-(2-aminoethoxy) ethan-1-ol, fluorescein derivative **4** with a short PEG spacer was obtained with 54% yield. From Cy³ mono NHS ester and following the same procedure, Cy3 derivative **5** was isolated with 47% yield. **4** or **5** were subsequently activated with *N,N'* disuccinimidyl carbonate (DSC) and the reaction mixture was gently stirred for 4h at room temperature. Activated intermediates **4'** or **5'**

were not isolated and directly added to **3**. After 2h of stirring at room temperature, the reaction mixture was diluted in CH₃CN for further RP-HPLC purification.

We first used standard eluting buffers (A: H₂O/TFA 0.1% and B: CH₃CN 90%/H₂O 10%/ TFA 0.09%) to purify the resulting acyl imidazole probes. In these conditions, acyl imidazole motif turned out instable and a part of the probe was hydrolysed (see Figure 38 for a representative probe **9** RP-HPLC profile in TFA conditions). When the pH of the eluting buffer was increased to pH=5,5 (A: 10 mM CH₃COONH₄ and B: CH₃CN), probes were purified and properly analysed with no detection of degradation compounds.

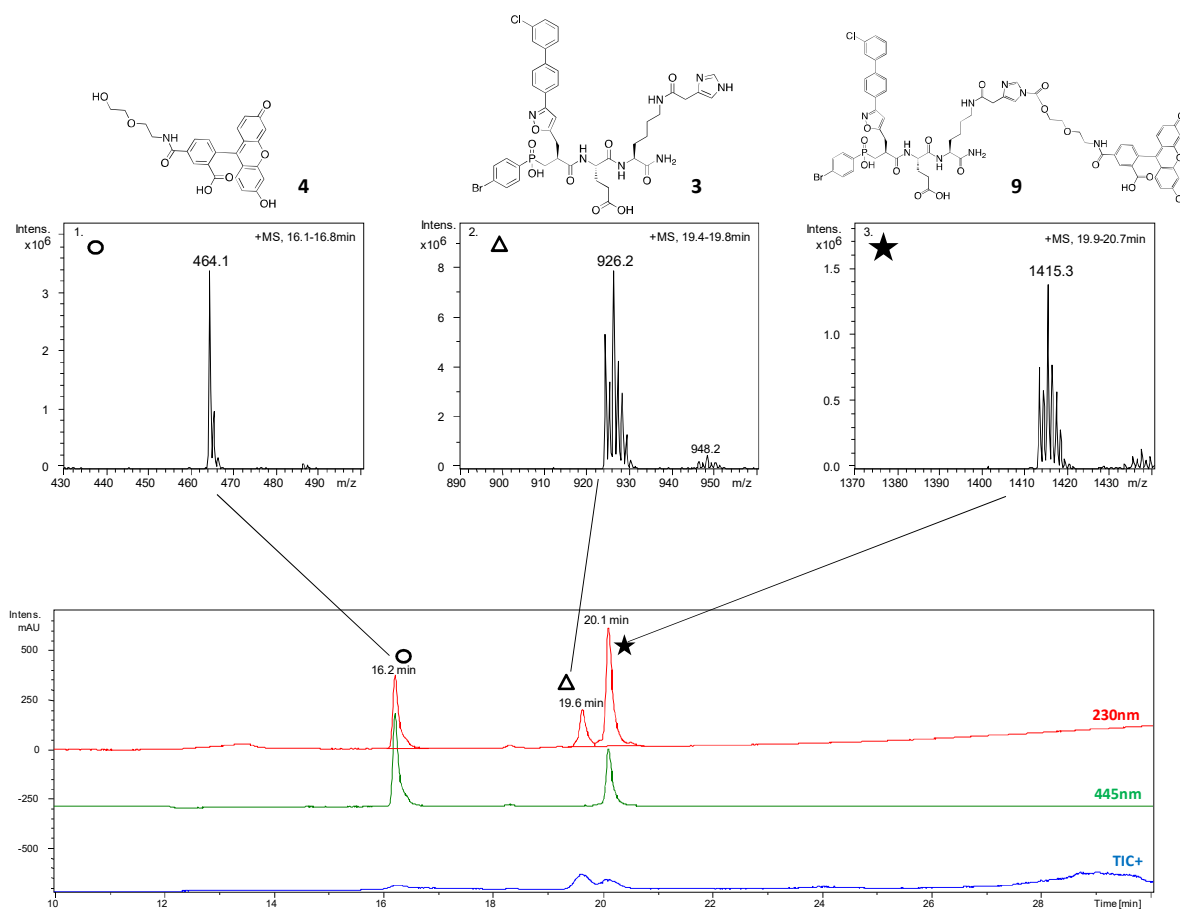


Figure 38: LC/MS profile of 9 analysed in TFA conditions using the following method: analytical XDB C18 column, flow rate: 0.6 mL.min⁻¹, Method: 0 to 5 min: 100% A, 5 to 25 min: 100% B with A: H₂O-TFA 0.1% and B: CH₃CN-TFA 0.09%, UV detection was performed at 230 nm (red) and 445 nm (green). Probe 9 and derivative 3 and 4 resulting from hydrolysis are marked with a black star, a white triangle and a white circle respectively.

In these optimised conditions of purification, **9** and **10** were isolated with 16% and 39% yield respectively. After characterisation using standard analytical methods, each probe was aliquoted (10 nmol per batch), freeze-dried and stored as a solid at -20°C away from light.

6.3. Choice of the labelling conditions.

In order to select the most appropriate conditions for performing labelling on hMMP12 catalytic domain, two parameters were considered: pH and chemical nature of the buffer.

Particularly, pH conditions can impact the stability of acyl imidazole motif in solution, the binding of RXP470.1-derived compounds to hMMP-12 as well as the reactivity of the targeted nucleophile within the protein core.

As described above, pH conditions can substantially impact the stability of acyl imidazole probe in solution. While very acidic pH can drastically accelerate hydrolysis rate of acyl imidazole motif, basic conditions have also a destabilizing effect. This was recently demonstrated by Hamashi and co-workers for benzenesulfonamide acyl imidazole derivative **B**⁸ (Figure 39).

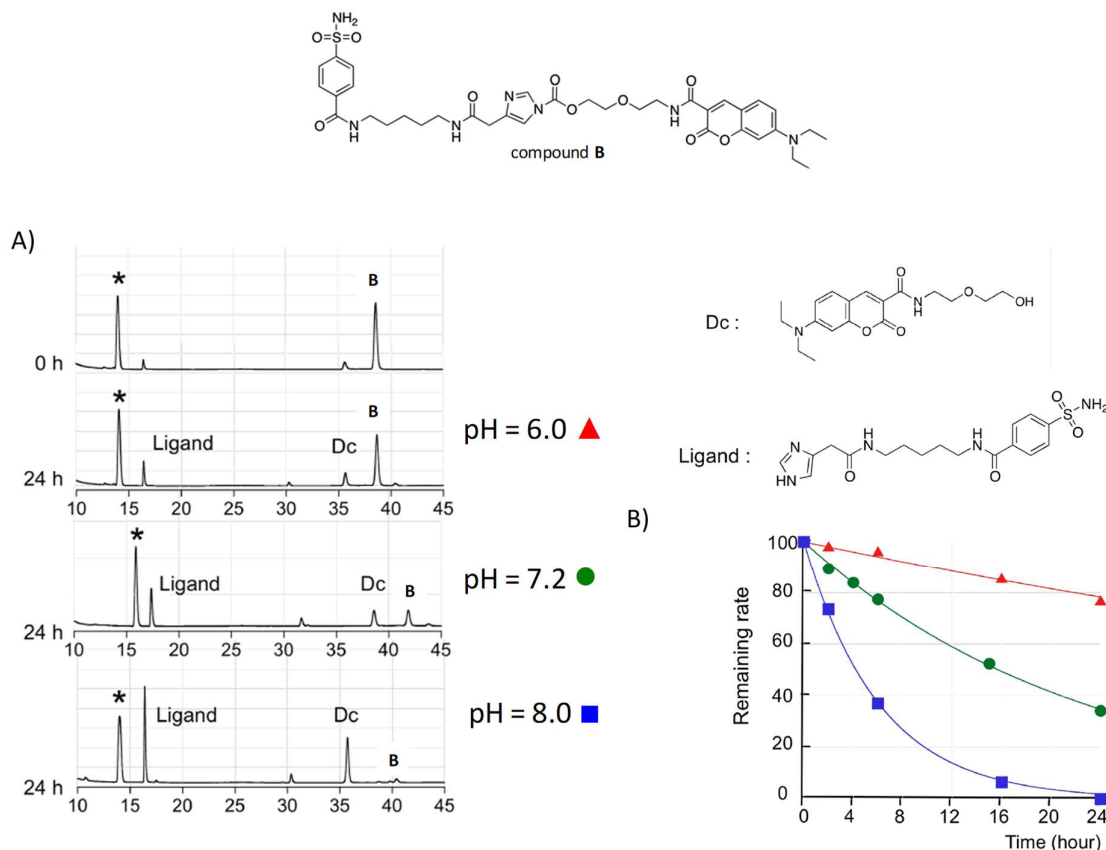


Figure 39. Evaluation of the hydrolysis stability of compound B under different pH conditions. (A) RP-HPLC profiles of B after a 37 °C incubation in aqueous buffer (50 mM HEPES) at different pH (6.0, 7.2 and 8.0). The peak marked with (*) corresponds to benzenesulfonamide as an internal standard. The structures of "Ligand" and "Dc" (7-diethylaminocoumarin) generated by the hydrolysis of B are shown on right side. (B) Time-trace plot of the remaining rate of B under the different pH conditions (50 mM HEPES buffer, 37 °C, pH = 6.0 (▲), 7.2 (●) and 8.0 (■))⁸.

As illustrated by Figure 39A, an increase in pH results in a hydrolysis rate acceleration of compound **B**. Thus, this compound displayed a half-life ranging from 4h at pH=8 to more than 24h at pH=6 (Figure 39B).

Recent studies in our lab showed that K_i values of RXP470.1 toward MMP-12 varied as function of pH^{6,12}. As shown by figure 8, RXP470.1 affinity constant can range from sub nano molar (0.2 nM at pH=6) to sub micro molar (340nM at pH= 9.5) values corresponding to a shift of a factor 1100.

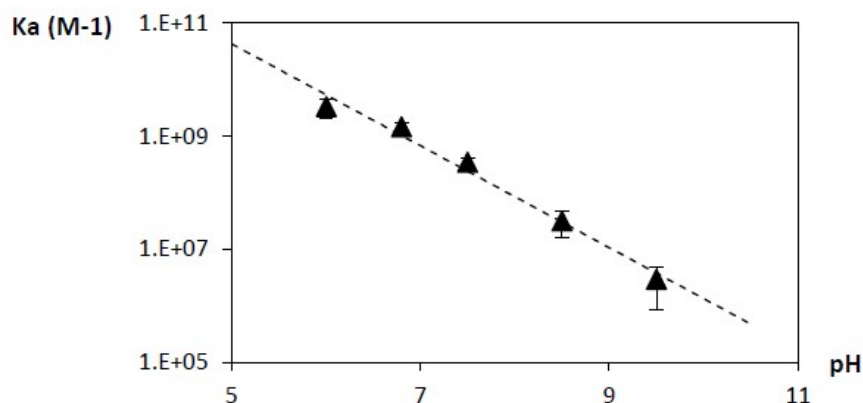


Figure 40. Change in RXP 470.1 affinity constant towards MMP-12 (Y-axis) as function of pH (X-Axis). Measurements were made in Tris buffer 20mM, NaCl 200 mM, CaCl₂ 3mM, ZnCl₂ 0,1 mM at 25 °C.

This pH dependence of inhibitor affinity has been correlated to a proton linkage upon binding¹².

As shown above, three potential nucleophiles are present within hMMP-12 S₃'region: Lys¹⁷⁷, Thr²¹⁰ and Tyr²⁴⁰. Considering its pKa value on threonine (pKa=13) and tyrosine (pKa=10) side chain, the alcohol function remains not protonated in a pH window of 6 to 9 and its nucleophilic character barely impacted. Conversely, with an approximate pKa of 10, the lysine ε-amino function is mainly protonated in this range of pH. Thus, an increase in pH enhances the proportion of not protonated species with a consequence on ε-amino function reactivity. In this regard, our group has showed a pH-dependence of hMMP12 photo labelling by a probe targeting a lysine residue within the S₁' cavity¹³.

Regarding the chemical nature of the buffer, we decided to avoid buffers with potential reactive functions (e.g.; TRIS buffer harbouring an amino group) that might may cross react with the acyl imidazole probes.

Based on these different considerations, we chose to perform labelling experiment in the following buffer: 20 mM HEPES, 200 mM NaCl, 5 mM CaCl₂, 0.1 mM ZnCl₂, 0,1% Brij-35 pH=7.4. Brij-35 as a polyoxyethylene surfactant was added to prevent aggregation of protein molecules.

6.4. Stability of Probes 9 and 10 in labelling buffer.

We first verified the stability of probes **9** and **10** over time in labelling buffer (20 mM HEPES, 200 mM NaCl, 5 mM CaCl₂, 0.1 mM ZnCl₂, 0,1% Brij-35 pH=7.4). Solutions of probe **9** and **10** (10 μM) were incubated for 24h at 37°C. At different time points (0 h, 1 h, 2 h, 4 h, and 24 h) samples were collected and analysed by RP-HPLC (Figure 41A).

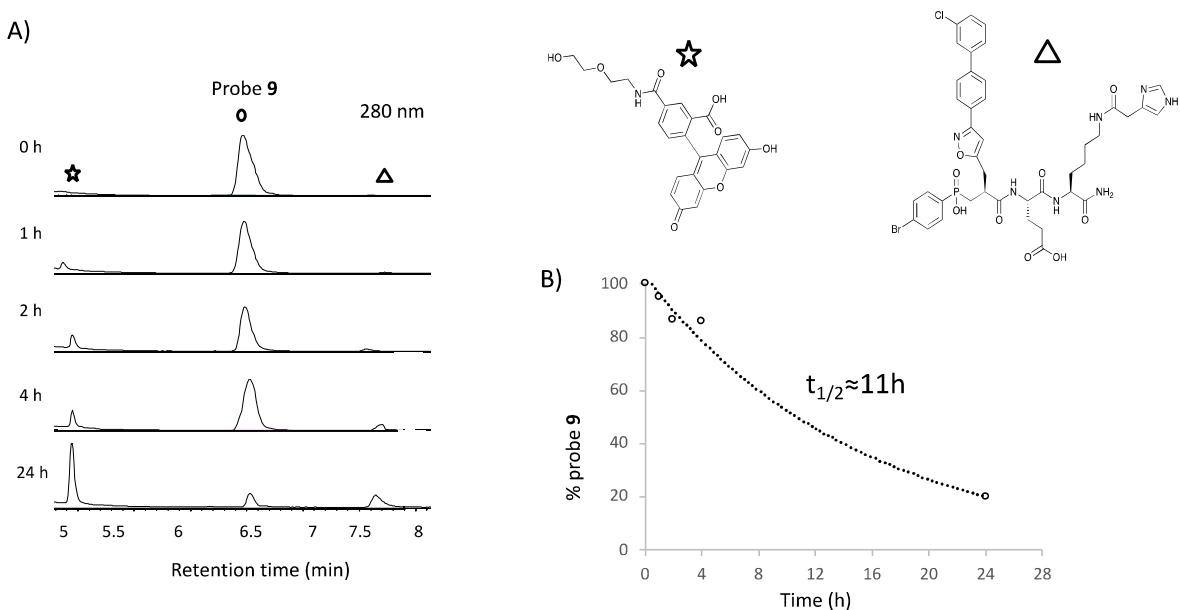


Figure 41. Evaluation of probe 9 hydrolysis stability in 20 mM HEPES buffer, pH=7.4, 5mM CaCl₂, 200 mM NaCl, 0.1 mM ZnCl₂ and 0.1 % Brij-35 at 37°C. A) Representative RP-HPLC profiles of samples collected at different time points (0 h, 1 h, 2 h, 4 h, and 24 h) in the following conditions: Column Ascentis® Express C18 (Supelco), 100 x 4.6 mm, particle size 2.7 μ, flow 0.6 mL.min⁻¹, Method: 0 -> 1 min: 0 -> 35% B, 1 min -> 9 min: 35% B -> 65% B, 9 min -> 10 min: 65% -> 100% with A: 10 mM CH₃COONH₄, pH=5.5 and B: CH₃CN. The analysis was performed at 280 nm. The peak marked with an empty circle corresponds to the starting probe 9. The products resulting from the hydrolysis are marked with an empty star and an empty triangle. B) Time trace plot of the percentage (Y-axis) of probe 9 remaining in solution over the time (X-axis).

From the RP-HPLC profiles at different time points, the relative amount of probe **9** and derivatives resulting from its hydrolysis was determined. This allowed generating a time trace plot of probe **9** percentage remaining intact in solution (Y-axis) over the time (X-axis). From this curve, a probe **9** half-life of approximately 11h was deduced. In the same conditions, probe **10** showed a slightly better hydrolysis stability with a half-life of 16 hours. These hydrolysis stability were comparable to those reported for other acyl imidazole probes in similar buffer and temperature conditions ⁷. This suggested that stability of such reagents was mainly governed by the intrinsic reactivity of the acyl imidazole moiety, with only a minor impact of the tag to which it was conjugated.

6.5. Determination of Probe 9 and 10 affinity constants

To assess impact of P₃' modification on probe 9 and 10 binding properties, we determined their affinity constants towards MMP-12 but also towards six other MMPs. In first approximation and despite their potential reactivity, we considered that probe 9 and 10 behaved as competitive inhibitors. The inhibitory assays were carried out in labelling buffer (20 mM HEPES, pH=7.5, 200 mM NaCl, 5 mM CaCl₂, 0.1 mM ZnCl₂ and 0.1% Brij-35) and continuous kinetic assays were performed by recording the fluorescence increase induced by the cleavage of a fluorogenic substrates (see part 14.3.1 for details). The results are presented in Table 2.

		Ki (nM)						
entry		hMMP-2	hMMP-3	hMMP-8	hMMP-9	hMMP-10	hMMP-12	hMMP-13
a	Probe 9	n.d.	n.d.	n.d.	n.d.	n.d.	3.4±0.2	n.d.
b	Probe 10	1355±310	1430±110	3500±200	> 10000	155±30	13.1±1.3	875±180
c	RXP470.1	330±20	345±15	780±80	840±120	98±16	1.1±0.1	74±7

Table 2. Ki values (nM) for probe 9, 10 and RXP470.1 on a set of MMPs in 20 mM HEPES, pH=7.5, 200 mM NaCl, 5 mM CaCl₂, 0.1 mM ZnCl₂ and 0.1% Brij-35. Ki values are determined at 25°C and are the mean ± SD of three experiments.

By comparison with its parent RXP470.1 (Ki =1.1 nM), probe 9 with a fluorescein moiety displayed very similar binding towards hMMP12 with an apparent affinity constant of 3.4 nM (entry a vs b vs c). The RXP470.1-derived probe 10 appeared slightly less potent (x 12) than its parent counterpart but remained very selective for hMMP-12 (entry b). Overall, these results confirmed that a substantial modification on P₃' position only moderately impacts probes affinity/selectivity profile towards a set of 7 MMPs.

6.6. Labelling of recombinant hMMP12 catalytic domain by probe 9 and 10

We then investigated the reactivity of probe 9 towards recombinant catalytic domain of hMMP-12. hMMP-12 catalytic domain was first produced as previously described¹⁴ and conditioned by dialysis in the appropriate labelling buffer (20 mM HEPES, pH=7.5, 200 mM NaCl, 5 mM CaCl₂, 0.1 mM ZnCl₂ and 0.1% Brij-35). The protein concentration was measured by UV ($\epsilon_{280}=26930 \text{ M}^{-1}\cdot\text{cm}^{-1}$) and fraction of active hMMP-12 was determined by titration experiment (see part 14.3.3). The probe 9 concentration was measured by UV considering a molar extinction coefficient of $\epsilon_{495}= 76\,900 \text{ M}^{-1}\cdot\text{cm}^{-1}$ (in pH 7,2). hMMP12 (5 μM) was incubated in presence of probe 9 (10 μM) in labelling buffer at 37°C. At selected time points (1, 2, 4 and

24h), samples were collected, resolved by SDS-PAGE in denaturing conditions and the fluorescence visualized at 460 nm with a fluorescent imager (Figure 42A).

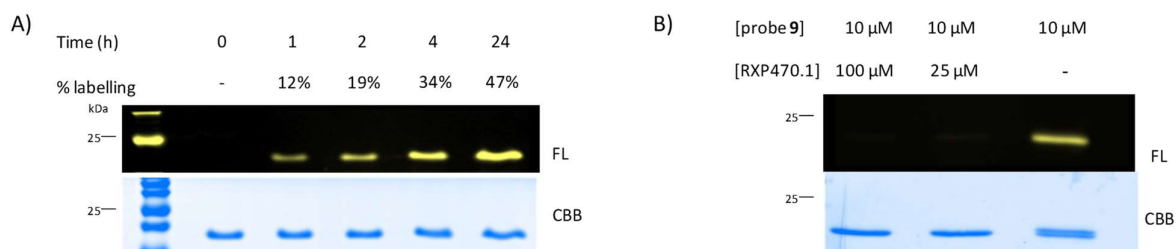


Figure 42. *hMMP-12 labelling by probe 9 and competitions experiment with RXP470.1. A) In-gel fluorescence analysis of hMMP12 (5 μM) labelled by probe 9 (10 μM) at different time points (1 h, 2 h, 4 h and 24 h). Samples were subjected to 12% SDS-PAGE and analysed by in-gel- fluorescence imaging (FL) and Coomassie brilliant blue (CBB) staining. B) In-gel fluorescence analysis of the labelling reaction after 24 h in presence of a competitive ligand RXP470.1 (25 μM and 100 μM), fluorescence imaging (FL) and Coomassie brilliant blue (CBB) staining.*

The labelling reaction proceeded in a time-dependent manner with a covalent modification of hMMP-12 already detectable after one hour. After 24h, the HPLC analysis of labelled and unlabelled hMMP-12 in mixture enabled determining their relative ratio (see 16.3), from which a labelling yield of $47 \pm 2\%$ was calculated. The yields at intermediate times (1 h, 2 h and 4 h) were deduced from that at 24 h by comparing relative bands intensity on the gel (ImageJ software, see part 14.4.1).

Through competition experiments in presence of RXP470.1 at two different concentrations (25 μM and 100 μM), we demonstrated that no significant labelling was observed after 24h (Figure 42B). This confirmed that hMMP-12 labelling by probe 9 was effectively driven by a ligand-protein recognition.

After 24 h, the labelling reaction was analysed by LC/MS in conditions enabling unambiguous separation between labelled and unlabelled hMMP12 (Figure 43). The labelled hMMP-12 (black star) displayed a multiple-charge ions mass profile associated to a molecular weight of 18081.2 Da corresponding to that of unlabelled MMP12 (17593.0 Da) incremented by the mass of one tag (488.2 Da). This indicated that a single labelling of hMMP-12 has occurred in these conditions.

The relative amount between labelled and unlabelled specie was determined by comparing peaks area of at 214 and 280 nm. The calculated yield was $47 \pm 2\%$ and corresponded to average values of experiments performed in triplicate. In this acidic condition contribution of fluorescein was not significant and the correction factor was not applied.

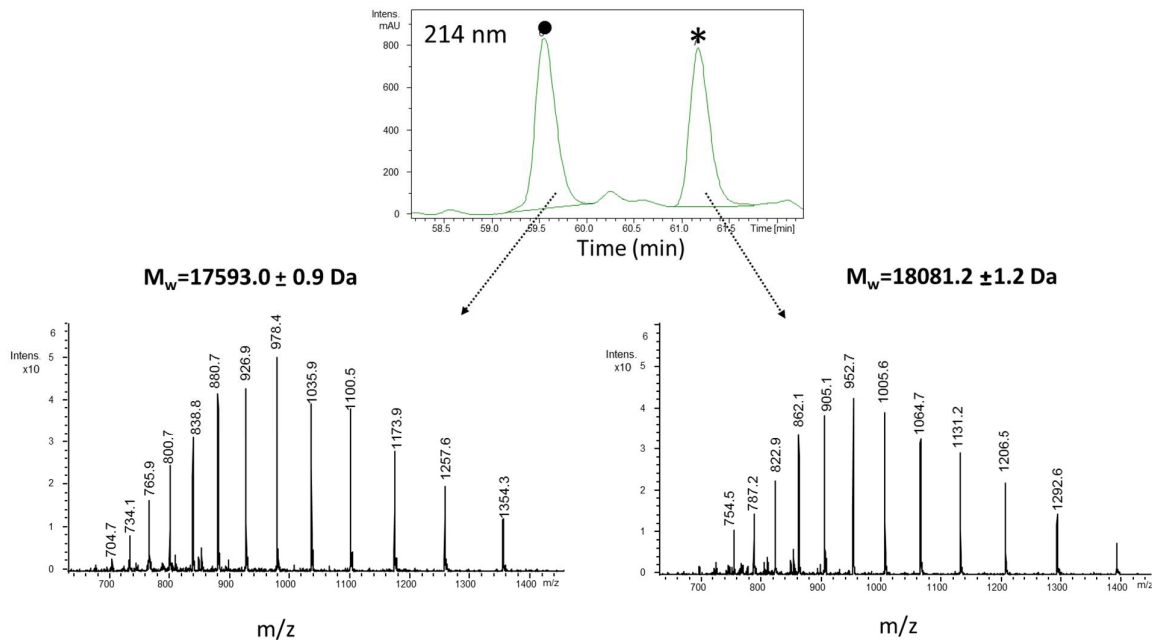


Figure 43. LC/MS analysis of the labelled and unlabelled MMP-12 in mixture after 24h of reaction. The mass spectra are not deconvoluted • unlabelled hMMP-12 ($M_w=17593.0$ Da), * singly labelled hMMP-12 ($M_w=18081.2$ Da). The LC conditions were the following: X Bridge BEH300 column (21 x 150 mm, 3.5 μ m, Waters), flow rate = 0.2 mL.min⁻¹, initial conditions: 5% B, 0 to 5 min: 5% B, 5 to 10 min: 20%, 10 to 65 min: 55%, 65 to 67 min: 100% B with A: H₂O/TFA 0.1% and B: CH₃CN 90%/H₂O 10%/ TFA 0.09%.

In the same conditions, we demonstrated that probe **10** (10 μ M) also reacted with the hMMP-12 catalytic domain (5 μ M) in a time dependant manner with a labelling efficiency of 48 ± 1 % after 24h (Figure 44A).

As for probe **9**, LC/MS analysis of the reaction mixture after 24h showed that only on Cy3 Tag was transferred to hMMP12 (Figure 44B). The labelling yield was calculated from peaks area integration at 214 and 280 nm (Figure 44B). At 280 nm, a correction factor of 1.44 was applied. This correction factor was calculated from an extinction coefficient of 12.000 M⁻¹.cm⁻¹ for Cy3 at this wavelength. Thus, the yields of hMMP12 labelling by probe **10** were estimated at $48,5\% \pm 1,1$ and $48,1\% \pm 0,5$ at 214 and 280 nm respectively, which corresponded to an average yield of 48,3%. This value was almost identical to that obtained for probe **9** (47%) despite a difference between their K_i values towards hMMP-12; 3.4 nM and 13.1 nM for probe **9** and **10** respectively.

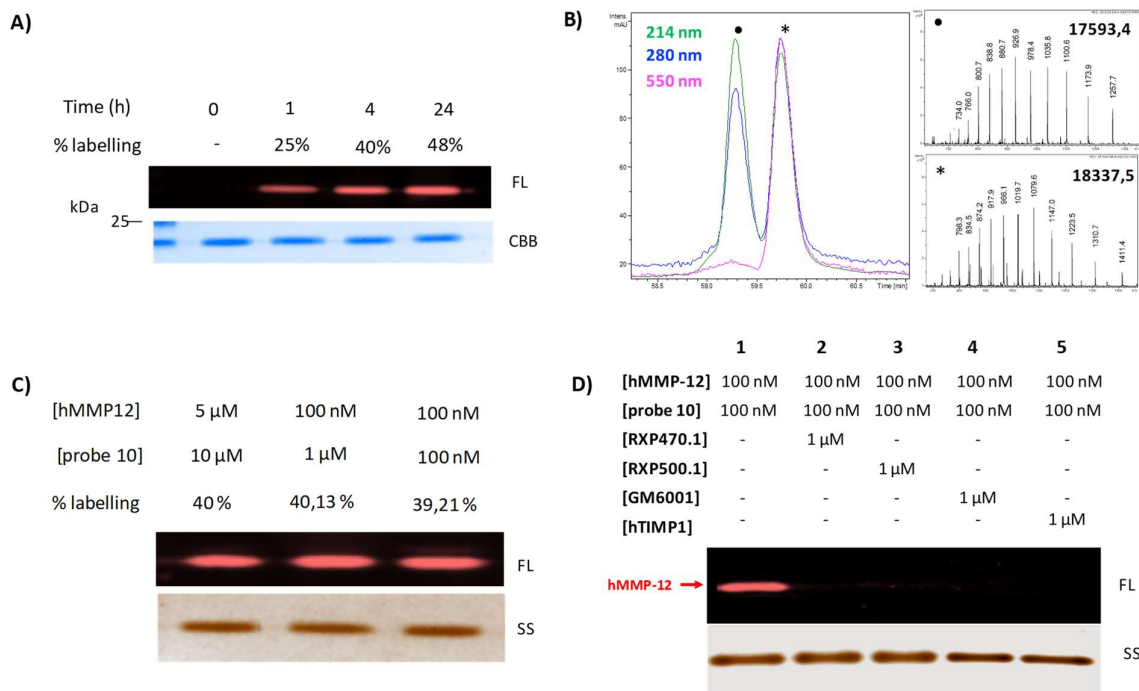


Figure 44. hMMP-12 labelling by probe 10 in labelling buffer and competitions experiment with RXP470.1, RXP500.1, GM6001 and hTIMP-1. **A)** In-gel fluorescence analysis of hMMP12 (5 μ M) labelled by probe 10 (10 μ M) at different time points (1 h, 4 h and 24 h). Samples were subjected to 12% SDS-PAGE and analysed by in-gel fluorescence imaging (FL) and Coomassie brilliant blue (CBB) staining. **B)** LC (214, 280 and 550 nm)/MS (electrospray, positive mode of ionization) analysis of the labelling reaction after 24h. The LC conditions were the following: X Bridge BEH300 column (21 x 150 mm, 3.5 μ m, Waters), flow rate = 0.2 mL.min⁻¹, initial conditions: 5% B, 0 to 5 min: 5% B, 5 to 10 min: 20%, 10 to 65 min: 55%, 65 to 67 min: 100% B with A: H₂O/TFA 0.1% and B: CH₃CN 90%/H₂O 10%/ TFA 0.09%. • unlabelled hMMP-12 (Mw=17593.4 Da), * singly labelled hMMP-12 (Mw=18337.5 Da). **C)** In-gel fluorescence analysis of the labelling reaction of hMMP-12 (5 μ M and 100 nM) with probe 10 (10 μ M, 1 μ M and 100 nM) in reaction buffer after 4h at 37°C. Samples were subjected to 12% SDS-PAGE and analysed by in-gel fluorescence imaging (FL) and silver staining (SS). **D)** In-gel fluorescence analysis of hMMP12 hMMP-12 (100 nM) pre-incubated with competitive inhibitors at 1 μ M; hMMP-12 selective inhibitor (RXP470.1, lane 2), broad-spectrum phosphinic pseudo peptide (RXP500.1, lane 3), a hydroxamate derivative (GM6001, lane 4) and hTIMP-1 (lane 5). The samples were subjected to 12% SDS-PAGE and analysed by in-gel fluorescence imaging (FL) and silver staining (SS).

To comment further this aspect, we estimated the percentage of probe 9 or 10 /hMMP12 complex generated in solution once the equilibrium is reached. This depends on both hMMP12-probe relative concentrations and values of probes inhibition constants (K_i) towards hMMP12. By solving a quadratic equation with only one possible solution, the theoretical percentage of probe/hMMP12 complex as function to those parameters can be calculated (Table 3).

In the conditions of concentration that we used (5 μ M of hMMP12 and 10 μ M of probe), the theoretical percentage of probe/hMMP12 is superior to 99% regardless of the probe (Table 3 entry a and b). Thus, in

this concentration range, difference in K_i values between **9** and **10** does not rule the first affinity step. This may explain a similar labelling yield between the two probes towards hMMP12.

Entry	Probe 9 or 10/[nM]	hMMP12 [nM]	% Probe/hMMP12
a	Probe 9 / 10 000 nM	5 000 nM	>99%
b	Probe 10 / 10 000 nM	5 000 nM	>99%
c	Probe 10 / 1 000 nM	100 nM	>98%
d	Probe 10 / 100 nM	100 nM	69.8%

Table 3. Theoretical % of probe 9 or 10/hMMP12 complex at equilibrium in labelling buffer. This value was calculated from quadratic equation with only possible solution considering K_i value of 9 towards hMMP12 equal to 3.4 nM and that of 10 to 13.1 nM.

Interestingly, the labelling yield after 4h was not very different to that after 24h (40% vs 48%, see Figure 44A). This led us to conduct short-time labelling reactions within 4h. In these conditions, we explored labelling reactions of hMMP12 at two different concentrations (5 μ M, 100 nM) by probe **10** at 10 μ M, 1 μ M and 100 nM. As shown by Figure 44C, regardless the hMMP-12-probe **10** relative concentrations, the labelling efficiency was maintained and labelling yield was not substantially impacted. Comparable yields between condition 1 (hMMP12 at 5 μ M and probe **10** at 10 μ M) and condition 2 (hMMP12 at 100 nM and probe **10** at 1 μ M) can be explained by a similar percentage of hMMP-12/probe **10** complex in solution (Table 3, entry b and c). More surprisingly, the labelling yield in condition 3 (hMMP12 at 100 nM and probe **10** at 100 nM) is also similar, while only 70% of the hMMP-12/probe **10** complex is theoretically present in solution (Table 3, entry d). This may be due to the fact that during an affinity labelling process several other parameters are in play including I) rate of labelling and II) probe residence time within enzyme active site.

Next, we evaluated hMMP-12 (100 nM) labelling by probe **10** (100 nM) in presence of inhibitors (1 μ M) with different structures: I) parent RXP470.1 as hMMP12 selective inhibitor, II) a phosphinic pseudo peptide RXP500.1 (see annex A) as broad spectrum inhibitor of MMPs, III) a hydroxamate derivative GM6001 (see annex A) as broad spectrum inhibitor of metalloproteases¹⁵ and, IV) recombinant hTIMP1 as endogenous MMP inhibitors. After inhibitors pre-incubation (30 min for RXP470.1, RXP500.1 and GM6001 and 1h for hTIMP1) followed by 4h of labelling reaction, no hMMP12 labelling was observed when the active site was occluded by these inhibitors (lane 2 to 5, Figure 44D), thus confirming the specificity of the labelling reaction, with hMMP-12 catalytic cleft specifically targeted in this case.

6.7. Determination of residue(s) identity covalently modified within hMMP- 12 S₃' region

After validation of the hMMP12 specific labelling by probe **9** and **10**, we identified the amino acids covalently modified within the hMMP12 catalytic cleft. This has been performed after proteolytic digestion of the labelled hMMP12 followed by peptide mapping in mass spectrometry.

Based on our probe design and as discussed above, we hypothesised that the residues potentially targeted by acyl imidazole motif were Lys¹⁷⁷, Thr²¹⁰ and Tyr²⁴⁰ located within S₃' region of hMMP12 catalytic domain. By using ExPASy bioinformatics resource portal (https://web.expasy.org/peptide_mass/) and based on hMMP12 sequence, it was possible to anticipate peptide fragments generated under standard trypsin digestion (Figure 45A).

A) MGPVWR_K_HYITYR_INNYTPDMNR_EDVDYAIR_K_AFQWWSNVTPLK_FSK_INTGMADILVVFAR_GAHGDDHAFDGK¹⁷⁷_GGILAHAFGPGSGIGGDAHFDEDEFWTTTHSGGT²¹⁰NLFLTAVHEIGHSLGLGHSSDPK_AVMFPTY²⁴⁰K_YVDINTFR_LSADDIR_GIQSLYG

↓ cleavage by trypsin

GGILAHAFGPGSGIGGDAHFDEDEFWTTTHSGGT²¹⁰NLFLTAVHEIGHSLGLGHSSDPK
 GAHGDDHAFDGK¹⁷⁷
 AVMFPTY²⁴⁰K

B) M_GPWW_RKHY_ITY_RINNY_TPDM_NREDVDY_AIRKAF_QWW_SNVTPK_KF_SKINTGM_ADIL_VF_ARGAHGDDHAF_DGK¹⁷⁷GGIL_AHAF_GPGSGIGGDAHF_DEDEF_W_TTHSGGT²¹⁰NL_F_L_TA_VHEIGHSL_GL_GHSSDPKAVM_FPTY²⁴⁰KY_VDINTF_RL_SADDIRGIQSL_Y_G

↓ cleavage by chymotrypsin

DGK¹⁷⁷GGIL
 TTHSGGT²¹⁰NL
 FPTY²⁴⁰ or FPTY²⁴⁰KY

Figure 45. A) amino acids sequence of hMMP-12 and theoretical fragments generated by trypsin digestion. B) amino acids sequence of hMMP-12 and theoretical fragments generated by chymotrypsin digestion. Lys¹⁷⁷, Thr²¹⁰ and Tyr²⁴⁰ are labelled and coloured in red, green and blue respectively.

In this case, the theoretical fragment containing Thr²¹⁰ was composed of 56 amino acids. This size may be prohibitive during peptide mapping by mass spectrometry due to potential poor ionization properties. Moreover, a potential covalent modification of Lys¹⁷⁷ may prevent proteolytic cleavage after this residue,

which could lead to a fragment of 68 amino acids containing both Lys¹⁷⁷ and Thr²¹⁰. In addition to possible poor ionization properties resulting in sequencing issue for this fragment, this may complicate unambiguous identification of covalently modified residue within the peptide sequence. Based on these hypotheses, we chose to use chymotrypsin which performs proteolytic cleavage on C-terminus of amino acids with an aromatic/hydrophobic side chain. In this case, the theoretical fragments generated were of reasonable sizes (Figure 45B), even with a covalent modification of Tyr²⁴⁰ that may impair proper cleavage. The mass as (M+H)⁺ of the theoretical fragments crosslinked by the fluorescein and Cy3 tag are presented in Table 4.

Peptide sequence/ (M+H) ⁺	MH+ of peptide fragment crosslinked with Fluorescein tag	MH+ of peptide fragment crosslinked with Cy3 tag
DGK ¹⁷⁷ GGIL / 659.4	1148.5	1402.6
TTHSGGT ²¹⁰ NL / 887.4	1376.5	1630.6
FPTY ²⁴⁰ / 527.2	1016.3	1270.4
FPTY ²⁴⁰ KY / 818.4	1307.5	1561.6

Table 4. (M+H)⁺ of peptide fragments under chymotrypsin digestion covalently modified by Fluorescein of Cy3 tag.

After separation of unlabelled and fluorescein-labelled hMMP12 by RP-HPLC in conditions described above (see Figure 43), the labelled specie was collected, lyophilised and dissolved in appropriate buffer for chymotrypsin digestion. The evolution of the digestion was monitored by SDS gel. The digest was then analysed by LC/MS (Figure 46A). Interestingly, among different peptide fragments detected at 214 nm only one absorbed at 450 nm, a wavelength corresponding to fluorescein absorption. Further, this peak displayed a (M+H)⁺ of 1148.5 Da in electrospray/positive mode of ionisation suggesting a targeting of Lys¹⁷⁷. This fraction was collected and the peptide was sequenced by MS/MS (MALDI, positive mode of ionisation) (Figure 46B) (see par 17 for details).

The peptide sequence was unambiguously confirmed through b and y ions visualization and fluorescein-tag covalent attachment was evidenced by its release under MS/MS condition (peak at 464.1261 Da, Figure 46B). This release can be associated to a specific spectral signature of covalently modified fragment(s) by fluorescein-tag. MALDI-MS analysis of the crude digest did not reveal any peaks at 1376.5 or 1016.3/1307.5 Da that could be related to a covalent modification of Thr²¹⁰ or Tyr²⁴⁰ respectively. In addition MS/MS sequencing of peaks that did not belong to native hMMP12 sequence did not allow highlighting other fragments with a characteristic spectral signature related to fluorescein release (loss of 464.13 Da). These results suggested that Lys¹⁷⁷ was the sole residue modified within hMMP-12 S₃' region.

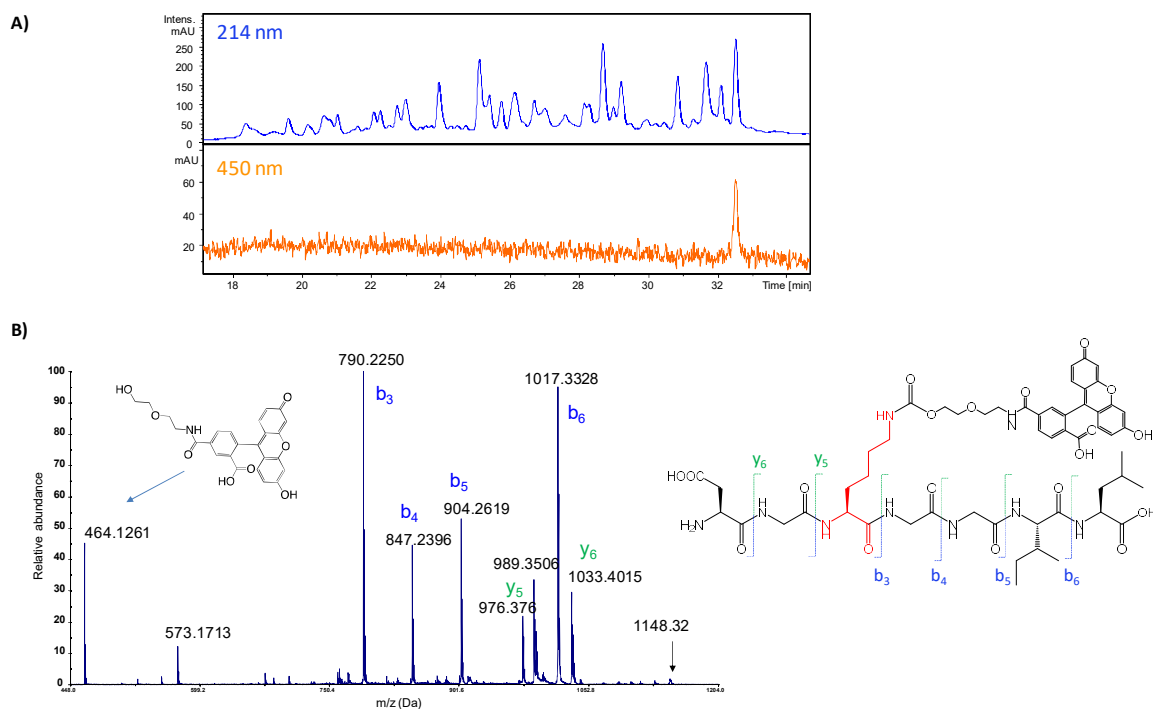


Figure 46. Identification of crosslinked residue(s) within fluorescein-labelled hMMP-12. A) Chromatogram of the chymotrypsin digest of fluorescein-labelled hMMP-12, (Bridge BEH300 column (21 x 150 mm, 3.5 μ m, Waters), flow rate = 0.2 mL.min⁻¹, initial conditions: 5% B, 0 to 5 min: 5% B, 5 to 10 min: 20%, 10 to 55 min: 70%, 55 to 57 min: 100% B with A: H₂O/TFA 0.1% and B: CH₃CN 90%/H₂O 10%/ TFA 0.09%). The analysis was performed at 214 nm and 450 nm. B) MS/MS sequencing of fluorescein-labelled peptide (1148.32 Da) in positive mode of ionisation, b ions are labelled in blue and y ions in magenta. Fluorescein tag released from the peptide appeared at 464.1261 Da.

Similarly, Cy3-labelled hMMP12 was submitted to chymotrypsin digestion and the resulting digest was analysed both by liquid chromatography coupled to fluorescence detection (Ex/Em= 550/570 nm) and by mass spectrometry (MALDI). As shown by Figure 47A, a single fluorescent fragment was detected. In mass spectrometry analysis, a mass of 1402.6 Da was measured and MS/MS sequencing unambiguously confirmed its identity (Figure 47B). Additional peaks that could be associated to covalent modification of Thr²¹⁰ or Tyr²⁴⁰ (1630.6, 1270.4 or 1561.6 Da) or peaks possessing a characteristic spectral signature (peak at 718.3 corresponding to a loss of Cy3 Tag) were not detected.

All these results showed an exclusive labelling of Lys¹⁷⁷ within hMMP12 S₃' region and validated our probe design. This lysine preference was in accordance with those previously reported for an acyl imidazole motif^{7,8,10}. In our case, the absence of labelling on Thr²¹⁰ and Tyr²⁴⁰ might be related to the nature of linker (lysine side chain) between the targeting moiety (pseudo peptide scaffold) and the reactive spacer. This linker could possess favourable topological features (length and flexibility) to induce a preferential Lys¹⁷⁷ labelling. In this regard, we do not exclude that other probes with linkers varying in length and flexibility would be able to target Thr²¹⁰ and Tyr²⁴⁰ with S₃ region.

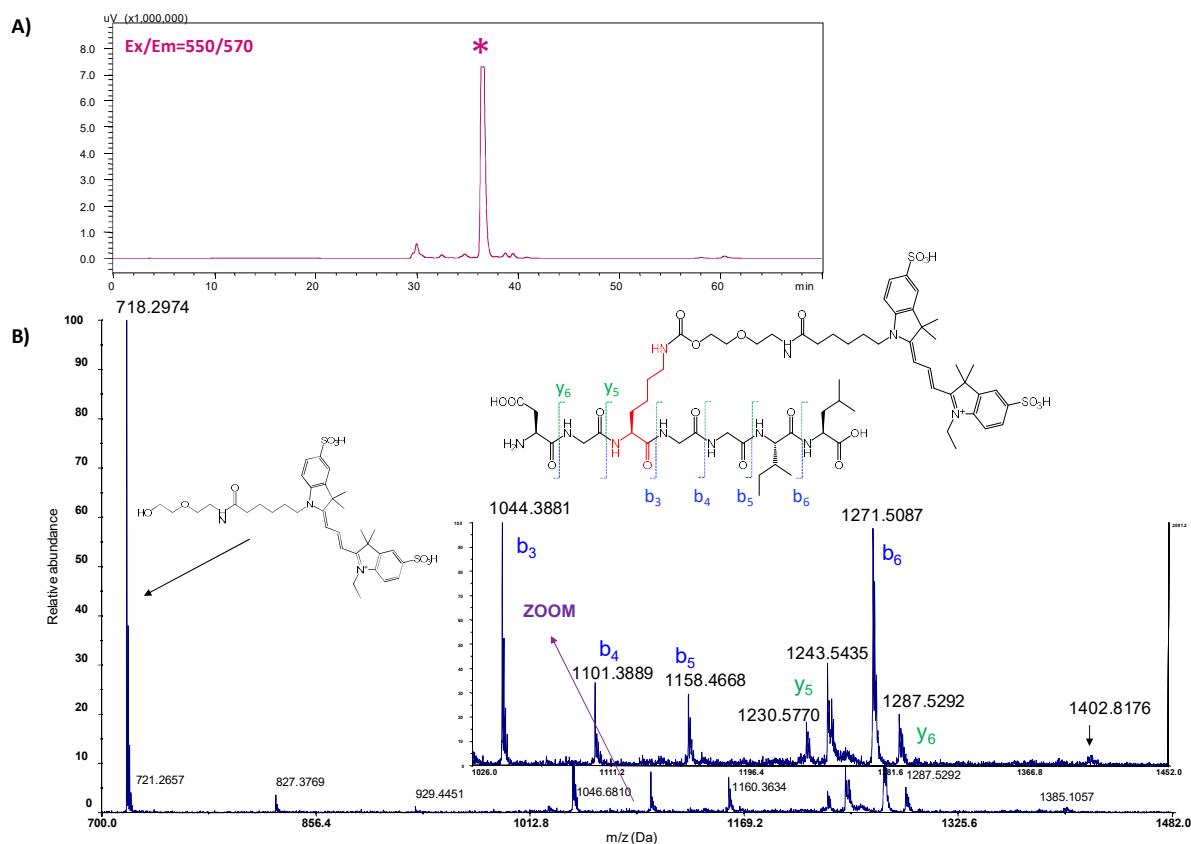


Figure 47. Identification of crosslinked residue(s) within Cy3-labelled hMMP-12. A) Chromatogram of the chymotrypsin digest of Cy3-labelled hMMP-12 in the following conditions: X Bridge BEH300 column, flow rate = 0.2 mL.min⁻¹, initial conditions: 5% B, 0 to 5 min: 5% B, 5 to 10 min: 20%, 10 to 65 min: 55%, 65 to 67 min: 100% B with A: H₂O/TFA 0.1% and B: CH₃CN 90%/H₂O 10%/ TFA 0.09%. Detection was performed in fluorescence (Ex/Em=550/570 nm). Fragment with fluorescent properties is labelled by a magenta star. b) MS/MS sequencing of peak at 1402.83 Da in positive mode of ionisation, b ions are labelled in blue and y ions in magenta. Cy3 tag released from the peptide appeared at 718.30 Da.

6.8. Impact of a labelling within hMMP12 S₃' region on its proteolytic activity.

We unambiguously demonstrated that a single labelling of Lys¹⁷⁷ occurred within the hMMP-12 S₃' region. In the next step, we wondered in which extent this modification could impact the hMMP12 proteolytic activity. Although lys¹⁷⁷ is located outside from the catalytic cleft (Figure 48A), its covalent modification by a bulky fluorescent reporter such as Cys3 could significantly perturb substrate binding and enzyme turn over.

To assess this hypothesis, the Cy3-labelled MMP-12 was first separated from unlabelled one by RP-HPLC in acidic conditions (Figure 44B). The concentration of isolated Cy3-MMP-12 was then determined by UV considering the extinction coefficient of Cy3 (150 000 M⁻¹.cm⁻¹) and, after dilution in activity buffer (1 nM final concentration), its proteolytic activity was evaluated in the presence of a synthetic substrate Mca-Pro-Leu- Gly-Leu-Dpa-Ala-Arg-NH₂ (Figure 48B for structure).

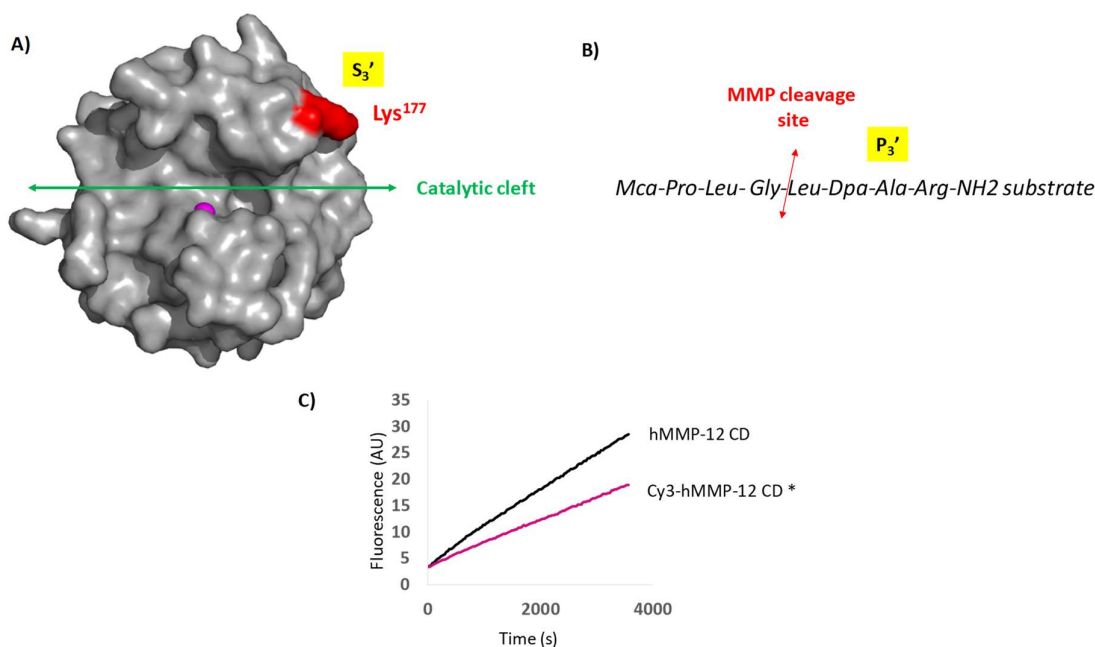


Figure 48. Evaluation of Cy3-labelled hMMP-12 proteolytic activity. **A)** Crystal structure of hMMP12 represented in surface representation and coloured in grey. Lys¹⁷⁷ is highlighted in red and catalytic zinc ion is a magenta sphere. Catalytic cleft is labelled by a green arrow. **B)** Sequence of synthetic fluorogenic substrate McaMat. The MMP cleavage site is marked with a red arrow and substrate P₃' position highlighted in yellow. **C)** Comparison between hMMP12 (1 nM) and Cy3-labelled hMMP12 (1 nM) proteolytic activity through a fluorogenic assay in 50 mM Tris-HCl buffer, pH = 6.8, 10 mM CaCl₂ at 25°C. Fluorescence increase induced by cleavage of Mca-Pro-Leu- Gly-Leu-Dpa-Ala-Arg-NH₂ substrate (9 μM) was recorded over 30 min.

Interestingly, the Cy3-hMMP-12 can efficiently cleave a fluorogenic substrate with however a slightly lower catalytic efficiency compared to that of unlabelled hMMP-12 (Figure 48C). In parallel, we showed that this protocol of purification did not impact the proteolytic activity of unlabelled hMMP-12. Thus, any loss of activity observed for Cy3-labelled hMMP-12 could be unambiguously assigned to the presence of a bulky hydrophobic cyanine 3 grafted on the distal Lys¹⁷⁷. This modification may affect I) proper hMMP12 refolding in the activity buffer II) substrate binding within catalytic cleft (K_M) and/or III) protease turnover (K_{cat}). Furthermore, it is worth mentioning that the used synthetic substrate for assessing proteolytic activity possesses a small side chain in P₃' (Figure 48B). The capacity of Cy3-labelled MMP-12 to process further substrates with different P₃' side chains and/or of different size, was not further explored. Nevertheless, we demonstrated that covalent labelling of hMMP-12 by probe **10** moderately perturbed its proteolytic activity. By comparison with standard activity-based probes directed towards proteases, this constitutes to our knowledge the first example of such probes described in the literature.

7. Labelling of others MMPs

7.1. A favorable structural context for extending the ligand-directed acyl imidazole chemistry to other MMPs

With the exception of their S_1' subsite, MMPs share high structural homology between their catalytic domains¹⁶. In this respect, a detailed analysis of the hMMP-2/3/8/9/10 and 13 S_3' region showed that these proteases displayed potential nucleophiles (Lys, Thr, Tyr, Ser or His) in comparable position and orientation to those found in hMMP12 (Figure 49A).

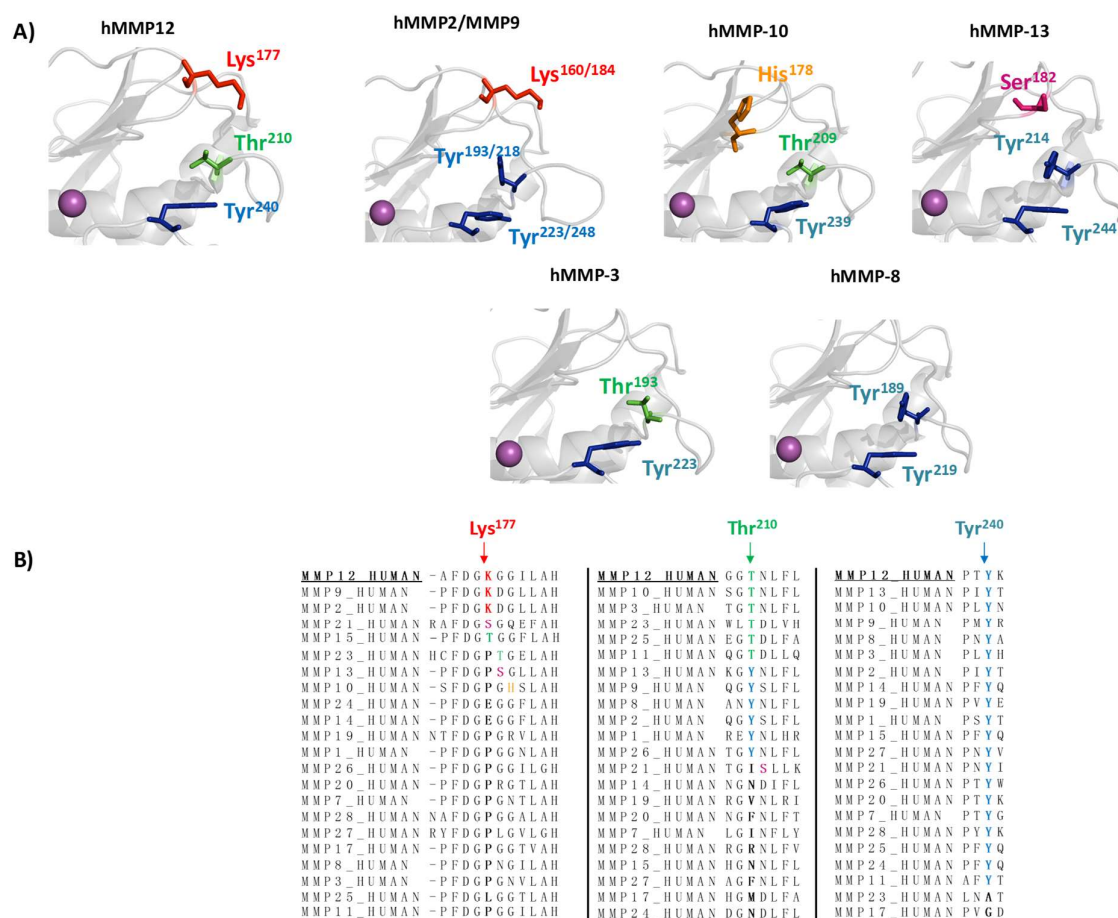


Figure 49. Comparison between the different S_3' regions of MMPs. A) Zoom on the S_3' region of hMMP12 (PDB code: 4GQL), hMMP2 (PDB code: 1QIB), hMMP3 (PDB code: 1QIA), hMMP8 (PDB code: 3TT4), hMMP9 (PDB code: 4H3X), hMMP10 (PDB code: 1Q3A) and hMMP13 (PDB code: 5B5O) catalytic domains. In the case of hMMP12, Lys¹⁷⁷, Thr²¹⁰ and Tyr²⁴⁰ are shown as red, green and blue sticks respectively. For the other MMPs, potential nucleophilic residues are shown as coloured stick according to the colour code used for hMMP12, in addition His (MMP10) and Ser (MMP13) residues are indicated in yellow and magenta respectively. The active site Zn_2^+ is shown as a magenta ball. B) Sequence alignment of 22 human MMPs, the positions equivalent to Lys¹⁷⁷, Thr²¹⁰ and Tyr²⁴⁰ within hMMP12 sequence were highlighted in bold. Potential nucleophilic residues are coloured according to the colour code used above.

Furthermore, a sequence alignment of 22 human MMPs showed that, except for hMMP17 that does not possess any, all these proteases display either one (MMP-7/14/19/20/24/27 and 28), two (MMP-1/3/8/11/15/23/25 and 26) or three (MMP-2/9/10/12/13 and 21) nucleophiles susceptible to be covalently modified by ligand-direct acyl imidazole chemistry. In this favourable structural context, we decided to assess the reactivity of probe **10** towards hMMP3 and 8 possessing two nucleophiles and hMMP2/9/10 and 13 with three ones within their S_3' subsites.

7.2. Evaluation of Probe 10 on a set of seven hMMPs

We first tested probe **10** (1 μ M) reactivity towards hMMP-2/3/8/9/10/12 and 13 (100 nM) over 4h at 37°C in labelling buffer. The labelling reaction was monitored at two time points (1h and 4h) by SDS-PAGE and in gel fluorescence imaging (Figure 50A and B).

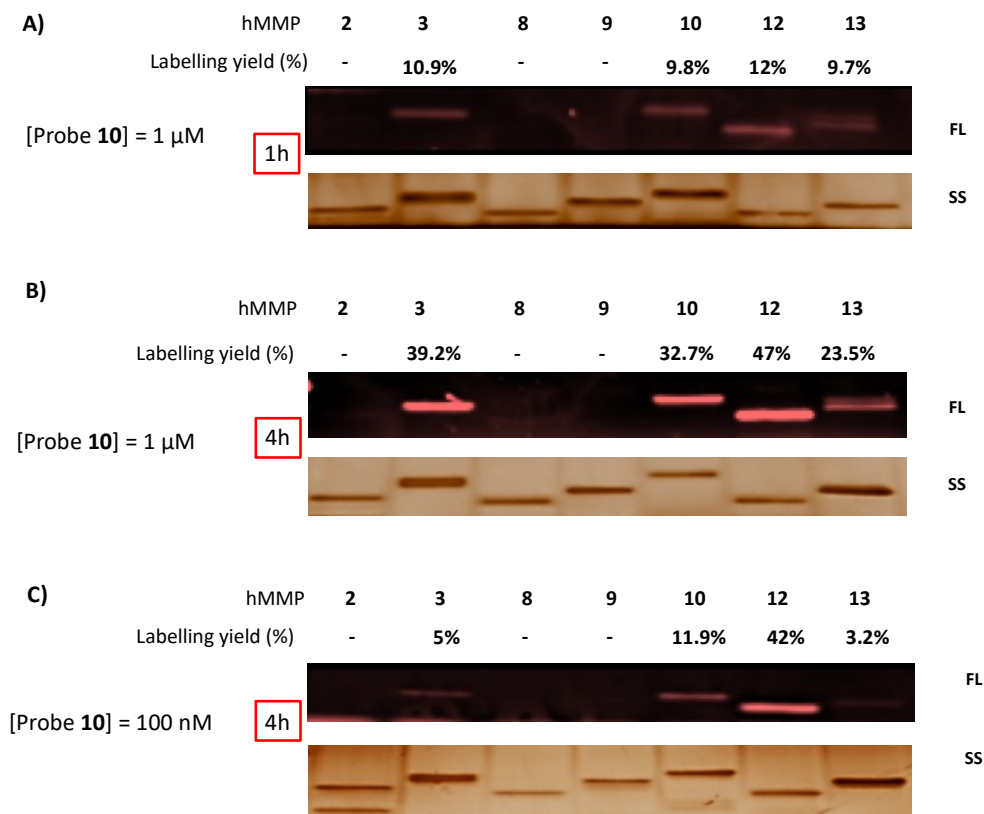


Figure 50. Labelling experiments of MMP-2/3/8/9/10/12 and 13 with probe 10. A) In-gel fluorescence analysis of hMMP catalytic domains (100 nM) labelled with probe 10 (1 μ M) after 1h of incubation at 37°C in labelling buffer. B) In-gel fluorescence analysis of same samples after 4 h of incubation. C) In-gel fluorescence analysis of hMMP catalytic domains (100 nM) labelled with probe 10 (100 nM) after 4h of incubation at 37°C in labelling buffer. All samples were subjected to 12% SDS-PAGE and analysed by in-gel- fluorescence imaging (FL). The presence of proteins was confirmed by silver staining (SS). For each condition/time, the percentage of labelling was determined from a standard (known amount of pre-labelled hMMP-12) loaded on the same gel after integration of the fluorescent bands.

Probe **10** (1 μ M) modified hMMP-12 in a privileged manner but also reacted with hMMP3, 10 and 13, with a labelling already detected after 1h, which significantly increased when the reaction time was prolonged to 4 h. These results could be commented considering the percentage of probe **10**/ hMMP complexes estimated in solution (Table 5).

% hMMP/probe 10 complex							
	hMMP2	hMMP3	hMMP8	hMMP9	hMMP10	hMMP12	hMMP13
Probe 10 [1 μM]	41%	40%	22%	<10%	85%	98%	52%
Probe 10 [100 nM]	<10%	<10%	14%	<1%	31%	70%	<10%

Table 5. Theoretical % of probe 10/hMMP complex at equilibrium in labelling buffer. This value was calculated from quadratic equation with only possible solution considering probe 10 K_i values towards hMMP determined in labelling buffer.

Particularly, the labelling of hMMP10 (32,7% yield at 4h) can be explained by a significant percentage of enzyme/probe **10** complex in solution (85%). Surprisingly, hMMP2, 3 and 13 are differently labelled while they displayed similar percentage of enzyme/probe **10** complex (41%, 40% and 52% respectively), with almost no detectable labelling for hMMP2 and a substantial labelling in the case of hMMP3 (39,2 % yield at 4h). These results illustrated again that beyond affinity step, the efficiency of labelling reaction was ruled by several other parameters including the reactivity/accessibility of targeted nucleophiles. When probe **10** was used at 100 nM, the selectivity in favour of hMMP12 was restored (Figure 50C), an observation in accordance with activity/selectivity profile determined for this probe towards a set of MMPs. Overall, these results suggested that nucleophiles within S_3' region of certain hMMPs were accessible for covalent modification.

7.3. Conception and validation of a broad-spectrum acyl imidazole probe directed towards hMMPs

The results obtained with probe **10** led us to envisage a second generation of probes that would possess a broad and efficient labelling capacity at low concentration. Notably, since the labelling efficiency is in part governed by the affinity step and residence time of the ligand within the active site, we decided to improve the probe binding constant towards MMP-2/3/8/9/10 and 13 by replacing the hMMP12 selective ligand part (RXP470.1-derived scaffold) with a broad-spectrum binder.

We previously demonstrated in phosphinic pseudo peptide series that a 3-(4-ethoxyphenyl) isoxazole P_1' side chain yielded (RXP500.1, Figure 51) a potent and pan-inhibitor of MMPs¹⁷. By relying on this

scaffold, we proposed the design of RXP500.1-derived probe **11** that harboured in P₃' the same Lys side chain conjugated to an acyl imidazole group and Cy3 tag than the one found in probe **10**.

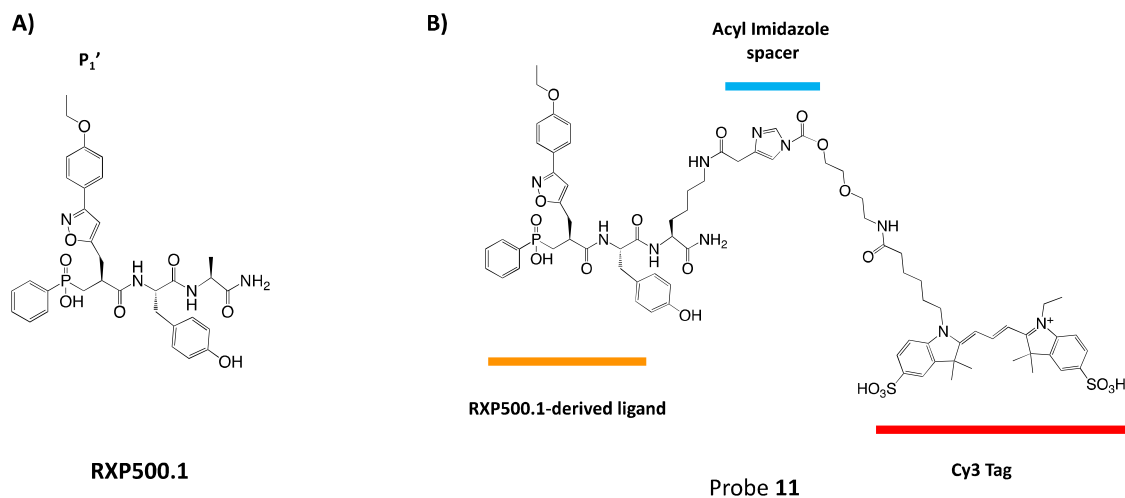


Figure 51. Chemical structure of A) RXP500.1 and B) RXP500.1-derived probe 11.

The synthesis of probe **11** was performed following the same chemical pathway as the one described for probe **9** and **10** (see experimental part 13.2.4 for details). The affinity and selectivity profile of **11** was then determined on a set of seven hMMPs (Table 6).

		Ki (nM)						
entry		hMMP-2	hMMP-3	hMMP-8	hMMP-9	hMMP-10	hMMP-12	hMMP-13
a	RXP500.1	2.0 ± 0.4	2600 ± 160	37 ± 17	0.8 ± 0.2	490 ± 40	1.7 ± 0.2	6 ± 1
b	Probe 11	35 ± 1	210 ± 30	530 ± 70	14 ± 3	92 ± 6	3.7 ± 0.3	117 ± 6
c	Probe 10	1355 ± 310	1430 ± 110	3500 ± 200	> 10000	155 ± 30	13.1 ± 1.3	875 ± 180

Table 6. Ki values (nM) of RXP500.1, probe 11 and probe 10 towards a set of MMPs in 20 mM HEPES, pH=7.5, 200 mM NaCl, 5 mM CaCl₂, 0.1 mM ZnCl₂ and 0.1% Brij-35. Ki values are determined at 25°C and are the mean ± SD of three experiments.

The P₃' modification of RXP500.1 resulted in a slight decrease of potency towards most hMMP except in the case of hMMP3 and 10 for which a gain of potency was surprisingly observed (Table 6 entry a vs b). We showed that, by comparison with probe **10**, probe **11** potency was improved for all tested

hMMPs with an affinity gain ranging from a factor 2 in the case of hMMP10 to a factor 710 for hMMP9 (entry b vs c).

Probe **11** was then tested at 100 nM on seven hMMP at the same concentration and the results presented in Figure 52.

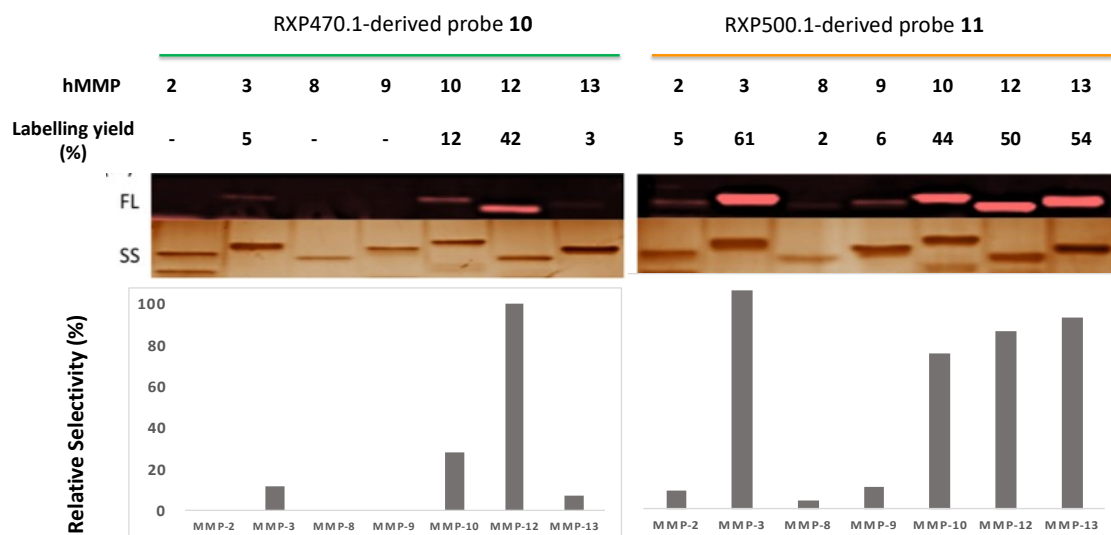


Figure 52. Comparison of hMMPs chemical labelling by probe **10** and **11**. In test tubes, hMMP-2/3/8/9/10/12 or 13 (100 nM) were incubated with probe **10** or **11** (100 nM) in labelling buffer. After 4h at 25°C, the samples were subjected to 12% SDS-PAGE and analyzed by in-gel fluorescence imaging (FL) and silver staining (SS). For each MMP, the yield of labelling was determined relatively to that of MMP-12.

By comparison with RXP470.1-derived probe **10**, RXP500.1-derived probe **11** was able to covalently modified the seven tested hMMPs with a substantial labelling of hMMP-3/10/12/13 and a faint but detectable one in the case of hMMP-2/8 and 9.

Thus, by increasing ligand binding capacity a change in labelling profile was induced, with probe **11** able to label seven hMMP while probe **10** only targeted 4 ones. Nevertheless, prolonging the probes residence time within the active-site does not ensure an efficient labelling for all MMPs members and other parameters have to be considered. This is first illustrated by the modest reactivity of probe **11** towards hMMP2 and 9 despite its excellent binding to these latter. In this case, despite a lysine in a comparable position to hMMP-12 Lys¹⁷⁷, the lack of reactivity may be explained by the presence of an adjacent acid aspartic with a negative charge that may stabilize lysine under its protonated state thus decreasing its intrinsic reactivity (Figure 53A).

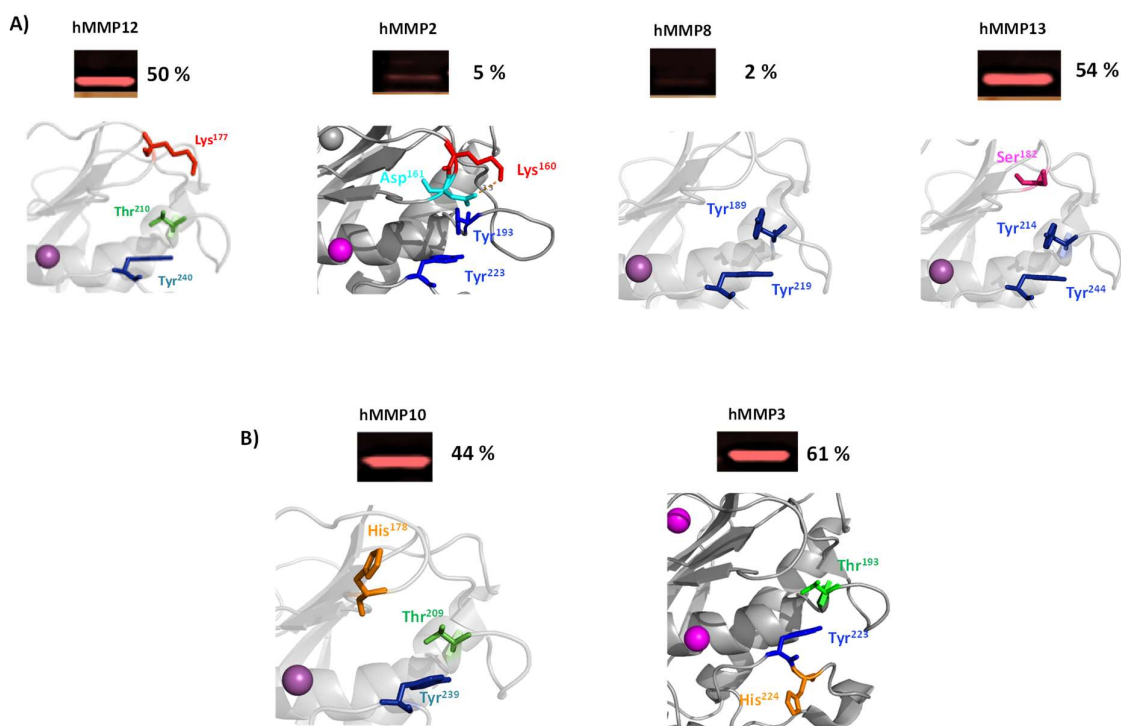


Figure 53. Comparison of hMMP12, 2, 8, 13, 10 and 13 S₃' region considering their labelling by probe 11. A) Comparison between hMMP12, 2, 8, 13 containing similar residues within S₃' region. B) Comparison between hMMP10 and 3 containing similar residues within S₃' region.

The modest labelling of hMMP2 and 9 also suggested a weak reactivity/accessibility of the two tyrosine (Tyr¹⁹³ and Tyr²²³ in the case of hMMP2, Figure 53A) towards probe **11**. This was consistent with the very weak labelling of hMMP8 only containing Tyrosine residues within its S₃' region. In this respect, the substantial labelling observed for hMMP13 suggested that residue preferentially targeted in this case was Ser¹⁸². Attempts to confirm this hypothesis was presented below.

A substantial labelling was observed for hMMP3 and 10. Interestingly, for both enzyme a Threonine and a Histidine are present with the S₃' region (Figure 53B). In the case of hMMP10, His¹⁷⁸ located within S₃' region upper part in similar position to that occupied by hMMP12 Lys¹⁷⁷ seems to be a reasonable candidate for covalent modification. On the other hand, His²²⁴ of hMMP3 does not seem appropriately oriented to react with acyl imidazole moiety likely pointing in the opposite direction. However, this His is located on a flexible loop and may adopt in solution a favourable orientation making it accessible for reaction. In addition, a strong reactivity of Thr residue common to the two hMMPs cannot be excluded. Attempts to confirm the residue(s) preferentially labelled within hMMP3 S₃' region are presented below.

In parallel, we compared the reactivity of probe **10** and **11** (100 nM) towards different concentration of hMMP12 (100, 50 and 25 nM, Figure 54)

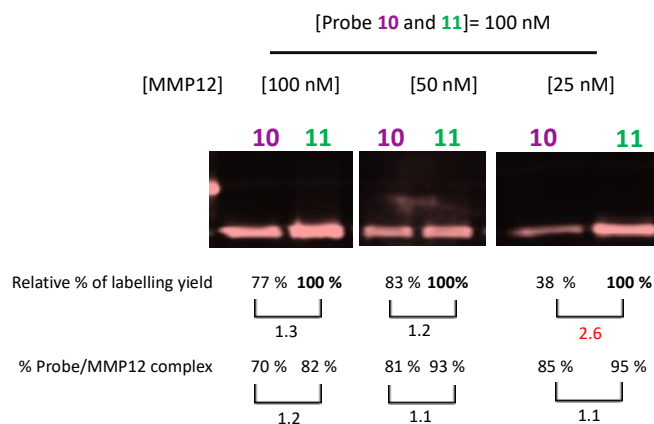


Figure 54. Comparison of hMMP12 chemical labelling by probe 10 and 11. In test tubes, hMMP12 (100 nM, 50 nM, 25 nM) was incubated with probe 10 or 11 (100 nM) in labelling buffer. After 4h at 25°C, the samples were subjected to 12% SDS-PAGE and analyzed by in-gel fluorescence imaging. The relative percentage of labelling was determined by integrating the bands fluorescent signal.

We first confirmed that probe **11** was slightly more reactive towards hMMP12 than probe **10**. In this range of concentration, the difference in K_i values between the two probes (13.1 nM for probe **10** vs 3.7 nM for probe **11**) resulted in difference of theoretical percentage of probe/hMMP12 complex in solution. At 100 or 50 nM of hMMP12, the difference in labelling yields between the two probes was in accordance with the percentage of probe/hMMP12, suggesting that the labelling reaction was mainly governed by the affinity step in this case. Very surprisingly, when hMMP12 was present at 25 nM, a discrepancy between relative percentage of labelling yield and percentage of probe/MMP12 complex was observed. This reliable observation is not fully understood but suggests either I) different physico-chemical properties (solubility and/or unspecific binding to the Eppendorf walls) between probe **10**/hMMP12 and probe **11**/hMMP12 complexes or II) different hydrolysis rate between the two probes that may impacts labelling yield at this relative ratio between hMMP12 and probe (only 25% of the probe is in complex with the protease). This aspect was not further explored and does not necessarily reflect probes behaviour in complex proteome.

Overall, by only changing the phosphinic peptide part, the probe efficiency and its selectivity profile were significantly modified, which results in a broad-spectrum probe competent for labelling of several hMMPs. This constitutes to our knowledge the first example of ligand-directed acyl imidazole chemistry validated in the context of selectivity within a family whose members are structurally very close.

7.4. Attempts to determine labelled residues within the S₃' region of hMMP- 13.

After observing significant labelling on hMMP-3/10/12/13 we were interested in defining the positions of a TAG also on others. hMMP13 was first examined and unlabelled and Cy-3 labelled hMMP13 were separated by RP-HPLC (the same conditions as for hMMP12). The labelled specie was collected, lyophilised and dissolved in BIC/ACN buffer (50% bicarbonate 100mM/ 50% acetonitrile pH=8) for trypsin digestion. After 12h of digestion in 25°C the digest was then analysed by RP-HPLC. Three different fragments were detected at 550 nm, a wavelength corresponding to Cy3 absorption. The fractions corresponding to these peaks were collected, freeze dried and analysed by MALDI-TOF. The fist peak A characterised by the highest intensity corresponded to the Cy3-TAG (718 Da). The fraction B comprised a peak which possessed a specific spectral signature 718 Da characteristic for labelled fragments. A part of the sequence close to Ser182 was identified what can suggest that Ser is the labelled nucleophile on hMMP13 however this result is ambiguous. The peak C corresponded to the mass 1673.72 while a specific spectral signature was not detected.

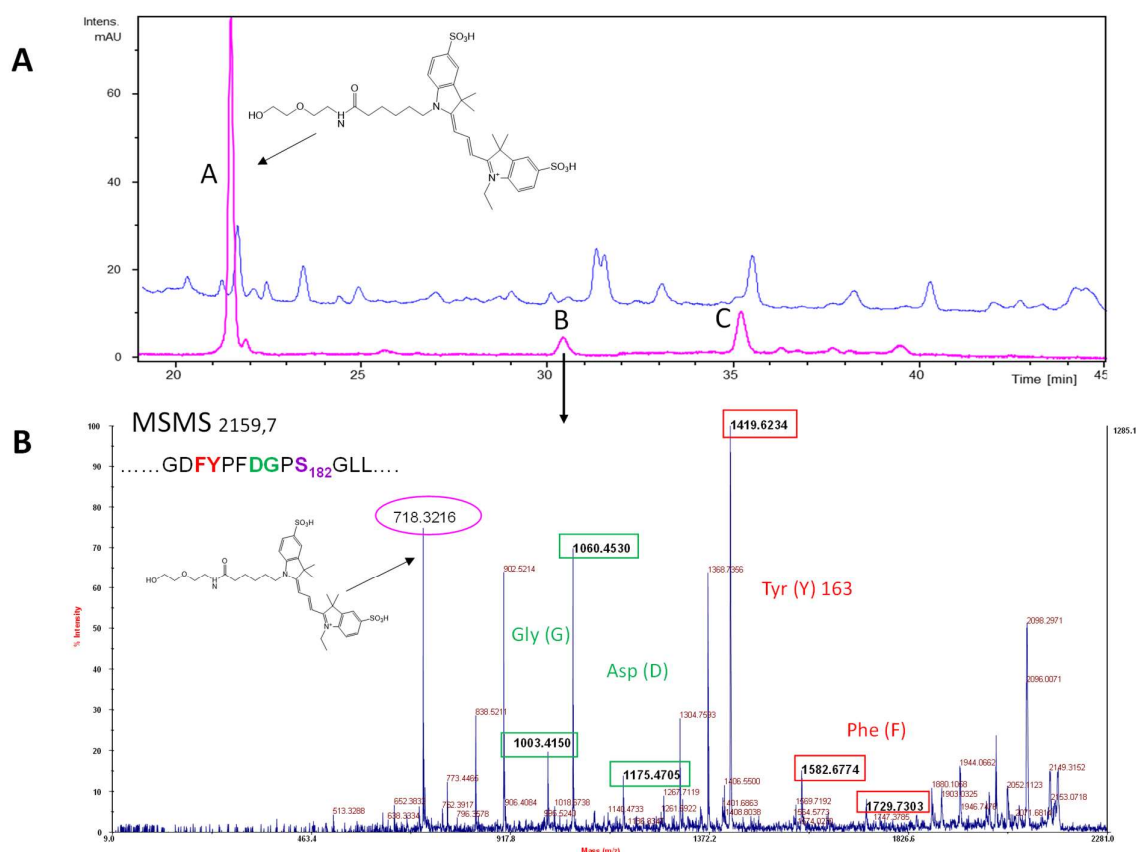


Figure 55. A)RP-HPLC analysis of tryptic digest of hMMP13 (X Bridge BEH300 column, flow rate = 0.2 mL.min⁻¹, initial conditions: 5% B, 0 to 5 min: 5% B, 5 to 10 min: 20%, 10 to 65 min: 55%, 65 to 67 min: 100% B with A: H₂O/TFA 0.1% and B: CH₃CN 90%/H₂O 10%/ TFA 0.09%) MS/MS of the peak 2159.7 Da.

8. Targeting hMMP12 active form in complex proteomes

Based on the results obtained in simple medium, we then explored the capacity of probes **9**, **10** and **11** to efficiently label recombinant hMMP12 catalytic domain spiked into media of increased complexity.

8.1. Labelling of hMMP-12 in presence of serum albumin.

First, the hMMP-12 labeling capacity of probe **9** was investigated in presence of human serum albumin (hSA). To this purpose, hMMP-12 (5 μ M) and increased concentration of hSA (5, 50 and 500 μ M) were incubated with probe **9** (10 μ M) at 37°C for 24 h (Figure 56A).

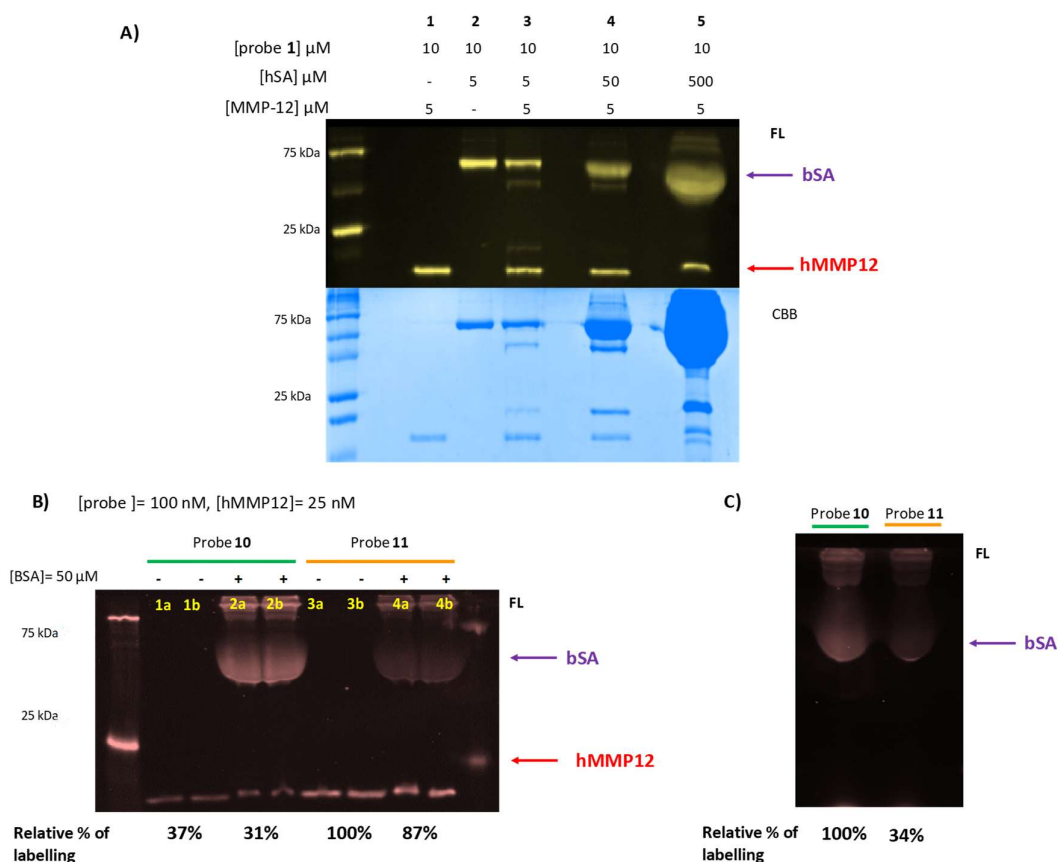


Figure 56. hMMP-12 labelling by probe 9, 10 or 11 in presence of Serum Albumin. A) MMP-12 (5 μ M) was incubated with probe 9 (10 μ M) in presence of increased concentration (5, 50 and 500 μ M) of human serum albumine (hSA) (YDRALBUM, LFB Biomedicaments, France). The labelling reaction was performed in labelling buffer for 24h at 37°C. B) MMP-12 (25 nM) was incubated with probe 10 or 11 (100 nM) in presence of bovine Serum Albumin (bSA) at 50 μ M for 4h at 37°C in labelling buffer. Relative % of labelling was determined by integrating the band intensity with labelling of hMMP12 by probe 11 corresponding to 100% (lane 3a/3b). C) Probe 10 or 11 (1 μ M) was incubated with 100 μ M of bSA for 4h at 37°C. Relative % of labelling was determined by integrating the band intensity with labelling of bSA by probe 10 corresponding to 100%. All the samples were resolved by 15% SDS-PAGE and analysed by in-gel fluorescence imaging (FL) and Coomassie brilliant blue (CBB) staining. Band corresponding to hSA or bSA is marked with a purple arrow and that of hMMP12 by red arrow.

Although partly consumed through a reaction with serum albumin, probe **9** conserved its capacity to react with hMMP12 regardless of hSA concentration. Remarkably, even when hMMP12/hSA ratio was 1/100, the labelling yield was not substantially affected (Figure 56A, lane 5).

We then compared the ability of Cy3-derived probes **10** and **11** to label hMMP12 in presence of bovine serum albumin (bSA). Thus, hMMP12 at 25 nM was incubated with either probe **10** or **11** at 100 nM and the labelling reaction was conducted in presence bSA at 50 μ M for 4h at 37°C. In this case, the ratio between hMMP12/bSA was 1/2000. For each probe, the labelling yield in presence of bSA was compared to that in absence of this latter. As shown by Figure 56B, the presence of 50 μ M of bSA did not significantly impact probe reactivity with a modest drop of labelling yield for the two probes (lane 1a/1b vs 2a/2b for **10** and lane 3a/3b vs 4a/4b for **11**). In addition, probe **11** appeared less prone to unspecific cross reaction with bSA than probe **10** (Figure 56B, lane 4a/4b vs 2a/2b). This was confirmed by incubating 100 μ M of bSA with 1 μ M of probe **10** or **11** for 4h at 37°C. As shown by Figure 56C, probe **11** reacted with bSA but in lesser extent relative to probe **10**, with a percentage of crosslink three times lower in this case.

The unspecific labelling component can be partly explained by a propensity of RXP470-targeting moiety to bind serum albumin¹⁸. Indeed, with a long polyaromatic side chain in P₁' and a negatively charged residue in P₂' position, RXP470.1 motif presents favourable features for binding to serum albumin. In this respect, shortening P₁' side chain and increasing its polarity (3-(4-ethoxyphenyl)isoxazole in the case of RXP500.1 motif) seems to reduce the unspecific component. The chemical nature of the Cy3 fluorescent tag could also contribute to unspecific binding but this aspect was not further investigated.

8.2. Labelling of hMMP12 in liver extract

We then examined the reactivity of probe **10** and **11** in mouse liver extract in which recombinant hMMP12 was added. The liver extract was prepared from harvested liver of C57B6 mouse solubilized in labelling buffer containing 1% v/v of protease inhibitor cocktail (no metalloprotease inhibitors in this case, see experimental part 16.1.1.1 for details). The content in proteins was measured by Bradford assay. All the hMMP12 labelling reactions were carried out in presence of 100 μ g of proteins liver extract and ran over 4h at 37°C.

We first demonstrated that probe **10** was able to detect active hMMP-12 spiked at 100 nM corresponding to 0.2% of the whole proteome (Figure 57A, lane 3 to 8). Although non-specific labelling of abundant proteins was observed, hMMP-12 was efficiently labelled by probe **10** at 1 μ M (Figure 57A, lane 2 and 3).

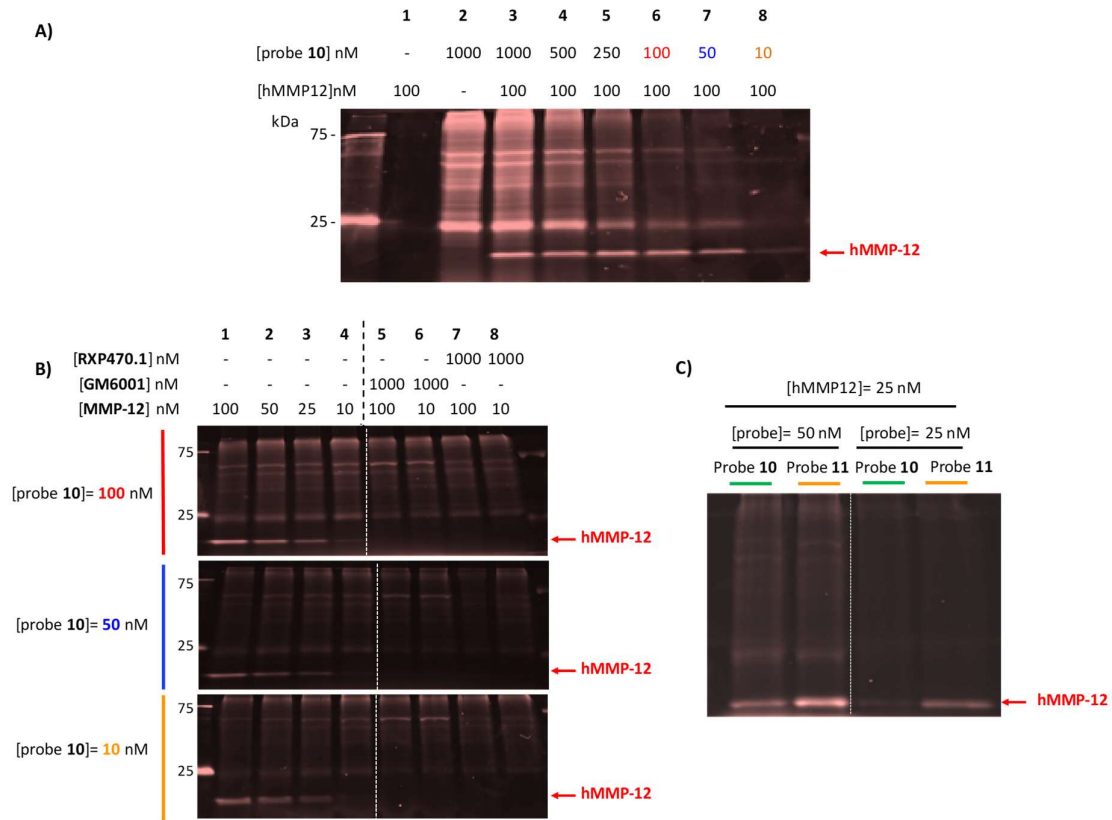


Figure 57. hMMP-12 labelling by probe 10 and 11 in mouse liver extract. A) In-gel fluorescence analysis of labelling reaction of hMMP-12 (100 nM, 200 ng, 0.2%) by probe 10 (1 μ M, 500 nM, 250 nM, 100 nM, 50 nM, and 10 nM) in mouse liver extract (100 μ g). B) In-gel fluorescence analysis of labelling reaction of hMMP-12 (100 nM, 50 nM, 25 nM and 10 nM) by probe 10 at different concentrations (100 nM red, 50 nM blue and 10 nM orange) in mouse liver extract (100 μ g). Competition experiments (lane 5 to 8) were carried out with RXP470.1 and GM6001 at 1 μ M and inhibitors were pre-incubated for 30 min before labelling. C) In-gel fluorescence analysis of labelling reaction of hMMP-12 (25 nM, 50 ng, 0.05%) by probe 10 and 11 at 50 nM and 25 nM. All the labelling reactions were performed for 4h at 37°C and samples were resolved by 12% SDS-PAGE followed by in gel-fluorescence imaging (λ_{ex} = 532 nm). Band corresponding to hMMP12 was identified by a red arrow.

More importantly, the unspecific component reduced while probe **10** concentration decreased (1 μ M, 500 nM, 250 nM, 100 nM, 50 nM and 10 nM, lane 2 to 8), with a selective labelling observed when the probe was used in a stoichiometric amount or as default relative to the target hMMP-12 (lane 6 to 8). We then further explored the labelling capacity of probe **10** at 100, 50 and 10 nM (Red, blue and orange panel respectively) towards decreasing quantities of hMMP12 (lane 1 to 4, Figure 57B). Irrespective of probe **10** concentration, up to 25 nM of hMMP12 can be efficiently labelled and detected, corresponding to 0.05% of whole proteome (lane 3). A detection limit was reached when hMMP12 and probe concentrations were used at 10 nM, with Cy3-labelled hMMP12 barely detected in this case (Figure 57B, orange panel, lane 4). In addition, pre-incubation of samples with either hMMP12

selective inhibitor RXP470.1 or hydroxamate GM6001 at 1 μ M prevented hMMP-12 labelling, thus confirming the labelling specificity (Figure 57B, line 5 to 8).

In the same complex proteome, we finally showed that 50 ng of hMMP12 (25 nM, 0.05% of the whole proteome) can be efficiently labelled and detected by probes **10** and **11**. However, probe **11** turned out more efficient and more selective than probe **10** to target hMMP12, specifically when used at 25 nM. The high labelling specificity observed for probe **11** was in accordance with its reduced propensity for unspecific interaction relative to **10**.

Overall, by relying on ligand-directed acyl imidazole chemistry up to 20 ng of hMMP12 spiked into 100 μ g of liver can be efficiently and selectively labelled. This quantity of active hMMP which corresponds to 0,02% of the whole proteins content, approximates the detection threshold displayed by previously reported photo labile probes for MMPs¹⁵.

A part of this work has been submitted as a full article to Chemical Science (see annex B). The article has been rejected in its current form and two major points were raised up by the referees. Both of them were critical about specificity of the approach and suggested to offer more promising data on the application of these probes to natural systems e.g. labelling of endogenous MMPs. However, we had the possibility to re submit this article if we were able to fully address the concerns raised by the reviewers. Since this review, the specificity of the probes has been further explored as shown above. Regarding the labelling of endogenous hMMPs, our attempts are presented in the following chapter.

9. Labelling of endogenous MMP12

The capacity of acyl imidazole probes to target endogenous MMP12 has been evaluated in three different systems: I) human dendritic cells stimulated by TNF- α and IL-10, II) mouse dendritic cells extracted from bone marrow and cultured and III) thioglycollate-stimulated mouse macrophages from peritoneal cavity. In this last case, acyl imidazole probes were tested according to two different protocols. In the first one, probes were assessed on cells extracted from the peritoneal lavage. In the second one, they were directly injected within the peritoneal cavity.

9.1. Labelling of human dendritic cells with acyl imidazole probe 10 and 11.

The expression and secretion of MMPs and TIMPs in monocyte-derived dendritic cell (DC) subpopulations has been recently described ¹⁹. Particularly, it seems that in response to activation signals (TNF α /IL10) MMP9 and 12 can be expressed by mature dendritic cells. In this case, MMP-9 and MMP-12 enzymes, act as relevant regulators in driving and directing dendritic cells migration. Noteworthy, in this study, the overexpression of MMP9 and 12 was only evidenced through transcriptomic data (variation in mRNA levels) and their proteolytic activity visualized by gelatinase zymography.

Preliminary to labelling experiments, we reinvestigated the binding capacity of probe **10** and **11** toward hMMP12 in TCNB buffer consisting of 50 mM Tris-HCl buffer, 10 mM CaCl₂, 150mM NaCl, 0.05% Brij, 1% v/v P8340 pH=7.5. This choice was guided by a recent study showing that MMPs proteolytic activity could be detected in human samples by using this buffer ²⁰. The two probes displayed comparable affinity constants in both labelling and TCNB buffers, with even a small gain in affinity in the case of probe **10** (Table 7).

	Ki (nM)/mMMP12		Ki (nM)/hMMP12	
	Activity buffer	Labelling buffer	Labelling buffer	TCNB buffer
Probe 10	14 \pm 1	150 \pm 21	13.1 \pm 1.3	4.9 \pm 0.5
Probe 11	9.5 \pm 1.1	43 \pm 5	3.7 \pm 0.3	3.5 \pm 0.3
RXP470.1	3.4 \pm 0.4	113 \pm 11	1.1 \pm 0.1	0.7 \pm 0.1

Table 7. Ki values (nM) of probes 10 and 11 as well as RXP470.1 towards mouse MMP12 (mMMP12) and human MMP12 (hMMP12). Ki are determined in i) Activity buffer: 50 mM Tris-HCl buffer, 10 mM CaCl₂, 0.1 % Brij-35, pH = 6.8, ii) TCNB buffer: 50 mM Tris-HCl buffer, 10 mM CaCl₂, 150mM NaCl, 0.05% Brij, 1% v/v P8340 pH=7.5 and iii) Labelling buffer: 20 mM HEPES, pH=7.5, 200 mM NaCl, 5 mM CaCl₂, 0.1 mM ZnCl₂ and 0.1% Brij-35. Ki values are determined at 25°C and are the mean \pm SD of three experiments.

Briefly, human CD14+ monocytes were purified by positive selection using magnetic microbeads and subsequently differentiated in monocyte-derived immature dendritic cells (iDC) by 5-day culture in presence of IL-4/GM-CSF. The secretion of MMPs was then induced in presence of TNF- α (10ng/ml) and IL-10 (40ng/ml) for two days at 37°C. At each step, the cells population was analyzed by flow cytometry and fluorescence-activated cell sorting (FACS), thus allowing to assess the efficiency of differentiation and stimulation (Figure 58A).

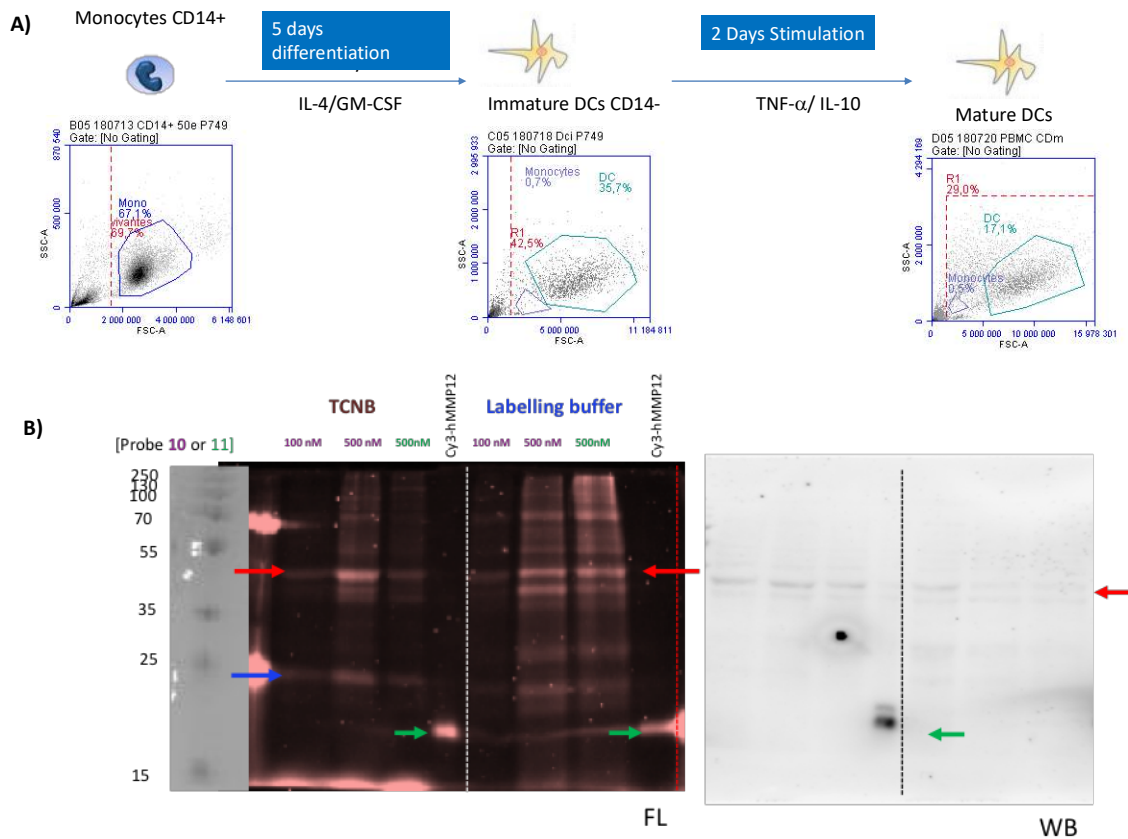


Figure 58. Human dendritic cells (DCs) labelled by probe 10 and 11. A) Human monocyte differentiation into immature DCs (iDCs) with IL-4/GM-CSF followed by iDCs stimulation in presence of TNF- α /IL-10. At each step, the cells population was analysed by flow cytometry and fluorescence-activated cell sorting (FACS) B) In-gel fluorescence analysis (FL) of labelling reactions on stimulated DCs in presence of probe 10 (100nM, 500nM) and 11 (500nM) in TCNB or labelling buffer. All the reactions were performed for 4h at 37°C and samples were resolved by 12% SDS-PAGE. After transfer from the gel to a PVDF membrane, the samples were stained with a primary antibody directed to mMMP12 (R&D, AF 3467 Mouse MMP-1, Polyclonal Goat Ig) followed by the incubation of secondary antibody (R&D, HAF 109 Goat IgG Peroxidase conjugated). The image of the Western blot (WB) was acquired using darkroom development techniques for chemiluminescence. Band potentially corresponding to hMMP12 were identified by a red arrow. Prelabeled Cy3-hMMP12 spiked into medium was marked with a green arrow.

At this stage, stimulated DCs were collected by trypsin treatment, washed, aliquoted (10^6 cells per batch) and centrifuged. After supernatant removal, cell pellets (10^6 cells) were then suspended in

either labelling or TCNB buffer (250 μ L) and the labelling reactions were performed in presence of probe **10** (100 nM or 500 nM) and probe **11** (500 nM) for 4h at 37°C. The samples were then centrifuged and the supernatant was removed for lyophilization. Resulting cells pellets and lyophilized supernatants were then suspended in Laemmli buffer (50 μ L) and samples were resolved by SDS-PAGE. Only the analyses of lyophilized supernatants are presented (Figure 58B).

Surprisingly, depending on the buffers significant differences in labelling were observed. Thus, several bands were visualized when labelling buffer was used while only a few was detected with TCNB buffer. This suggested a significant part of unspecific labelling in labelling buffer, an unspecific component that is reduced in TCNB buffer. This could be explained by a short half-life of the acyl imidazole probes in TCNB buffer that contains TRIS. As a consequence, in TRIS buffer, acyl imidazole probes could be more rapidly degraded than in labelling buffer and would only label proteins with which they potentially (and specifically?) interact. Regardless the nature of the buffer, two major fluorescent bands were observed: one at 40 KDa (marked with a red arrow) and one at 25 KDa (marked with a blue arrow). These two bands could be associated to the presence of MMPs active form labelled by probe **10** and **11**. However, these bands are less intense when probe **11** was used, an observation which was not consistent with observed difference in labelling capacity between the two probes specifically towards hMMP12.

In order to determine the identity of the labelled proteins at 25 and 40 KDa, a western blot was performed with an antibody directed to mMMP12. This antibody was not optimal but since it displayed approximately 20% of cross reactivity with human MMP-12, we considered it as a valuable tool for assessing the eventual presence of hMMP12 within the samples. Further, we demonstrated that Cy3-labelled hMMP12 (10 nM) spiked into the same cells samples can be I) recovered intact in the lyophilized supernatant (Figure 58B, lane Cy3-hMMP12, 1 pmol loaded, green arrow) and II) further detected by WB when mMMP12-directed antibody was used. Interestingly, only the band at 40KDa was stained by this antibody (Figure 58B). Based on these observations, we could postulate that this band corresponded to active hMMP12 still conjugated to its haemopexin domain. Importantly, competition experiments with GM6001 (5 μ M) did not unambiguously confirm the labelling specificity.

9.2. Labelling of endogenous mMMP-12

9.2.1. Validation of mMMP-12 labelling with acyl imidazole probe **10** and **11**

Before assessing acyl imidazole probes **10** and **11** in complex proteomes susceptible to contain endogenous mMMP-12, we needed to confirm the labelling capacity of these two probes towards this enzyme. Noteworthy, mMMP-12 only possess 64% sequence identity with the human form, with possible consequences on its binding property as well as its reactivity towards the two probes.

The inhibition constants of **10** and **11** towards mMMP-12 were first determined in labelling buffer. As shown in table 5, the two probes were ten times less potent towards mMMP-12 by comparison to hMMP-12. This drop of potency was also observed in the case of RXP470.1. In parallel, we assessed probes potency in activity buffer (50 mM Tris-HCl buffer, 10 mM CaCl₂, 0.1 % Brij-35, pH = 6.8). Importantly, at pH=6.8, a nano molar potency was restored for both probes as well as for RXP470.1. This gain in affinity was in accordance with our previous observations with a pH dependence upon phosphinic peptides binding to MMPs (see part 6.3 Figure 40). This substantial gain of affinity (10 fold) was critical since it allowed envisaging to perform affinity labelling experiment at lower probes concentration than those that could be used in the labelling buffer.

We first evaluated and compared probe **10** and **11** (100 nM) reactivity towards mMMP-12 and hMMP-12 (100, 50 and 25 nM) in labelling buffer. As illustrated by figure Figure 59, regardless the enzymes concentration the two probes were systematically more efficient to label hMMP12 relative to mMMP12 with a labelling capacity reduced by a factor 3 in all cases. This can be explained in part by a percentage of probe/MMP12 complexes which are 1.6-times (probe **11**) and 2.2-times (probe **10**) lower for mMMP12 than for hMMP12, a decrease related to a drop in **10** and **11** potency toward mMMP12 in labelling buffer.

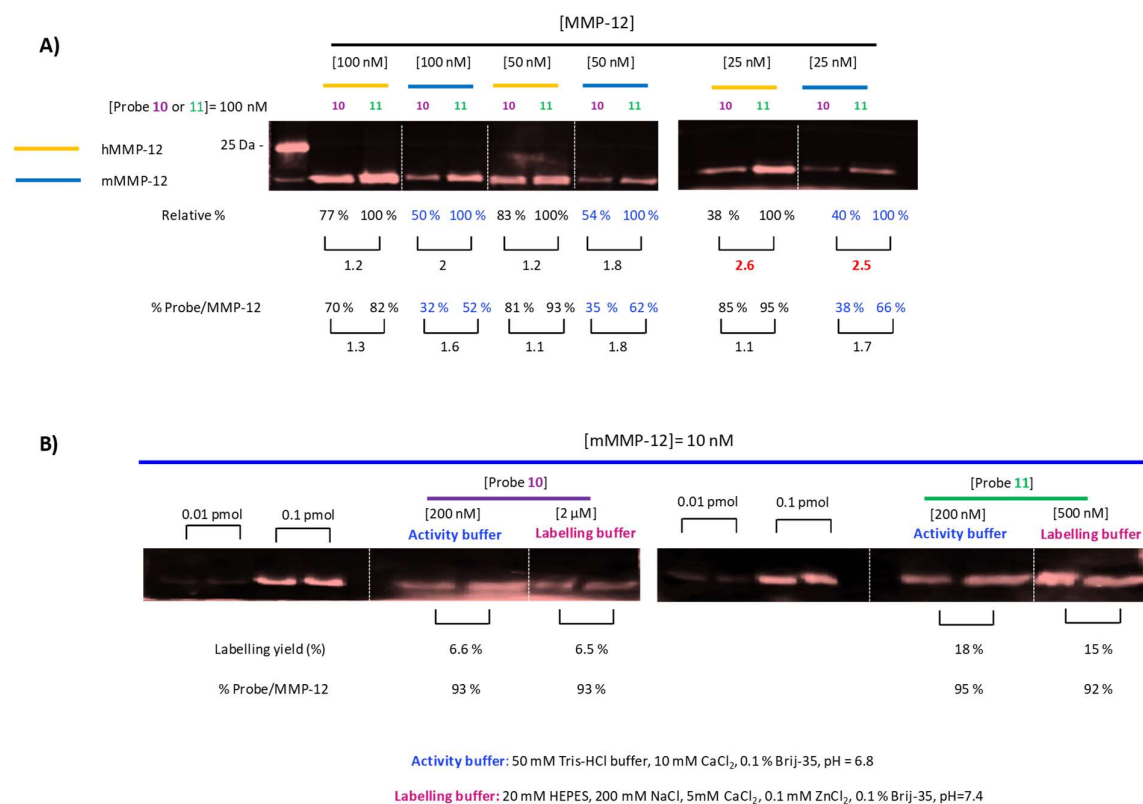


Figure 59. Comparison of hMMP12 and mMMP12 chemical labelling by probe 10 and 11. A) In test tubes, hMMP12 or mMMP12 (100 nM, 50 nM, 25 nM) were incubated with probe 10 or 11 (100 nM) in labelling buffer. After 4h at 25°C, the samples were subjected to 12% SDS-PAGE and analyzed by in-gel fluorescence imaging. The relative percentage of labelling was determined by integrating the bands fluorescent signal. B) In test tubes mMMP12 (10 nM) was incubated with probe 10 (200 nM, 2 μM) or 11 (200 nM, 500 nM) in activity (50 mM Tris-HCl buffer, 10 mM CaCl₂, 0.1 % Brij-35, pH = 6.8) and in labelling buffer (20 mM HEPES, pH=7.5, 200 mM NaCl, 5 mM CaCl₂, 0.1 mM ZnCl₂ and 0.1 % Brij-35) The experiments were performed in duplicate. After 4h at 25°C, the samples were subjected to 12% SDS-PAGE and analyzed by in-gel fluorescence imaging. The yields of labelling were determined from standards (0.01 and 0.1 pmol of Cy3-labelled hMMP12) loaded and imaged on the same gel.

Interestingly, as observed for hMMP12, probe **11** reacted 2-times more efficiently with mMMP-12 than probe **10**. This behaviour turned out critical when labelling experiments were performed at low concentration (25 nM). In this case, the Cy3-labelled mMMP-12 was barely detectable when probe **10** was used while it could be still visualized when labelled by probe **11**.

We also examined the capacity of probe **10** and **11** to label 10 nM of mMMP-12 conditioned either in activity or labelling buffer. Depending on the buffers, the probes concentrations were adjusted to afford more than 90% of probe/mMMP12 complex in solution. After 4h at 25°C, mMMP12 was covalently labelled by **10** with a yield of 6.5% in both buffers. In the case of probe **11**, the labelling yield was improved by a factor 3 and was similar in the two buffers. These results showed that labelling

efficiency was mainly governed by the percentage of probe/mMMP12 in solution with minor impact of the buffer. Particularly, the possible differences in probes half-life as function to pH and buffer did not seem to affect the reaction rate, at least in the conditions of time and temperature that we used.

We also determined the identity of the residue(s) modified within mMMP12 core. We first verified the eventual presence of nucleophilic residues within mMMP12 S₃' region. In absence of three-dimensional structure, this can only be assessed by aligning mMMP12 and hMMP12 sequences. Interestingly, mMMP12 possessed similar lysine (K²⁸¹), threonine (T²¹⁴) and Tyrosine (Y²⁴⁴) in comparable positions to those found within hMMP12 sequence (Figure 60).

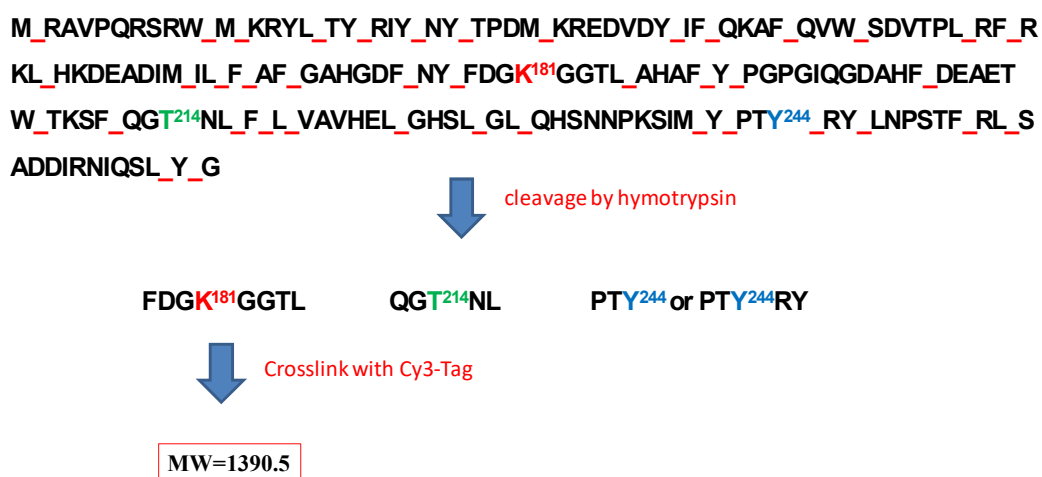


Figure 60. A) amino acids sequence of mMMP-12 and theoretical fragments generated by chymotrypsin digestion Lys¹⁸¹, Thr²¹⁴ and Tyr²⁴⁴ are coloured in red, green and blue respectively.

Based on these observations, we postulated that these three residues were targetable by probe **10** and chose chymotrypsin to generate three (or four) small peptides fragments potentially containing the crosslinked amino acids. As shown in Figure 61, after partial chymotrypsin digestion of Cy3-labelled mMMP12 followed by LC/fluo analysis of the digest, two major peaks were observed. These two peaks were collected and subsequently analysed by MALDI (MS and MS/MS sequencing). We thus demonstrated that one of the two peaks corresponded to the covalent modification of Lys¹⁸¹, a result in accordance with that obtained for hMMP12. More surprisingly was the presence of second peak corresponding to Cy3-tag. Indeed, before chymotrypsin digestion, Cy3-labelled mMMP12 was purified by RP-HPLC. Accordingly, the presence of the tag in the chymotrypsin digest would be more likely related to the labelling a second residue whose covalent bond with the Cy3-tag was unstable in the basic conditions of chymotrypsin digestion. However, this hypothesis needs to be further explored by modifying the conditions of digestion (pH, temperature).

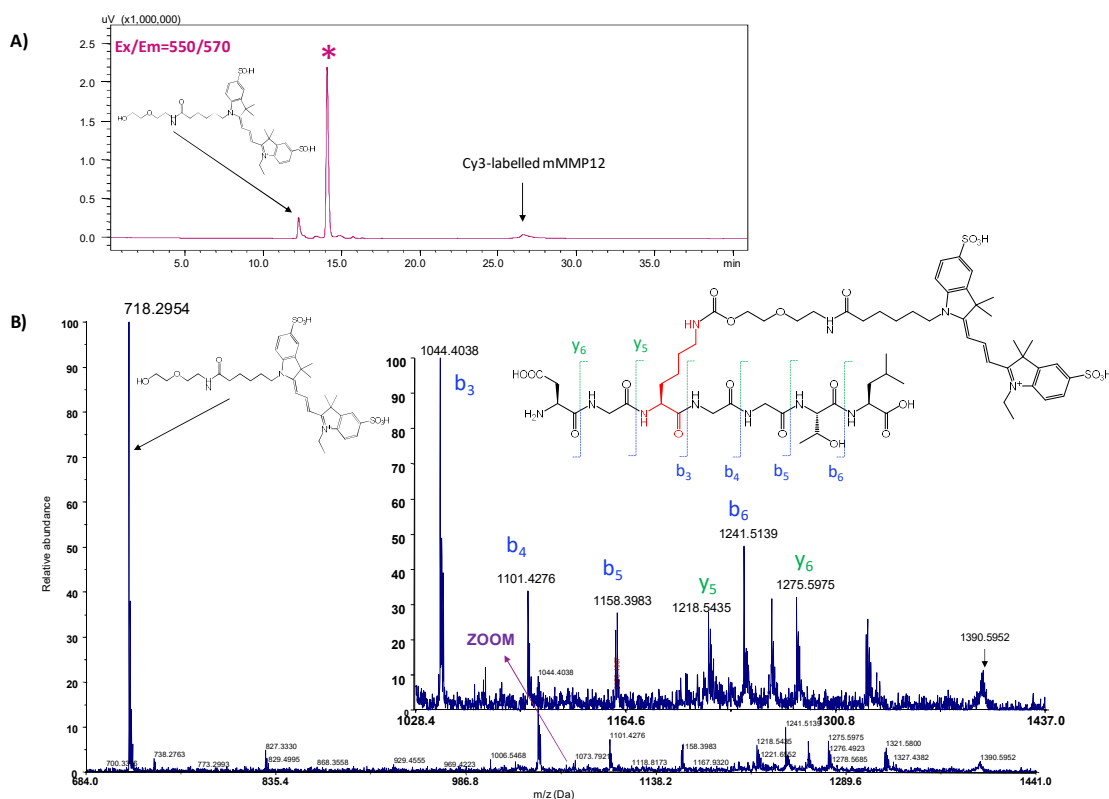


Figure 61. Identification of crosslinked residue(s) within Cy3-labelled mMMP-12. A) Chromatogram of the chymotrypsin digest of Cy3-labelled mMMP-12 in the following conditions: X Bridge BEH300 column, flow rate = 0.2 mL.min⁻¹, initial conditions: 5% B, 0 to 5 min: 5% B, 5 to 10 min: 20%, 10 to 65 min: 55%, 65 to 67 min: 100% B with A: H₂O/TFA 0.1% and B: CH₃CN 90%/H₂O 10%/ TFA 0.09%. Detection was performed in fluorescence (Ex/Em=550/570 nm). B) MS/MS sequencing of peak at 1390.5 Da in positive mode of ionisation, b ions are labelled in blue and y ions in magenta. Cy3 tag released from the peptide appeared at 718.2954 Da.

Overall, we demonstrated that both probes **10** and **11** could react with mMMP12.

9.2.2. Labelling of endogenous mMMP12 secreted by dendritic cells

As mentioned above, dendritic cells could be a source of endogenous MMPs particularly of MMP12. In this context, we decided to test probe **10** and **11** on murine dendritic cells stimulated by GMCSF and IL-4.

Briefly, bone marrow was obtained from tibias and femurs of C57BL6J mice collected under sterile conditions. Both ends of the bone were cut and a needle of a syringe was inserted into the bone cavity to rinse the bone marrow out of the cavity into a sterile culture dish with RPMI medium. After cells filtration and several lysis and centrifugation steps (see experimental part), cells were suspended in IMDM (Iscove's Modified Dulbecco's Medium) counted and cultured for 3 days at 37°C in presence of

GMCSF (10 ng) and IL-4 (10 ng). At day 3, DCs were collected from the supernatant. After trypsin treatment, centrifugation, washing and counting (11.10^6 DCs/mL), DCs were re suspended in IMDM and cultured in presence of GMCSF and IL-4 for three additional days at 37°C. At this stage, stimulated DCs were isolated from the supernatant by centrifugation. After supernatant removal, the cells pellets were washed, suspended in PBS buffer, aliquoted (5.10^6 DCs per batch) and centrifuged.

The labeling experiments were carried out on 5.10^6 of DCs cells after supernatant removal and resuspension in activity buffer (200 μ L, Tris buffer 50mM, $CaCl_2$ 10mM, pH=6.8) containing 0.1% v/v of P8340 inhibitors cocktail. Probe **10** and **11** were incubated at 1 μ M for 4h at 37°C. Competition experiments with either RXP470.1 or RXP500.1 (50 μ M) were performed in parallel. In addition, mMMP12 (10 nM) was spiked into cell samples in absence or in presence of RXP470.1 at 50 μ M. After 4h, the samples were centrifuged and supernatants were collected and freeze-dried. After solubilization in Laemmli buffer (50 μ L), the resulting samples were resolved by SDS-PAGE (Figure 62).

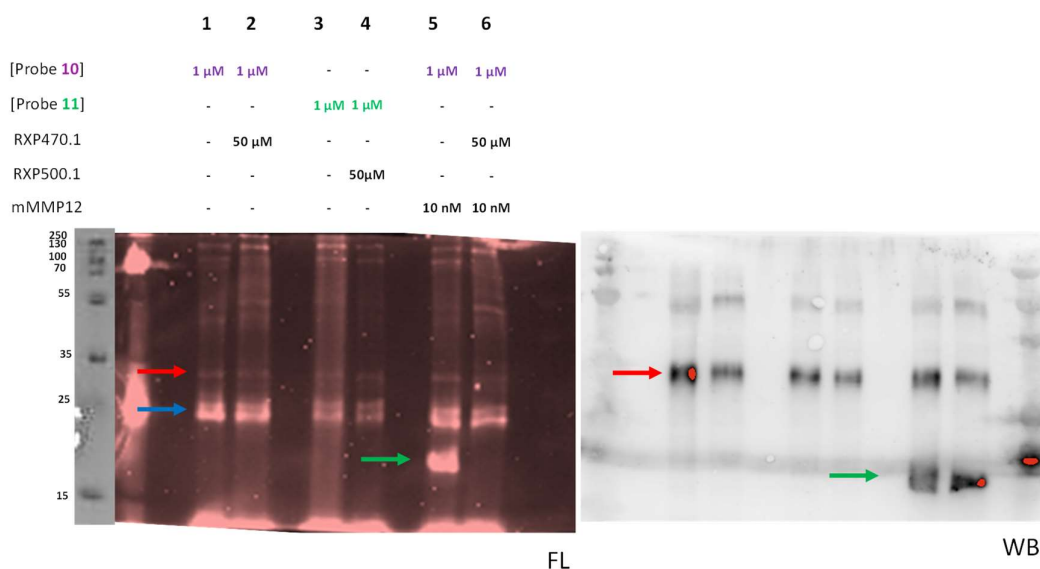


Figure 62. Labelling of murine DCs. In gel-fluorescence analysis (FL) of DCs supernatants after 4h labelling at 37°C by probe 10 (lane 1) or 11 (lane 3) at 1 μ M in absence or in presence of competitive inhibitors RXP470.1 (lane 2) or RXP500.1 (lane 4) inhibitor. Lane 5: supernatant containing pre-spiked recombinant mMMP12 (10nM). Lane 6: same conditions with 50 μ M of RXP470.1. All samples were resolved by 12% SDS-PAGE. After transfer from the gel to a PVDF membrane, the samples were stained with a primary antibody directed to mMMP12 (R&D, AF 3467 Mouse MMP-1, Polyclonal Goat Ig) followed by the incubation of secondary antibody (R&D, HAF 109 Goat IgG Peroxidase conjugated). The image of the Western blot (WB) was acquired using darkroom development techniques for chemiluminescence. Band corresponding to endogenous mMMP12 was marked by a red arrow, that corresponding to recombinant mMMP12 by a green arrow.

As shown by Figure 62, the 4h-treatment by probe **10** and **11** led to the observation of three major bands: two possessing a molecular weight around 25KDa (Figure 62, blue arrow) and a faint one around 30 KDa (red arrow). The labelling of band at 30kDa was slightly prevented by the presence of

competitive inhibitors (lane 2 and 4). Importantly, recombinant mMMP12 at 10nM (green arrow) was unambiguously labelled by probe **10** (lane 5) and the presence of RXP470.1 clearly abolished its labelling (lane 6). Western blot of the gel with an antibody directed to mMMP12 showed that only the band at 30 KDa was stained. In addition, recombinant mMMP12 was unambiguously stained by the antibody. From these observations, some conclusions were drawn. First, although protein at 30kDa did not clearly respond to competition, it could correspond to an endogenous form of mMMP12 since it was revealed by an mMMP12-direct antibody. Furthermore, such molecular weight is consistent with that reported for endogenous mMMP12 detected through elastin zymography ²¹. Based on WB analysis, the two bands at 25KDa (blue arrow) did not seem corresponding to mMMP12. These labelled bands could be associated to the presence of other active MMPs. However, competition experiments did not clearly confirm the labelling specificity.

In any event, our data suggest that probe **10** and **11** can react with a protein that may correspond to an endogenous form of mMMP12. Nevertheless, as shown by the presence of additional fluorescent bands of higher intensity, a significant nonspecific labelling also occurs.

9.2.3. Labelling of mMMP12 secreted by thioglycollate-stimulated mouse macrophages

The thioglycollate-stimulated mouse macrophages have been reported as a source of endogenous mMMP12 ²¹⁻²⁵. In all these studies, while mMMP12 overexpression has been evidenced both at the gene (transcriptomic approach) and protein level (western blot with mMMP12-directed polyclonal antibodies), the transient presence of mMMP12 under its active form has been visualized only indirectly through casein ²⁴ or elastin zymography ²¹.

According to previously reported protocols ²⁵, injection of thioglycollate within the peritoneal cavity of C57BL6J mice induced an acute inflammation that leads to the recruitment of macrophages. After 4 days of inflammation, thioglycollate-stimulated macrophages were collected from the peritoneal cavity by using a lavage solution cooled at 4°C (PBS containing 0.1% v/v of P8340 inhibitors cocktail). The lavage solution was then centrifuged and the cells pellets were collected and resuspended in PBS for counting. Cells were then dispatched in aliquot (5.10⁶ cells per batch), centrifuged, and resuspended in 200 µL of activity buffer (Tris buffer 50mM, CaCl₂ 10mM, pH=6.8) containing 0.1% v/v of P8340 inhibitors cocktail. The labelling reaction was performed over 4h at 37°C with probe **10** or **11** at 1 µM and 100 nM in presence or in absence of competitors. In parallel, labelling experiments were also performed on cells samples containing recombinant mMMP12 at 10nM.

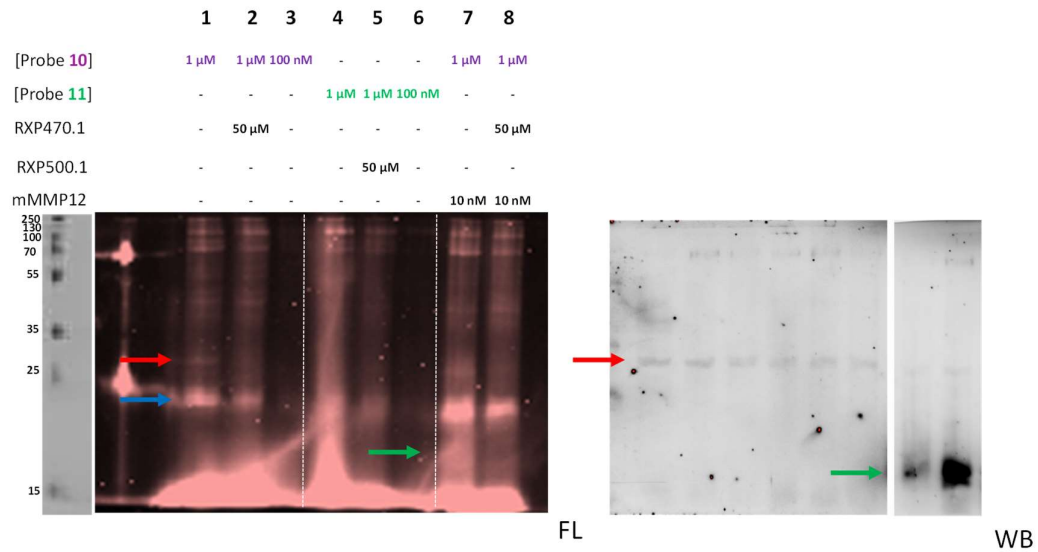


Figure 63. Labelling of murine thioglycolate-stimulated macrophages. In gel-fluorescence analysis (FL) of supernatants after 4h labelling at 37°C by probe 10 (1 μ M-lane 1 and 100 nM-lane 3) or 11 (1 μ M-lane 4 and 100 nM-lane 6). Lane 2: Competition experiment in presence of competitive inhibitors RXP470.1 at 50 μ M, lane 5: Competition experiment in presence of competitive inhibitors RXP470.1 at 50 μ M. lane 7: supernatant containing pre-spiked recombinant mMMP12 (10nM). Lane 8: same conditions with 50 μ M of RXP470.1. All samples were resolved by 12% SDS-PAGE. After transfer from the gel to a PVDF membrane, the samples were stained with a primary antibody directed to mMMP12 (R&D, AF 3467 Mouse MMP-1, Polyclonal Goat Ig) followed by the incubation of secondary antibody (R&D, HAF 109 Goat IgG Peroxidase conjugated). The image of the Western blot (WB) was acquired using darkroom development techniques for chemiluminescence. Band corresponding to endogenous mMMP12 was marked by a red arrow, that corresponding to recombinant mMMP12 by a green arrow.

As described in the case of DCs, the samples were then centrifuged and supernatants were collected and freeze-dried. After solubilization in Laemmli buffer (50 μ L), the resulting samples were resolved by SDS-PAGE (Figure 63).

Interestingly, we observed two main fluorescent bands, with similar molecular weight than those observed in the case of DCs: one at 25KDa (blue arrow) and another at 30 KDa (red arrow). Importantly, the presence of RXP470.1 prevented the labelling of 30KDa band (Lane 1 vs 2). Disappointingly, when probe 10 was used at 100 nM no band was detected at 30 KDa (lane 3). The result obtained with probe 11 were more difficult to interpret and will have to be repeated. Similarly, in the case of recombinant mMMP12 spiked into cells sample, the labelling and competition experiments (lane 7 and 8) were not clearly explicit. In accordance with our observation on DCs, western blot analysis revealed that band at 30KDa could be associated to an mMMP12 endogenous form.

Based on these results, we decided to inject probe 10 directly in the peritoneal cavity after four days of inflammation. Such a protocol reduced the number of handling steps on samples and accordingly

could limit eventual degradation of MMPs under their active forms. As illustrated by Figure 64A, after four days of inflammation, a 4°C lavage solution (Tris buffer 50mM, CaCl₂ 10mM, pH=6.8, 0.1% v/v of P8340 inhibitors cocktail) containing probe **10** at 1 μM was used to collect the stimulated-macrophages. The solution was incubated for 4h at 37°C and then centrifuged. The supernatant was collected for subsequent freeze drying and subsequently resolved in duplicate by SDS-PAGE followed by in-gel fluorescent imaging (Figure 64B).

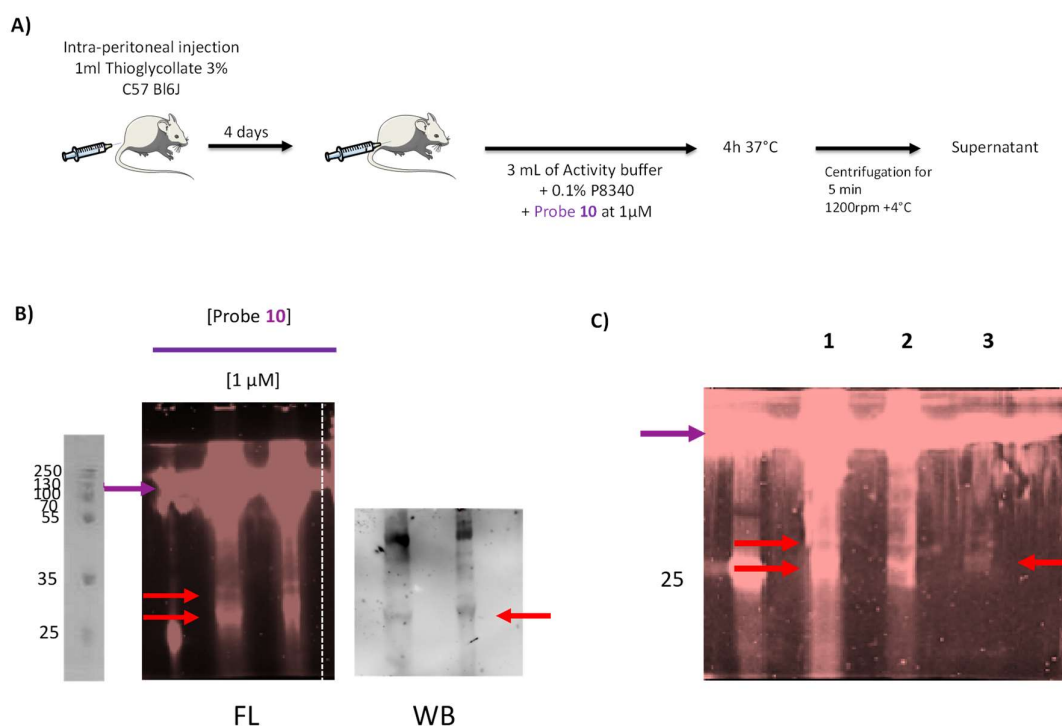


Figure 64. Labelling of murine thioglycolate-stimulated macrophages in the peritoneal cavity. *A) Schematic representation of the labelling protocol consisting in labelling the macrophages directly in the peritoneal cavity. B) In gel-fluorescence analysis (FL) of supernatant after 4h labelling at 37°C by probe **10** (1 μM). The sample samples were resolved by 12% SDS-PAGE. After transfer from the gel to a PVDF membrane, the samples were stained with a primary antibody directed to mMMP12 (R&D, AF 3467 Mouse MMP-1, Polyclonal Goat Ig) followed by the incubation of secondary antibody (R&D, HAF 109 Goat IgG Peroxidase conjugated). The image of the Western blot (WB) was acquired using darkroom development techniques for chemiluminescence. C) In gel-fluorescence analysis of supernatant before (lane 1) and after immunocapture (lane 2), fluorescent proteins released from the beads functionalized by mMMP12-directed antibody (Lane 3). Band corresponding to endogenous mMMP12 was marked by a red arrow and that corresponding to serum albumin was marked by a purple arrow.*

Three fluorescent bands were observed: one at high molecular weight likely associated to unspecific labelling of serum albumin (purple arrow) and two bands whose molecular weights were comprised between 25 and 30 KDa (red arrow). Importantly, these two bands were stained by mMMP12-directed antibody. In parallel, we showed that these bands could be selectively immunocaptured by

Dynabeads™ Protein G (ThermoFisher Scientific) on which mMMP12-directed antibody was installed (Figure 64C). In-gel digestion of these fluorescent bands by either trypsin or chymotrypsin did not allow to unambiguously confirm the identity of the crosslinked protein. Due to the low amount of proteins on the gel, these procedures have to be further optimized. In parallel, biotin analogues of probe **10** and **11** (see experimental part 13.2.4) were recently synthesized and could turn out useful to address this issue.

All of our data are consistent with the labelling of endogenous forms of mMMP12 by acyl imidazole probes **10** and **11**. If unambiguously confirmed, this would constitute the first example of labelling of MMPs endogenous forms without any photo activation. Our data also showed that these affinity probes provide a significant unspecific labelling of proteins in high abundance (e.g. serum albumin).

10. Comparison between Ligand-directed tosyl and acyl imidazole chemistry.

By comparison with ligand-directed acyl imidazole chemistry, the tosyl chemistry displays some limitations including a rather slow labelling rate and limited reactive amino acids (His, Tyr and Glu)²⁶ Nevertheless, a limited reactivity of chemically sensitive spacer could also allow limiting unspecific labelling component in complex proteomes. In this context, we synthesised a RXP470.1-derived probe harbouring a tosyl group in place of acyl imidazole spacer (probe **19**, Figure 65A) and evaluated its labelling capacity towards seven hMMPs

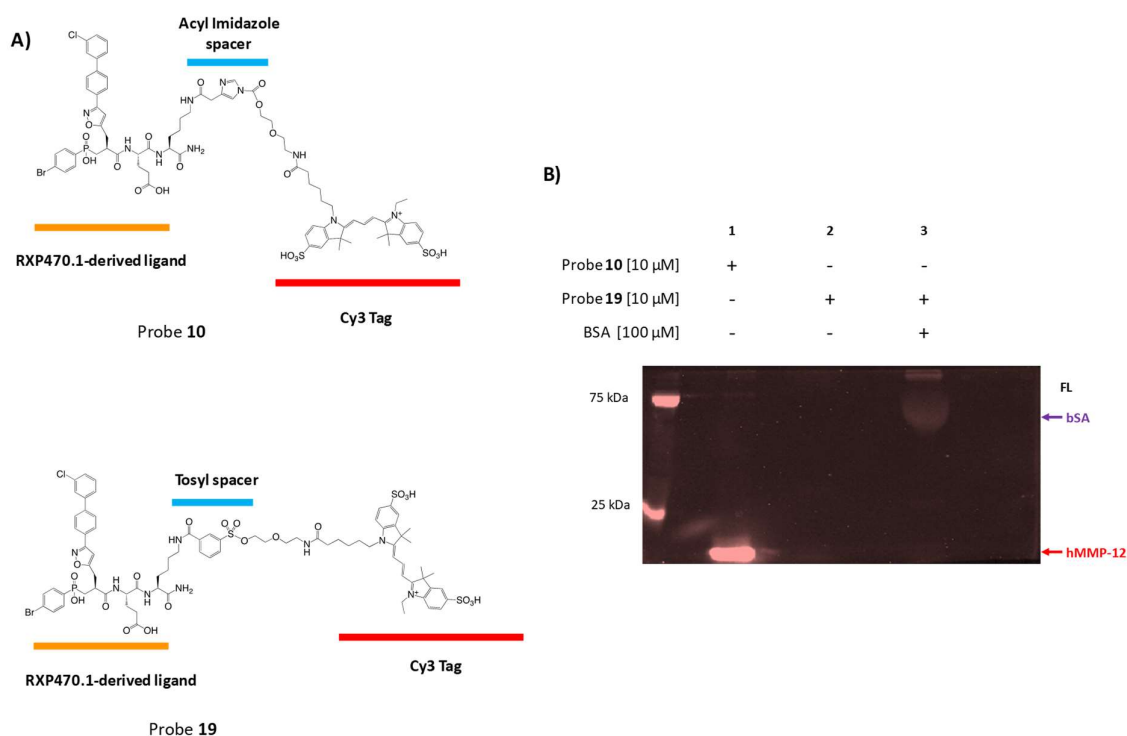


Figure 65. hMMP-12 labelling capacity comparison between acyl imidazole probe **10** and tosyl probe **19**. **A)** Structure of RXP470.1-derived probe **10** and **19** with an acyl imidazole and a tosyl chemically sensitive spacer respectively. **B)** In-gel fluorescence imaging of hMMP12 (1 μ M) labelled with probe **10** (lane 1) and probe **19** (lane 2) at 10 μ M after 24h at 37°C. In the same conditions, the labelling of bSA (100 μ M) by probe **19** was also analysed (lane 3). All the samples were resolved by 15% SDS-PAGE. Band corresponding to bSA is marked with a purple arrow and that of hMMP12 by red arrow.

Probe **19** was synthesised in a single step from amino acid precursor **1**, 3-Chlorosulfonyl benzoyl chloride and Cy3 derivative **5** (see experimental part 13.2.6 for details). Its apparent affinity constant towards hMMP-12 catalytic domain was determined in labelling buffer and was similar to that of probe **10** (2.28 vs 13.1 nM). This stressed again the minor impact of P₃' position on inhibitors binding properties. We then tested probe **19** (10 μ M) towards hMMP12 at 2 μ M. The labelling reaction was

performed at 37°C and the reaction progress was monitored at 3 times point (4h, 24 h and 48h). Regardless of the analysis time, no labelling reaction was observed (Figure 65B, lane 2 for result of hMMP-12 labelling after 24h). This was not due to an absence of probe reactivity since probe **19** was competent to modestly labelled bSA after 24h of incubation (Figure 65B, lane 3).

These results can be explained if we considered the following aspects: I) probe **19** structure with a P₃' lysine side chain directing tosyl reactive moiety to the upper part of the S₃' region, II) presence of a single reactive lysine (Lys¹⁷⁷) in this region and III) lack of reactivity of tosyl group towards lysine side chain.

More surprisingly, probe **19** did not display any reactivity towards the six other MMPs. Particularly, hMMP10 that however possesses a Histidine residue favourably oriented within S₃' region upper part (His¹⁷⁸, Figure 53) was not modified by probe **19**.

Overall, this result confirmed that the choice of acyl imidazole as chemically sensitive spacer was the most appropriate.

11. New Activity-based Probes for Mass spectrometry profiling of Metalloproteases: preliminary data.

The identification of a new generation of activity-based probes able to covalently modify MMPs without any photo activation allows envisaging further applications including the profiling of this enzyme *in vivo*. Since MMPs under their active form are present only transiently at potentially very low concentrations (nM to sub nM concentration), this “photoactivation-free” strategy has to be associated to a detection method of high sensitivity. In this context, we proposed to explore a new proteomic strategy illustrated in Figure 66.

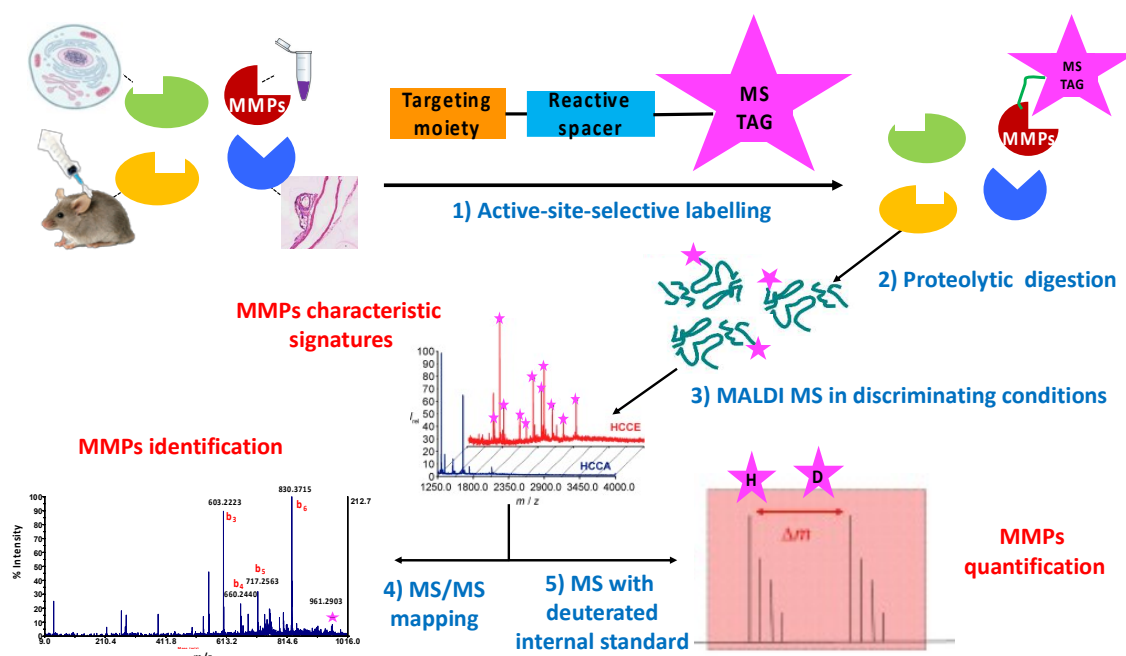


Figure 66. Detection of native MMPs within various complex proteomes by using a new proteomic approach exploiting both a new generation of probes and a mass signal enhancer.

The originality of the approach relies on a targeted proteomic approach allowing an active-site-selective transfer of a mass signal enhancer (MS Tag) to MMP active forms.

As a MS Tag, we propose to use a 4-hydroxycinnamic acid tag (HCCA tag) developed by G. Subra and S. Cantel (University of Montpellier). Indeed, when conjugated to peptides and used in combination with HCCCE (alpha-cyano-4-hydroxycinnamic methyl ester) as MALDI MS (matrix-assisted laser desorption/ionization mass spectrometry) matrix, this tag induces a HCCA-discriminating effect resulting in a preferential detection of HCCA-peptides²⁷. Particularly, this enables a very sensitive detection of HCCA-peptides (down to 50 attomoles in the most favourable cases) and affords

a substantial signal to noise ratio improvement up to 100, making this HCCA-tagging a method of choice for the detection of low-abundance peptides.

After proteolytic digestion, the resulting MMP digest containing unlabelled and HCCA tagged-peptides will be analysed by MALDI MS in HCCA discriminating conditions. The crosslinked MMPs will be thus identified by combining information on tagged-peptides masses in MS and corresponding peptide fragmentation patterns in MS/MS. We also propose a quantification of active MMPs by comparing the intensity of the MMPs characteristic tagged-fragments with that of their deuterated (heavy) version spiked into biological samples.

This strategy would involve a limited number of handling steps on sample, with no enrichment steps that might lead to unspecific capture of peptides. Accordingly, this will significantly reduce potential changes in MS peptides profiles coming from variabilities in sample manipulation and processing, thus increasing the robustness of the strategy.

As a proof of concept, we first synthesised a HCCA version of RXP500.1-derived probe **11** (Figure 67).

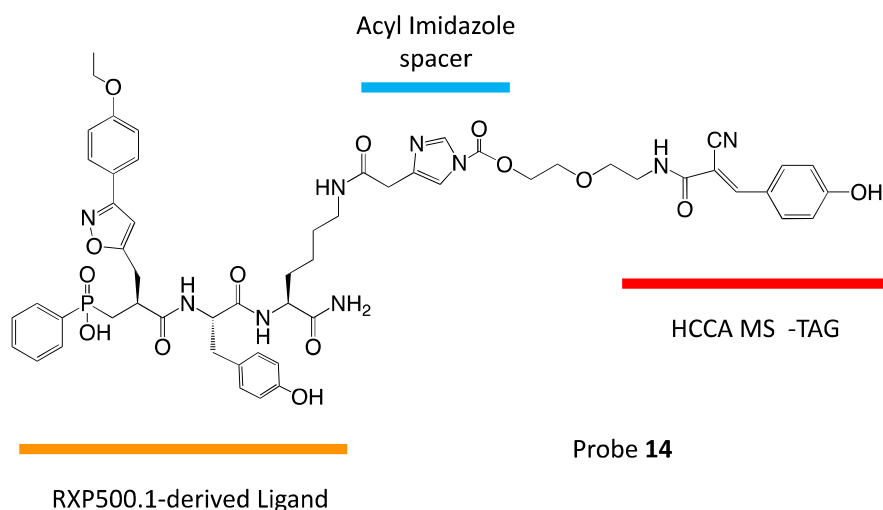


Figure 67. Chemical structure of HCCA probe 14 with a RXP500.1 binding motif.

Probe **14** was obtained according to a pathway similar to that described for probe **9** and **10** (see experimental part 13.2.4 for details). The probe **14** reactivity was then assessed at 10 μ M towards hMMP12 (1 μ M) in labelling buffer at 37°C. After 24h, the reaction mixture was analysed by LC/MS (Figure 68A).

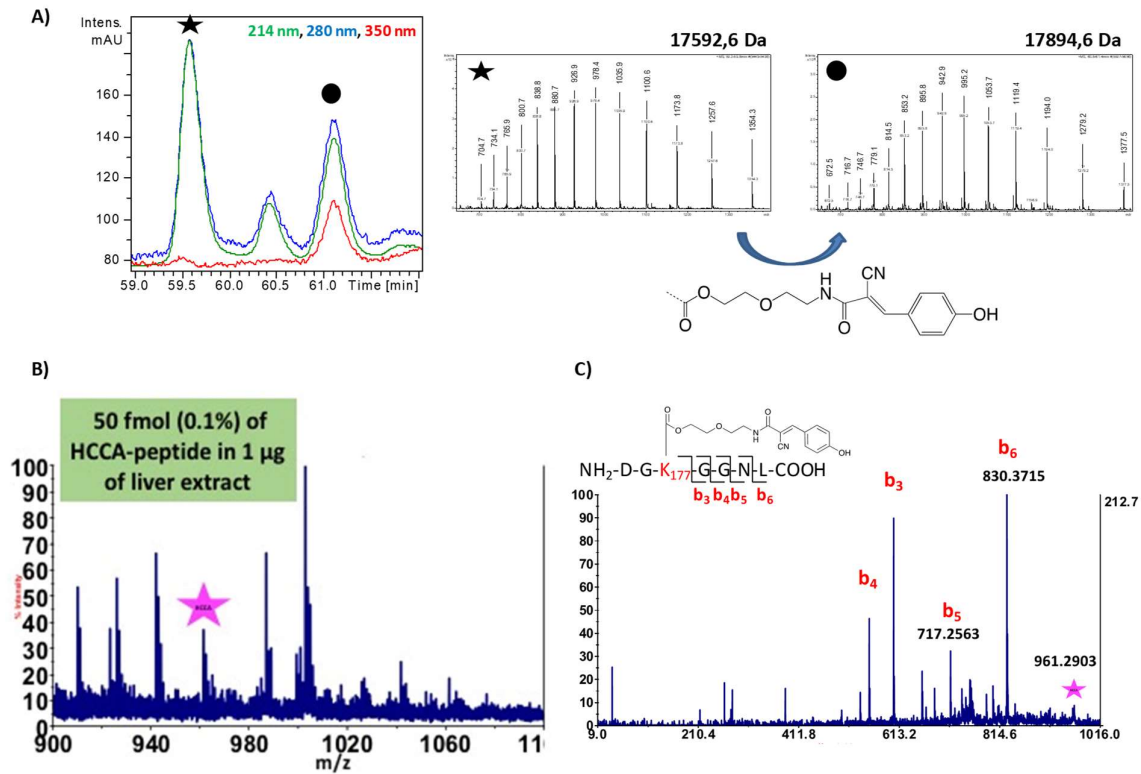


Figure 68. Labelling of hMMP12 by probe 14. A) LC/MS analysis of the HCCA-labelled and unlabelled MMP-12 in mixture after 24h of reaction. The mass spectra are not deconvoluted * unlabelled hMMP-12 (Mw=17592.6), • singly HCCA-labelled hMMP-12 (Mw=17894.2). The LC conditions were the following: X Bridge BEH300 column (21 x 150 mm, 3.5 µm, Waters), flow rate = 0.2 mL.min⁻¹, initial conditions: 5% B, 0 to 5 min: 5% B, 5 to 10 min: 20%, 10 to 65 min: 55%, 65 to 67 min: 100% B with A: H₂O/TFA 0.1% and B: CH₃CN 90%/H₂O 10%/ TFA 0.09%. B) MALDI MS analysis of HCCA-MMP12 digest spiked into 1 µg of liver extract. HCCA matrix was used as MALDI matrix. Peak corresponding to a peptide sequence compatible with the crosslinked of lys¹⁷⁷ was marked with a magenta star. C) MS/MS sequencing of peptide fragment at 961.3 Da, b ions were labelled in red.

As attested by the mass profile, only one HCCA tag was transferred to MMP12 (Figure XA). This in accordance with previous observations made with probe 9 and 10. After isolation of the HCCA-labelled hMMP12 and digestion in presence of chymotrypsin, 50fmol of the resulting digest was spiked into 1 µg of liver extract. This corresponded to 0.1% of whole protein content. Importantly in this case, the fragment containing lys¹⁷⁷ crosslinked with HCCA was detected (MW=961.3 Da, Figure 68B) and MS/MS sequencing confirmed unambiguously its identity (Figure 68C).

We estimated these preliminary data as sufficiently encouraging for applying to an “ANR” grant. The project has been particularly well received and a three-year financial support was obtained: ANR PRoMap, 2019-2021.

12. Towards substrate-derived acyl imidazole probes?

In the frame of this project, we also explored the possibility to modify the nature of binding motif susceptible to transfer a tag to MMPs. In this respect, we wondered whether substrate-derived probes would be able to react with MMPs. To assess the capacities of such probes, we synthesized four substrates possessing an acyl imidazole motif conjugated to linkers of variable lengths and flexibility (Figure 69A).

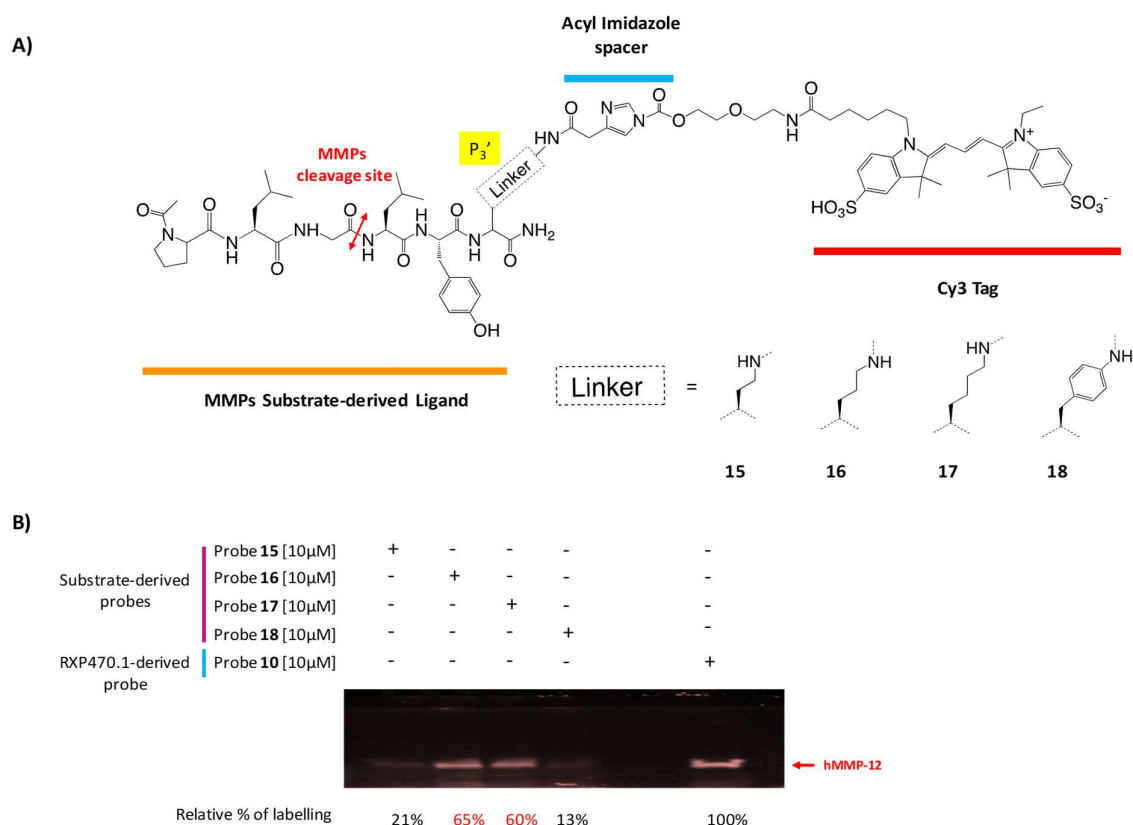


Figure 69. *hMMP-12 labelling with substrate-derived probes 15, 16, 17 and 18. A) Chemical structure of probes 15, 16, 17 and 18 with a P₃' side chain varying in length and flexibility. B) In-gel fluorescence imaging of hMMP12 (1 μM) labelled with probes 15, 16, 17 and 18 at 10 μM after 24h at 37°C. In the same conditions, the labelling experiment was also performed with probe 10 (10 μM) as an internal control. All the samples were resolved by 15% SDS-PAGE. Relative % of labelling were estimated through comparison of bands intensity. 100% was attributed to the labelling of hMMP12 by probe 10. Band corresponding to Cy3-labelled hMMP12 is marked by a red arrow.*

The chosen peptide sequence was derived from that of McaMat substrate (see experimental part 14.3.1), a broad-spectrum substrate that can be processed by the vast majority of MMPs. The acyl imidazole was installed onto a P₃' side chain to target nucleophiles within MMP S₃' region. We postulated that the chemical nature of P₃' side chain could substantially impact labelling efficiency of

substrate-derived probes whose residence time within MMP active site is potentially shorter than that of ligand-derived probes with nano molar affinity.

The peptide sequences were synthesized on solid support. After cleavage, P₃' position was conjugated in solution to acyl imidazole moiety and Cy3 tag incorporated in presence of N,N' disuccinimidyl carbonate (DSC) according to the procedure described in ligand series. Each resulting substrate-derived probe (**15** to **18**) was aliquoted as solid and stored at -20°C (see experimental for details).

Each probe (10 µM) was individually incubated with hMMP12 catalytic domain (1 µM) for 24h at 37°C. The samples were collected, resolved by SDS-PAGE in denaturing conditions and the fluorescence visualized at 532nm as described. A control labelling experiment was carried out with probe **10** in the same conditions of concentration, time and temperature. The labelling yield for each probe was estimated as function to that obtained for probe **10** (100%). As shown by Figure 69, probe **16** and **17** with an ornithine and a lysine P₃' linker respectively yielded a substantial and comparable labelling of 60% towards hMMP12. Conversely, when the linker is shorter (probe **15**) or less flexible (probe **18**), a significant drop of reaction yield was observed.

These data showed that, despite a short residence time within the active site, substrate-derived probes enabled hMMP12 labelling. Importantly, the labelling reaction occurred efficiently with linker of specific length, thus confirming the specificity of the reaction. These results also stressed that a minimum of three methylene group are necessary to target Lys¹⁷⁷ within S₃' region, thus validating our initial design. Surprisingly, at this relative range of concentration (10 µM of probes and 1µM of hMMP12), probe **16** and **17** labelling capacities are almost comparable to that of probe **10**. Accordingly, the labelling capacities of these substrate-derived probes have to be investigated at lower concentration.

These very encouraging data pave the way for the development of a new generation of substrate-based probes which would allow in a single experiment both reporting a proteolytic activity and identifying the protease(s) responsible of the cleavage. To our knowledge, such chemical tools have not been described yet and would turn out valuable for exploring the specificity of peptide sequences directed to one specific sub class of proteases in complex proteome. Furthermore, this change in paradigm may allow better addressing the unspecific component observed in the case of ligand-based probes. In this respect, a peptide sequence composed of natural amino acids is potentially less prone to unspecific interactions e.g. with serum albumin than pseudo peptides with hydrophobic cores.

These preliminary data allowed us to apply for an ANR grant (Break-Bright-Mass).

BIBLIOGRAPHY II

1. Devel, L. *et al.* Development of Selective Inhibitors and Substrate of Matrix Metalloproteinase-12. *J. Biol. Chem.* **281**, 11152–11160 (2006).
2. Johnson, J. L. *et al.* A Selective Matrix Metalloproteinase-12 Inhibitor Retards Atherosclerotic Plaque Development in Apolipoprotein E–Knockout Mice. *Arterioscler Thromb Vasc Biol* **31**, 528–535 (2011).
3. Lim, N. H. *et al.* In Vivo Imaging of Matrix Metalloproteinase 12 and Matrix Metalloproteinase 13 Activities in the Mouse Model of Collagen-Induced Arthritis. *Arthritis & Rheumatology* **66**, 589–598 (2014).
4. Marchant, D. J. *et al.* A new transcriptional role for matrix metalloproteinase-12 in antiviral immunity. *Nat. Med.* **20**, 493–502 (2014).
5. Ella, E. *et al.* Matrix metalloproteinase 12 promotes tumor propagation in the lung. *J. Thorac. Cardiovasc. Surg.* **155**, 2164–2175.e1 (2018).
6. Czarny, B. *et al.* Molecular Determinants of a Selective Matrix Metalloprotease-12 Inhibitor: Insights from Crystallography and Thermodynamic Studies. *J. Med. Chem.* **56**, 1149–1159 (2013).
7. Fujishima, S., Yasui, R., Miki, T., Ojida, A. & Hamachi, I. Ligand-Directed Acyl Imidazole Chemistry for Labeling of Membrane-Bound Proteins on Live Cells. *J. Am. Chem. Soc.* **134**, 3961–3964 (2012).
8. Matsuo, K. *et al.* One-step construction of caged carbonic anhydrase I using a ligand-directed acyl imidazole-based protein labeling method. *Chem. Sci.* **4**, 2573–2580 (2013).
9. Miki, T. *et al.* LDAI-Based Chemical Labeling of Intact Membrane Proteins and Its Pulse-Chase Analysis under Live Cell Conditions. *Chemistry & Biology* **21**, 1013–1022 (2014).
10. Yamaura, K., Kiyonaka, S., Numata, T., Inoue, R. & Hamachi, I. Discovery of allosteric modulators for GABA_A receptors by ligand-directed chemistry. *Nature Chemical Biology* **12**, nchembio.2150 (2016).
11. Bordenave, T. *et al.* Synthesis and in Vitro and in Vivo Evaluation of MMP-12 Selective Optical Probes. *Bioconjug. Chem.* **27**, 2407–2417 (2016).
12. Rouanet-Mehouas, C. *et al.* Zinc-Metalloproteinase Inhibitors: Evaluation of the Complex Role Played by the Zinc-Binding Group on Potency and Selectivity. *J. Med. Chem.* **60**, 403–414 (2017).
13. Dabert-Gay, A.-S. *et al.* Covalent Modification of Matrix Metalloproteinases by a Photoaffinity Probe: Influence of Nucleophilicity and Flexibility of the Residue in Position 241. *Bioconjugate Chem.* **20**, 367–375 (2009).
14. Dabert-Gay, A.-S. *et al.* Molecular Determinants of Matrix Metalloproteinase-12 Covalent Modification by a Photoaffinity Probe INSIGHTS INTO ACTIVITY-BASED PROBE DEVELOPMENT AND CONFORMATIONAL VARIABILITY OF MATRIX METALLOPROTEINASES. *J. Biol. Chem.* **283**, 31058–31067 (2008).

15. Saghatelian, A., Jessani, N., Joseph, A., Humphrey, M. & Cravatt, B. F. Activity-based probes for the proteomic profiling of metalloproteases. *Proc Natl Acad Sci U S A* **101**, 10000–10005 (2004).
16. Devel, L. *et al.* Third generation of matrix metalloprotease inhibitors: Gain in selectivity by targeting the depth of the S1' cavity. *Biochimie* **92**, 1501–1508 (2010).
17. Bregant, S. *et al.* Detection of Matrix Metalloproteinase Active Forms in Complex Proteomes: Evaluation of Affinity versus Photoaffinity Capture. *J. Proteome Res.* **8**, 2484–2494 (2009).
18. Bordenave, T. *et al.* Synthesis, in vitro and in vivo evaluation of MMP-12 selective optical probes. *Bioconjug Chem* **27**, 2407–2417 (2016).
19. Kis-Toth, K. *et al.* Monocyte-derived dendritic cell subpopulations use different types of matrix metalloproteinases inhibited by GM6001. *Immunobiology* **218**, 1361–1369 (2013).
20. Miller, M. A. *et al.* Proteolytic Activity Matrix Analysis (PrAMA) for simultaneous determination of multiple protease activities. *Integr Biol (Camb)* **3**, 422–438 (2011).
21. Tian, J. H. *et al.* Genetic regulation of protective immune response in congenic strains of mice vaccinated with a subunit malaria vaccine. *J. Immunol.* **157**, 1176–1183 (1996).
22. Banda, M. J. & Werb, Z. Mouse macrophage elastase. Purification and characterization as a metalloproteinase. *Biochem J* **193**, 589–605 (1981).
23. Jeng, A. Y. *et al.* Mouse macrophage metalloelastase expressed in bacteria absolutely requires zinc for activity. *J. Biochem.* **117**, 216–221 (1995).
24. Shipley, J. M., Wesselschmidt, R. L., Kobayashi, D. K., Ley, T. J. & Shapiro, S. D. Metalloelastase is required for macrophage-mediated proteolysis and matrix invasion in mice. *Proc Natl Acad Sci U S A* **93**, 3942–3946 (1996).
25. Werb, Z. & Gordon, S. Elastase secretion by stimulated macrophages. Characterization and regulation. *J. Exp. Med.* **142**, 361–377 (1975).
26. Algar, W. R., Dawson, P. & Medintz, I. L. *Chemoselective and Bioorthogonal Ligation Reactions: Concepts and Applications*. (John Wiley & Sons, 2017).
27. Lascoux, D. *et al.* Discrimination and selective enhancement of signals in the MALDI mass spectrum of a protein by combining a matrix-based label for lysine residues with a neutral matrix. *Angew. Chem. Int. Ed. Engl.* **46**, 5594–5597 (2007).

CHAPTER III

GENERAL DISCUSSION AND CONCLUSION

Accurately detecting and quantifying MMPs under their functional states in a spatial and temporal manner, remains of particular importance considering the implication of these enzymes in numerous physiological and pathological processes. This, in correlation with studies aiming to identify MMPs substrates, would enable to better decipher the complex biology of these enzymes. Furthermore, this would allow not only to validate several preclinical models but also to define the most appropriate therapeutic window for treating diseases in which MMPs are proposed as potential therapeutic targets.

Over the last fifteen years, several chemical probes have been devoted to the monitoring of MMPs activation *in vivo* but none of them have really provided direct and unambiguous evidences of their presence. This relative failure can be explained by the fact that MMPs are mainly overexpressed as inactive zymogens and/or inactivated fractions in a given biological samples, with active form present only transiently in very low amounts. In addition, photo affinity probes directed to MMPs detection have displayed a limited scope. Accordingly, *in vivo* profiling of these enzymes has not been achieved yet.

In this context, the new generation of ABPs developed in this study would enable to take a step in this direction. By relying on the acyl imidazole chemistry and by exploiting the crystal structure of a phosphinic pseudo peptide inhibitor (RXP470.1) in interaction with its privileged target, we indeed demonstrated that it was possible to design activity-based probes able to label MMPs covalently without requiring to photo activation. These RXP470-derived affinity probes with a reactive acyl imidazole in their P₃' position can react within hMMP12 S₃' region yielding a single and unambiguous covalent modification of Lys¹⁷⁷. The two active-site-directed probes **9** and **10** only target functional states of hMMP12 and spare forms whose active site is occluded either by synthetic inhibitors or natural hTIMP-1. Importantly, the capacity of these probes to target recombinant MMP12 spiked into complex proteomes was also demonstrated. In this case, down to 50 ng of active hMMP12 catalytic domain corresponding to 0.01 % of the whole proteome, can be efficiently detected by in-gel fluorescence analysis. In addition to a sensitivity limit compatible with the profiling of low abundance proteins, probe **10** turns out highly selective for its privileged target.

We also showed that this “photo activation free” method could be applied to other MMPs. As illustrated by the change in the labelling profile between probe **10** and **11**, increasing the ligand binding capacity could significantly improve its labelling efficacy. However, prolonging the probe residence time within MMP active-site does not ensure an efficient labelling for all MMPs members and other parameters have to be considered. In this respect, a targetable lysine within MMP2 and 9 S₃' region cannot be modified efficiently. This can be explained by the presence of an adjacent acid aspartic with

a negative charge that could stabilize the lysine under its protonated state thus decreasing its intrinsic reactivity. Regarding the differential reactivity of nucleophiles within the S_3' sub-site, the results obtained on hMMP3 and **8** are particularly informative. Indeed, these MMPs possess two potential nucleophiles in this region, two tyrosine in the case of hMMP8 and a threonine and a tyrosine for MMP-3 both in comparable positions, and only hMMP3 displays a significant reactivity. This first suggests that hMMP-3 threonine is more reactive than the hMMP8 tyrosine. Further, the canonical tyrosine found in almost all MMPs is not accessible for chemical modification with the probe that we designed. Thus, in addition to intrinsic nucleophile reactivity that may vary in function of local environment, other parameters are at play including distance and orientation between the two reactive partners as well as their relative dynamics. Although the dynamics are rather difficult to anticipate, a favourable orientation of the acyl imidazole moiety towards its target nucleophiles can be achieved by optimizing the length and flexibility of the linker. Accessing to pan-MMPs probes could also require to modify the position of the chemically sensitive spacer along the phosphinic peptide backbone as other potential nucleophiles are present within the MMPs catalytic cleft. Alternatively, another type of ligand-directed chemistry could be exploited such as ligand-directed N-Sulfonyl pyridone recently reported by Hamachi and co-workers.

We also demonstrated that probes **10** and **11** could target endogenous form of mMMP12. In this case, the strict identity of mMMP12 could not been achieved unambiguously but several data including competitions experiments, western blot analysis as well as immunocapture with mMMP12-directed antibody reinforced this view. To further address this particular point, we recently synthesised biotin analogues and they are currently under investigation. If confirmed, this would constitute to our knowledge, the first example of endogenous MMPs detection by using an affinity-based approach without any external trigger.

Our experiments in complex media also stressed that probe **10** and **11** presented certain limitations with notably a non-negligible unspecific labelling. In an affinity-labelling approach, limiting unspecific component while maintaining labelling efficiency could be obtained by decreasing probes concentration without impacting their binding capacity. In a unique way, phosphinic pseudo peptides offer such a possibility by simply modulating the pH of the medium. In this respect, performing labelling at slightly acidic pH (6-6.5) might improve the acyl imidazole probes selectivity. In addition, as serum albumin seems to be one of the main binding partners of these probes, another option would also consist in adding some PEG extension within probes **10** and **11** structure. Furthermore, we do not exclude that the chemical nature of the fluorescent reporter impacts probes unspecific binding and the use other fluorophore (e.g. with a zwitterionic character) might turn out critical.

We also realized that in-gel fluorescent imaging displays certain limits not necessarily compatible with the sensitive detection of MMPs active forms likely present in very low amounts. By replacing the fluorescent tag by a mass signal enhancer, this would allow overcoming this limitation. Moreover, this targeted proteomic approach would permit the direct profiling of MMPs active forms with a limited number of handling steps, which constitutes a major advantage with proteases only present transiently and susceptible to degradation.

By developing the first “photo activation-free” strategy to covalently modify active forms of MMPs, the unresolved proteomic profiling of native MMPs should be now accessible both in complex proteomes and *in vivo*. Particularly, we believe that RXP470- derived AfBPs might be useful to study the complex cell compartmentalization of active MMP-12 which can either localize at the cell surface or translocate to the nucleus. Thus, such probes with a negative net charge would target favourably the extracellular portion of MMP12 while sparing the intracellular one. Furthermore, as the labelling of S₃' region moderately impacts the MMP-12 proteolytic activity, it should be possible to study MMP12 active form in complex systems. In this respect, substrate-derived probes with a very short residence time within MMP active site might appear as real traceless probes allowing monitoring of native MMPs *in vivo*.

Finally, by employing appropriate targeting moieties and using the ligand-directed chemistry, we believe that the proteomic strategy described here might be effectively transferred more widely to other metalloprotease families and further to proteases for which the development of activity-based probes has remained problematic.

CHAPTER IV

MATERIALS AND METHODS

13. Probes synthesis and analytical characterization

13.1. General information.

13.1.1. Materials

All commercially available reagents and solvents were used without further purification.

4-Imidazoleacetic acid hydrochloride (Ref: 219991), N-(3-Dimethylaminopropyl)-N'-ethylcarbodiimide hydrochloride (EDC. HCl, Ref: 03449), 2-(2-Aminoethoxy)ethanol (Ref: A54059), 5-Carboxyfluorescein N-succinimidyl ester (Ref: 92846), Cy[®]3 Mono NHS Ester (Ref: GEPA13104), (+)-Biotin NHS Ester (Ref: H1759), N,N'-Disuccinimidyl carbonate, (DSC, Ref: 225827), 3-Chlorosulfonyl benzoyl chloride (Ref: CDS003205), anhydrous pyridine (Ref: 270970), N,N-Diisopropylethylamine (DIEA Ref: D125806), Diisopropylcarbodiimide (DIC, Ref: D125407), dry N,N-Dimethylformamide (DMF, Ref: 227056), Triisopropylsilane (Ref: 233781), and Trifluoroacetic acid (TFA, Ref: T6508) were from Sigma Aldrich. Rink amide resin[®] (200-400 Mesh, 0.71 mmol. g⁻¹) and Fmoc-AA-OH were purchased from Merck. 6-Chloro-1-Hydroxybenzotriazole di-hydrate (ClHOBt, Ref: 23283170) was from Molekula. Pseudo peptide synthesis was performed manually in polypropylene syringe (Ref: 57026, Supelco) equipped with a polyethylene frit and a stopper. The synthesis of Phosphynic block A and phosphynic block B were previously described ^{1,2}.

13.1.2. Instrumentation

Microwave experiments were performed on a Discover apparatus (CEM μ Wave) using the open vessel mode with the SPS kit. Analytical or semi preparative RP-HPLC separations and analyses were performed on a Shimadzu apparatus (LC-20AB for pump module, PD-20A for UV detector and RF-20AXS for fluorescent detector) or an Agilent system (1100 series) using an i) Analytical Ascentis[®] Express C18 column (Supelco, 100 x 4.6 mm, 2.7 μ m), ii) Analytical Synchronis C18 column (Thermo, 150 x 4.6 mm, 3 μ m), iii) Analytical XDB C18 column (Agilent, 150 x 4.6 mm, 5 μ m) or a iv) semi-Preparative column Grace[®] Vision HT C18 HL (250 x 10 mm, 5 μ m). Retention times (Rt) are reported in minutes.

¹H NMR spectra were recorded on a 500 MHz Bruker instrument (Bruker Daltonics) for compounds **1**, **2**, **3** and **4**. Chemical shifts are reported in ppm relative to the residual solvent peak (DMSO d₆ = 2.50). Data are reported as follows: chemical shift, multiplicity (s= singlet, d= doublet, t= triplet, q= quartet, br= broad, m= multiplet), coupling constants (Hz) and integration.

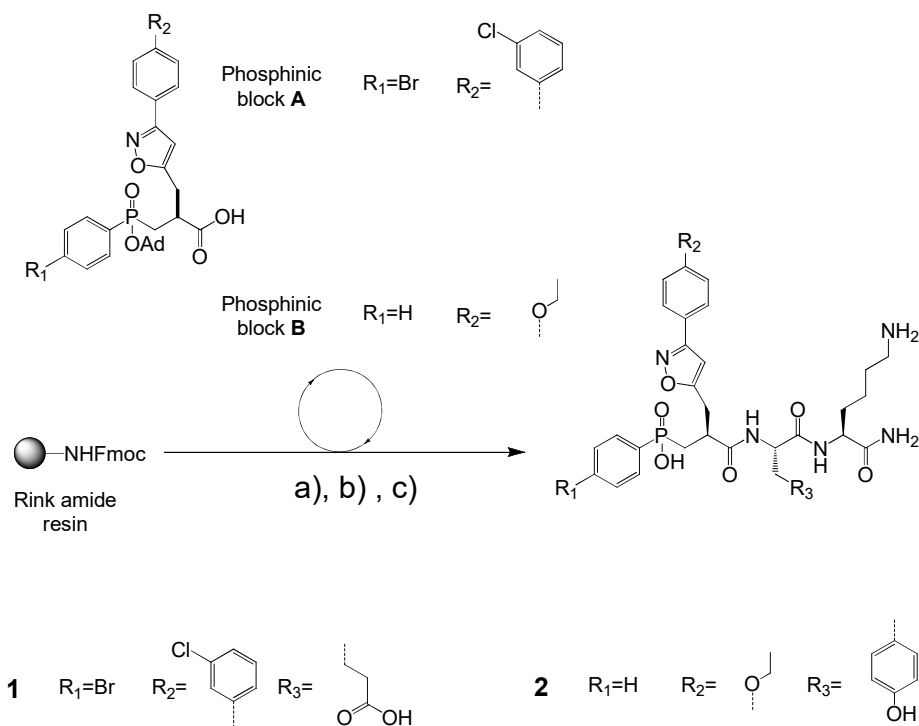
Mass spectrometry data were registered using a 4800 MALDI-TOF mass spectrometer (Applied Biosystems) or an ion trap Esquire HCT spectrometer (Bruker Daltonics). Amino acid compositions were performed on an aminoTac JLC-500/V amino acids analyser (JEOL, Tokyo, Japan). DO measurements were performed on a UV-1800 spectrophotometer (Shimadzu). Fluorescent measurements were carried out on a CLARIOstar microplate reader (BMG LABTECH).

For each compound, the molar extinction coefficient was calculated from the absorbance value of a solution whose concentration was first determined by amino acid composition. The identity and purity of each newly synthesized compound were assessed by analytical RP-HPLC, NMR, and high-resolution mass spectrometry (HRMS, 4800 MALDI-TOF mass spectrometer).

13.2. Synthetic protocols and compounds characterisation

13.2.1. Solid phase synthesis of pseudo peptides 1 and 2.

Standard Fmoc methodology was used to build the amino acid sequence on rink amide resin. The general pathway is illustrated in Scheme 1.

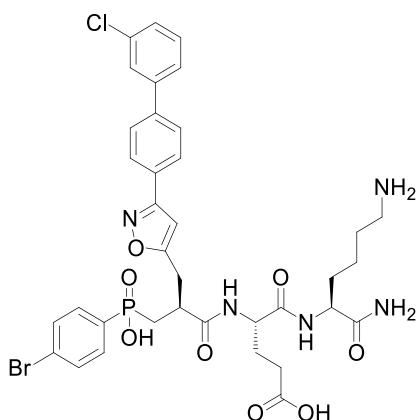


Scheme 2: Synthesis of compound 1 and 2. Reaction conditions: a) Fmoc solid phase synthesis, Fmoc-AA-OH, ClHOBT/DIC in DMF, 60°C 10 min, followed by Phosphinic block A or B incorporation, ClHOBT/DIC, DMF, 60°C, 60min, b) TFA/TIS/H₂O: 95/2.5/2.5 c) RP-HPLC separation

After Fmoc removal (piperidine 20% in DMF, 3 × 2 min, 60 °C, 25 W) and washing steps (2 x 3ml DMF followed by 2 x 3ml DCM), Fmoc-Lys (Boc)-OH and Fmoc-Glu(OtBu)-OH (10 equivalents, [100 mM]) were sequentially incorporated on the solid support following a standard activation protocol in presence of DIC (10 eq) and ClHOBT (10 eq) in DMF. The coupling reaction was carried out under microwave irradiation (45 W) at 60 °C for 10 min and was repeated once. After Fmoc removal and washing, 1.2 equivalents of phosphinic block A¹ was first activated with DIC (3 eq) and ClHOBT (3 eq) and incorporated to the support at room temperature overnight to access compound 1.

The same protocol was carried out with building block B² to lead compound 2. The phosphinic pseudo peptides were then cleaved from the support with Trifluoroacetic acid/Trisopropylsilane/water 95:2.5:2.5 cocktail (3 × 45 min) and Trifluoroacetic acid/DCM solution 1:1 (2 × 45 min).

Compound 1.



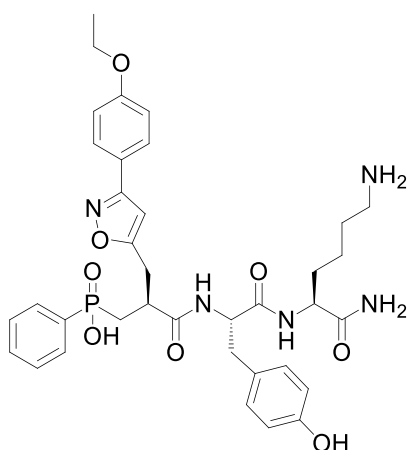
Chemical Formula: C₃₆H₄₀BrClN₅O₈P

Exact Mass: 815,15

Molecular Weight: 817,06

$\epsilon_{272} = 26,900 \text{ M}^{-1} \cdot \text{cm}^{-1}$ (MeOH/H₂O:1/1)

Compound 2.



Chemical Formula: C₃₆H₄₄N₅O₈P

Exact Mass: 705,29

Molecular Weight: 705,75

$\epsilon_{262} = 18,400 \text{ M}^{-1} \cdot \text{cm}^{-1}$ (MeOH/H₂O:1/1)

Note that compounds **1** and **2** are obtained as a mixture of diastereomers (**1(R)** and **1(S)**, Figure 70A and **2(R)** and **2(S)**, Figure 70B respectively) varying in the configuration of their P1' position.

Diastereomers **1(R)** and **1(S)** were separated by RP-HPLC using the following conditions: semi preparative Grace Vision HT C18 HL column, flow rate: 4 mL.min⁻¹, Method: 0 to 2 min: 30% B, 2 to 28 min: 60% B, 28 to 30 min: 100% B with A: H₂O/0.1% TFA and B: CH₃CN/0.09% TFA, UV detection at 230 nm and 280 nm (Figure 70A).

Diastereomers **2(R)** and **2(S)** were separated by RP-HPLC using the following conditions: semi preparative Grace Vision HT C18 HL column, flow rate: 4 mL.min⁻¹, Method: 0 to 2 min: 23% B, 2 to 28 min: 53% B, 28 to 30 min: 100% B with A: H₂O/0.1% TFA and B: CH₃CN/0.09% TFA, UV detection at 230 nm and 280 nm (Figure 70B).

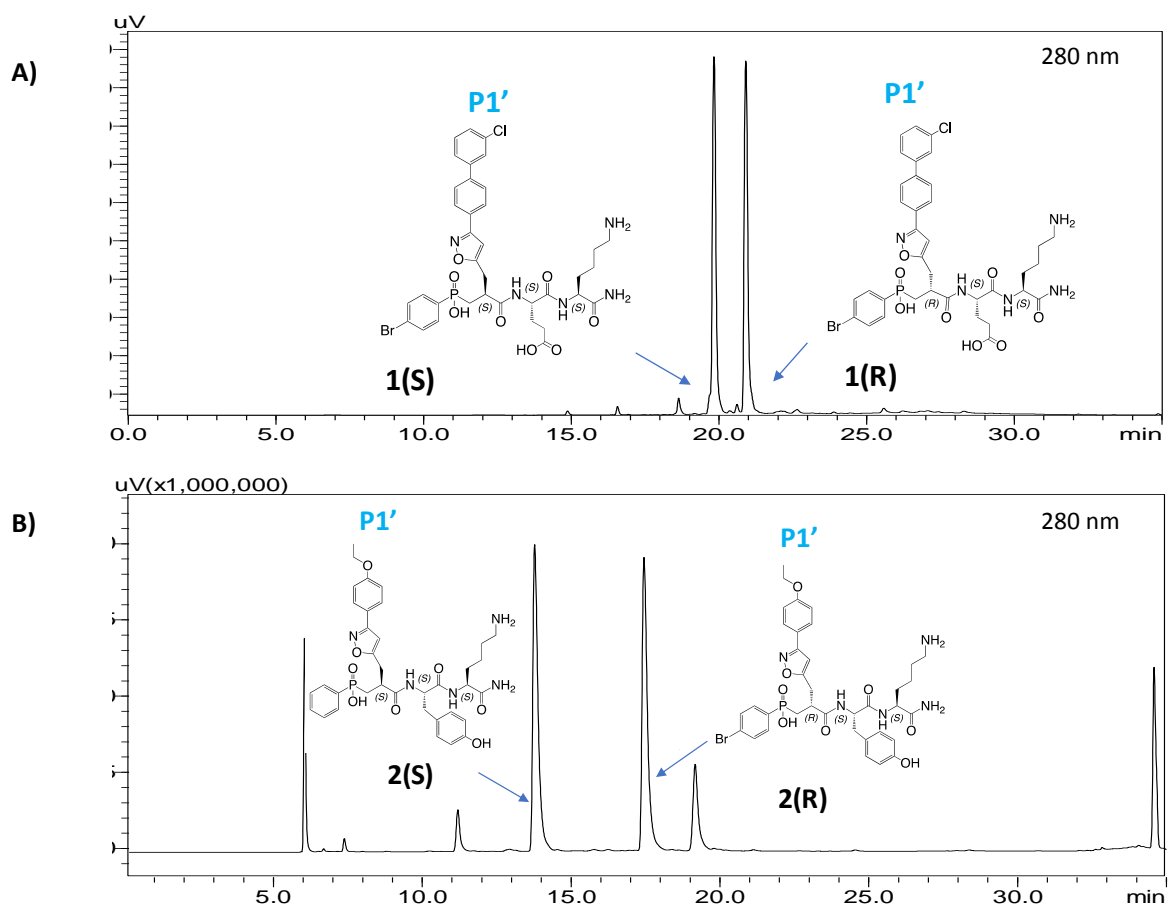


Figure 70: RP- HPLC profiles of crude compounds 1 and 2. A) Profile of crude compound 1 corresponding to a mixture of two diastereomers (1a and 1b) differing in the configuration of their P1' position. B) Profile of crude compound 2 corresponding to a mixture of two diastereomers (2a and 2b). UV detection was performed at 280 nm.

During the HPLC separation, fractions were collected to purify both compounds. Chromatograms and HRMN spectra of each purified compounds is presented in Figure 72 to Figure 74. In these conditions of purification, the first peak eluted from the column (phosphinic pseudo peptide with **1(R)** or **2(R)** with a (R) configuration in P1') corresponds to the diastereomer of interest. For simplification reasons, diastereomers **1(R)** and **2(R)** will be named **1** and **2** respectively. After freeze drying, **1** (5mg) and **2** (7mg) were isolated as a white powder with 34% and 55% yield respectively.

LC/MS data – compound 1:

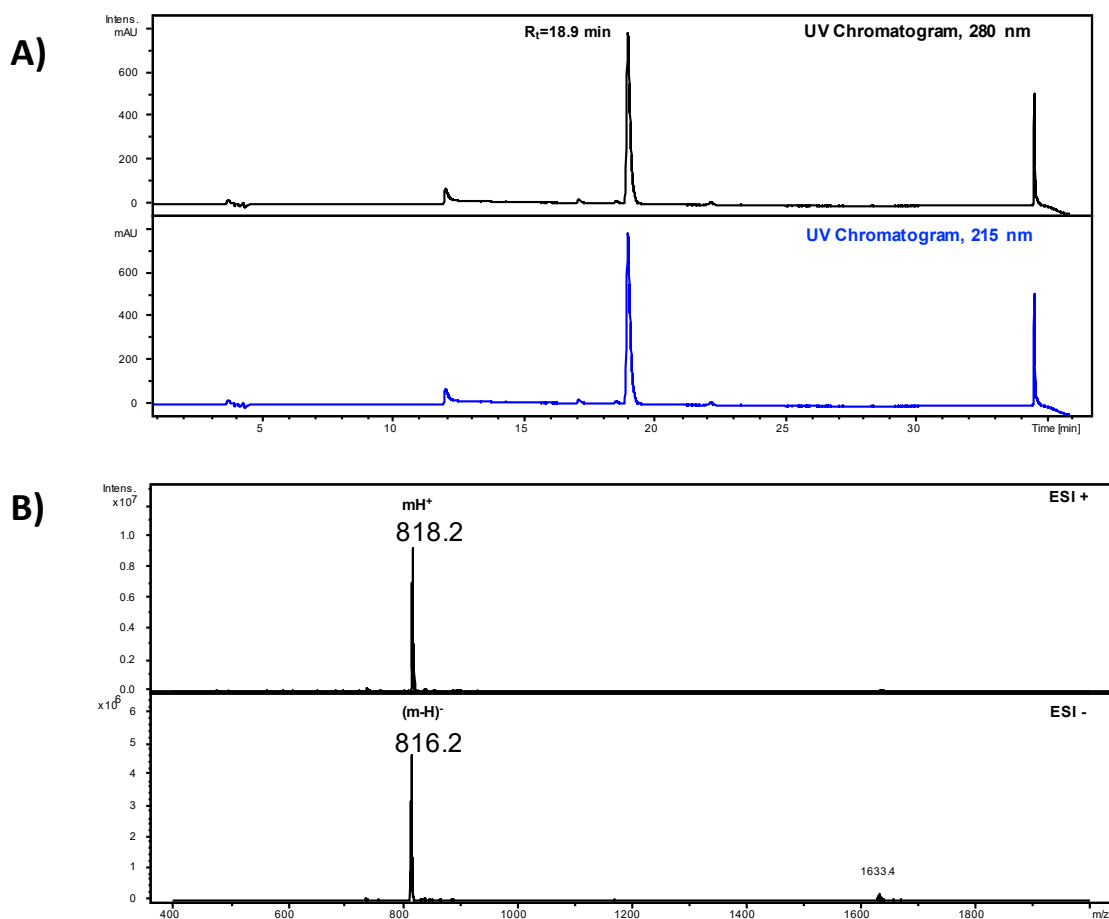


Figure 71: LC/MS profile of purified compound 1. A) RP-HPLC profile of 1 ($R_t = 18.9$ min) in the following conditions: analytical XDB C18 column, flow rate: $0.6 \text{ mL}\cdot\text{min}^{-1}$, Method: 0 to 5 min: 100% A, 5 to 25 min: 100 % B with A: 10mM AcONH₄ and B: CH₃CN, UV detection was performed at 215 nm and 280 nm. B) Mass profile of 1 analysed in ESI/positive mode of ionisation ($mH^+=818.2$) and ESI/negative mode of ionisation ($(m-H)^-=816.2$).

H NMR analysis have been performed on the compounds 1 and 2 and the results are presented in Figure 72 and Figure 74.

¹H NMR experimental data -compound 1:

¹H NMR (500 MHz, d₆- DMSO) δ : 1.24-1.34 (m, 2H), 1.44 (m, 2H), 1.55 (m, 1H), 1.63 (m, 1H), 1.81 (m, 1H), 1.96 (m, 2H), 2.28 (m, 3H), 2.66 (m, 2H), 2.93 (m, 1H), 3.05 (m, 2H), 4.05 (m, 1H), 4.15 (m, 1H), 6.81 (s, 1H), 7.07 (s, 1H), 7.35 (br, 1H), 7.49 (d, 1H, $J = 7.9$ Hz), 7.54 (t, 1H, $J = 7.9$ Hz), 7.65 (m, 3H), 7.72 (m, 3H), 7.82 (s, 1H), 7.86 (d, 2H, $J = 8.3$ Hz), 7.94 (d, 2H, $J = 8.3$ Hz), 8.20 (br, 1H), 8.46 (d, 1H, $J = 6.75$ Hz); HRMS m/z for [C₃₆H₄₀BrClN₅O₈P]⁺ calcd 816.1564, found 816.1594

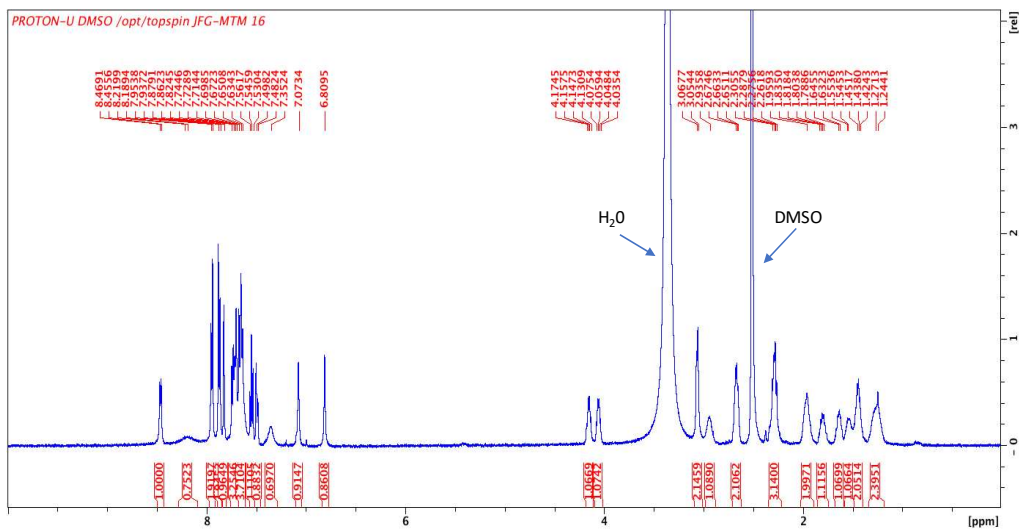


Figure 72: ^1H NMR profile of compound 1.

LC/MS data – compound 2:

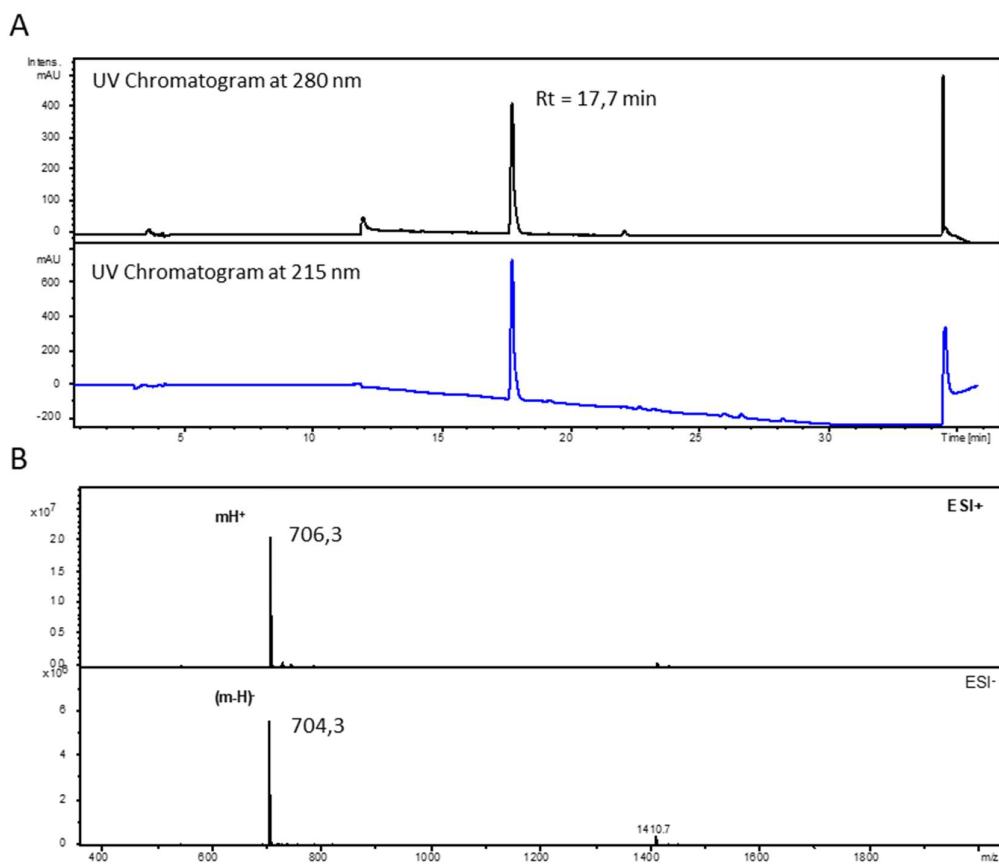


Figure 73: LCMS profile of purified compound 2. A) RP-HPLC profile of 2 ($R_t = 17.7$ min) in the following conditions: XDB C18 column, flow rate: $0.6 \text{ mL}\cdot\text{min}^{-1}$, Method: 0 to 5 min: 100% A, 5 to 25 min: 100% B with A: 10mM AcONH₄ and B: CH₃CN, UV detection was performed at 215 nm and 280 nm. B) Mass profile of 2 analysed in ESI/positive mode of ionisation ($m\text{H}^+ = 706.3$) and ESI/negative mode of ionisation ($(m\text{-H})^- = 704.3$).

¹H NMR experimental data -compound 2:

¹H NMR (600 MHz, d₆-DMSO) δ; 1.22-1.33 (m, 2H), 1.36 (t, 3H, J = 7 Hz), 1.47 (m, 2H), 1.56-1.83 (m, 3H), 2.08 (m, 1H), 2.62-2.82 (m, 4H), 3.08 (m, 1H), 4.09 (q, 2H, J = 7 Hz), 4.20 (m, 2H), 6.65 (m, 2H), 7.05 (m, 5H), 7.44 (m, 2H), 7.50 (m, 1H), 7.68 (m, 4H), 8.46 (bs, 1H), 9.19 (s, 1H); HRMS m/z for [C₃₆H₄₄ClN₅O₈P]⁺ calculated 706.3006, found 706.3021. HRMS m/z for [C₃₆H₄₄ClN₅O₈P]⁺ calculated 706.3006, found 706.3021.

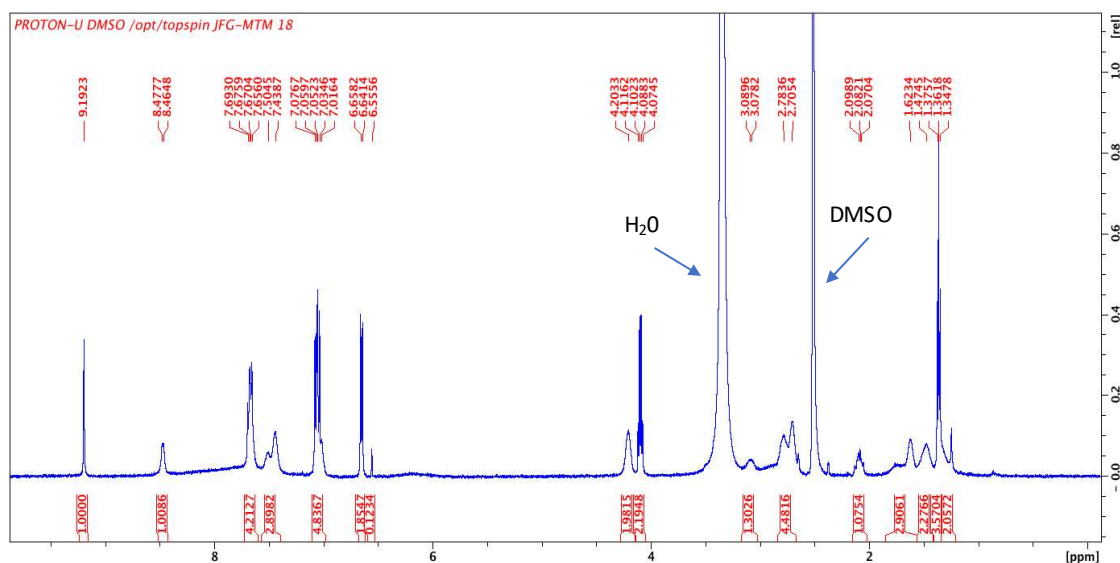


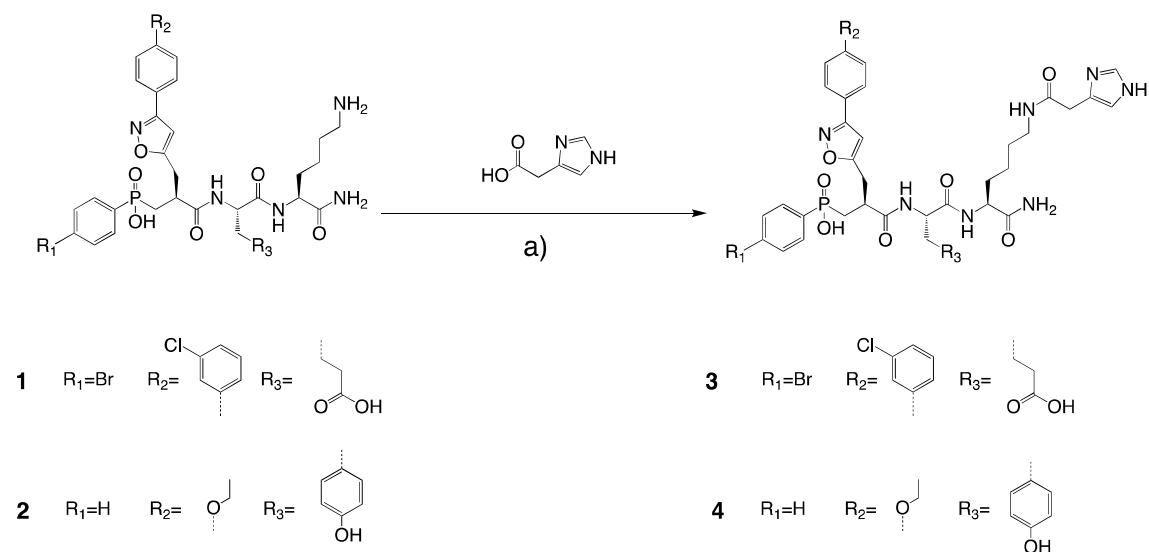
Figure 74: ¹H NMR profile of compound 2.

13.2.2. Incorporation of 4-Imidazole acetic acid and access to compounds 3 and 4.

A solution of compound **1** or **2** (5 μmol), 4-Imidazole acetic acid hydrochloride (50 μmol, 10 eq), EDC.HCl (15 μmol, 3 eq), ClHOBT (15 μmol, 3 eq) and DIEA (150 μmol, 30 eq) in dry DMF (230 μL, [**1** or **2**] = 20 mM) was stirred overnight at room temperature. The reaction mixture was then diluted with a H₂O/CH₃CN: 1/1 solution (500 μL) and the resulting crude was purified by RP-HPLC.

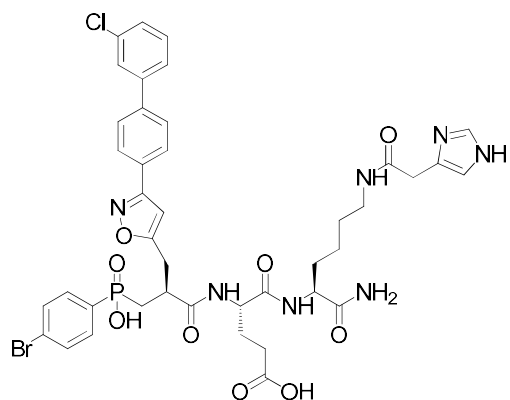
Compound **3** (R_t = 19.5 min) and **4** (R_t = 15.4 min) were purified on semi preparative Grace Vision HT C18 column, flow rate: 4 mL.min⁻¹ using the following program: 0 to 30 min: 100% B, with A: H₂O/0.1% TFA and B:CH₃CN/0.09% TFA, UV detection was performed at 230 nm and 280 nm. **3** (55%) and **4** (59%) were obtained as a white powder after freeze drying.

The Scheme 3 illustrates the pathways of synthesis of compounds 3 and 4 from 1 and 2.



Scheme 3: Synthesis of compounds 3 and 4. Reaction conditions: a) 4-Imidazoleacetic acid hydrochloride (10 eq), EDC, ClHOBT (3 eq), DIEA (30 eq) in DMF, o. n., r. t.

Compound 3:



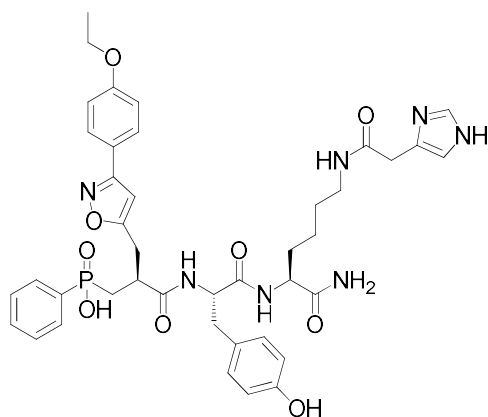
Chemical Formula: $\text{C}_{41}\text{H}_{44}\text{BrClN}_7\text{O}_9\text{P}$

Exact Mass: 923,18

Molecular Weight: 925,17

$\epsilon_{270} = 23,300 \text{ M}^{-1} \cdot \text{cm}^{-1}$ (MeOH/H₂O:1/1)

Compound 4:



Chemical Formula: $\text{C}_{41}\text{H}_{48}\text{N}_7\text{O}_9\text{P}$

Exact Mass: 813,33

Molecular Weight: 813,85

$\epsilon_{258} = 24,000 \text{ M}^{-1} \cdot \text{cm}^{-1}$ (MeOH/H₂O:1/1)

LC/MS data – compound 3:

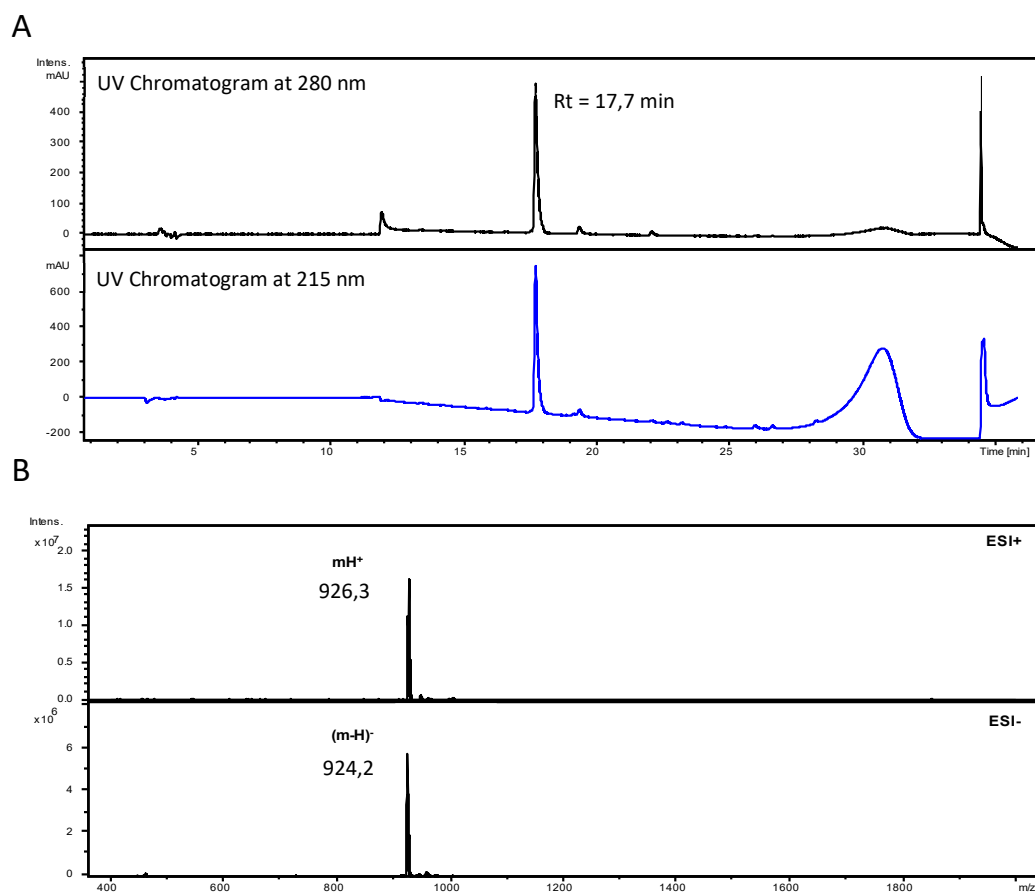


Figure 75: LC/MS profile of purified compound 3. A) RP-HPLC profile of 3 (Rt = 17.7 min) in the following conditions: analytical XDB C18 column, flow rate: 0.6 mL.min⁻¹, Method: 0 to 5 min: 100% A, 5 to 25 min: 100 % B with A: 10mM AcONH₄ and B: CH₃CN, UV detection was performed at 215 nm and 280 nm. B) Mass profile of 3 analysed in ESI/positive mode of ionisation (mH⁺=926.3) and ESI/negative mode of ionisation ((m-H)⁻=924.2).

¹H NMR experimental data -compound 3:

¹H NMR (500 MHz, d₆-DMSO) δ; 1.24-1.42 (m, 2H), 1.65 (m, 1H), 1.87-2.01 (m, 2H), 2.27-2.37 (m, 2H), 2.76 and 2.86 (br, 2H), 2.98-3.13 (m, 3H), 3.42 (m, 3H), 3.49 (m, 3H), 3.65 (m, 1H), 4.06-4.12 (m, 2H), 4.58 (br, 1H), 6.56 (s, 2H), 6.74 (s, 1H), 7.09 (s, 1H), 7.45 (s, 1H), 7.48 (d, 1H, J = 7.8 Hz), 7.53 (t, 1H, J = 7.8 Hz), 7.64 (m, 4H), 7.73 (d, 1H, J = 7.7 Hz), 7.82 (s, 1H), 7.86 (d, 2H, J = 8.2 Hz), 7.94 (d, 2H, J = 8.2 Hz), 8.61 (br, 1H), 8.89 (s, 1H). HRMS m/z for [C₄₁H₄₅BrClN₇O₉P]⁺ calcd 924.1888, found 924.1876.

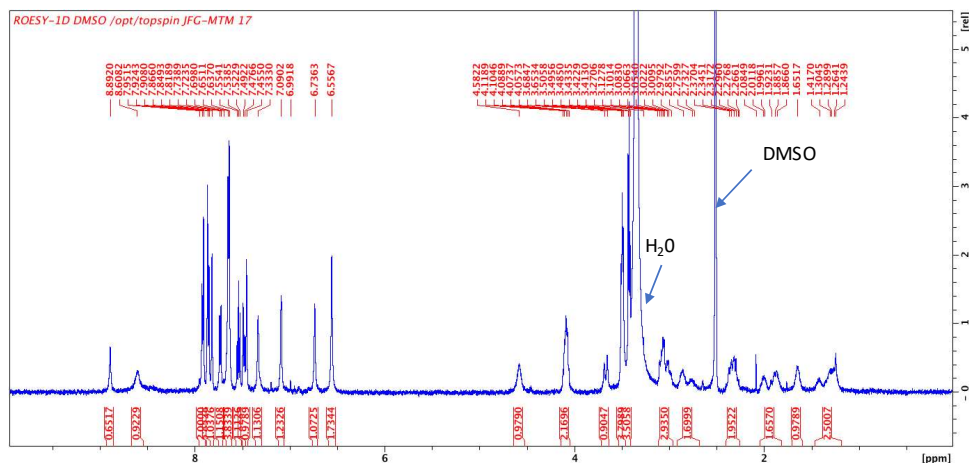


Figure 76 ^1H NMR profile of compound 3.

LC/MS data – compound 4:

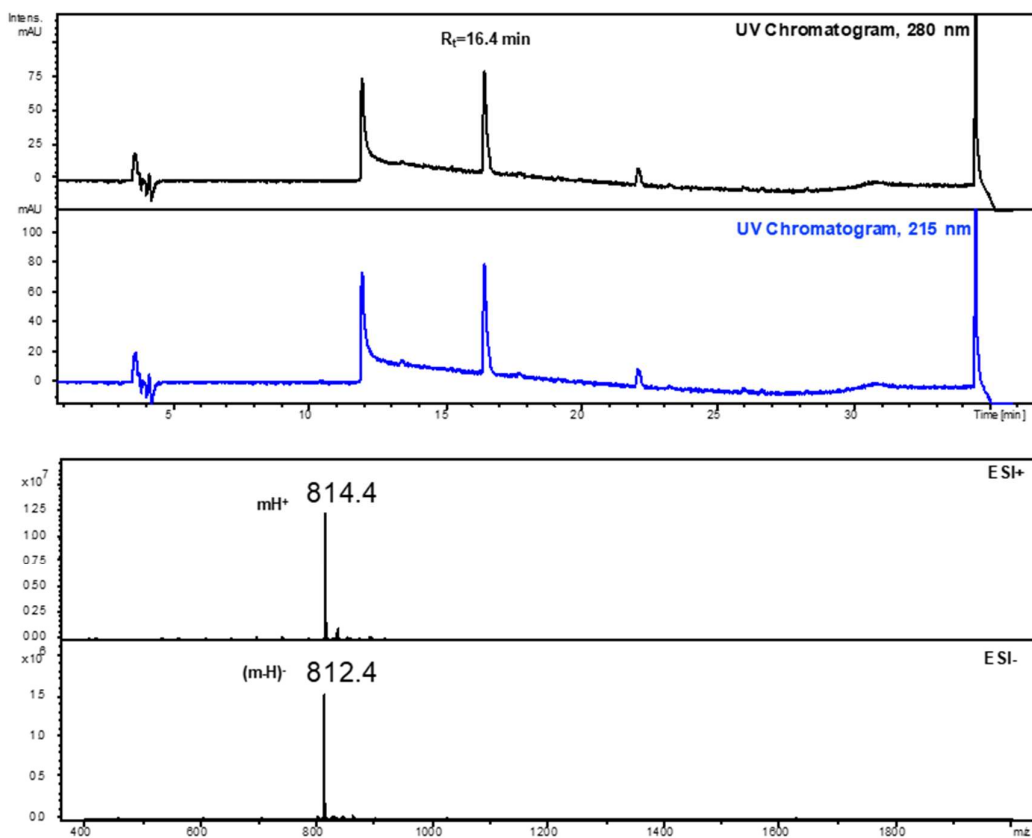


Figure 77: LC/MS profile of purified compound 4. A) RP-HPLC profile of 4 ($R_t = 16.4$ min) in the following conditions: analytical XDB C18 column, flow rate: $0.6 \text{ mL} \cdot \text{min}^{-1}$, Method: 0 to 5 min: 100% A, 5 to 25 min: 100% B with A: 10mM AcONH₄ and B: CH₃CN, UV detection was performed at 215 nm and 280 nm. B) Mass profile of 4 analysed in ESI/positive mode of ionisation ($m\text{H}^+ = 814.4$) and ESI/negative mode of ionisation ($(m\text{-H})^- = 812.4$).

^1H NMR experimental data (compound 4):

^1H NMR (600 MHz, d_6 -DMSO) δ : 1.16-1.33 (m, 1H), 1.36 (t, 4H, $J = 7$ Hz), 1.62 (m, 2H), 1.84 (m, 1H), 2.10 (m, 1H), 2.71- 2.82 (m, 2H), 2.84-3.06 (m, 4H), 3.42 (m, 2H), 3.49 (m, 1H), 3.57 (m, 1H), 4.09 (q, 2H, $J = 7$ Hz), 4.13 (m, 1H), 4.26 (m, 1H), 4.58 (bs, 1H), 6.25 (s, 1H), 6.55 (s, 1H), 6.64 (d, 2H, $J = 8.4$ Hz), 7.05 (m, 5H), 7.30 (bs, 1H), 7.41 (s, 1H), 7.46 (m, 2H), 7.54 (m, 1H), 7.68 (m, 4H), 8.38 (bs, 2H), 8.57 (s, 1H), 8.86 (s, 1H), 9.20 (s, 1H). HRMS m/z for $[\text{C}_{41}\text{H}_{49}\text{N}_7\text{O}_9\text{P}]^+$ calcd 814.3329, found 814.3347.

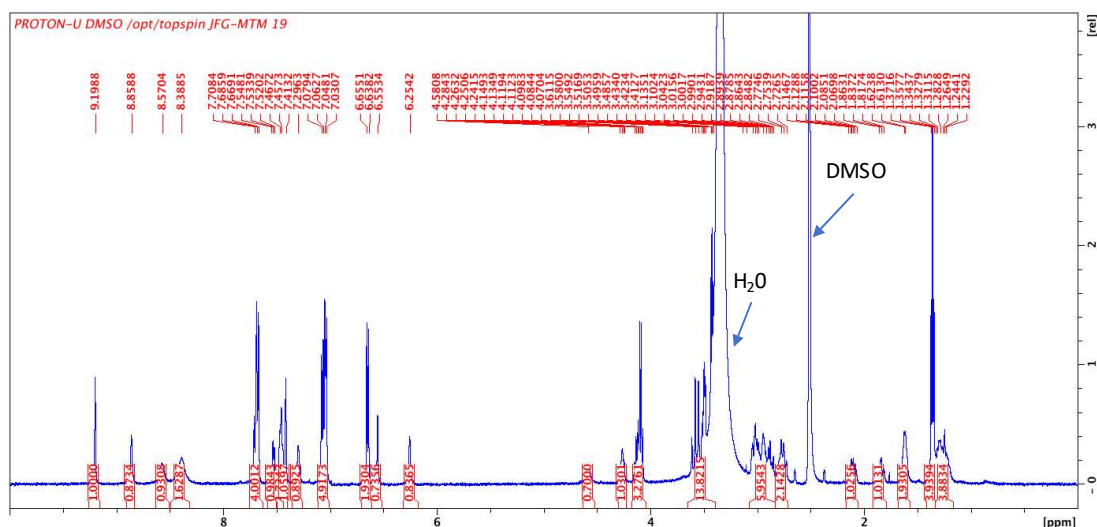


Figure 78 ^1H NMR profile of compound 4.

13.2.3. Synthesis of precursors 5, 6, 7, and 8

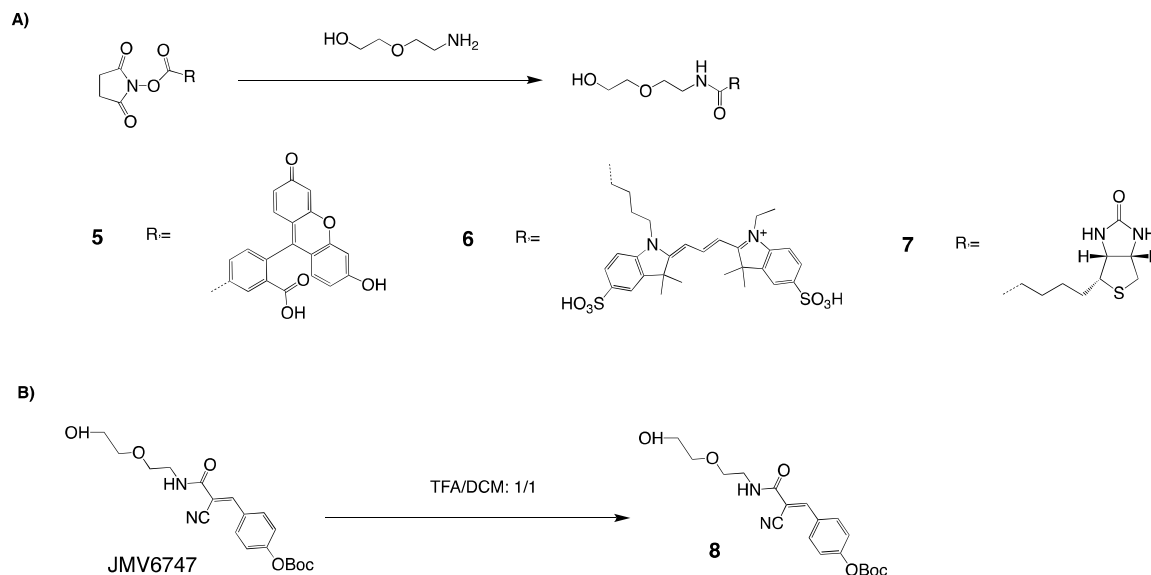
Compounds **5**³, **6**³ and **7** were synthesized from 5-Carboxyfluorescein (5mg, 10.6 μmol , Aldrich Ref: 92846), Cy[®]3 (5mg, Aldrich, 6.9 μmol , Aldrich Ref: GEPA13104) and (+)-Biotin (10mg, 29 μmol , Aldrich Ref: H1759) mono NHS Ester respectively.

The activated ester (50mM) was first dissolved in anhydrous DMF. 2-(2-aminoethoxy) ethan-1-ol (1 eq) and DIEA (10 eq) were successively added. The reaction mixture was kept under stirring for 60 minutes at room temperature.

The Scheme 4 illustrate the pathways of synthesis of compounds 5, 6 and 7.

After dilution in H₂O/CH₃CN:1/1 (1 mL), the crude solutions were directly purified by RP-HPLC on semi preparative Grace Vision HT C18 HL column (flow rate: 4 mL.min⁻¹) using the following conditions: I) compounds **5**, 0-5 min 20% B, 5-25 min 50% B, 25- 30 min 100% B with A: H₂O/0.1% TFA and B:CH₃CN/0.09% TFA, UV detection at 230 nm and 280 nm, II) compound **6**, 0 to 40 min: 100% B, with

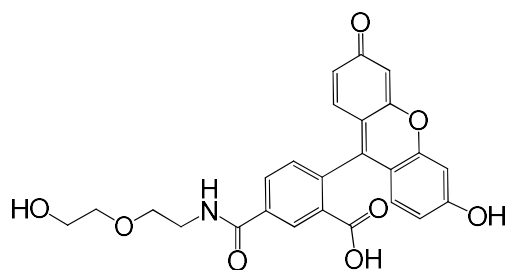
A: H₂O/0.1% TFA and B:CH₃CN/0.09% TFA, UV detection at 230 nm and 280 nm and III) compound **7**, 0 to 20 min: 100% B, with A: H₂O/0.1% TFA and B:CH₃CN/0.09% TFA, UV detection at 215 nm. After freeze drying, compound **5**, **6** and **7** were isolated with 54%, 47% and 84% yield respectively.



Scheme 4: Synthesis of precursors **5, **6**, **7** and **8**. A) Activated NHS-ester (1eq) and 2-(2-aminoethoxy) ethan-1-ol (1eq), DMF, r.t. B) TFA/DCM: 1/1, o. n., r.t.**

After dilution in H₂O/CH₃CN:1/1 (1 mL), the crude solutions were directly purified by RP-HPLC on semi preparative Grace Vision HT C18 HL column (flow rate: 4 mL.min⁻¹) using the following conditions: I) compounds **5**, 0-5 min 20% B, 5-25 min 50% B, 25- 30 min 100% B with A: H₂O/0.1% TFA and B:CH₃CN/0.09% TFA, UV detection at 230 nm and 280 nm, II) compound **6**, 0 to 40 min: 100% B, with A: H₂O/0.1% TFA and B:CH₃CN/0.09% TFA, UV detection at 230 nm and 280 nm and III) compound **7**, 0 to 20 min: 100% B, with A: H₂O/0.1% TFA and B:CH₃CN/0.09% TFA, UV detection at 215 nm. After freeze drying, compound **5**, **6** and **7** were isolated with 54%, 47% and 84% yield respectively.

Compound 5:



Chemical Formula: C₂₅H₂₁NO₈

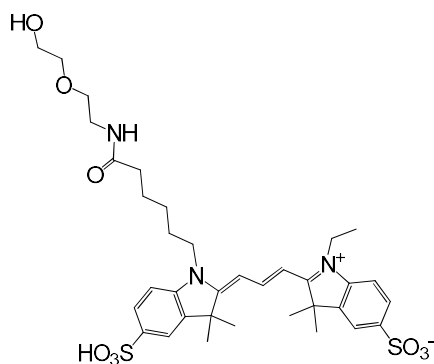
Exact Mass: 463,13

Molecular Weight: 463,44

$\epsilon_{498} = 76,900 \text{ M}^{-1} \cdot \text{cm}^{-1}$ (PBS 1X, pH=8)

Fluorescence: $\lambda_{\text{ex}} 494 / \lambda_{\text{em}} 520$

Compound 6:



Chemical Formula: C₃₅H₄₇N₃O₉S₂

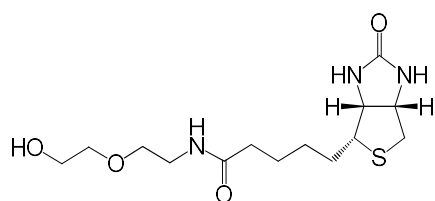
Exact Mass: 717,28

Molecular Weight: 717,89

$\epsilon_{550} = 150,000 \text{ M}^{-1} \cdot \text{cm}^{-1}$ (CH₃CN/H₂O:1/1),

Fluorescence: $\lambda_{\text{ex}} 549 / \lambda_{\text{em}} 563$

Compound 7:



Chemical Formula: C₁₄H₂₅N₃O₄S

Exact Mass: 331,16

Molecular Weight: 331,43

Compound **8** was obtained from precursor JMV6747 provided by Gilles Subra's Team (Université de Montpellier, France). The Boc removal of JMV6747 (2 μmol) was performed at room temperature in presence of DCM/TFA: 1/1 (500 μL). After an overnight stirring, the solvent was evaporated, the crude was dissolved in H₂O/CH₃CN: 7/3 (1 mL) and lyophilized. **8** was not further purified and directly engaged in the following step.

LC/MS data – compound 5:

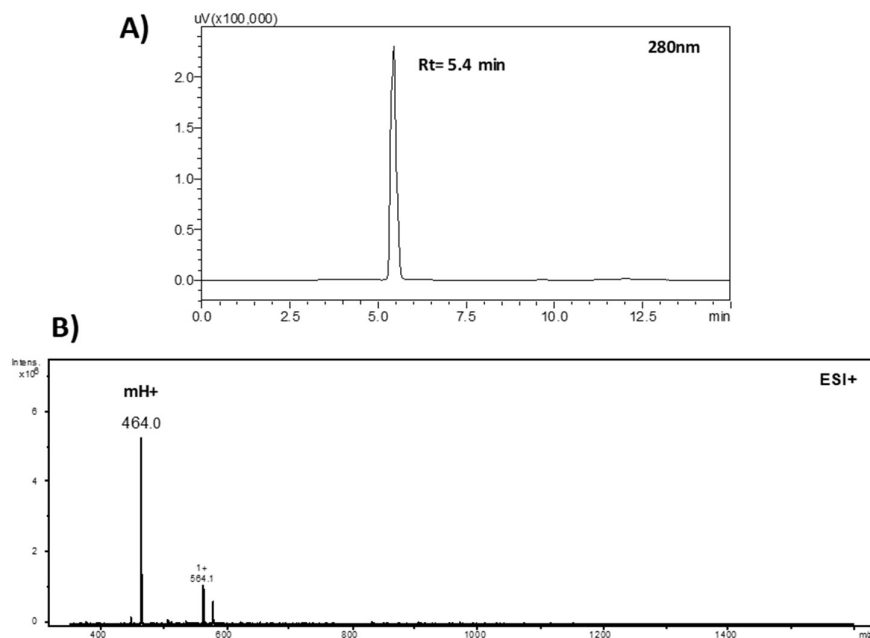


Figure 79: RP-HPLC and mass profiles of 5. A) RP-HPLC profile of 5 obtained on analytical Grace Vision HT C18 HL column (flow rate: 1,2 mL.min⁻¹) using the following method: 0 to 1 min: 20% B, 1 to 9 min: 50% B, 9 to 10 min: 100% B, with A: H₂O/0.1% TFA and B:CH₃CN/0.09% TFA, UV detection was performed at 230 nm and 280 nm. B) Mass profile of 5 in ESI/positive mode of ionisation, mH+=464.0.

LC/MS data – compound 6:

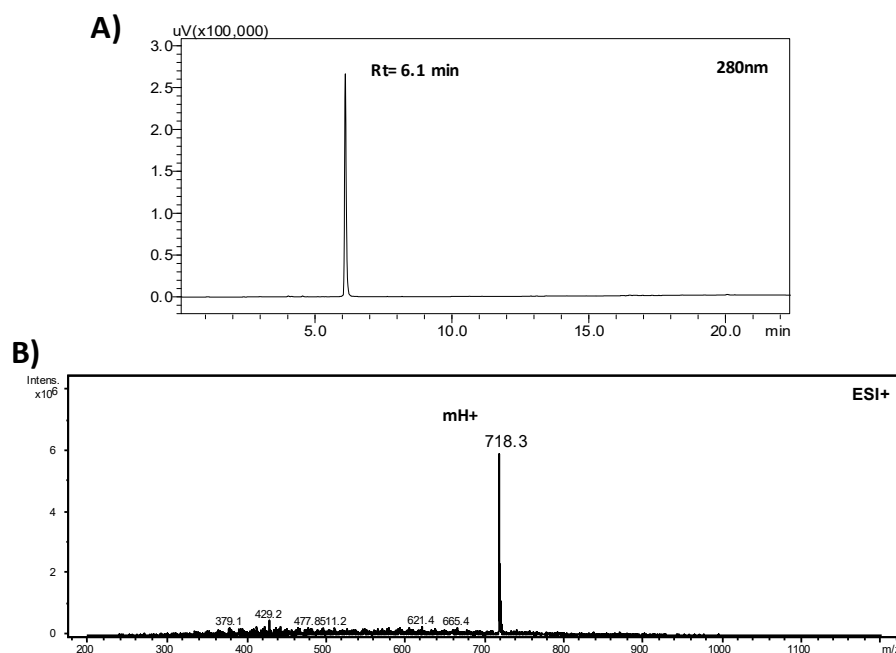


Figure 80: RP-HPLC and mass profiles of 6. A) RP-HPLC profile of 6 obtained on analytical Ascentis express C18 column (flow rate: 1,2 mL.min⁻¹) using the following method: 0 to 20 min: 100 % B, with A: H₂O/0.1% TFA and B:CH₃CN/0.09% TFA, UV detection was performed at 230 nm and 280 nm. B) Mass profile of 6 in ESI/positive mode of ionisation, mH+=718.3.

LC/MS data – compound 7:

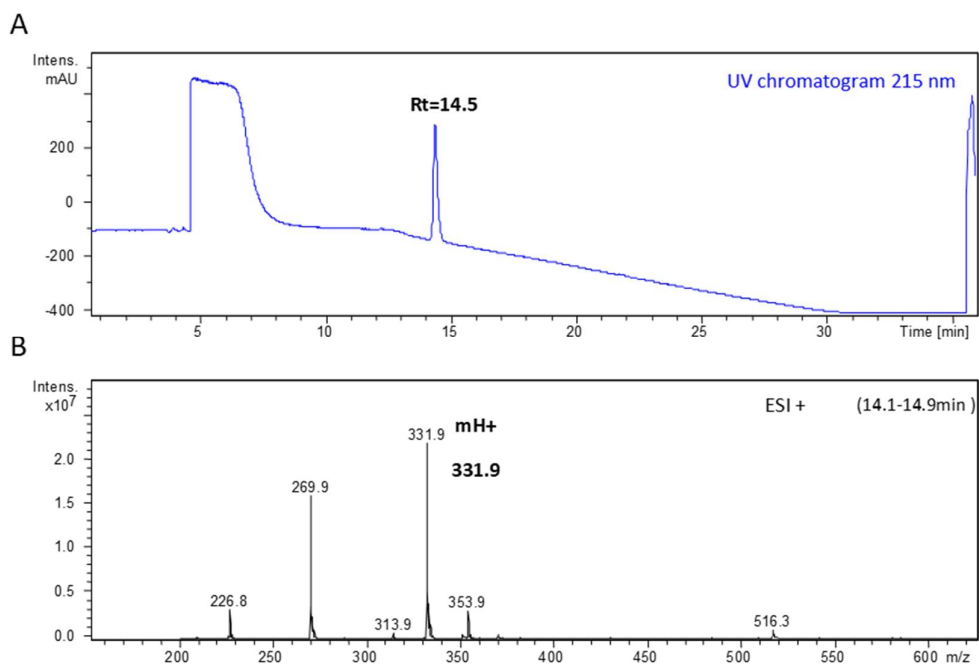
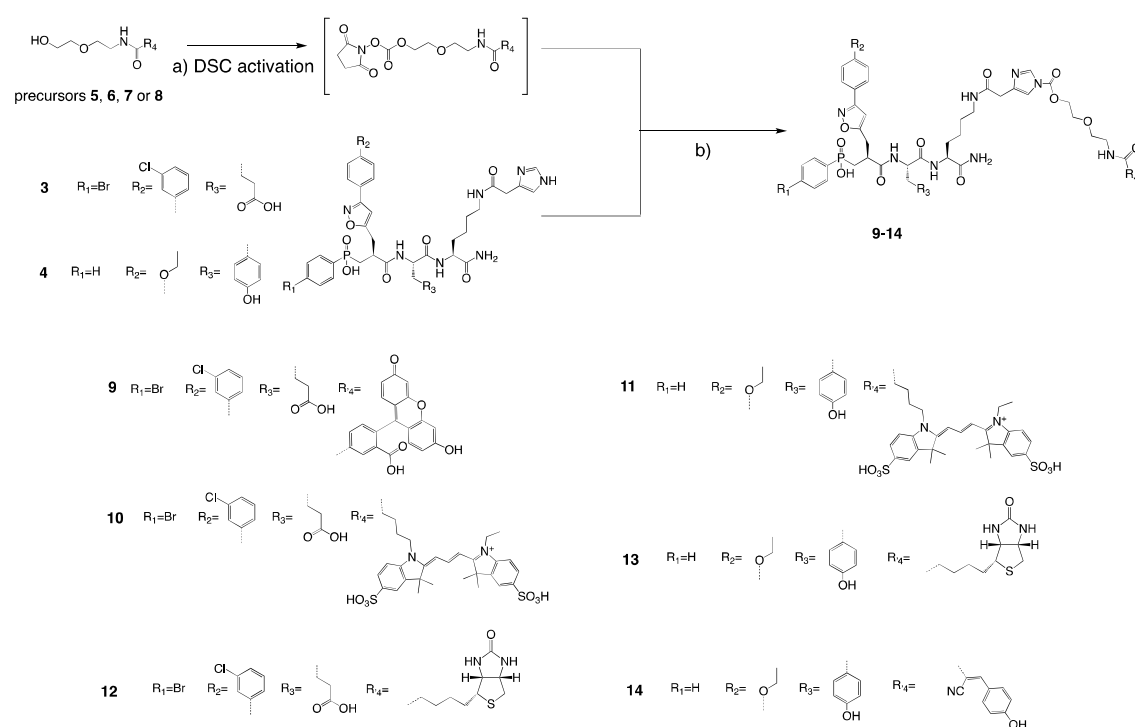


Figure 81: LCMS profile of purified compound 7. A) RP-HPLC profile of 7 ($R_t = 14.5$ min) in the following conditions: analytical XDB C18 column, flow rate: $0.6 \text{ mL}\cdot\text{min}^{-1}$, Method: 0 to 5 min: 100% A, 5 to 25 min: 100 % B with A: 10mM AcONH₄ and B: CH₃CN, UV detection was performed at 215 nm. B) Mass profile of 7 analysed in ESI/positive mode of ionisation, $mH^+=331.9$.

13.2.4. Synthesis of ligand-derived acyl imidazole probes 9 to 14.

A DSC solution was first prepared in DMF/DMSO: 2/1 (0.1 mg/ μ L, 390 mM). Precursor (**5**, **6**, **7** or **8**) was then activated in presence of DSC (1 eq) and DIEA (5 eq) in dry DMF ([precursor] = 80 mM) for 4h at room temperature. The reaction mixture was then added to imidazole derivatives (**3** or **4**, 1 eq) solubilized in dry DMF containing anhydrous pyridine (5 eq), [**3** or **4**]_{final} = 40 mM. The reaction solution was stirred for 2 h at room temperature and then diluted with CH₃CN (500 μ L). The resulting crude was purified by RP-HPLC.



Scheme 5: Synthesis of acyl imidazole probes 9-14. Reaction conditions: a) Precursors 5, 6, 7 or 8 (1eq), DSC (1.5 eq), DIEA (5 eq), anhydrous DMF, [5, 6, 7 or 8] = 80 mM, r.t. 4h b) Reaction mixture added to 3 or 4 (1 eq), pyridine (5 eq) DMF, [3 or 4]_{final} = 40 mM. r.t. 2h.

Probe **9** (R_t = 12.8 min) was purified on semi preparative Grace Vision HT C18 HL column (flow rate: 4 mL·min⁻¹, UV detection at 230 nm and 280 nm) using the following method: 0 to 30 min: 100% B, with A: 10mM AcONH₄ and B: CH₃CN, to yield a pale-yellow powder (16%) after freeze drying.

Probe **10** (Rt=13.7 min) was purified on semi preparative Grace Vision HT C18 HL column (flow: 4 mL.min⁻¹, UV detection at 230 nm and 280 nm) using the following method: 0 to 30 min: 100% B, with A: 10mM AcONH₄ and B: CH₃CN to yield a pink powder (39%) after freeze drying.

Probe **11** (Rt=13.1 min) was purified on semi preparative Grace Vision HT C18 HL column (flow: 4 mL.min⁻¹, UV detection at 230 nm and 280 nm) using the following method: 0 to 1 min: 18% B, 1 to 29 min: 48% B, 29 to 30 min: 100% B with A: 10mM AcONH₄ and B: CH₃CN, to yield a pink powder (33%) after freeze drying.

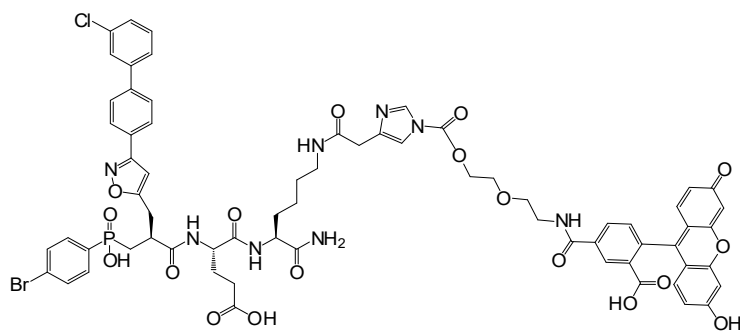
Probe **12** (Rt=13.0 min) was purified on semi preparative Grace Vision HT C18 HL column (flow: 4 mL.min⁻¹, UV detection at 230 nm and 280 nm) using the following method: 0 to 1 min: 38% B, 1 to 29 min: 68 %B, 29 to 30 min: 100% B with A: 10mM AcONH₄ and B: CH₃CN to yield a white powder (19%) after freeze drying.

Probe **13** (Rt=12.2 min) was purified on semi preparative Grace Vision HT C18 HL column (flow: 4 mL.min⁻¹, UV detection at 230 nm and 280 nm) using the following method: 0 to 1 min: 33% B, 1 to 29 min: 63 %B, 29 to 30 min: 100% B with A: 10mM AcONH₄ and B: CH₃CN to yield a white powder (19%) after freeze drying.

Probe **14** (Rt=17.1 min) was purified on semi preparative Grace Vision HT C18 HL column (flow: 4 mL.min⁻¹, UV detection at 230 nm and 280 nm) using the following method: 0 to 40 min: 100% B with A: 10mM AcONH₄ and B: CH₃CN to yield a white powder (10%) after freeze drying.

Each acyl imidazole probe (**9** to **14**) was aliquoted (10 nmol per batch), lyophilized and stored as solid at -20 °C away from light.

Compound 9:



Chemical Formula: $C_{67}H_{63}BrClN_8O_{18}P$

Exact Mass: 1412,29

Molecular Weight: 1414,61

$\epsilon_{498} = 76,900 \text{ M}^{-1} \cdot \text{cm}^{-1}$ (PBS 1X, pH=8)

Fluorescence: $\lambda_{ex} 496 / \lambda_{em} 524$

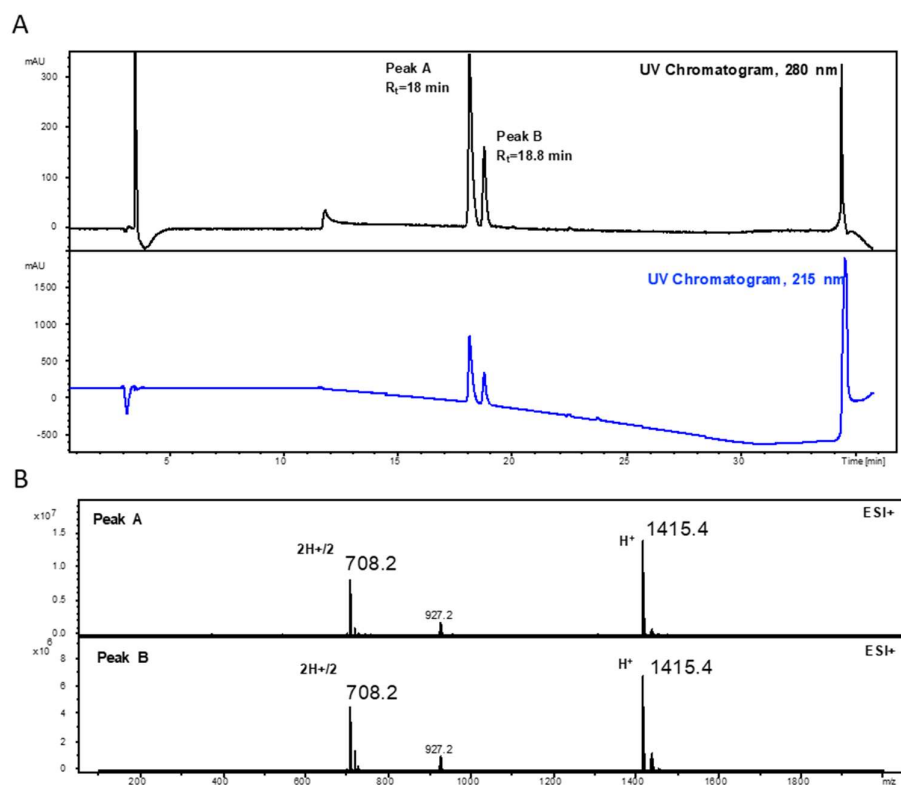
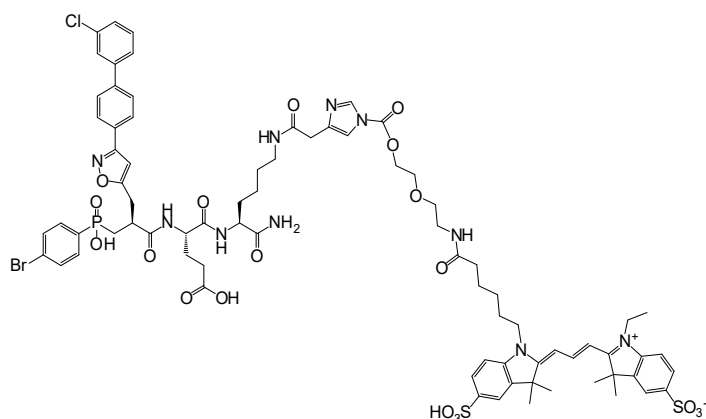


Figure 82: LC/MS profile of purified probe 9. A) RP-HPLC profile of 9 (peak A, $R_t = 18 \text{ min}$ and Peak B, 18.8 min) in the following conditions: analytical XDB C18 column, flow rate: $0.6 \text{ mL} \cdot \text{min}^{-1}$, Method: 0 to 5 min: 100% A, 5 to 25 min: 100% B with A: 10mM AcONH₄ and B: CH₃CN, UV detection was performed at 215 nm and 280 nm. B) Mass profile of 9 (peak A and B) analysed in ESI/positive mode of ionisation ($mH^+=1415.4$, $m2H^+/2= 708.2$).

HRMS m/z for $[C_{67}H_{64}BrClN_8O_{18}P]^+$ calculated 1413.2948, found 1413.2825.

Compound 10:



Chemical Formula: C₇₇H₈₉BrClN₁₀O₁₉PS₂

Exact Mass: 1666,44

Molecular Weight: 1669,05

$\epsilon_{550} = 150,000 \text{ M}^{-1} \cdot \text{cm}^{-1}$ (CH₃CN/H₂O:1/1)

Fluorescence: $\lambda_{\text{ex}} 553 / \lambda_{\text{em}} 568$

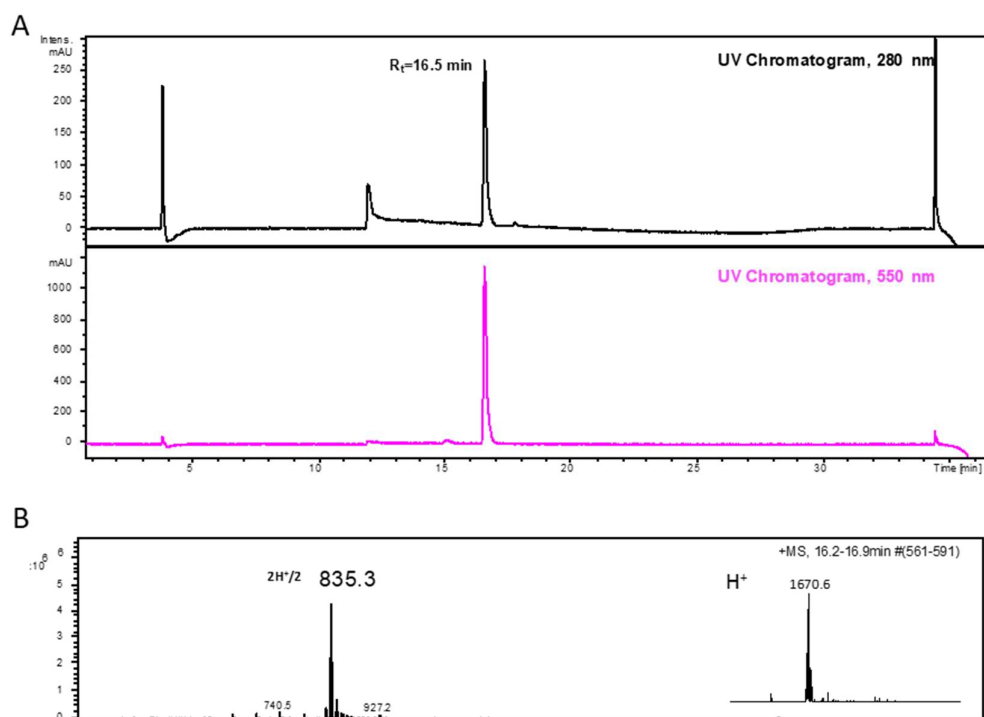
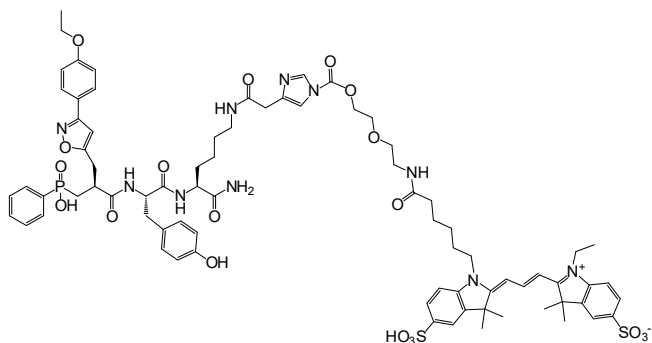


Figure 83: LCMS profile of purified probe 10. A) RP-HPLC profile of 10 ($R_t=16.5\text{min}$) in the following conditions: XDB C18 column, flow rate: $0.6 \text{ mL}\cdot\text{min}^{-1}$, Method: 0 to 5 min: 100% A, 5 to 25 min: 100 % B with A: 10mM AcONH₄ and B: CH₃CN, UV detection was performed at 280 nm and 550 nm. B) Mass profile of 10 analysed in ESI/positive mode of ionisation ($mH^+=1670.6$, $m2H^+/2=835.3$).

HRMS m/z for [C₇₇H₉₀BrClN₁₀O₁₉PS₂]⁺ calculated 1667.4434, found 1667.4381.

Compound 11:



Chemical Formula: $C_{77}H_{93}N_{10}O_{19}PS_2$

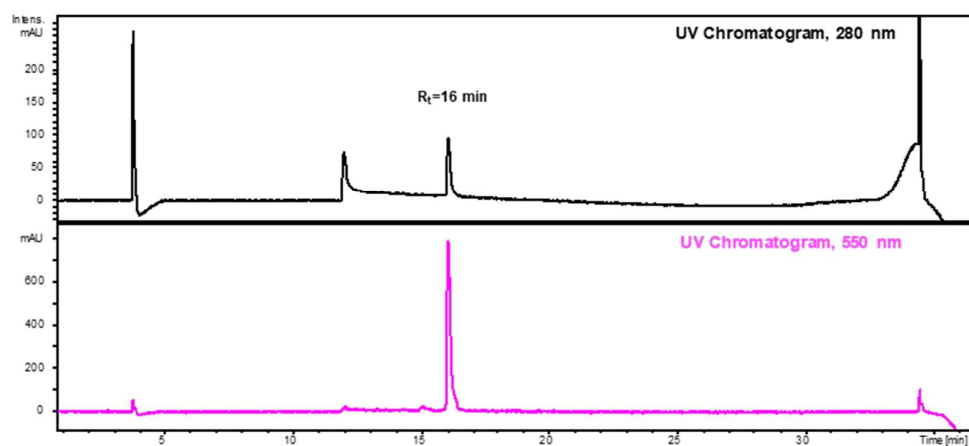
Exact Mass: 1556,58

Molecular Weight: 1557,72

$\epsilon_{550 \text{ nm}} = 150,000 \text{ M}^{-1} \cdot \text{cm}^{-1}$ ($\text{CH}_3\text{CN}/\text{H}_2\text{O}:1/1$)

Fluorescence: $\lambda_{\text{ex}} 552 / \lambda_{\text{em}} 566$

A



B

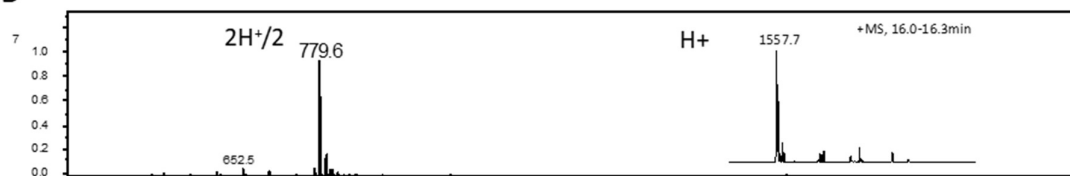


Figure 84: LCMS profile of purified probe 11. A) RP-HPLC profile of 11 ($R_t=16 \text{ min}$) in the following conditions: XDB C18 column, flow rate: $0.6 \text{ mL}\cdot\text{min}^{-1}$, Method: 0 to 5 min: 100% A, 5 to 25 min: 100 % B with A: 10mM AcONH₄ and B: CH₃CN, UV detection was performed at 280 nm and 550 nm. B) Mass profile of 11 analysed in ESI/positive mode of ionisation ($m\text{H}^+=1557.7$, $m2\text{H}^+/2=779.6$).

HRMS m/z for $[C_{77}H_{94}N_{10}O_{19}PS_2]^+$ calculated 1557.5875, found 1557.5870.

Compound 12:

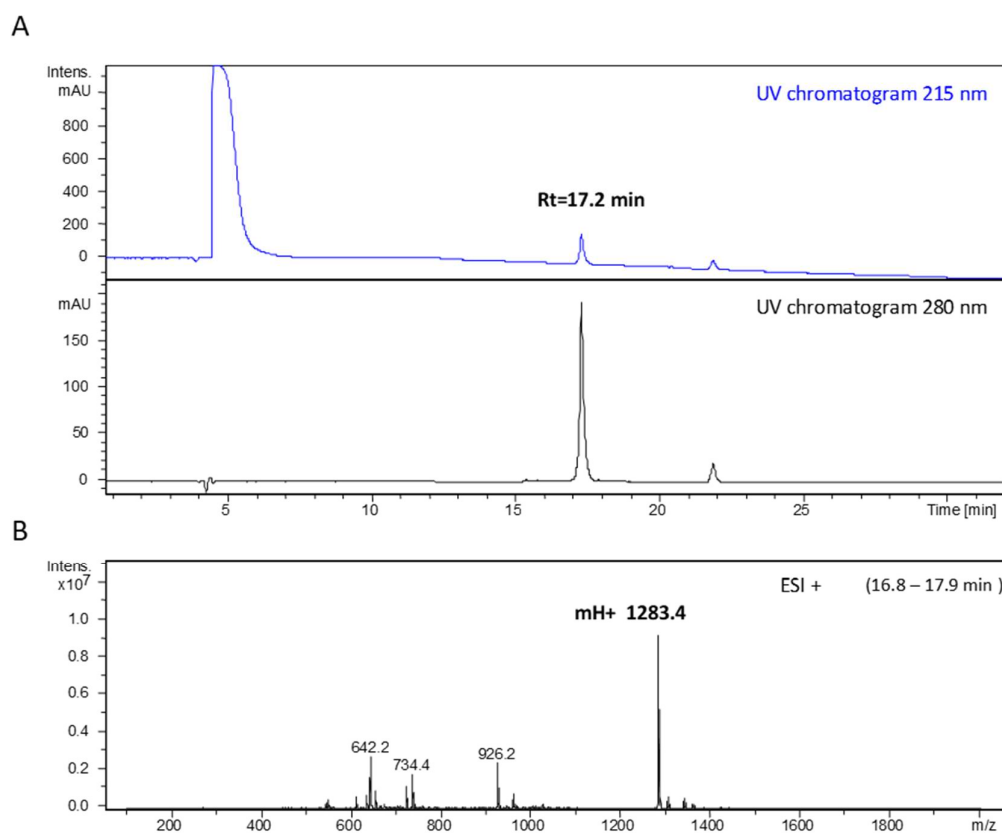
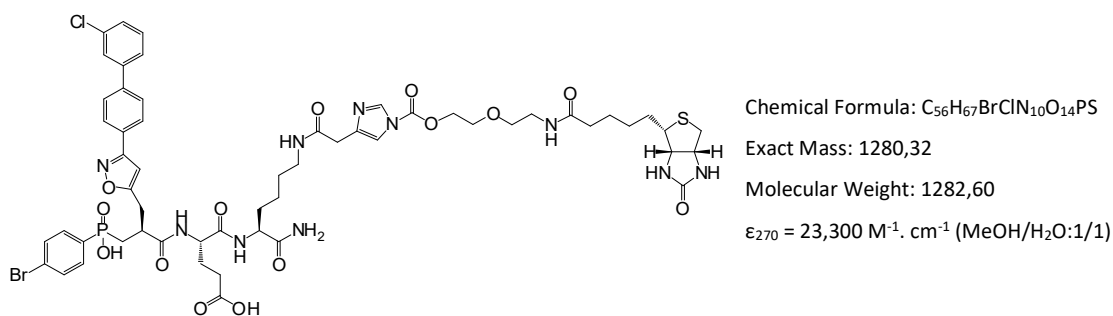
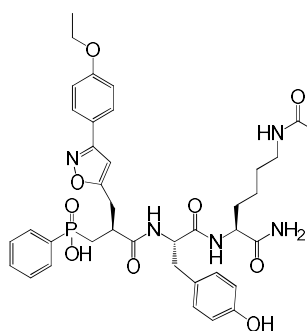


Figure 85: LCMS profile of purified probe 12. A) RP-HPLC profile of 12 (Rt=17.2 min) in the following conditions: analytical XDB C18 column, flow rate: 0.6 mL.min⁻¹, Method: 0 to 5 min: 100% A, 5 to 25 min: 100 % B with A: 10mM AcONH₄ and B: CH₃CN, UV detection was performed at 215 nm and 280 nm. B) Mass profile of 12 analysed in ESI/positive mode of ionisation (mH+=1283.4, m2H+/2=642.2).

HRMS m/z for [C₅₆H₆₇BrClN₁₀O₁₄PS]⁺ calculated 1281.3246, found 1281.3285.

Compound 13:



Chemical Formula: C₅₆H₇₁N₁₀O₁₄PS

Exact Mass: 1170,46

Molecular Weight: 1171,27

$\epsilon_{258} = 24,000 \text{ M}^{-1} \cdot \text{cm}^{-1}$ (MeOH/H₂O:1/1)

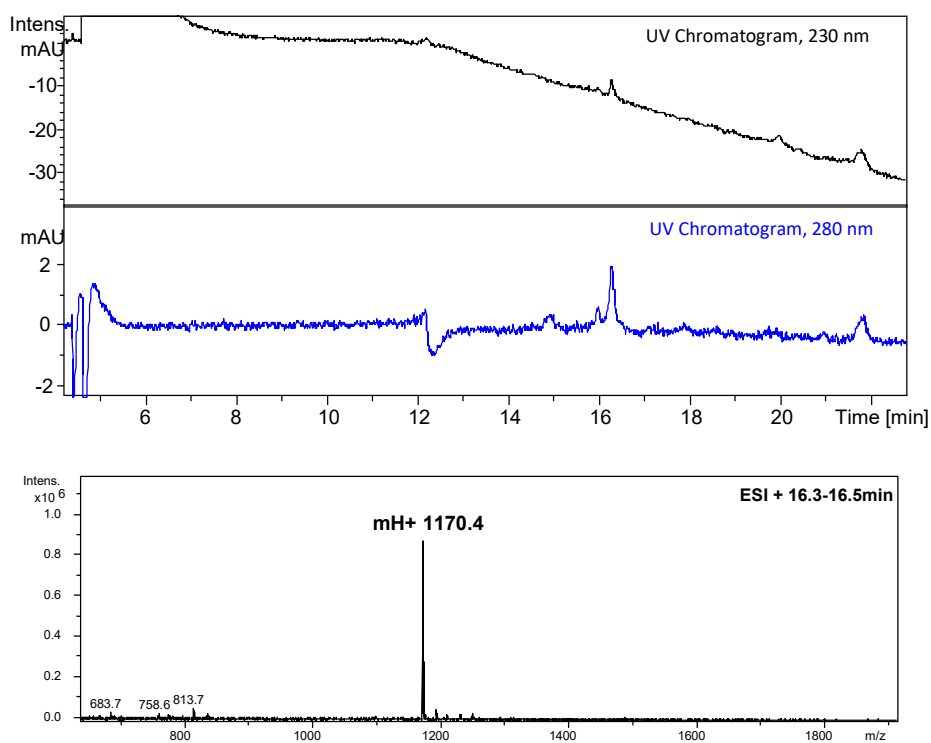
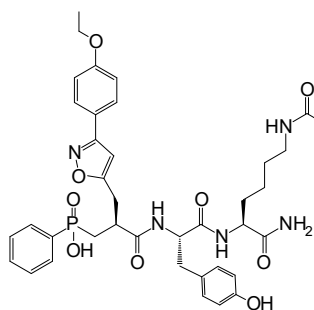


Figure 86: LCMS profile of purified probe 13. A) RP-HPLC profile of 12 (Rt=16.3 min) in the following conditions: analytical XDB C18 column, flow rate: 0.6 mL.min⁻¹, Method: 0 to 5 min: 100% A, 5 to 25 min: 100% B with A: 10mM AcONH₄ and B: CH₃CN, UV detection was performed at 215 nm and 280 nm. B) Mass profile of 13 analysed in ESI/positive mode of ionisation (mH+=1170.4).

HRMS m/z for [C₅₆H₇₂N₁₀O₁₄PS]⁺ calculated 1171.4688, found 1171.4697

Compound 14:



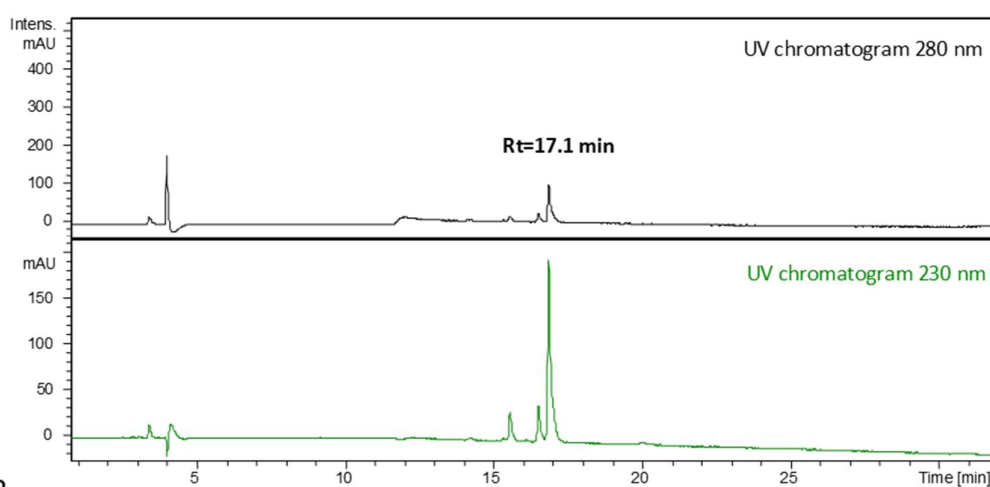
Chemical Formula: C₅₆H₆₂N₉O₁₄P

Exact Mass: 1115,42

Molecular Weight: 1116,12

$\epsilon_{258} = 24,000 \text{ M}^{-1} \cdot \text{cm}^{-1}$ (MeOH/H₂O:1/1)

A



B

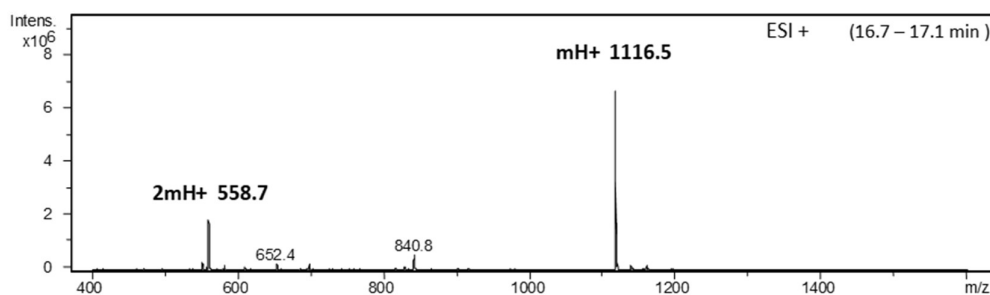
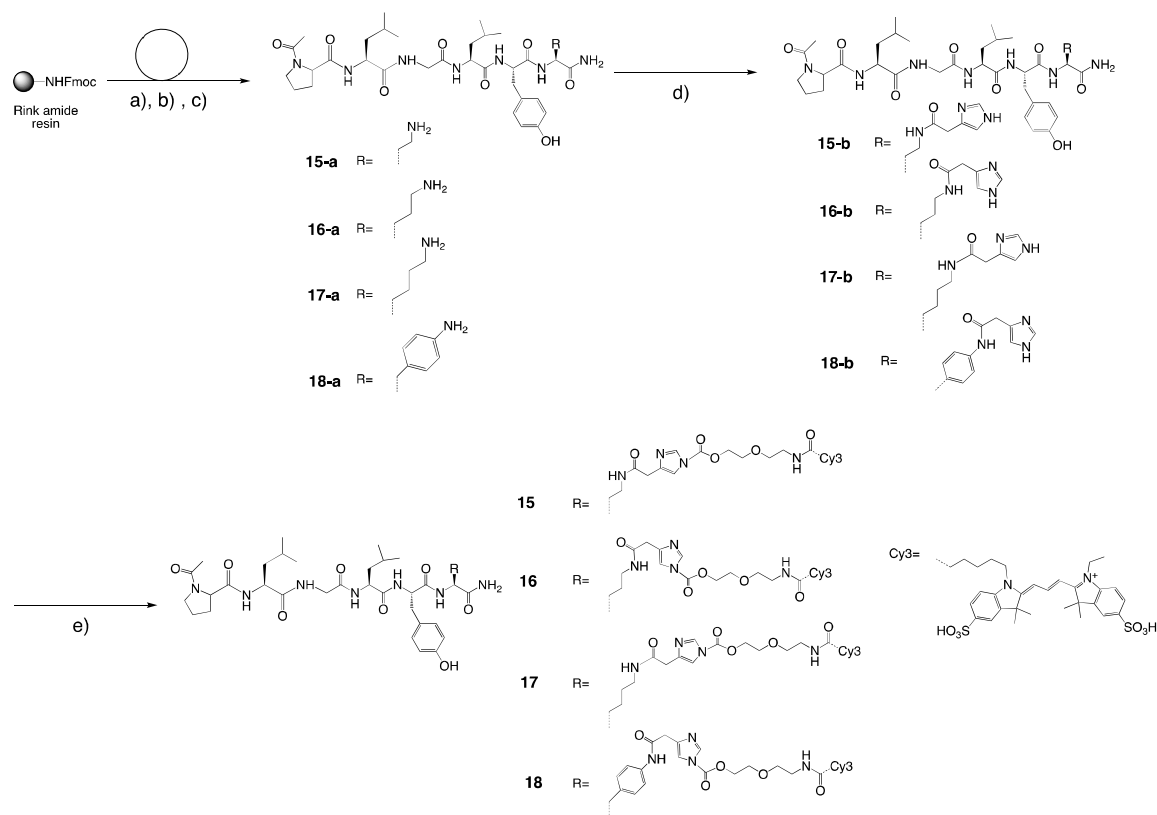


Figure 87: LCMS profile of purified probe 14. A) RP-HPLC profile of 14 (Rt=17.1 min) in the following conditions: analytical XDB C18 column, flow rate: 0.6 mL.min⁻¹, Method: 0 to 5 min: 100% A, 5 to 25 min: 100 % B with A: 10mM AcONH₄ and B: CH₃CN, UV detection was performed at 230 nm and 280 nm. B) Mass profile of 14 analysed in ESI/positive mode of ionisation (mH+=1116.5, m2H+/2=558.7).

HRMS m/z for [C₅₆H₆₃N₉O₁₄P]⁺ calculated 1116.4232, found 1116.4248

13.2.5. Synthesis of substrate-derived acyl imidazole probes 15, 16, 17, and 18



Scheme 6: Synthesis of acyl imidazole probes 15-18. Reaction conditions: a) Fmoc solid phase synthesis, Fmoc-AA-OH (10 eq), ClHOBT/DIC (10 eq) in DMF, 60°C 10 min, followed by acylation step in presence of acetyl imidazole (10eq), b) TFA/TIS/H₂O: 95/2.5/2.5 c) RP-HPLC purification, d) 4-Imidazoleacetic acid hydrochloride (10 eq), EDC, ClHOBT (3 eq), DIEA (30 eq) in DMF, o. n., r.t followed by RP-HPLC purification, e) Compound 6 (1eq), DSC (1.5 eq), DIEA (5 eq), anhydrous DMF, [6] = 80 mM, r.t. 4h, the reaction mixture was then added to 15b, 16b, 17b or 18b (1 eq), pyridine (5 eq) DMF, [15b, 16b, 17b or 18b] = 40 mM. r.t. 2h. followed by RP-HPLC purification.

Peptide sequence was synthesized manually on solid support (Rink amide, Novabiochem) using standard Fmoc chemistry. After Fmoc removal (piperidine 20% in DMF, 3 × 2 min, 60 °C, 25 W) and washing steps (2 x DMF followed by 2 x DCM), Fmoc-AA-OH (10 eq, [100 mM]) were sequentially incorporated on the solid support using a standard activation protocol in presence of DIC (10 eq) and ClHOBT (10 eq) in DMF. In future P3' position of **15a**, **16a**, **17a** and **18a**, Fmoc-(Dab)-OH, Fmoc-Orn(Mtt)-OH, Fmoc-Lys(Boc) and Fmoc pNH₂BocPhe-OH were incorporated respectively. The coupling reaction was carried out under microwave irradiation (45 W) at 60 °C for 10 min and was repeated once. After sequence building and removal of the N-*ter* Fmoc protection, the acetylation step was performed in presence of 1-acetyl Imidazole (10 eq). The resulting peptides were then cleaved from the support with TFA/TIS/H₂O: 95/2.5/2.5. After RP-HPLC purification (Vision HT C18 HL column, flow

rate: 4 mL.min⁻¹ using the following program: 0 to 2 min: 15% B%, 2 to 28 min: 45%, 28 to 30 min: 100% B with A: H₂O/0.1% TFA and B:CH₃CN/0.09% TFA, UV detection at 230 nm and 280 nm), the collected fractions containing the expected peptides (Mass analysis) were dosed by UV ($\epsilon_{280}=1490 \text{ M}^{-1}\text{cm}^{-1}$). Peptides **15a**, **16a**, **17a** and **18a** were isolated with 26%, 29%, 29% and 33% respectively. Each peptide was lyophilized and subsequently engaged in the following step. Imidazole derivatives **15b**, **16b**, **17b** and **18b** were obtained from 4-Imidazole acetic acid hydrochloride (10 eq) using the conditions described for the synthesis of compounds **3** and **4**. LC/MS analyses of crude **15b**, **16b**, **17b** and **18b** indicated an incomplete acetyl imidazole incorporation onto P3' amino function (see Figure 88 for LC/MS profile of **15b** in mixture with its amino precursor **15a**). Since the amino precursor and the imidazole derivative were particularly difficult to separate, the two compounds were collected in mixture, lyophilized and directly engaged in the following step. Note that the yield was not calculated in this case. For the subsequent reaction, the respective concentrations of **15b**, **16b**, **17b** and **18b** were estimated by UV by considering the tyrosine extinction coefficient ($\epsilon_{280}=1490 \text{ M}^{-1}\text{.cm}^{-1}$).

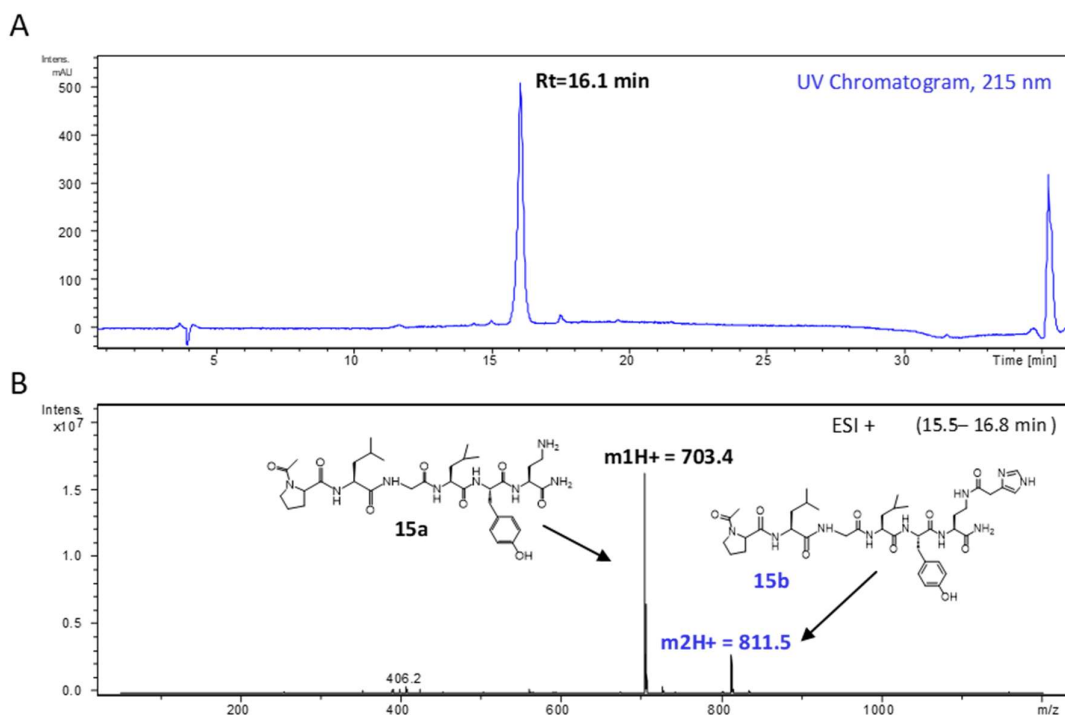
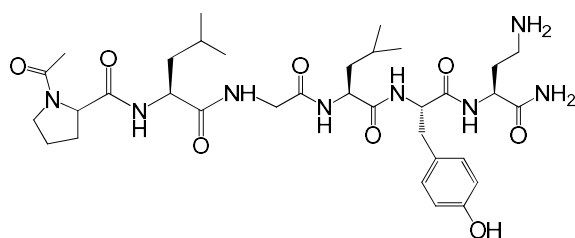


Figure 88: LC/MS profile of 15b in mixture with its amino precursor 15a. A) RP-HPLC profile is obtained after collection of the fraction and analysis in the following conditions: analytical XDB C18 column, flow rate: 0.6 mL.min⁻¹, Method: 0 to 5 min 100%A, 5 to 25 min: 100% B, with A: H₂O/0.1% TFA and B:CH₃CN/0.09% TFA, UV detection was performed at 280 nm. B) Mass profile in ESI/positive mode of ionisation. The analysis of the mass profile revealed that imidazole derivative 15b (mH+=811.5) co elute with its amino precursor 15a (mH+=703.4).

Substrate-derived acyl imidazole probes were synthesized according to the protocol described for ligand-derived probes. After RP-HPLC purification (semi preparative Vision HT C18 HL column, flow rate: 4 mL.min⁻¹ using the following program: 0 to 30 min: 100% B with A: 10mM AcONH₄ and B: CH₃CN, UV detection at 230 nm and 280 nm). Compound **15**, **16**, **17** and **18** were aliquoted (10 nmol per batch), lyophilized and stored at -20°C away from light. **15**, **16**, **17** and **18** were obtained with 9%, 12%, 7% and 7% yield respectively.

Compound 15a:



Chemical Formula: C₃₄H₅₄N₈O₈

Exact Mass: 702,41

Molecular Weight: 702,84

ϵ_{280} =1490 M⁻¹cm⁻¹ (MeOH/H₂O:1/1)

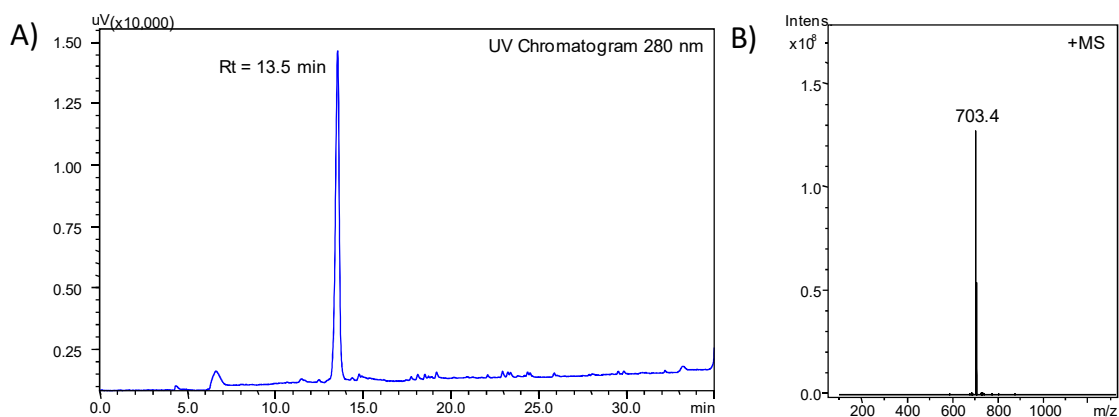
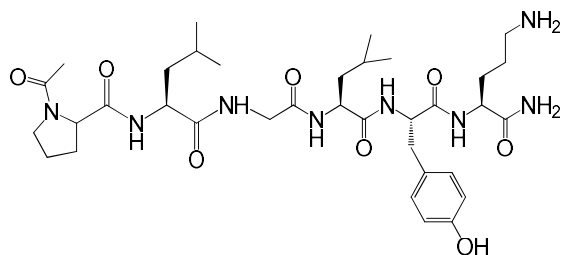


Figure 89: RP-HPLC and mass spectrometry profiles of purified 15a. A) RP-HPLC profile of 15a (Rt=13.5 min) in the following conditions: semi preparative Vision HT C18 HL column, flow rate: 4 mL.min⁻¹, Method: 0 to 30 min: 100% B, with A: H₂O/0.1% TFA and B:CH₃CN/0.09% TFA, UV detection was performed at 280 nm. B) Mass profile of 15a analysed in ESI/positive mode of ionisation (mH⁺=703.4).

Compound 16a:



Chemical Formula: C₃₅H₅₆N₈O₈

Exact Mass: 716,42

Molecular Weight: 716,87

ϵ_{280} =1490 M⁻¹cm⁻¹ (MeOH/H₂O:1/1)

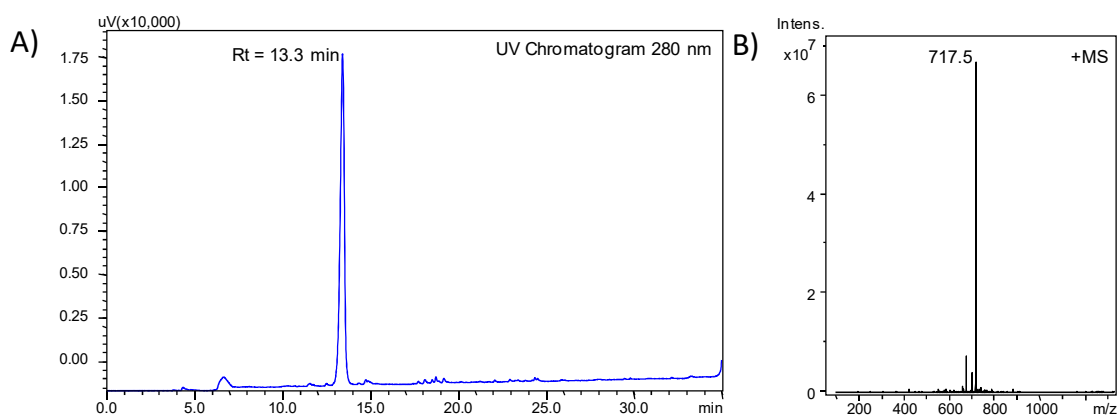
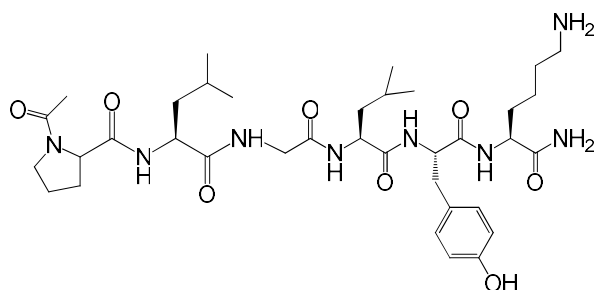


Figure 90: RP-HPLC and mass spectrometry profiles of purified 16a. A) RP-HPLC profile of 16a (Rt=13.3 min) in the following conditions: semi preparative Vision HT C18 HL column, flow rate: 4 mL.min⁻¹, Method: 0 to 30 min: 100% B, with A: H₂O/0.1% TFA and B:CH₃CN/0.09% TFA, UV detection was performed at 280 nm. B) Mass profile of 16a analysed in ESI/positive mode of ionisation (mH⁺=717.5).

Compound 17a:



Chemical Formula: $C_{36}H_{58}N_8O_8$

Exact Mass: 730,40

Molecular Weight: 730,89

$\epsilon_{280} = 1490 \text{ M}^{-1}\text{cm}^{-1}$ (MeOH/H₂O:1/1)

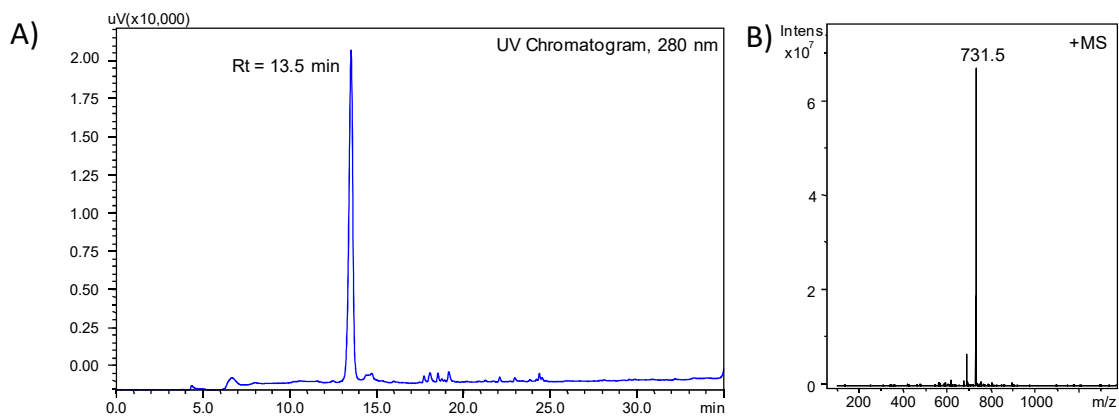
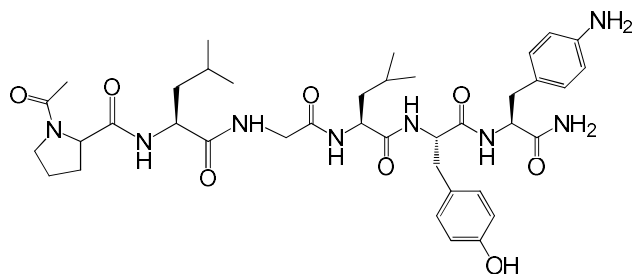


Figure 91: RP-HPLC and mass spectrometry profiles of purified 17a. A) RP-HPLC profile of 17a ($R_t=13.5 \text{ min}$) in the following conditions: semi preparative Vision HT C18 HL column, flow rate: $4 \text{ mL}\cdot\text{min}^{-1}$, Method: 0 to 30 min: 100% B, with A: $\text{H}_2\text{O}/0.1\% \text{ TFA}$ and B: $\text{CH}_3\text{CN}/0.09\% \text{ TFA}$, UV detection was performed at 280 nm. B) Mass profile of 17a analysed in ESI/positive mode of ionisation ($mH^+=731.5$).

Compound 18a:



Chemical Formula: $C_{39}H_{56}N_8O_8$

Exact Mass: 764,42

Molecular Weight: 764,91

$\epsilon_{280}=1490 \text{ M}^{-1}\text{cm}^{-1}$ (MeOH/H₂O:1/1)

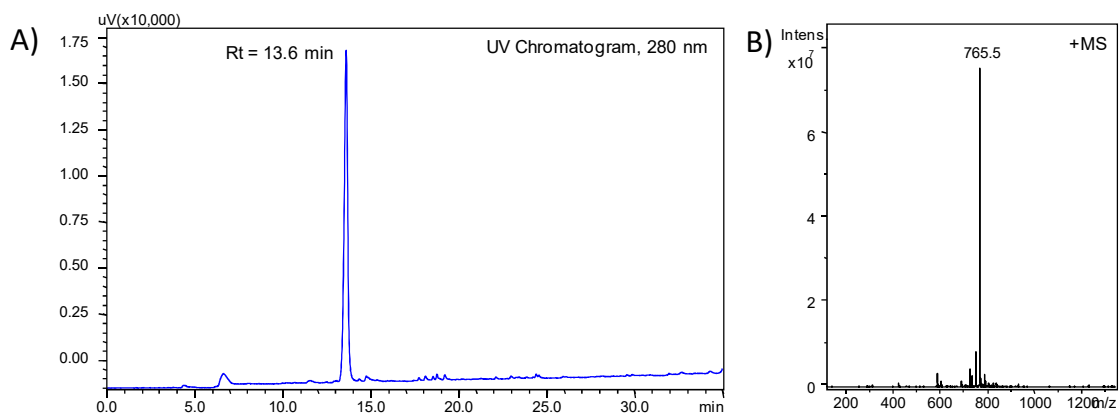
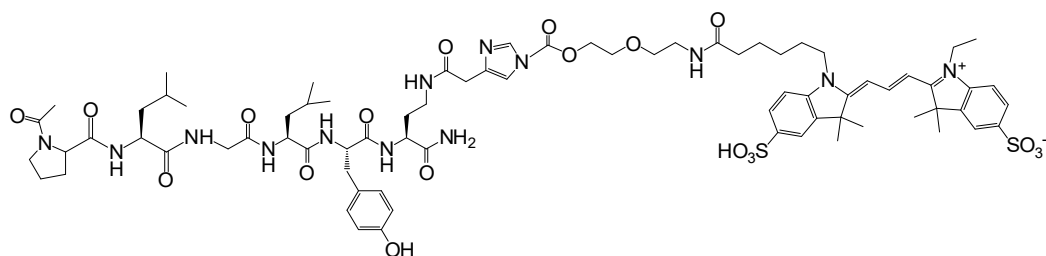


Figure 92: RP-HPLC and mass spectrometry profiles of purified 18a. A) RP-HPLC profile of 18a (Rt=13.6 min) in the following conditions: semi preparative Vision HT C18 HL column, flow rate: 4 mL.min⁻¹, Method: 0 to 30min: 100% B, with A: H₂O/0.1% TFA and B:CH₃CN/0.09% TFA, UV detection was performed at 280 nm. B) Mass profile of 18a analysed in ESI/positive mode of ionisation (mH⁺=765.5).

Compound 15:



Chemical Formula: $C_{75}H_{103}N_{13}O_{19}S_2$

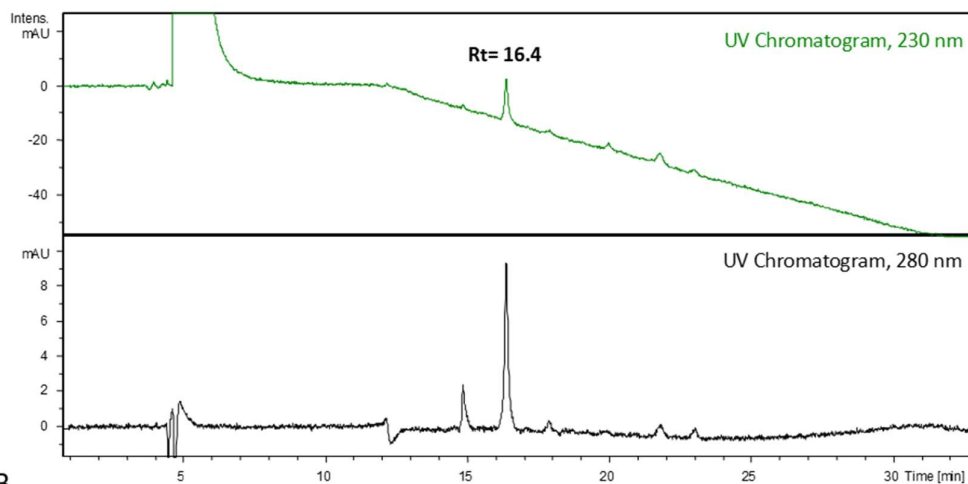
Exact Mass: 1553,69

Molecular Weight: 1554,83

$\epsilon_{550 \text{ nm}} = 150,000 \text{ M}^{-1} \cdot \text{cm}^{-1}$ ($\text{CH}_3\text{CN}/\text{H}_2\text{O}:1/1$)

Fluorescence: $\lambda_{\text{ex}} 551 / \lambda_{\text{em}} 565$

A



B

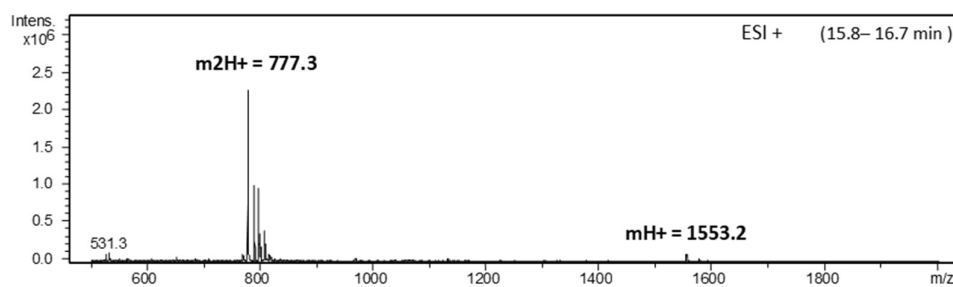
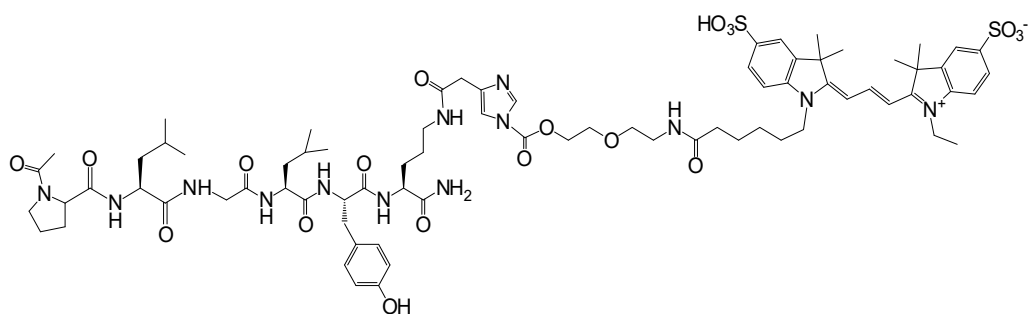


Figure 93: LCMS profile of purified probe 15. A) RP-HPLC profile of 15 ($R_t=16.4 \text{ min}$) in the following conditions: analytical XDB C18 column, flow rate: $0.6 \text{ mL}\cdot\text{min}^{-1}$, Method: 0 to 5 min: 100% A, 5 to 25 min: 100% B with A: 10mM AcONH₄ and B: CH₃CN, UV detection was performed at 230 nm and 280 nm. B) Mass profile of 15 analysed in ESI/positive mode of ionisation ($mH^+=1553.2$, $m2H^+/2=777.3$).

HRMS m/z for $[C_{75}H_{104}N_{13}O_{19}S_2]^+$ calculated 1554.7012, found 1554.7045

Compound 16:



Chemical Formula: $C_{76}H_{105}N_{13}O_{19}S_2$

Exact Mass: 1567,71

$\epsilon_{550 \text{ nm}} = 150,000 \text{ M}^{-1} \cdot \text{cm}^{-1}$ ($\text{CH}_3\text{CN}/\text{H}_2\text{O}:1/1$)

Molecular Weight: 1568,85

Fluorescence: $\lambda_{\text{ex}} 551 / \lambda_{\text{em}} 565$

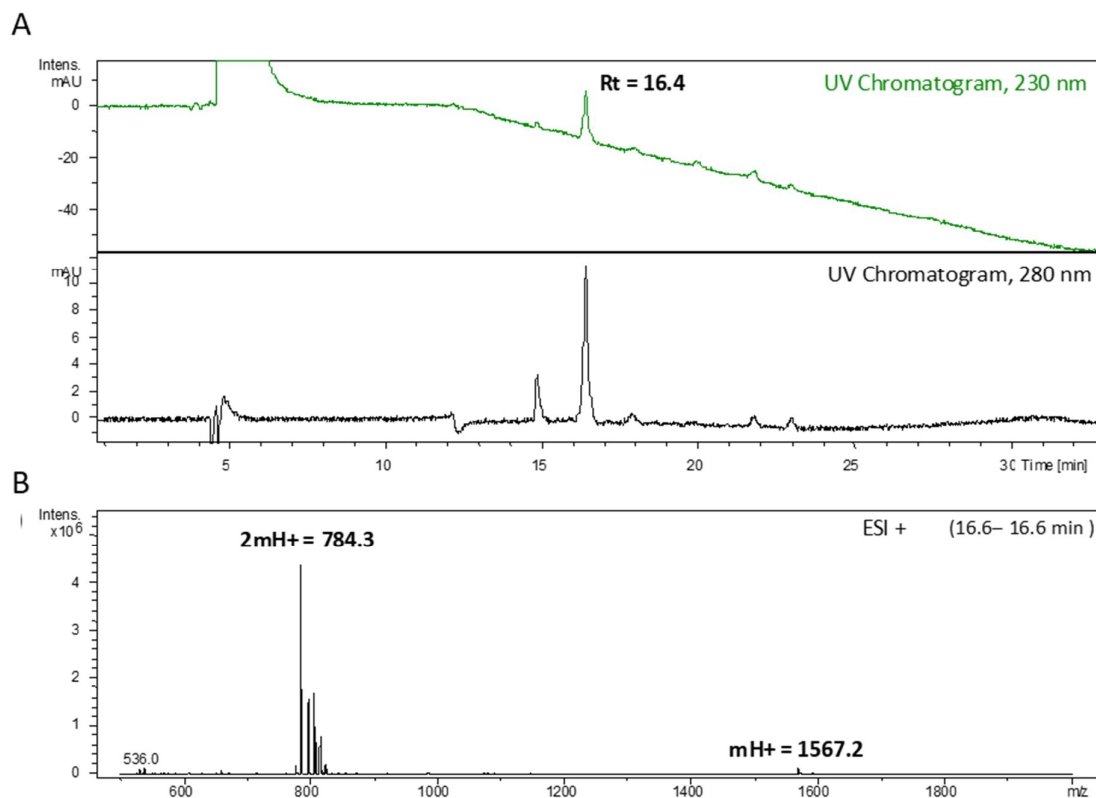
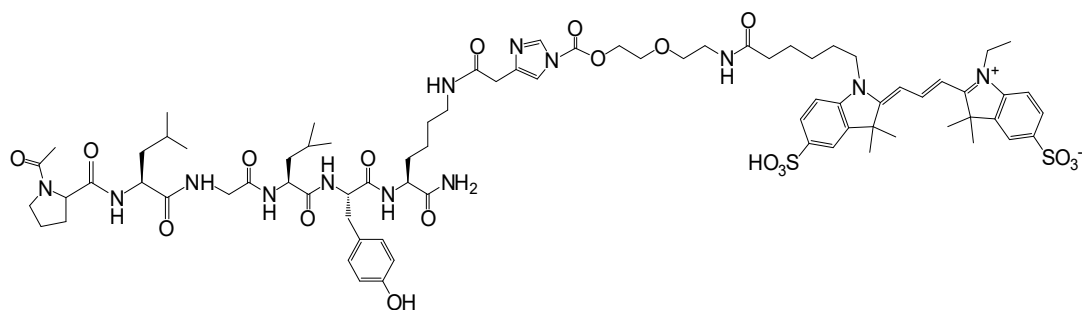


Figure 94: LCMS profile of purified probe 16. A) RP-HPLC profile of 16 (Rt=16.4 min) in the following conditions: analytical XDB C18 column, flow rate: 0.6 mL.min⁻¹, Method: 0 to 5 min: 100% A, 5 to 25 min: 100% B with A: 10mM AcONH₄ and B: CH₃CN, UV detection was performed at 230 nm and 280 nm. B) Mass profile of 16 analysed in ESI/positive mode of ionisation (mH+=1567.2, m2H+/2=784.3).

HRMS m/z for $[C_{76}H_{106}N_{13}O_{19}S_2]^+$ calculated 1568.7169, found 1568.7250

Compound 17:



Chemical Formula: $C_{77}H_{107}N_{13}O_{19}S_2$

$\epsilon_{550 \text{ nm}} = 150,000 \text{ M}^{-1} \cdot \text{cm}^{-1}$ ($\text{CH}_3\text{CN}/\text{H}_2\text{O}:1/1$)

Exact Mass: 1581,72

Fluorescence: $\lambda_{\text{ex}} 553 / \lambda_{\text{em}} 565$

Molecular Weight: 1582,88

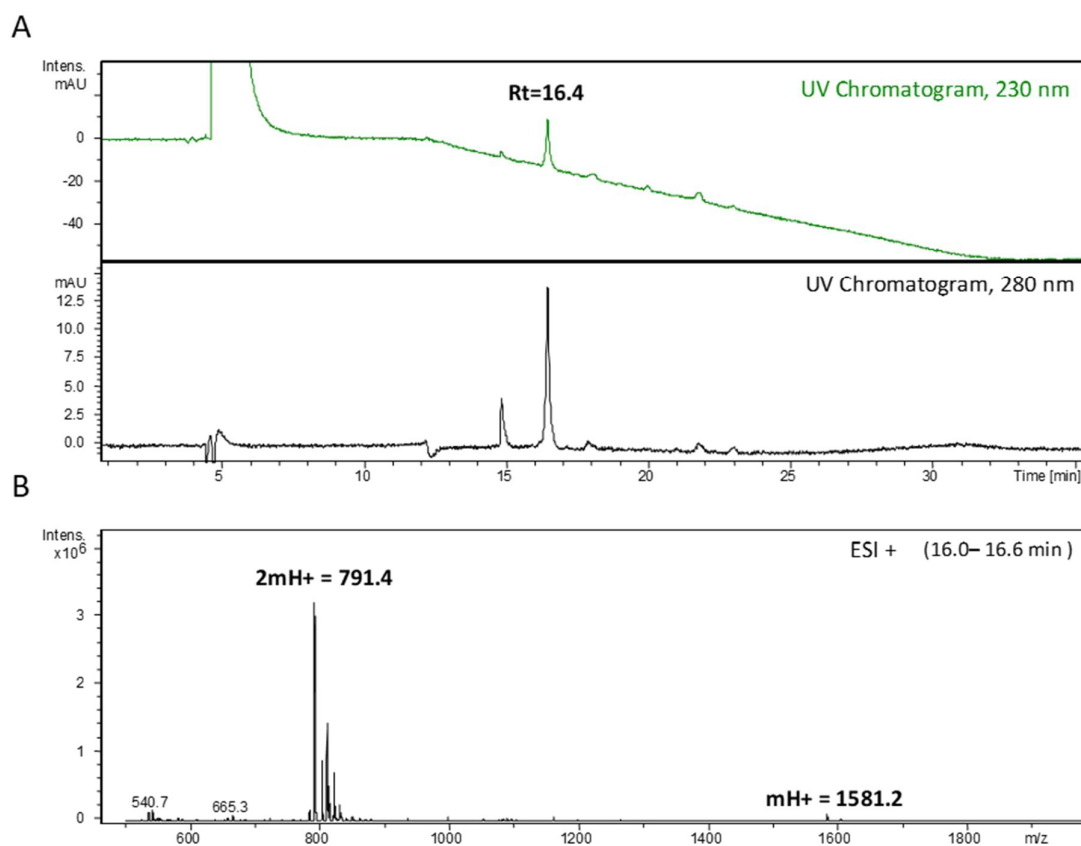
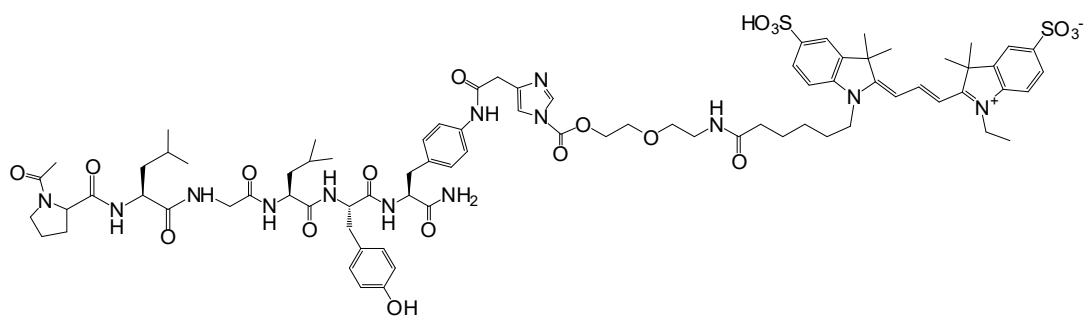


Figure 95: LCMS profile of purified probe 17. A) RP-HPLC profile of 17 ($R_t=16.4$ min) in the following conditions: analytical XDB C18 column, flow rate: $0.6 \text{ mL} \cdot \text{min}^{-1}$, Method: 0 to 5 min: 100% A, 5 to 25 min: 100% B with A: 10mM AcONH₄ and B: CH₃CN, UV detection was performed at 230 nm and 280 nm. B) Mass profile of 17 analysed in ESI/positive mode of ionisation ($mH^+=1581.2$, $2mH^+/2=791.4$).

HRMS m/z for $[C_{77}H_{108}N_{13}O_{19}S_2]^+$ calculated 1582.7325, found 1582.7351

Compound 18:



Chemical Formula: $C_{80}H_{105}N_{13}O_{19}S_2$

$\epsilon_{550\text{ nm}} = 150,000\text{ M}^{-1}\cdot\text{cm}^{-1}$ ($\text{CH}_3\text{CN}/\text{H}_2\text{O}:1/1$)

Exact Mass: 1615,71

Fluorescence: $\lambda_{\text{ex}} 551 / \lambda_{\text{em}} 565$

Molecular Weight: 1616,90

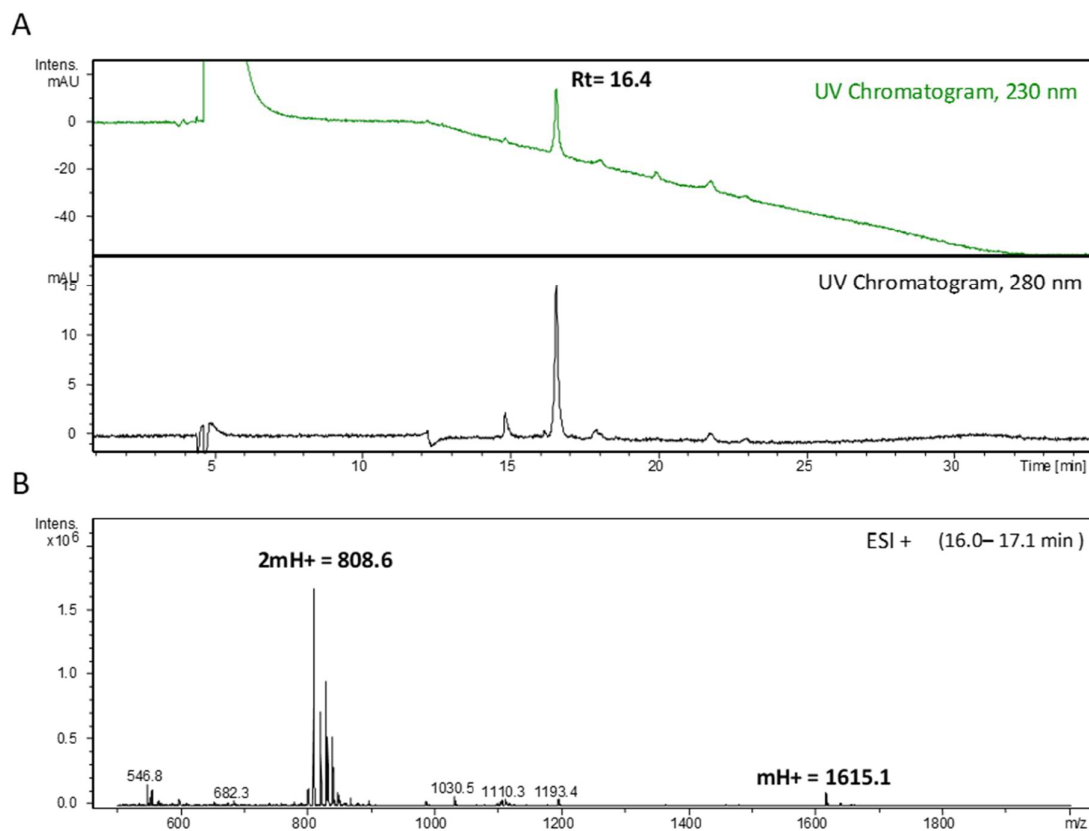
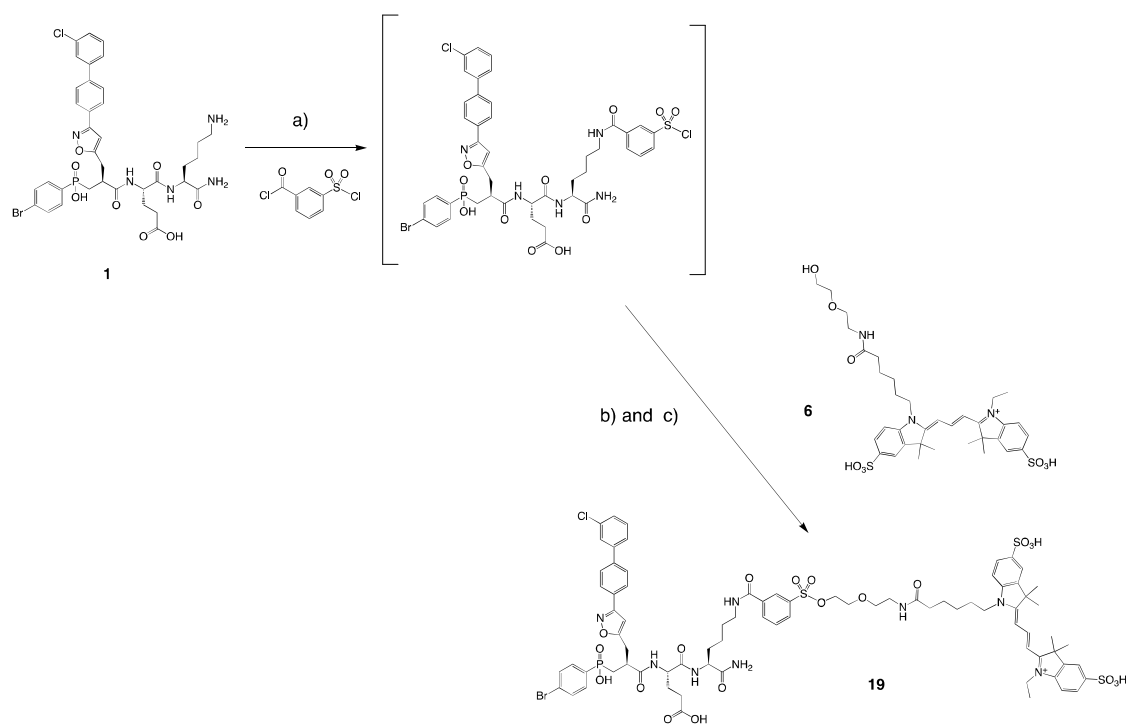


Figure 96: LCMS profile of purified probe 18. A) RP-HPLC profile of 18 ($R_t=16.4$ min) in the following conditions: analytical XDB C18 column, flow rate: $0.6\text{ mL}\cdot\text{min}^{-1}$, Method: 0 to 5 min: 100% A, 5 to 25 min: 100% B with A: 10mM AcONH₄ and B: CH₃CN, UV detection was performed at 230 nm and 280 nm. B) Mass profile of 18 analysed in ESI/positive mode of ionisation ($mH^+=1615.1$, $m2H^+/2=808.6$).

HRMS m/z for $[C_{80}H_{106}N_{13}O_{19}S_2]^+$ calculated 1616.7169, found 1616.7180

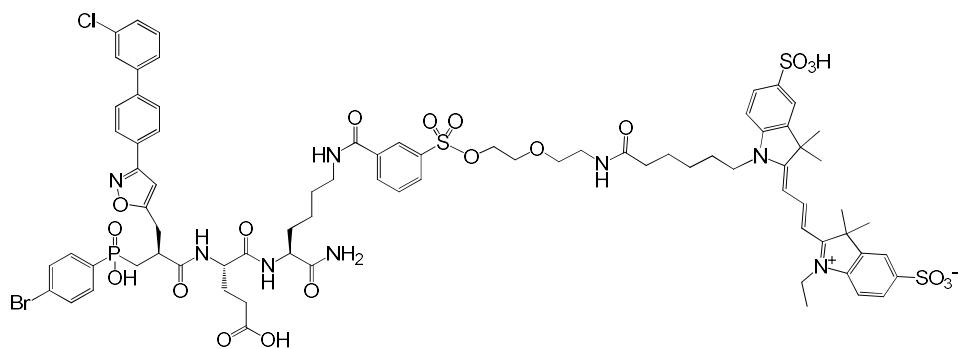
13.2.6. Synthesis of Tosyl probe 19.



Scheme 7: Synthesis of compound 19. Reaction conditions: a) compound 1 (1 eq), DIEA (10 eq), 3-Chlorosulfonyl benzoyl chloride (1.2 eq), DMF/DIEA:90/10, [2]=60 mM, 0°C for 30 min and r.t. for 1h30 b) to the activated intermediate was then added 6 (0.6 eq) in DMF, [activated 1]=45 mM, [6]= 30 mM, r.t., 1h, c) DMAP (0,09 eq), 3h, r.t.

Compound **1** (1.1 μmol , 1 eq) was first dissolved in anhydrous DMF and the solution was cooled to 0°C (ice bath). 3-Chlorosulfonyl benzoyl chloride (3-Chlorosulfonyl benzoyl chloride (1.3 μmole , 1.2 eq, 1 μL of a solution at 3mg in 10 μL of DMF) and DIEA (11 μmole , 10 eq) was then added and the reaction mixture was stirred for 30 min at 0°C followed by 1h30 stirring at room temperature. To the activated intermediate was added **6** (0.66 μmol , 0.6 eq) dissolved in anhydrous DMF ([activated **1**] = 45 mM), [**6**] = 30 mM). After 1h stirring at room temperature, DMAP (1 μL of a DMF solution at 98 mM, 0.098 μmol , 0,09) was added and the reaction mixture was left under stirring for additional 3h at room temperature. The crude solution was then diluted with 300 μL of H₂O/CH₃CN:1/1 and purified on semi-preparative Grace vision HT C18 HL column (4 mL.min⁻¹) using the following program: 0 to 1 min: 35% B, 1 to 29 min: 65% B, 29 to 30 min: 100% B with A: CH₃COONH₄ 10mM and B: CH₃CN, UV detection was performed at 230 nm and 280 nm. **19** was aliquoted (10 nmol per batch), lyophilized and stored at -20°C away from light. Compound **19** was isolated as a pink solid with 12% yield.

Compound 19:



Chemical Formula: $C_{78}H_{89}BrClN_8O_2PS_3$

Exact Mass: 1698,40

$\epsilon_{550\text{ nm}} = 150,000\text{ M}^{-1}\cdot\text{cm}^{-1}$ ($\text{CH}_3\text{CN}/\text{H}_2\text{O}:1/1$)

Molecular Weight: 1701,11

Fluorescence: $\lambda_{\text{ex}} 551 / \lambda_{\text{em}} 565$

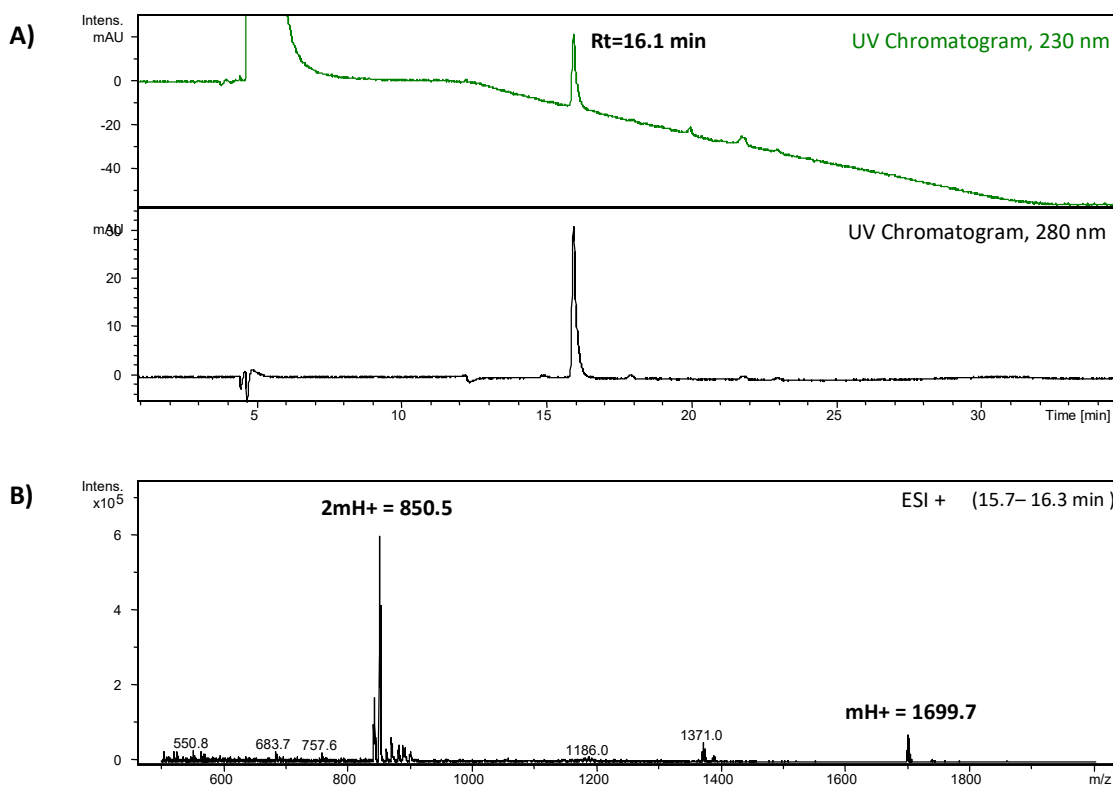


Figure 97: LCMS profile of purified probe 19. A) RP-HPLC profile of 19 (Rt=16.1 min) in the following conditions: analytical XDB C18 column, flow rate: 0.6 mL.min⁻¹, Method: 0 to 5 min: 100% A, 5 to 25 min: 100% B with A: 10mM AcONH₄ and B: CH₃CN, UV detection was performed at 230 nm and 280 nm. B) Mass profile of 19 analysed in ESI/positive mode of ionisation (mH⁺=1699.7, m2H⁺/2=850.5).

HRMS m/z for $[C_{78}H_{90}BrClN_8O_{20}PS_3]^+$ calculated. 1699.4043, found 1699.3997

13.3. Stability of probe 9 and 10

The stability assay was performed in 20 mM HEPES buffer, pH=7.5, 5mM CaCl₂, 200 mM NaCl, 0.1 mM ZnCl₂ and 0.1 % Brij-35. **9** or **10** (10 μM) were incubated at 37°C. At different time points (0 h, 1 h, 2 h, 4 h, and 24 h), samples were collected (20 μL) and analysed by RP-HPLC in the following conditions: analytical Column Ascentis® Express C₁₈ (flow 0.6 mL.min⁻¹), Method: 0 to 1 min: 35% B, 1 to 9 min: 65 % B, 9 to 10 min: 100% with A: 10 mM CH₃COONH₄, pH=5.5 and B: CH₃CN. The detection was performed at 280 nm. For each probe, analysis has been performed in triplicate. Figure 98 shows representative profiles obtained for probe 10 at different time points.

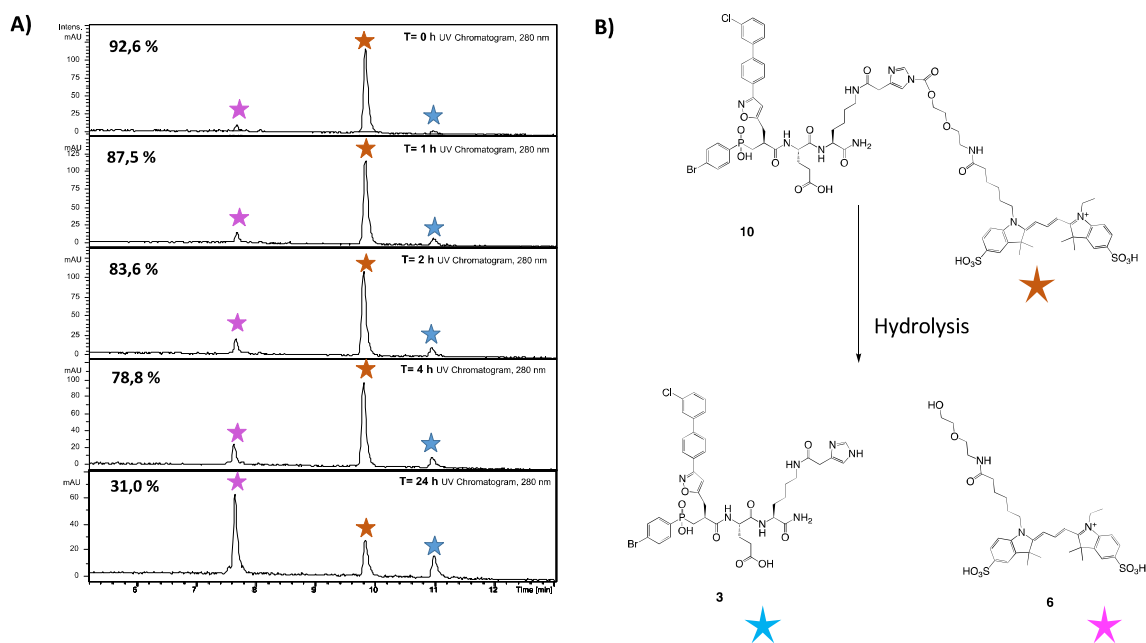


Figure 98: A) RP-HPLC profiles of probe 10 (brown star) at different time points (0, 1h, 2h, 4h and 24h) after incubation in 20 mM HEPES buffer, pH=7.5, 5mM CaCl₂, 200 mM NaCl, 0.1 mM ZnCl₂ and 0.1 % Brij-35 at 37°C. B) Hydrolysis of probe 10 (brown star) resulting in formation of imidazole 3 (blue star) and Cy3 6 (pink star) derivatives

The peak marked with a brown star corresponds to the starting probe **10**. The products resulting from the hydrolysis: Imidazole derivatives **3** and fluorescent moiety **6** are marked with a blue star and a pink star respectively. Their respective identities were unambiguously confirmed by mass spectrometry analyses coupled to RP-HPLC elution. At each time point, peak area of each compound was integrated and their relative ratio calculated.

14. MMPs production and characterization

The catalytic domains of human MMP-2, MMP-3, MMP-8 and MMP-10 were purchased from Giotto Biotech (Italy). The catalytic domains of human MMP-9, MMP-12 and MMP13 as well as that of murine MMP-12 were produced and purified in our laboratory according to protocols previously described ^{4,5}. Proteins concentrations were assessed by UV absorbance and proteins quality were evaluated by SDS-PAGE. MMPs catalytic activity was determined through continuous kinetic assays by recording the fluorescence increase induced by the cleavage of fluorogenic substrates: Mca-Pro-Leu- Gly-Leu-Dpa-Ala-Arg-NH₂ substrate (Mca Mat, Enzo life Science) in the case of human MMP-2, 8, -9, -10, -12, -13 and murine MMP-12 and Mca-Arg-Pro-Lys-Pro-Val-Glu-Nval-Trp-Arg-Lys-(Dnp)-NH₂ (McaMMP-3, R&D systems) for human MMP-3. To determine the accurate active enzyme concentration for each MMP, titration experiments were carried out with a broad-spectrum potent MMP inhibitor ⁶ in presence of McaMMP-3 substrate and in case of hMMP3 in presence of MCAmat substrate. A defined quantity of MMP active form was associated to a variation of fluorescence (ΔF). Substrate mother solution are prepared in DMSO ($\epsilon_{328} = 21470 \text{ M}^{-1} \text{ cm}^{-1}$). Unless otherwise indicated, dilutions of substrate solution were prepared in the DMSO. All enzymatic assays were performed using black, flat-bottomed, 96-well non-binding surface plates (Corning-Costar, Schiphol-Rijk, Netherlands) and fluorescence signals were monitored using a Fluoroskan Ascent photon counter spectrophotometer (Thermo- Labsystems, Courtaboeuf, France) equipped with a temperature control device and a plate shaker. Once appropriately characterized and dosed, each MMP catalytic domain has been conditioned in a buffer consisting of 3 mM CaCl₂, 0.1 mM ZnCl₂ 200 mM NaCl, 20 mM TrisHCl, pH 7.5, aliquoted and stored at -80°C.

14.1. Production of mMMP12 catalytic domain

Synthetic gene encoding the catalytic domain of the mMMP-12 (for sequence see Figure 99 A) was obtained from Geneart (Geneart-AG, Germany). This gene was inserted into the pET24a vector, between the NdeI and BamHI site, for expression under the PT7 promoter. Recombinant protein was expressed in *E. coli* BL21(DE3 star) cells carrying the mMMP-12 catalytic domain-encoding plasmids. Bacteria were grown at 37 °C in LB (Lysogeny broth/ Luria-Bertani) medium supplemented with kanamycin (50 µg/ml). At an absorbance (600 nm) of 0.6, protein expression was induced with 0.5 mM isopropyl- β -thiogalactopyranoside (IPTG). Five hours after induction, cells were harvested by centrifugation at 5000 $\times g$ for 30 min at 4 °C. The pellets were re-suspended in 100 mM Tris-HCl, pH 8.5, 5 mM benzamidinohchloride, 5 mM 2-mercaptoethanol and incubated with lysozyme (0.25 mg/mL) in presence of PMSF (Protease Inhibitor, Phenylmethylsulfonyl fluoride, Sigma 329-98-6) (0.25 mM) for 30 min at 4 °C. 2µL of benzonase (10 mM) and 200µL of MgCl₂ (1M) were added and the solution

was stirred for 30 min at 4 °C. The suspension was then passed through a cell disruption system at 4 °C and centrifuged at 4 °C for 45 min (8000 × g). The pellet was washed three times with 100 mM Tris-HCl, pH 8.5, 2 M urea, 5 mM 2-mercaptoethanol and then solubilized in buffer 100 mM Tris-HCl, pH 8.5, 8 M urea (Figure 99B, lane S4'). Refolding and purification steps were carried out through three successive dialyses in Tris-HCl, pH 7.5 by decreasing urea (3M to 0) and CaCl₂ (10, 5 and 3mM) concentrations⁴. mMMP-12 refolded catalytic domain was analysed by SDS-PAGE and found to migrate as a single band. Protein molecular weight were determined by electrospray ionization mass spectrometry (Figure 99C).

A) **MR**AVP**QR**SR**WM**KRY**LT**YRIY**NY**TP**DM**KRE**DV**YIF**Q**KAF**Q**V**W**SD**V**T**PL**R**FR**KL**HK**DE**AD**IM**IL**FA**FG**A**H**GD**FN**Y**FD**GK
GGTL**AH**AF**YP**GP**GI**Q**G**DA**HF**DE**AE**T**WT**K**S**F**Q**GT**N**LF**V**AV**HE**L**GH**SL**GL**Q**HS**N**NP**K**S**IM**YP**TY**RY**L**NP**ST**FR**LS**AD**DI**RNI**
QSL**YG**

MW=18572,9 g/mol

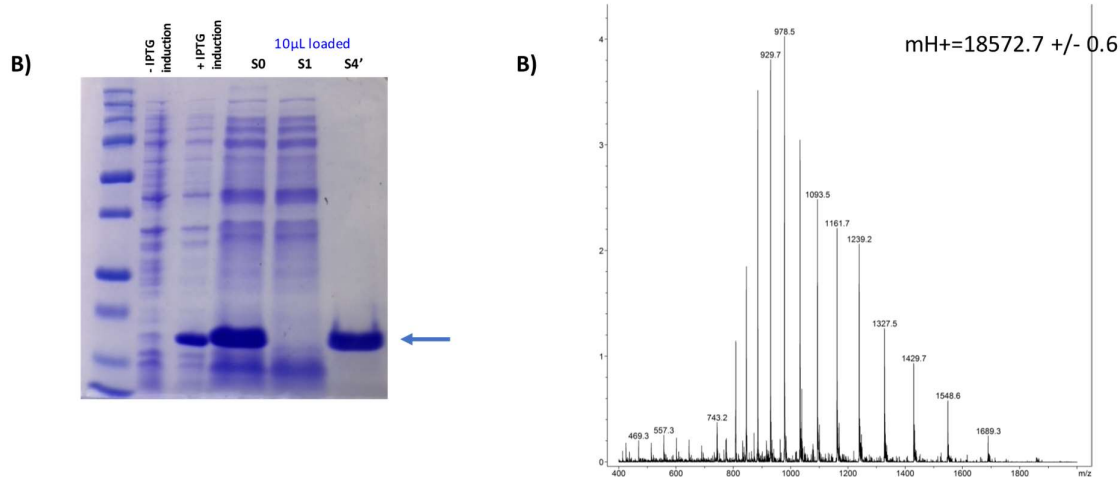


Figure 99 A) Sequence of mMMP12 catalytic domain and theoretical molecular weight (MW) calculated using Expsy ProtParam program. B) SDS-gel of mMMP12 during different phases of production: with or without induction with IPTG and solubilisation of inclusion bodies (Lane S4'), C) Mass profile of mMMP12 catalytic domain analysed in positive mode of ionisation (ESI+). mMMP12 presents a multiple-charge ion mass spectrum, from which a molecular weight (MW= 18572 ± 0.6) can be deduced.

14.2. MMPs UV dosing

The catalytic domains of human MMP-2, MMP-3, MMP-8 and MMP-10 were first solubilized in aqueous buffer (20 mM HEPES, pH=7.5, 200 mM NaCl, 5 mM CaCl₂, 0.1 mM ZnCl₂ and 0.1% Brij-35). The catalytic domains of human MMP-9, MMP-12 and MMP-13 as well as that of murine MMP-12 were conditioned in buffer (20 mM HEPES, pH=7.5, 200 mM NaCl, 5 mM CaCl₂, 0.1 mM ZnCl₂ and 0.1% Brij-35) after final step of dialysis/refolding.

The protein concentration was determined by UV absorbance. By using expasy program (<https://web.expasy.org/protparam>), the theoretical molar extinction coefficient of each protein can be calculated from its composition in tyrosine and tryptophan. This theoretical value is given at 280 nm with $\epsilon_{280}(\text{Tyr}) = 1490 \text{ M}^{-1} \cdot \text{cm}^{-1}$ and $\epsilon_{280}(\text{Trp}) = 5500 \text{ M}^{-1} \cdot \text{cm}^{-1}$. Absorbance measurements were performed on the Shimadzu UV-spectrophotometer (model UV 1800 240V IVDD) and analysed by software UV Probe 2.42.

The protein concentration was calculated from the following formula:

$$[\text{protein}] = \frac{A_{280}}{\epsilon_{280}}$$

with [protein] corresponding to the protein concentration in aqueous buffer, A₂₈₀ to the absorbance measured at 280 nm and ϵ_{280} to the protein molar extinction coefficient calculated with expasy program. [protein] is expressed in M, ϵ_{280} in $\text{M}^{-1} \cdot \text{cm}^{-1}$ and path length is equal to 1 cm. The results are summarised in Table 8.

	hMMP2	hMMP3	hMMP8	hMMP9	hMMP10	hMMP12	mMMP12	hMMP13
ϵ_{280}								
$\text{M}^{-1} \cdot \text{cm}^{-1}$	32430	28420	28420	33920	29910	26930	32890	34505
[protein]								
μM	4,84	3,87	3,76	4,42	3,34	5,2	3,15	3,74

Table 8 theoretical ϵ 280 nm and the concentration of mother solutions of used MMPs.

14.3. MMPs catalytic activity

14.3.1. General principle of the enzymatic assay with fluorogenic substrate.

A peptide substrate functionalized by a quencher group and a fluorescence emitter group was used in the enzyme's tests. Activity tests were performed using MMP and MCA-Mat whereas MCA-MMP3 was used for MMP titration and MMP3 activity measurement.

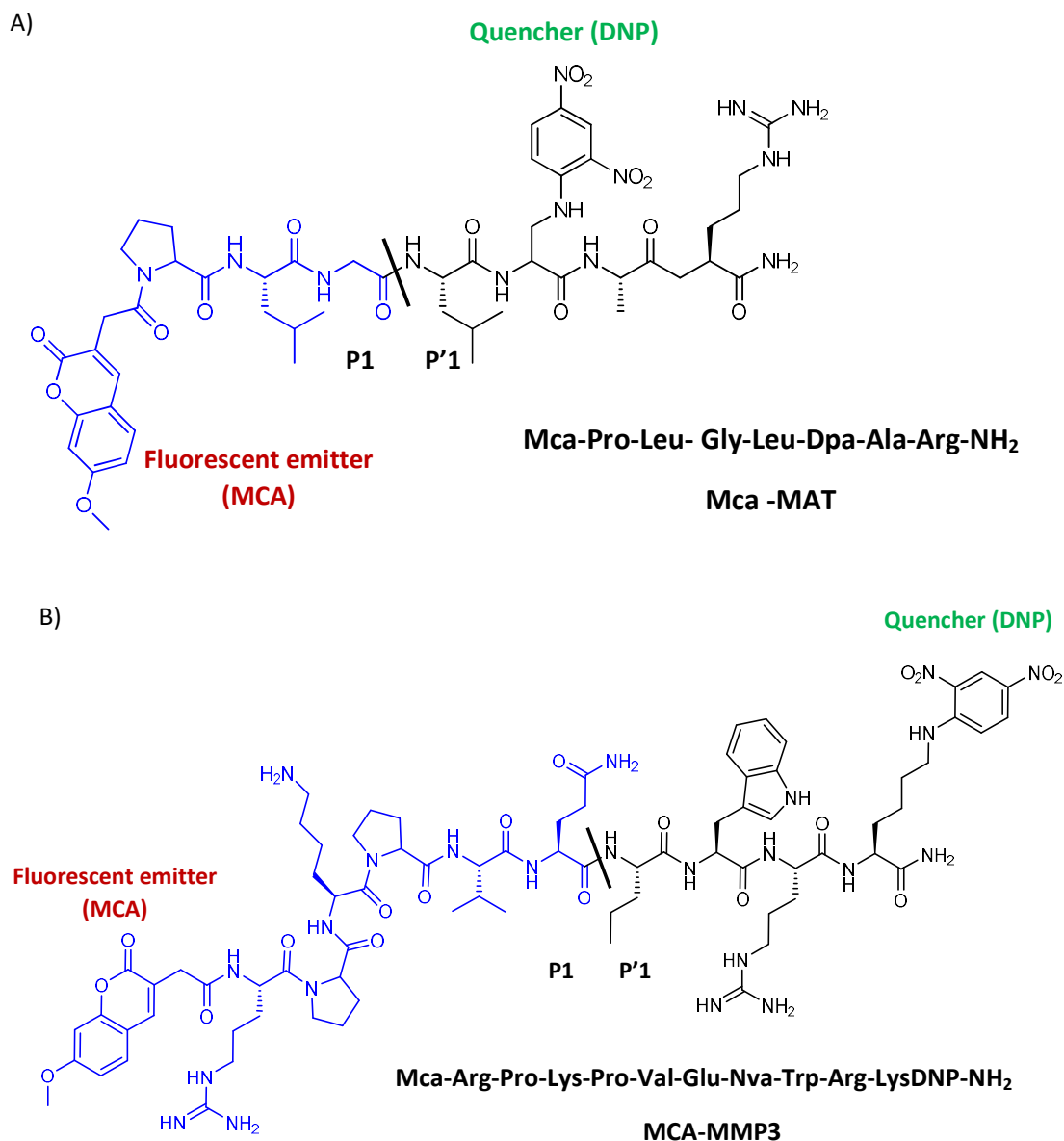


Figure 100. Chemical structure of A) MCA-MAT and B) MCA-MMP.

The activity assay consists in measuring the emission of fluorescence upon peptide sequence proteolytic cleavage. In absence of cleavage, the quencher group (Di Nitro Phenyl DNP, Figure 100) prevents the emission of the fluorescence by the emitter group (Methoxy coumarin, Mca, $\lambda_{ex}/\lambda_{em} = 328/400\text{nm}$, Figure 100). The quencher effectiveness depends on its proximity to the emitter group. When the quencher and the emitter are spatially separated (upon proteolytic cleavage) a fluorescence signal is emitted and then detected and registered by using a fluorimeter. The Mca-Mat and McaMMP-3 substrates are cleaved by MMPs between P1 glycine/P1' leucine and P1 glutamine/P1' norvaline respectively.

14.3.2. MMPs activity

Activity assays were carried out in 50 mM Tris-HCl buffer, pH = 6.8, 10 mM CaCl₂ at 25°C. In this case, continuous kinetic assays were performed by recording the fluorescence increase induced by the cleavage of Mca-Pro-Leu- Gly-Leu-Dpa-Ala-Arg-NH₂ substrate in the case of MMP-2, -8, -9, -10, -12, and 13 and Mca-Arg-Pro-Lys-Pro-Val-Glu-Nva-Trp-Arg-LysDNP-NH₂ for MMP-3. In a typical assay, the protease concentration is comprised between 0.1 to 5 nM (Table 10) and the concentration of fluorogenic substrates was at 9 μM. Activity assay was performed in 96-well non-binding surface plates and final volume in the well was 100μL. Experiment was performed in triplicate.

Materials and equipment

- | | |
|----------------------|---|
| Reagents | <ul style="list-style-type: none"> • Activity buffer (50 mM Tris-HCl buffer, 10 mM CaCl₂ ,pH=6.8) • Mother solutions of enzymes (MMPs catalytic domain) whose concentration have been determined by titration (see below 14.3.3) • Solution of substrates (Mca-MAT or Mca MMP3 1.8mM in DMSO) |
| Reagent setup | <ul style="list-style-type: none"> • Mother solution of enzyme was diluted in activity buffer to concentration 100nM. (for example MMP-12 =[5,2 μM], dilution 52 times) |
| Equipment | <ul style="list-style-type: none"> • fluorescence reader (Fluoroskan Ascent, Thermolab Systems) • black, flat-bottomed, 96-well non-binding surface plates (Corning-Costar, Schiphol-Rijk, Netherlands) |

Procedure

- Step 1.** 99 μL of activity Tris buffer was loaded in the well.
- Step 2.** 1 μL of MMP solution was added to reach a final concentration of 0.1 to 5 nM depending of MMP (see Table 10).
- Step 3.** 0.5 μL of McaMat substrate or Mca MMP3 (1.8mM in DMSO) was added to the well to reach final concentration 9 μM
- Step 4.** The plate was under gentle stirring for 10s.
- Step 5.** The plate was read (fluorescence reading) during 30 min.
- Step 6.** ΔF value was determined. It was associated with MMP activity

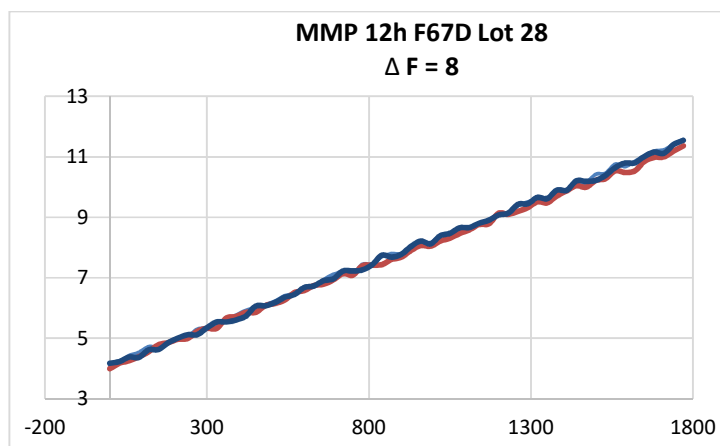


Figure 101. A graph of MMP12h activity (triplicate).

14.3.3. MMPs Titration

To determine the accurate active enzyme concentration for each MMP, titration experiments were carried out with a broad-spectrum potent MMP inhibitor (RXP500.1, Table 9) ⁶ in presence of McaMMP-3 at 18 μM . The enzyme concentration was chosen to ensure evaluation of an initial rate (less than 10% of the substrate consumption) and it should be at least ten times higher than the inhibitor K_i value. The titration was performed in 50 mM Tris-HCl buffer, pH = 6.8, 10 mM CaCl_2 at 25°C.

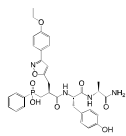
		Ki (nM)						
		hMMP-2	hMMP3	hMMP-8	hMMP-9	hMMP-10	hMMP-12	hMMP-13
RXP500.1 								
		0,009	2,6	0,09	0,004	0,99	0,019	0,027

Table 9 Ki (nM) value of RXP 500.1 towards a set of hMMPs. The affinity constant was determined in 50 mM Tris/HCl buffer, pH 6.8, 10 mM CaCl₂ at 25 °C (see below for the inhibition assay part 15).

Materials and equipment

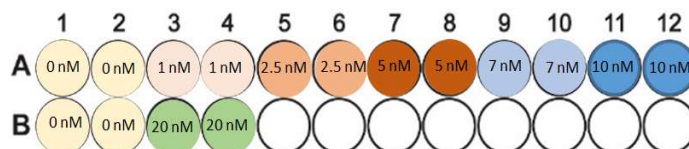
- Reagents**
- Activity buffer (50 mM Tris-HCl buffer, pH = 6.8, 10 mM CaCl₂, pH=6.8 containing 0.01% in volume of brij-35.)
 - Mother solutions of enzymes (MMPs catalytic domain) whose concentration have been determined by UV measurement.
 - Solution of inhibitor RXP 500.1
- Reagent setup**
- Mother solution of enzyme was diluted in activity buffer to reach the concentration 200nM (a dilution was performed in activity buffer (sequential dilutions, minimum volume handled for each intermediate solution -> 2 µL) to obtain a 200 nM solution. Minimum volume of final solution at the concentration 200 nM was 90 µL (for a 16 wells experiment). The solution was stored at + 4°C (Ice bath))
 - Preparation of RXP500.1 solutions: S_{1µM} and S_{100nM}.
 The concentration of RXP500.1 mother solution (1.6 mM, EtOH/H₂O:1/1) was accurately determined by amino acids dosing. From this solution, sequential dilutions in EtOH/H₂O:1/1 were performed.
 S_{1µM}: d₁₆ (4µL in 60µL) followed by d₁₀ (20 µL in 180 µL)
 S_{100nM}: d₁₀ (20 µL in 180 µL) of S_{1µM}
 NB: Both solutions were properly labelled and stored at -20°C for future titration experiments.
- Equipment**
- fluorescence reader (Fluoroskan Ascent, Thermolab Systems)
 - black, flat-bottomed, 96-well non-binding surface plates (Corning-Costar, Schiphol- Rijk, Netherlands)

Procedure

The final volume in the well was 100 μ L. For one given concentration of inhibitor, the measurement was carried out in duplicate.

- Step 1.** 95 μ L of activity buffer was added to each well.
- Step 2.** 5 μ L of 200 nM MMP solution was added to each well \rightarrow [MMP]_{final}=10 nM
- Step 3.** RXP500.1 solutions was distributed to reach the following final concentrations in the wells 0, 1nM, 2.5 nM, 5 nM, 7 nM, 10 nM, 20 nM.

[RXP500.1] _{final}	V S _{1μM} or S _{100nM} (μ L)
0	-
1 nM	1 μ L/S _{100nM}
2.5 nM	2.5 μ L/S _{100nM}
5 nM	0.5 μ L/S _{1μM}
7 nM	0.7 μ L/S _{1μM}
10 nM	1 μ L/S _{1μM}
20 nM	2 μ L/S _{1μM}



- Step 4.** MMP and inhibitor were pre incubated for 45 min under gentle stirring at RT (25°C)
- Step 5.** 1 μ L of McaMMP-3 substrate (MCAmat in case of hMMP3) at 1.8 mM concentration (DMSO solution) was added \rightarrow [McaMMP-3]= 18 μ M followed by 10s of gentle stirring and fluorescence reading for 30 min.
- Step 6.** The percentage of inhibition for each RXP500.1 concentration was then determined using the ratio between its initial rate and the one from the reference activity (no inhibitor in the well): % = 1-V_{inh}/V_{ref}.
- A graph was built (kaleidagraph) by reporting inhibitor concentration (X axis) in function of percentage of inhibition (y- axis) in log scale (Figure 102). By using a linear regression, the amount of active MMP was determined ⁷.

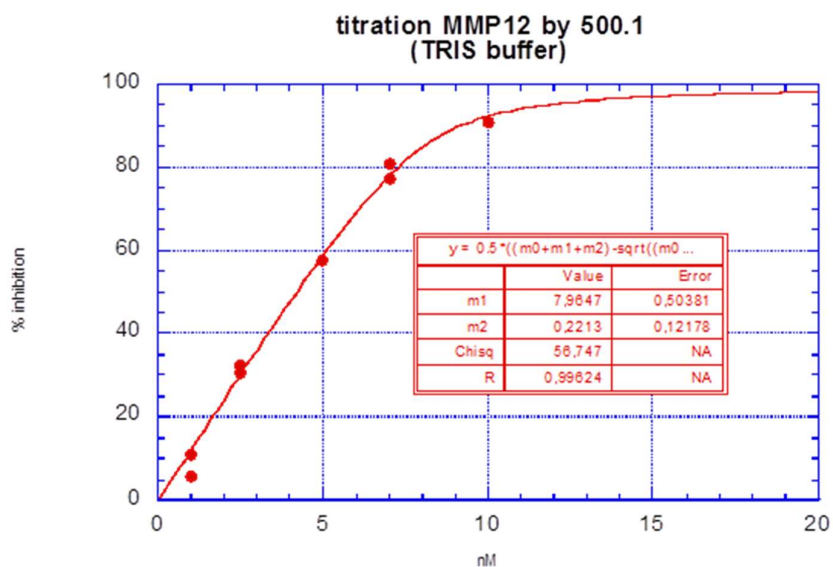


Figure 102. Titration MMP12 by RXP 500.1 in Tris buffer.

Once the amount of active MMP was determined, enzyme activity was measured as reference activity (Table 10). Every time MMP was handled for labelling and other experiments the enzyme reference activity was checked following the protocol described below.

	hMMP-2	hMMP-3*	hMMP-8	hMMP-9	hMMP-12	mMMP-12	hMMP-13	hMMP-14
[MMP] final (nM)	0.05	3.5	0.1	0.05	1	1	0.1	0.1
ΔF (AU)	14	15	13	17	8	5	12	8

Table 10. ΔF values for each MMP catalytic domain (various concentration according to MMP) in presence of 9 μM of McaMat and after 30 min reading.

Ki (nM) of MMP3 for RXP500.1 is much lower compared to others MMPs (2,5 nM) and the titration is less precise. In case of hMMP-3 titration, MCAmat substrate was used at 9 μM final concentration.

14.4. Analysis of MMP catalytic domain by SDS-PAGE

14.4.1. Principle of one-dimensional electrophoresis in denaturing conditions

SDS-PAGE (Sodium dodecyl sulphate polyacrylamide gel electrophoresis) is the most widely used analytical method for the separation of macromolecules in mixtures by their molecular mass in an electric field. The polyacrylamide gel is generated by the polymerization of acrylamide and N, N'-methylenebisacrylamide (bis-acrylamide), forming a network of elastic polymer chains in which proteins migrate. The polymerization step is catalysed by ammonium persulfate (APS) (or potassium persulphate) and N, N, N', N'-tetramethylethylenediamine (TEMED). SDS (Sodium dodecyl sulphate) is a negatively charged surfactant that covers the proteins intrinsic charge and confers to them very similar charge-to-mass ratios. The proteins intrinsic charges are negligible in comparison to the SDS loading. Upon application of a constant electric field, proteins thus migrate towards the anode according to their molecular weight.

The SDS-PAGE gel is composed of a stacking gel pH 6.8 and a resolving gel pH 8.8 (Table 11). The stacking gel is supposed to concentrate the protein at the start of the migration so that all of them start from the same point.

	Resolving gel	Stacking gel
Acrylamide 35%	4 mL	625 µL
Buffer TRIS	4 mL TRIS 1,5 M pH 8,8	1,2 mL TRIS 1,5 M pH 6,8
H ₂ O distilled	5 mL	3 mL
SDS 10 %	200 µL	50 µL
APS	75 µL	50 µL
TEMED	20 µL	10 µL

Table 11 Composition of electrophoresis gels for 2 gels.

Gels were prepared in SureCast Gel Handcast System (thermo Fisher)

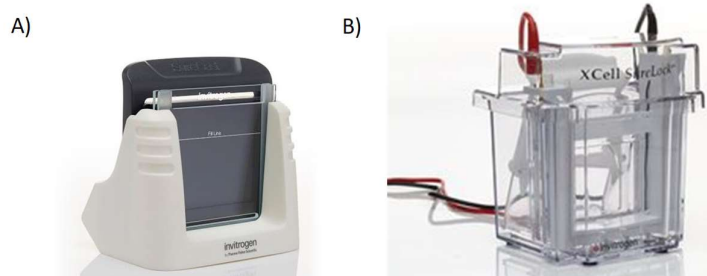


Figure 103. A) SureCast Gel Handcast System B) XCell SureLock electrophoresis system

Ingredients were mixed in order showed in Table 11. It is important that APS and TEMED were added in the end. After polymerization of gels (stacking gel 30 min, resolving gel 45 min), they were immersed in the MiniProtean III system in the presence of migration buffer (25 mM Tris, 192 mM glycine, 0.1% SDS, pH 8.3).

Samples were mixed with a sample buffer (NuPage LDS Sample buffer 4X, Invitrogen) and heated during 5 min in 95°C and then loaded on the gel. Electrophoresis was performed in XCell SureLock system during 1h 100 mA. Proteins are visualized on the gel by using coomassie blue or silver staining.

14.4.1.1. Coomassie blue staining

Materials and equipment

- | | |
|------------------|---|
| Reagents | <ul style="list-style-type: none">• SimplyBlue™ SafeStain Thermo Fisher• Ultrapure water |
| Equipment | <ul style="list-style-type: none">• Gel Doc™ EZ imager (Biorad)• Staining tray• Rotary shaker |
-

Procedure

- Step 1.** A gel was washed 3 times for 5 minutes with 100 mL deionized water to remove SDS and buffer salts, which interfere with binding of the dye to the protein. Water was discarded after each rinse.
- Step 2.** The gel was stained with enough SimplyBlue™ SafeStain (~20 mL) to cover the gel. The staining was performed during 1 hour at room temperature under gentle shaking.
- Step 3.** The gel was then washed with 100 mL of water for 1–3 hours.
- Step 4.** When the clearest background was obtained, the gel was scanned by Gel Doc™ EZ imager.

14.4.1.2. Silver staining

Materials and equipment

Reagents	<ul style="list-style-type: none">• SilverQuest™ Silver Staining Kit:<ul style="list-style-type: none">○ 250 ml Sensitizer○ 25 ml Stainer○ 250 ml Developer○ 2ml Developer Enhancer○ 250 ml Stapper Solution• Ultrapure water• 100% ethanol• Acetic acid
Reagent setup	<p>Reagents provided in the kit were diluted following protocol:</p> <ul style="list-style-type: none">• Sensitizing solution (ethanol 30 mL, sensitizer 10 mL, ultrapure water to 100 mL)• Staining solution (stainer 1 mL, ultrapure water to 100 mL)• Developing solution (developer 10 mL, developer enhancer 1 drop, ultrapure water to 100 mL)• Fixative solution (40% ethanol, 10% acetic acid, made with ultrapure water)• 30% ethanol (made with ultrapure water)
Equipment	<ul style="list-style-type: none">• Gel Doc™ EZ imager (Biorad)• Staining tray (a polypropylene)• Rotary shaker

Procedure

- Step 1.** Dilution of reagents were performed as describes above.
- Step 2.** After electrophoresis, a gel was rinsed with ultrapure water.
- Step 3.** The gel was fixed in 100 mL of fixative solution for 20 minutes or overnight with gentle rotation.
- Step 4.** The fixative solution was then decanted and the gel was washed in 30% ethanol for 10 minutes

- Step 5.** The ethanol was decanted and 100 mL of Sensitizing solution was added to the gel and incubated for 10 minutes.
- Step 6.** The sensitizing solution was decanted and the gel was washed in 100 mL of 30% ethanol for 10 minutes.
- Step 7.** The gel was washed in 100 mL of ultrapure water for 10 minutes.
- Step 8.** Next the gel was incubated in 100 mL of staining solution for 15 minutes.
- Step 9.** After the staining the gel was washed with 100 mL of ultrapure water for 20–60 seconds.
- Step 10.** At the end the gel was incubated in 100 mL of developing solution for 4–8 minutes until bands appeared.
- Step 11.** When the appropriate staining was achieved, 10 mL of Stopper was immediately added directly to the gel.
- Step 12.** After few minutes the Stopper solution was decanted and the gel was washed with 100 mL of ultrapure water for 10 minutes.
- Step 13.** The gel was scanned by Gel Doc™ EZ imager.

14.4.1.3. Representative SDS-Page gel

From MMP mother solution, 30 μ L corresponding to 3 pmol were loaded on the gel. After electrophoresis silver staining was performed and the gel was scanned by Gel Doc™ EZ imager.

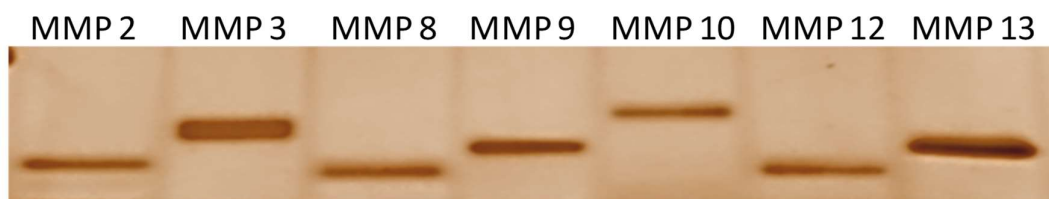


Figure 104. Profile of MMPs on silver stained SDS-PAGE gel.

15. Inhibitory potency of probes vs MMPs.

The Inhibition assays were carried out in three different buffers and MCA-Mat substrate (McaMMP3 in case of hMMP3) was used at 4,5 μM concentration. The percentage of inhibition was determined in duplicate, at four inhibitor concentrations chosen to reach a 20–80% range of inhibition. K_i values were determined using the method proposed by Horovitz and Leviski ⁸.

Materials and equipment

- Reagents**
- Buffer A: Reaction buffer (20 mM HEPES, 200 mM NaCl, 5 mM CaCl_2 , 0.1 mM ZnCl_2 and 0.1% Brij-35, pH=7.5)
 - Buffer B: Activity buffer (50 mM Tris-HCl buffer, 10 mM CaCl_2 , pH=6.8)
 - Mother solution of catalytic domain of enzyme.
 - Mother solution of an inhibitor (e.g RXP470.1 – compound 1)

Reagent setup Mother solution of enzyme was diluted in an appropriate buffer to reach the concentration 100nM. (the dilution was prepared in the same buffer in which inhibition assay was performed, the solution was stored at + 4°C (Ice bath))

- Equipment**
- fluorescence reader (Fluoroskan Ascent, Thermolab Systems)
 - black, flat-bottomed, 96-well non-binding surface plates (Corning-Costar, Schiphol-Rijk, Netherlands)

Procedure

Step 1. 200 μl of one examined buffer was distributed in 96-well non-binding surface plate.

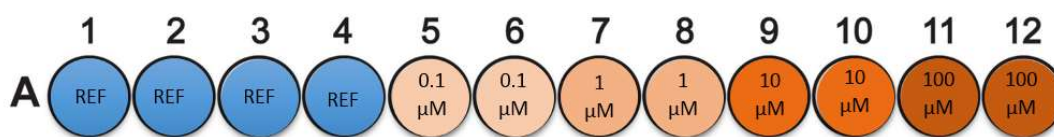


Figure 105. Example of distribution of the inhibitor for a K_i measurement

Step 2. 1 μl of MMPs was diluted in buffer. The final concentration of enzyme in each well was 1 nM.

Step 3. Inhibitor was distributed in wells according to the figure above. Before adding the MCA-Mat substrate, the plate was incubated for 45 minutes with at 25 C.

Step 4. 0.5 μ L MCA-Mat 1.8 mM (100% DMSO storage) was added to wells. The reading was performed at the same temperature for 30 minutes.

The titration curve was obtained via KaleidaGraph by reporting the percentage of the inhibition (calculated in the same way described in titration section) obtained at each concentration of the inhibitor, considering reference (without inhibitor).

The sigmoid was obtained by non-linear regression (least squares method) which allowed to read K_i directly. Its value corresponds to the concentration of inhibitor for which 50% of the enzyme is inhibited ($[S] \lll K_m$).

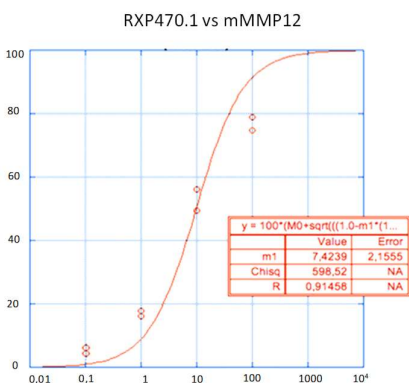


Figure 106. Sigmoid representing the inhibition constant of mMMP12 against RXP470.1 (compound 1).

The inhibitory assays were carried out towards a set of metalloproteases to determine K_i values (nM) in appropriate buffer for several compounds. The Table 12 shows K_i values for hMMP-2/3/8/9/12/and 13 in a buffer A (20 mM HEPES, pH=7.5, 200 mM NaCl, 5 mM $CaCl_2$, 0.1 mM $ZnCl_2$ and 0.1% Brij-35) for compound 9, 10, 11, RXP470.1, RXP500.1, GM6001 and humanTIMP1.

	Ki (nM)						
	hMMP-2	hMMP-3	hMMP-8	hMMP-9	hMMP-10	hMMP-12	hMMP-13
Probe 9	n.d.	n.d.	n.d.	n.d.	n.d.	3.4±0.2	n.d.
Probe 10	1355±310	1430±110	3500±200	>10000	155±30	13.1±1.3	875±180
Probe 11	35±1	210±30	530±70	14±3	92±6	3.7±0.3	117±6
RXP470.1	330±20	345±15	780±80	840±120	98±16	1.1±0.1	74±7
RXP500.1	2.0±0.4	2600±160	37±17	0.8±0.2	490±40	1.7±0.2	6±1
GM6001	n.d.	n.d.	n.d.	n.d.	n.d.	0,07±0.01	n.d.
hTIMP-1	n.d.	n.d.	n.d.	n.d.	n.d.	3,6±0.6	n.d.

Table 12 Ki values (nM) for probe 9, 10, 11, RXP470.1, RXP500.1, GM6001 and humanTIMP1 towards a set of metalloproteases.

16. Labelling of MMPs with probes

Labelling experiments were performed on MMPs in appropriate buffer (Reaction buffer A (20 mM HEPES, 200 mM NaCl, 5 mM CaCl₂, 0.1 mM ZnCl₂ and 0.1% Brij 35, pH=7.5), Reaction buffer B (50mM Tris buffer, 10mM CaCl₂, pH=6.8), Reaction buffer C (50 mM Tris-HCl buffer, 10 mM CaCl₂, 150mM NaCl, 0.05% Brij, pH=7.5)).

Prior to labelling, each MMP was first conditioned in the reaction buffer. Regarding the hMMP-9/12 and 13 as well as the mMMP-12 produced in the laboratory, we distinguish two different situations. For labelling at µM concentration, MMP storage buffer was exchanged to reaction buffer by dialysis during 6h at 4°C using Spectra/Por7 Dialysis Membrane (MWCO 3.5 kD). For labelling at sub µM concentration, a simple dilution into the reaction buffer was performed. In the case of hMMP-2/3/8 and 10, as they were supplied in 20 mM TRIS buffer, pH=7.2, 300 mM NaCl, 10 mM CaCl₂, 0.1 mM ZnCl₂ containing 0.2-0.5 M of Acetohydroxamic Acid (AHA) 0.2-0.5 M, samples were dialyzed using Spectra/Por7 Dialysis Membrane (MWCO 3.5 kD) for 6h at 4°C. This mainly aims removing AHA and conditioning MMP in the appropriate buffer for labelling experiment. The protein concentration was

verified by UV dosing, the purity was assessed by 12% SDS-PAGE gel and the fraction of active protease was determined by titration experiments as described above.

Labelling experiments were performed in few different medias, with or without spiked MMPs, in presence of serum albumin and in complex proteomes like mouse liver extract, murine macrophages, human and murine dendritic cell described in the paragraph below.

16.1. Production of complex proteomes

16.1.1. Murine sources of complex proteomes

16.1.1.1. Mouse liver extract.

Harvested livers from C57BL/6 mice (Charles River Laboratories, France) were suspended in the reaction buffer A (20 mM HEPES, pH=7.5, 200 mM NaCl, 5 mM CaCl₂, 0.1 mM ZnCl₂ and 0.1% Brij 35) used for the labelling experiments (46 mg/mL). The liver solubilisation was performed in presence of a protease inhibitor cocktail (2% v/v of a DMSO solution, P8340, Sigma Aldrich). The suspension was manually crushed at 4°C within a potter to provide an extract that was centrifuged (5000 rpm, Centrifuge 5430R (Eppendorf) for 30 min at 4°C. the supernatant was then isolated from the pellet and the resulting homogeneous liver extract was stored at -80°C after Bradford's dosage of proteins.

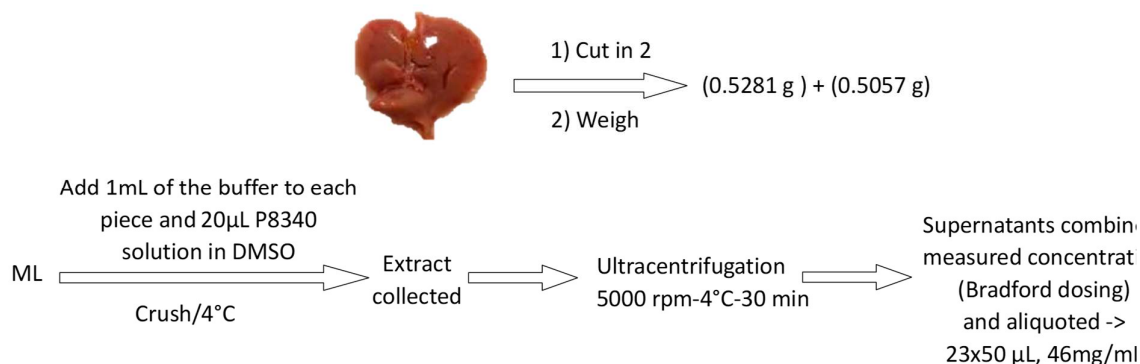


Figure 107. Preparation of liver extract.

The Bradford protein assay spectroscopic analytical procedure was used to measure the total amount of protein in complex media. By this method it is possible to detect from 1 to 20 µg (<25 µg/ml). The procedure for determining the protein concentration uses the phenomenon of dye-protein complex formation (Coomassie Brilliant Blue G-250, *Figure 108*).

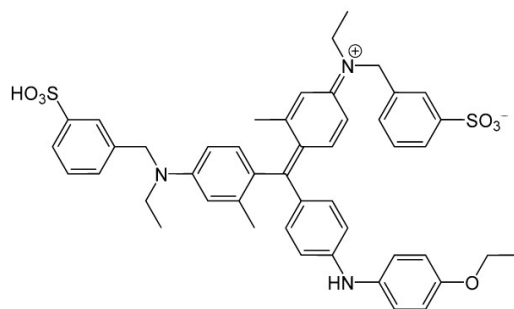


Figure 108. Coomassie Brilliant Blue G-250 structure.

This dye forms a strong, noncovalent complex with proteins (Van der Waals force and electrostatic interactions). The protein-dye complex shifts the wavelength corresponding to the dye maximum absorption from 465 to 595 nm. The absorbance value is proportional to the protein concentration. Bovine albumin is used as the protein standard.

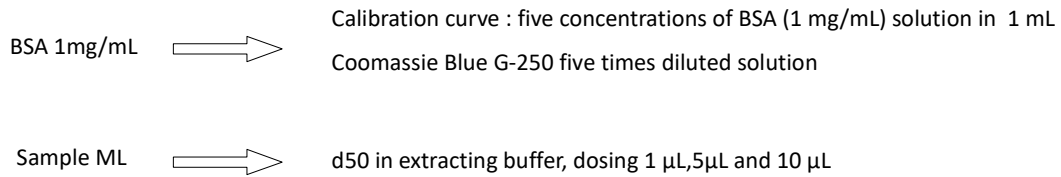
Materials and equipment

- | | |
|----------------------|--|
| Reagents | <ul style="list-style-type: none"> • Bio-Rad Protein Assay Dye Reagent Concentrate Ref. 5000006 (a solution contains Coomassie brilliant blue G-250 dye) • Bovine Serum Albumin (BSA) (Sigma-Aldrich) • distilled water |
| Reagent setup | <ul style="list-style-type: none"> • stock solution of Coomassie Blue G-250 was first diluted to 1 / 5th in distilled water • BSA solution was prepared with the concentration 1mg/ml |
| Equipment | <ul style="list-style-type: none"> • Spectrophotometer (UV Shimadzu, UV-1800) • Polystyrene spectrophotometer cuvettes (Sigma-Aldrich) |

Procedure

- Step 1.** Five standard solutions were prepared by mixing 1ml of Coomassie Blue G-250 diluted solution and Bovine Serum Albumin (BSA): 0 µg; 2.5 µg; 5 µg; 7.5 µg; 10 µg. Solutions were performed in duplicate in cuvettes adapted for spectrometric measurement.

Step 2. A tested sample (1, 5 and 10 μL) was added to cuvettes containing 1 mL of diluted Bradford solution (in duplicate).



Step 3. All samples were incubated during 10 min in the dark in room temperature.

Step 4. The absorbance was measured at 595 nm.

Step 5. The measurements were evaluated relatively to the range of BSA.

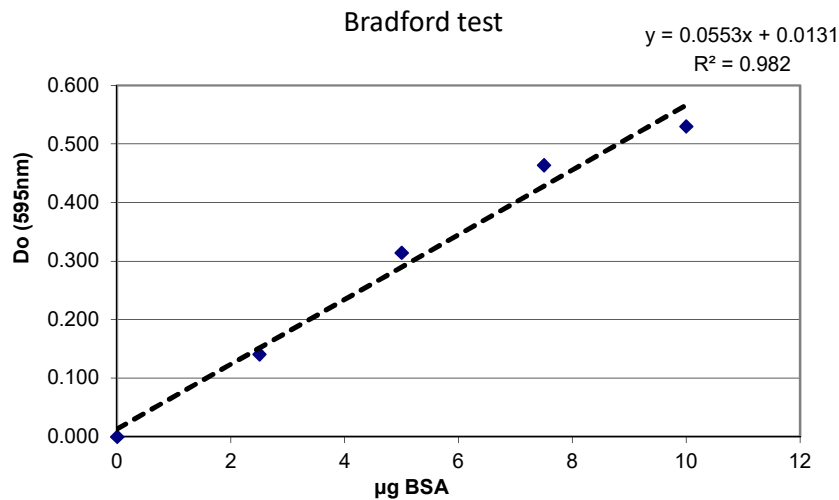


Figure 109. Bradford test – calibration curved of BSA (μg)

From the BSA calibration curve (Figure 109), the protein concentration (d50) can be deduced: 0.92 ± 0.03 corresponding to 46mg/mL for the mother solution (Table 13).

ML d50			
	ML	ML	ML
Vol (μl)	1,0	5,0	10,0
DO	0,060	0,263	0,509
C(mg/ml)	0,94	0,91	0,89

Table 13. Measurements of Bradford test of mouse liver extract.

16.1.1.2. Dendritic cells

Materials and equipment

- Animal**
- Donor mouse C57 Bl6J
- Reagents**
- recombinant murine granulocyte-macrophage colony stimulating factor (GM-CSF) (PeproTech, USA), RPMI
 - interleukin-4 (IL-4) (PeproTech, USA)
 - Iscove's Modified Dulbecco's Media (IMDM)
 - ACK (Ammonium-Chloride-Potassium- Lysing Buffer)
 - Trypsin solution
- Equipment**
- Centrifuge 5430R (Eppendorf)
 - 50-ml conical centrifuge tube (filter 100µm)
 - Flasks (150 mm²)
 - counting-chamber (hemocytometer)
-

Procedure

Day 0

- Step 1.** C57BL6J mouse was euthanized, the skin from each hind leg was peeled. The hind legs were cut off and bones (tibias and femurs) were recovered.
- Step 2.** Bones were washed first in ethanol and then two times in RPMI buffer.
- Step 3.** A needle was inserted into bone marrow cavity of femur or tibia. The bones cavities were flushed with ~ 20 ml RPMI medium, or until bone cavity appeared white. Wash medium was collected in sterile 50ml conical centrifuge tube on ice (filter 100µm) and then the sample was centrifuged (1500 RPM 5min 4C).
- Step 4.** The supernatant was discarded and the cell pellet was resuspended in 20 ml of ACK and centrifuged.
- Step 5.** The supernatant was again discarded and the cell pellet was resuspended in 10 ml of IMDM.
- Step 6.** Cells were counted on counting-chamber (hemocytometer)- 40×10^6

Step 7. Cells were resuspended in 30 ml IMDM buffer containing 10ng GM-CSF and 10 ng IL -4 . 3 flasks (150 mm²) were prepared where each contained 13,3 x 10⁶ cells.

Step 8. The cells were cultured at 37°C in an incubator containing 5% CO₂.

Day 3

Step 9. Supernatant was collected to recover dendritic cells.

Step 10. 4 ml of cold trypsin solution was added to the supernatant and the solution was centrifugated during 4 min (1500 RPM, 20 C).

Step 11. The pellet was resuspended in a IMDM buffer and the cells were counted on counting-chamber (hemocytometer)

Step 12 The cells were again resuspended in 30 ml IMDM buffer containing 10ng GM-CSF and 10 ng IL-4. 2 flasks (150 mm²) were prepared where each contained 11,0 x 10⁶ cells

Day 6

Step 13 Step 9, 10 11 were repeated

Stimulated DCs were isolated from the supernatant by centrifugation. The supernatant was removed and the pellets were washed in PBS buffer and aliquoted (5.10⁶ DCs per batch).

Step 14 Obtained cells were used for labelling experiment and Western Blot

16.1.1.3. Macrophages

The thioglycollate-stimulated mouse macrophages were used as a source of endogenous mMMP12. The collection of cells and labelling was performed in two pathways: A or B.

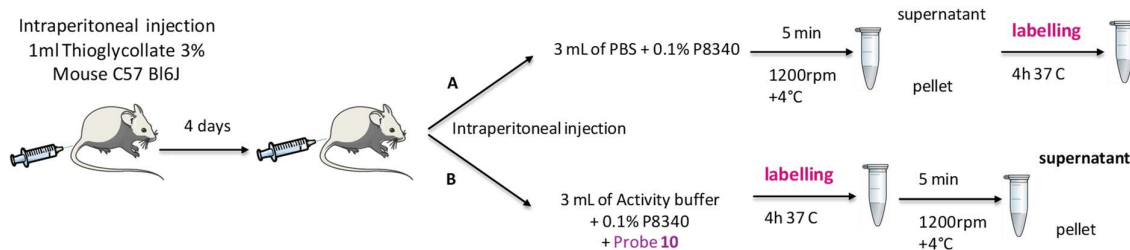


Figure 110 Scheme of the protocol of murine macrophages collection.

Materials and equipment

Animal	<ul style="list-style-type: none">• mouse C57 Bl6J
Reagents	<ul style="list-style-type: none">• 1ml of thioglycollate 3% solution• buffer (PBS or reaction buffer B (50mM Tris buffer, 10mM CaCl₂, pH=6.8))• Protease Inhibitor Cocktail (Aldrich, P8340) for use with mammalian cell and tissue extracts, DMSO solution
Equipment	<ul style="list-style-type: none">• Centrifuge 5430R (Eppendorf)• syringes (5ml)• needles 30-cc• scissors• tweezers

Procedure

Day 0

Step 1. 1ml of thioglycollate 3% solution was injected intraperitoneally into a mouse C57 Bl6J. During four days thioglycollate solution caused inflammatory response in peritoneal cavity.

Day 4

Step 2. The mouse was euthanized by cervical dislocation.

Step 3. 3 ml of a buffer (PBS or Tris activity buffer, with or without probe, see Figure 110) containing 0,1 % v/v of inhibitors P8340 was injected intraperitoneally.

A or B

Step 4. The abdomen of mouse was properly sterilized (70% alcohol) and prepared for opening of peritoneal cavity.

Step 5. After opening of peritoneal cavity, injected in step 3 solution was collected using a syringe (without a needle).

Step 6. A Collected solution (around 2 -2.5 ml) (Figure 110) was kept in ice, then centrifuged (5000 rpm) and cell pellet was resuspended in PBS, counted and divided in aliquots (5.10⁶ cells per batch).

See part 17.2 for labelling pathway A and B

16.1.2. Human sources of complex proteomes

16.1.2.1. Human dendritic cells

Procedure

- Step 1.** Buffy –coats from healthy individuals were provided by “Établissement Français du Sang” (EFS, Rungis, France). They were collected from anonymous donors after signature of informed consent and following EFS guidelines.
- Step 2.** PBMCs were isolated by Ficoll-Paque PLUS density gradient centrifugation (GE healthcare).
- Step 3.** CD14+ monocytes were purified by positive selection using magnetic microbeads (Miltenyi Biotec) and differentiate in monocyte-derived immature dendritic cells (iDC) by 5-days culture in AIM-V medium (Invitrogen) supplemented with 1000 units/ml rhIL-4 and rhGM-CSF (both from R&D system).
- Step 4.** iDC were activated in the same medium with a cocktail of TNF (10 ng/ml) and IL-10 (40 ng/ml) and incubated at 37 C for two days.
- Step 5.** Cells were removed from the flask by trypsin treatment, washed and centrifuged into dry pellets.
- Step 6.** At each step, the cells population was analysed by flow cytometry and FACS (see figure Figure 58).

16.2. Procedures of labelling

Materials and equipment

- Reagents**
- Reaction buffer A (20 mM HEPES, 200 mM NaCl, 5 mM CaCl₂, 0.1 mM ZnCl₂ and 0.1% Brij 35, pH=7.5)
 - Reaction buffer B (50mM Tris buffer, 10mM CaCl₂, pH=6.8)
 - Reaction buffer C (50 mM Tris-HCl buffer, 10 mM CaCl₂, 150mM NaCl, 0.05% Brij, pH=7.5).

Mother solution of MMP: MMP catalytic domain conditioned in storage buffer, in case of hMMP-2/3/8 and 10 buffer A (after dialysis), in case of hMMP9/12/13 and mMMP12 buffer A (after dialysis) or 20 mM Tris buffer 3 mM CaCl₂, 200 mM NaCl, 0,1 mM ZnCl₂, pH=7,5 (without dialysis).

- Probe **9-18** at 1 mM in DMSO. From this stock solution, sequential dilutions in DMSO-> [probe] = 100µM, 10µM, 1µM.
- RXP470.1 at 11.2 mM in H₂O neutralized NH₃ 33%,
- GM6001 at 5mM in EtOH/H₂O:1/1,
- RXP500.1 at 1.6 mM, EtOH/H₂O:1/1
- hTIMP-1 at 1 mg/ml H₂O

From these stock solutions, sequential dilutions in buffer were prepared-> [Competitor] = 100µM, 10µM or 1µM.

- Protease Inhibitor Cocktail (Aldrich, P8340) for use with mammalian cell and tissue extracts, DMSO solution
- Human serum albumin hSA 200 g/l (YDRALBUM, LFB Biomedicaments, France)
- Liver extract at 46mg/mL in reaction buffer A (see part 16.1.1.1 for preparation and dosing)
- Murine dendritic cells (see part 16.1.1.2 for preparation)
- Murine macrophages from peritoneal cavity (see part 16.1.1.3 for preparation)
- Human dendritic cells (see part 16.1.2.1 for preparation)
- Sample loading buffer: NuPAGE™ LDS Sample Buffer (4X) or Laemmli Sample Buffer (4x Biorad 1610747)
- Cells washing buffer: PBS 1X containing 0.05% v/v of Tween.

- Equipment**
- Protein LoBind tube (Eppendorf AG).
 - ThermoMixer C (Eppendorf)
 - Centrifuge 5430R (Eppendorf)
-

Labelling procedure in reaction buffer

- Step 1.** MMP catalytic domain was conditioned or diluted in the appropriate reaction buffer A, B or C -> final concentration [MMP]= 1 μ M, 100nM, 50nM, 25nM, 10nM or 1nM.
- Step 2.** In the case of competition experiments, competitors were added (1 μ l) and incubation was performed at 37°C for 30 min under gentle stirring (ThermoMixer C, 800rpm). For hTIMP-1, the time of pre-incubation was 90 min.
- Step 3.** 1 μ L of probe in DMSO solution was added-> final probe concentration [probe]= 10 μ M, 1 μ M, 100 nM or 10 nM.
- Step 4.** The labelling reaction solution was gently stirred (ThermoMixer C, 800 rpm) at 37°C
- Step 5.** At specific time point (for 4h, 8h etc or 24h), the reaction was either quenched by addition of loading buffer for subsequent SDS-PAGE or acidify with TFA (0.1% v/v) for subsequent RP-HPLC analysis.
-

Labelling procedure in presence of serum albumin

- Step 1.** MMP catalytic domain was conditioned or diluted in the appropriate reaction buffer A.
- Step 2.** hSA (1 μ L) was added-> final concentration [hSA]=500 μ M, 100, 50 μ M or 10 μ M
- Step 3.** 1 μ L of probe solution was added-> final concentration [probe 9, 10 or 11]= 10 μ M or 1 μ M
- Step 4.** The labelling reaction solution was gently stirred (ThermoMixer C, 800rpm) at 37°C
- Step 5.** At specific time point (24h), the reaction was quenched by addition of loading buffer for subsequent SDS-PAGE.

Labelling procedure in presence of mouse liver extract

- Step 1.** Liver extract (46 mg/mL) was dissolved in reaction buffer A -> 100 µg
- Step 2.** Recombinant hMMP-12 was added -> final concentration [MMP-12] = 100nM, 50 nM, 25nM or 5nM.
- Step 3.** In the case of competition experiments 1 µL of competitor in DMSO solution was added-> final concentration [RXP470.1] = [GM6001] = [RXP500.1] = [hTIMP-1] = 1 µM
- The competitors were first incubated for 30 min with hMMP-12 catalytic domain, for hTIMP-1, the time of pre-incubation was 90 min.
- Step 4.** 1 µL of probe solution was added -> final concentration [probe 10]= 1µM, 100 nM, 50 nM or 10 nM.
- Step 5.** The labelling reaction solution was gently stirred (ThermoMixer C, 800rpm) at 37°C.
- Step 6.** The reaction was quenched by addition of loading buffer and protein mixture was resolved by SDS-PAGE
-

Labelling procedure on murine macrophages

Pathway A (see Figure 110 part 16.1.1.3)

- Step 1.** Each aliquot ($5 \cdot 10^6$ cells per batch) was resuspended in 200 µL of activity buffer (Tris buffer 50mM, CaCl₂ 10mM, pH=6.8) containing 0.1% v/v of P8340 inhibitors cocktail
- Step 2.** The probes 10 and 11 were added to obtain final concentration 1 µM and 100 nM.
- Step 3.** The labelling reaction solutions was gently stirred (ThermoMixer C, 800rpm) at 37°C during 4h.
- Step 4** The samples were centrifuged, supernatants were collected and concentrated by freeze drying and then solubilized in Laemmli buffer (50µL) and resolved by SDS-PAGE.

Pathway B (see Figure 110 part 16.1.1.3)

- Step 1** 3 ml of a Tris activity buffer B (0,1 % v/v of inhibitors P8340) containing probe 10 at 1 μ M was injected directly intraperitoneally.
- Step 2** The solution was then collected, incubated for 4h at 37°C and centrifuged. The supernatant was collected, freeze drying and then solubilized in Laemmli buffer (50 μ L) and resolved by SDS-PAGE.

Labelling procedure on murine dendritic cells

- Step 1.** Murine dendritic cells ($5 \cdot 10^6$) were suspended in in activity buffer (200 μ L, Tris buffer 50mM, CaCl₂ 10mM, pH=6.8) containing 0.1% v/v of P8340 inhibitors cocktail.
- Step 2.** Probe 10 and 11 were added to obtain final concertation 1 μ M.
- Step 3.** The samples were incubated during 4 h in 37 °C.
- Step 4.** After labelling the samples were centrifuged and supernatants were collected and freeze-dried.
- Step 5.** The samples were solubilised in Laemmli buffer (50 μ L) and protein mixture was resolved by SDS-PAGE.

Labelling procedure on human dendritic cells

- Step 1.** Human dendritic cells (10^6 cells per batch) were suspended in 250 μ L TCNB buffer (50 mM Tris-HCl buffer, 10 mM CaCl₂, 150mM NaCl , 0.05% Brij, 1% v/v P8340 pH=7.5.)
- Step 2.** Probe **10** was added to obtain final concertation 100 nM or 500 nM and probe **11** to obtain 500 nM.
- Step 3.** The labelling solutions were gently stirred (ThermoMixer C, 800rpm) during 4h at 37°C.
- Step 4.** The samples were centrifuged.
- Step 5.** The supernatant was removed and freezdried.
- Step 6.** The cell pellets and lyophilized supernatants were suspended in Laemmli buffer (50 μ L) an resolved by SDS-PAGE.

16.3. RP-HPLC samples analysis and labelling yield determination

The RP-HPLC analyses of the reaction mixture containing labelled and unlabelled MMPs were performed as followed:

- Step 1.** The labelling was performed in following conditions: hMMP12 5 μ M, buffer A, 24h, 37 C, probe **9** or **10** at 10 μ M, 100 μ l of mixture for each measurement.
- Step 2.** The labelling mixture was first acidified with TFA (0.1% v/v)
- Step 3.** 100 μ L of the resulting solution was injected and eluted on X Bridge BEH300 column (21 x 150 mm, 3.5 μ m, Waters, flow rate = 0.2 mL.min⁻¹) using the following program: initial conditions: 5% B, 0 to 5 min: 5% B, 5 to 10 min: 20%, 10 to 65 min: 55%, 65 to 67 min: 100% B with A: H₂O/TFA 0.1% and B: CH₃CN 90%/H₂O 10%/ TFA 0.09%. Detection of MMPs labelled with a fluorescein tag was performed at 215/280/450 nm and at 215/280/550 nm for those labelled with Cy3 tag (see Figure 111 for representative chromatograms).

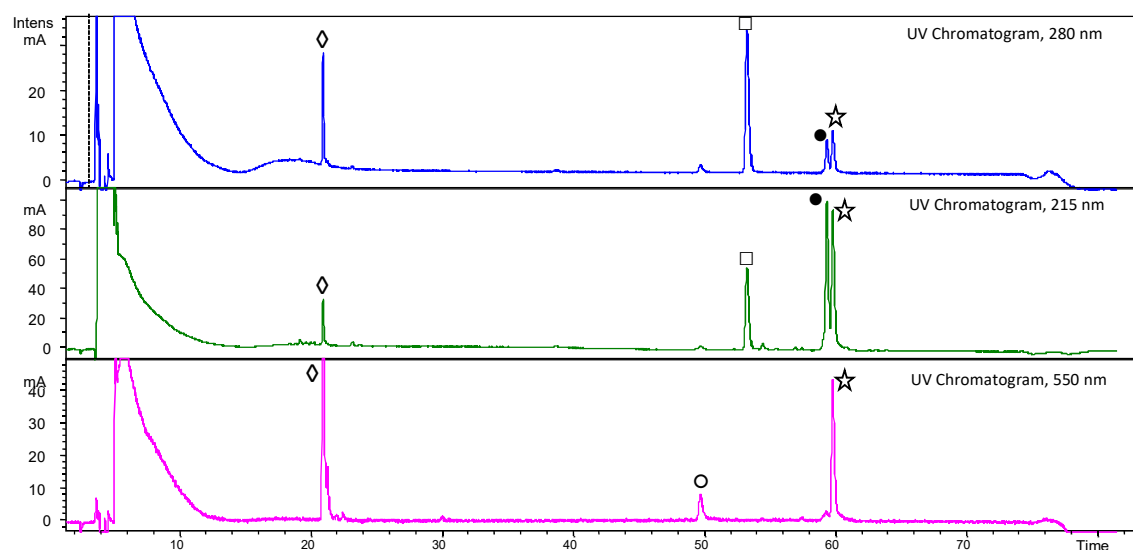


Figure 111: Representative LC/MS profile of reaction of hMMP-12 labelling by probe 10 (Cy3-tagged hMMP-12 in mixture with its unlabelled counterpart after 24h of reaction. Cy3-tagged MMP-12 (Rt=60 min, marked with ☆) was preferentially detected at 550nm while its unlabelled counterpart (Rt=59min marked with ●) is visualized at 215 and 280 nm. Intact probe 10 (Rt=49.1min, marked with ○) and Imidazole (Rt=54 min, marked with □) and Cy3 (Rt=21,5 min, marked with ◇) derivatives resulting from probe 10 hydrolysis were also detected on the chromatograms.

In these conditions of detection (UV/visible detector Agilent 1100 series, G1315B DAD), up to 5 pmol of Cy3-labelled MMP can be detected.

In the same RP-HPLC conditions, when the elution device was coupled to a fluorescence detector (RF-20A XS/Shimadzu, Ex/Em= 550/570 nm, gain x4 and medium sensitivity) up to 0.01 pmol of Cy3-tagged MMP is detected (Figure 112).

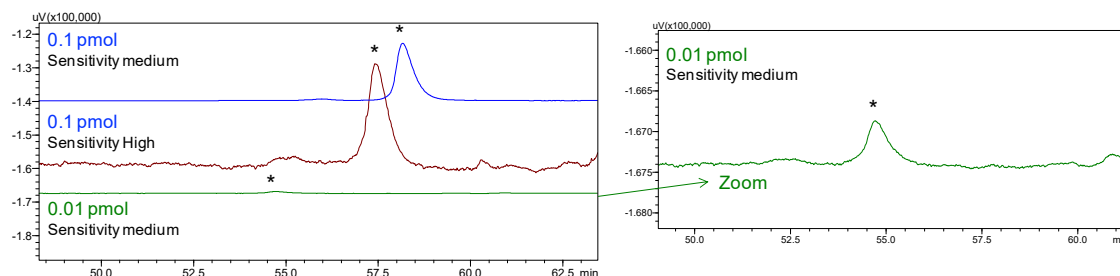


Figure 112: RP-HPLC profile of Cy3-tagged hMMP-12 detected with a fluorescent detector (Ex/Em= 550/570 nm, gain x4 and medium sensitivity). Cy3-tagged MMP-12 is marked with a black star. The detection limit is 0.01 pmol.

With a maximum injection volume of 50 μ L, this corresponds to a Cy3-tagged MMP at 10 nM concentration in solution.

The labelling yield was calculated both at 214 and 280 nm. At 280 nm, a correction factor was calculated considering the molar extinction coefficient of the Cy3 dye ($\epsilon_{280}=12.000 \text{ M}^{-1}\cdot\text{cm}^{-1}$). The applied correction factor for labelled hMMP12 by Cy3 was 1,44 (Figure 113 B) compared to native hMMP12. At 280 nm for fluorescein dye considering acidic conditions of elution ($\text{pH} < 2$) a correction was not significant and not applied in these calculations (Figure 113 A).

The calculated yields corresponded to average values of experiments performed in triplicate.

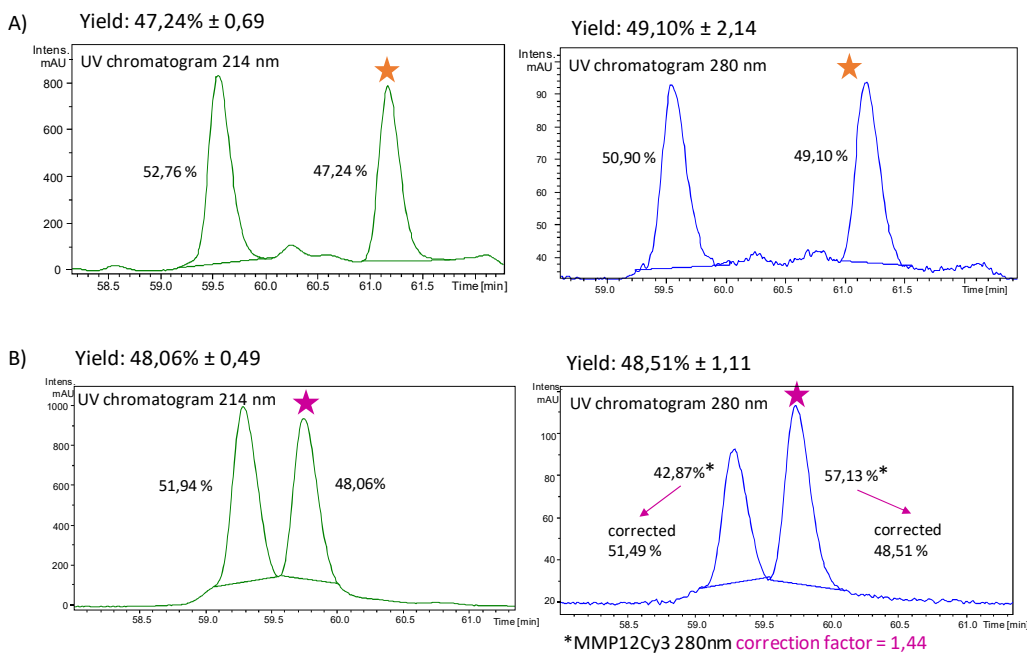


Figure 113: Representative RP-HPLC profiles of A) fluorescein-tagged hMMP-12 ★ in mixture with unlabelled hMMP12 at 280 and 215 nm. B) Cy3 -tagged hMMP-12 ★ in mixture with unlabelled hMMP12 at 280 and 215 nm. Their relative ratios were calculated from picks area integration at both wavelengths. At 280 nm, correction factor of 1,44 was applied for Cy3 -tagged hMMP-12.

Mass of unlabelled and labelled MMP eluted from the reversed phase column were also analysed in positive mode of ionization using a Bruker Esquire HCT Ion Trap mass spectrometer. Ion trap parameters were set as follows: electrospray potential, ± 4000 V; skimmer voltage, ± 40 V; capillary exit, 226 V; and a source temperature of 365 °C. The MS survey scan was m/z 400-3000 Da with a target mass fixed at m/z 1800 Da and a 5-spectrum scan average.

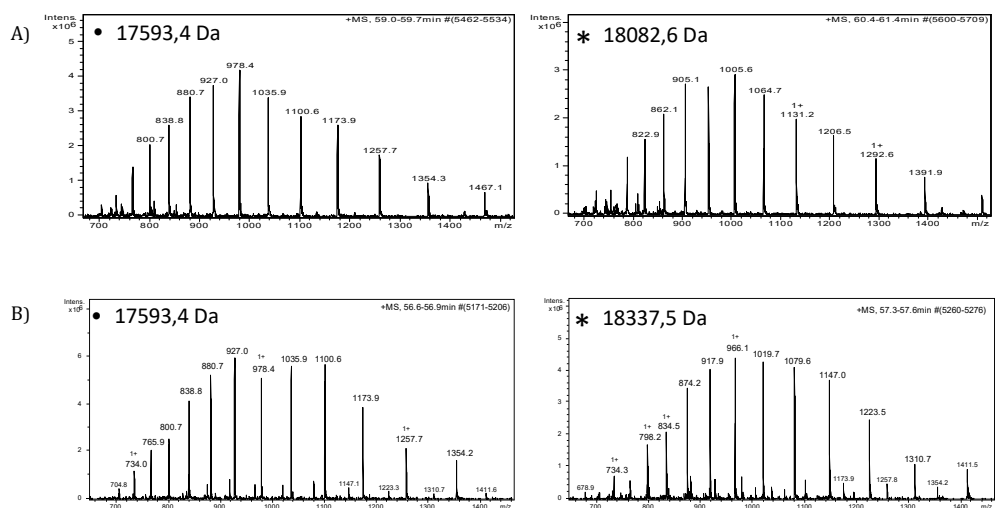
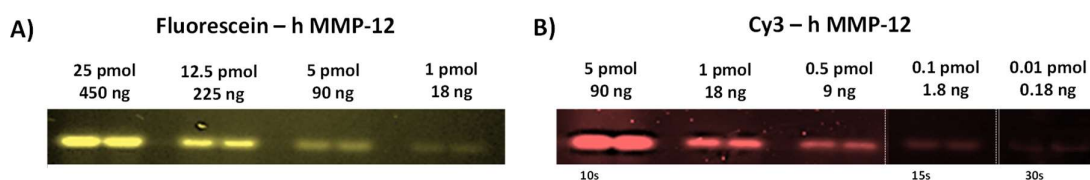


Figure 114 Representative ESI profiles of A) hMMP-12 ● and fluorescein-tagged hMMP-12 * B) hMMP-12 ● and Cy3 -tagged hMMP-12 *.

16.4. Samples analysis by SDS-Page followed by In gel fluorescence imaging and western blot.

The samples were resolved by 12% SDS-PAGE gel according to the procedure described in part 14.4. The Fluorescein tag labelled proteins were visualized at $\epsilon_{ex} = 460$ nm on a Luminescent imager analyser (Image Quant LAS 4000 Mini, General Electric, USA) and the Cy3 tagged proteins at $\epsilon_{ex} = 532$ nm with a Typhoon 9200 (Amersham, USA) or Molecular Imager® VersaDoc™ MP 4000 (BioRad) fluorescence gel scanner. All the resulting images were analysed with ImageJ software. When an internal standard was loaded on the gel, integration of the fluorescent bands allowed estimating the amount of labelled MMP and then deducing the labelling yield. The internal standard was a known amount of Fluorescein/Cy3-tagged MMP-12 that was first isolated by RP-HPLC (see above 16.3 step 3), lyophilized and solubilized in appropriate buffers. Its concentration was then determined by measuring the absorbance at 495 nm (fluorescein in pH=7.2) and 550 nm (Cy3) and applying the beer lambert law with $\epsilon_{495} = 76\,900\text{ M}^{-1}\text{cm}^{-1}$ and $\epsilon_{550} = 150\,000\text{ M}^{-1}\text{cm}^{-1}$.

As illustrated by Figure 115, the threshold of detection in fluorescein-tagged and Cy3-tagged hMMP-12 are 1pmol (18 ng) and 0.01pmol (0.18 ng) respectively. This detection limit can be improved by increasing the time of reading.



**Figure 115: Comparison of detection threshold through in-gel fluorescence imaging a) fluorescein -hMMP12
b) Cy3-hMMP12**

Specific detection of the MMP-12 (unlabelled or labelled) band can be selectively achieved through a western blot using MMP12 selective polyclonal antibodies. The western blot was performed according the following procedure.

Materials and equipment

- Reagents**
- Primary antibody ref: AF 3467 Mouse MMP 12 (Polyclonal Goat Ig)
 - Secondary antibody ref :HAF 109 Goat IgG Peroxydase conjugated
 - Blocking buffer - TBS/ 0,01%Tween/ 1% BSA
 - TBST - TBS/ 0,01% Tween
 - Trans-Blot® Turbo™ 5x Transfer buffer (Biorad)
200ml of concentrated buffer was mixed with 600 ml ultrapure water and 200 ml of ethanol to make of 1L of transfer buffer.
 - Clarity™ Western ECL Blotting Substrates (Clarity Western Peroxide Reagent and Clarity Western Luminol/Enhancer Reagent)
- Equipment**
- Trans-Blot® Turbo™ mini-size PVDF membrane (7.1 x 8.5 cm, Biorad)
 - Trans-Blot® Turbo™ mini-size transfer stacks (7.1 cmx8.5 cm, BioRad)
 - Trans-Blot® Turbo™ Transfer System
 - Luminescent imager analyser (Image Quant LAS 4000 Mini, General Electric, USA)
-

Procedure

- Step 1.** A SDS gel was prepared following the procedure 14.4.1
- Step 2.** The membrane was activated by wetting it in ethanol for 30 seconds then soaking it briefly in distilled water followed by 1X transfer buffer.
- Step 3.** Transfer stacks were soaked in transfer buffer.
- Step 4.** The transfer “sandwich” was assembled by placing respectively on the bottom cassette transfer stacks, membrane, gel, transfer stacks (Figure 116). The blot roller was used to remove any air bubbles in the assembled transfer pack and provide consistent contact between the layers.

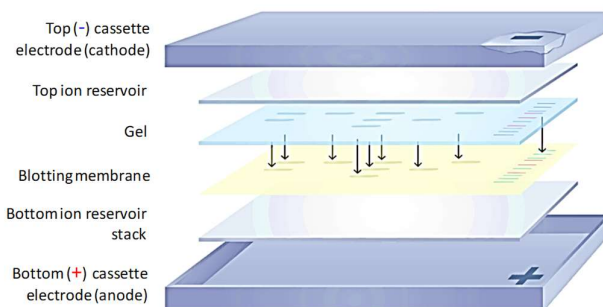


Figure 116. Blotting „sandwich”

- Step 5.** The top cassette was settled on the transfer “sandwich” and it was properly closed.
- Step 6.** The cassette was sliced into the Trans-Blot Turbo Transfer System and the migration of single Mini Gel run in 25 V, 2.5 A, 14 min.
- Step 7.** Blocking of the membrane was performed in blocking buffer at room temperature for 1h.
- Step 8.** The primary antibodies were diluted in a ratio 1/500 in TBS/ 0,01% Tween -2µg/ml (50 µl in 10 ml). The membrane was incubated overnight in 4°C under gently stirring.
- Step 9.** The blot was rinsed 3 times for 10 min with TBS/ 0,01% Tween/ 1% BSA.
- Step 10.** The secondary antibodies were diluted in a ratio 1/1000 in 10 ml of TBS/ 0,01% Tween buffer (10 µl in 10 ml). The membrane was incubated in the solution for 1h at room temperature.
- Step 11.** The blot was rinsed 3 times for 10 min with TBS/ 0,01% Tween/ 1% BSA.
- Step 12.** Clarity ECL substrates were mixed in a 1:1 ratio (for a mini-sized membrane (7.1 x 8.5 cm), 2 ml of solution was sufficient).
- Step 13.** The membrane was covered by prepared solution.
- Step 14.** Chemiluminescence signal was detected by Luminescent imager analyser during 6 min of exposition (Figure 117).

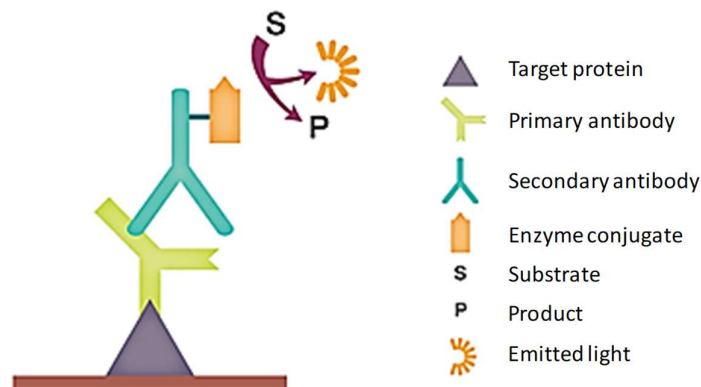


Figure 117 Chemiluminescence detection (Biorad Clarity ECL substrates).

The secondary antibody which binds the antibody specific for the protein of interest, is conjugated to an enzyme, which catalyzes a reaction leading to light emission. Luminol oxidized by HRP in the presence of a peroxide leads to the formulation of a 3-aminophthalate dianion and the release of light. In these conditions, unlabelled and labelled MMP can be detected indifferently. As illustrated by Figure 118.

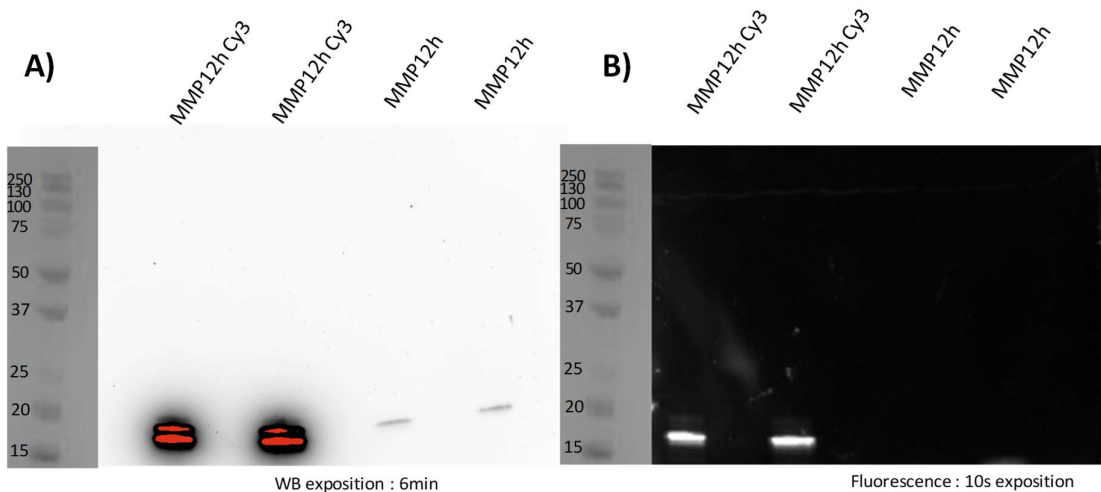


Figure 118 A) Western Blot and B) in-gel fluorescence of hMMP12 Cy3 and hMMP12

17. Proteomics

17.1. Determination of the position of MMP12 labelling by RXP 470.1 derived probes.

In order to identify the position of the tag on MMP-12 after labeling of MMP12 with RXP470.1 derived probes, the following procedure was applied. The general workflow is illustrated in Figure 119.

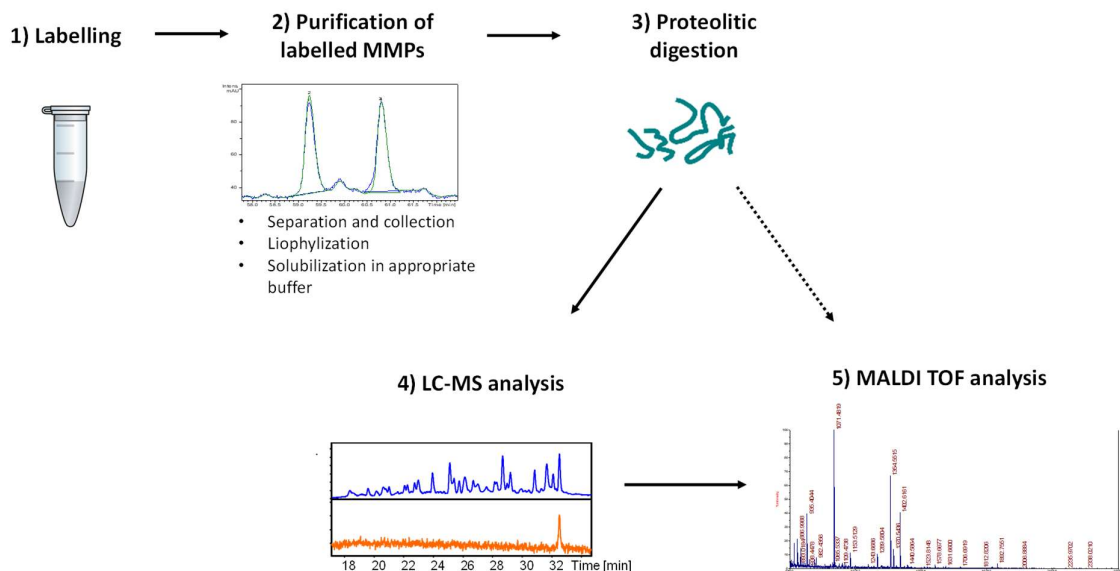


Figure 119 General work flow to isolate and identify labelled MP fragment.

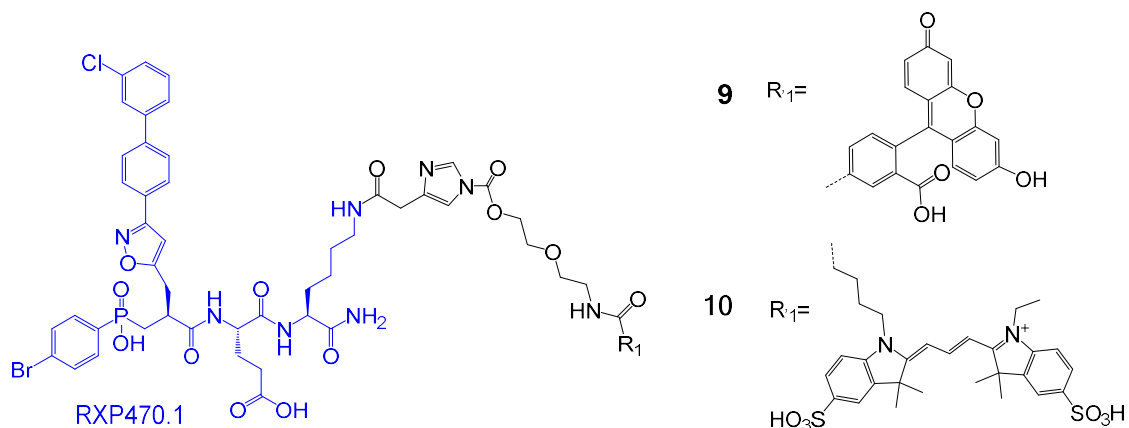


Figure 120. Probe 9 and 10 structure.

First, MMP12 was labeled by mixing MMP12 solution with an excess of probe (probe 9 or 10, Figure 120). The reaction mixture was then purified by liquid chromatography monitored at 214 nm and 450 nm or 550 nm together with ESI-MS to isolate the labeled MMP12 (Figure 121 A and Figure 123 A respectively for probe 9 and 10). This fraction of MMP12 was then freeze-dried and dissolved in Tris buffer 100 mM pH 7,8 10 mM CaCl₂. The sample was then digested by chymotrypsin. The mixture of peptides (digest) was purified by LC coupled to ESI-MS and monitoring at 450 nm (550 nm for Cy3) fluorescent MMP12 peptide fragment was isolated (Figure 121 B, Figure 123 B).

The collected fragment was then freeze dried and dissolved in water. The sample was analyzed by MALDI-TOF. The MS experiment allowed to detect the mass of modified fragment (1148,7 Da for probe 9 experiment and 1402,6 Da for probe 10 experiment). MS/MS experiments led to the identification of the position of the tag on the protein sequence (Figure 121C, Figure 123C). The MS/MS spectra indicated for both probe that the labelled peptide was modified on Lys 177 belonging to DGKGGIL sequence of hMMP-12.

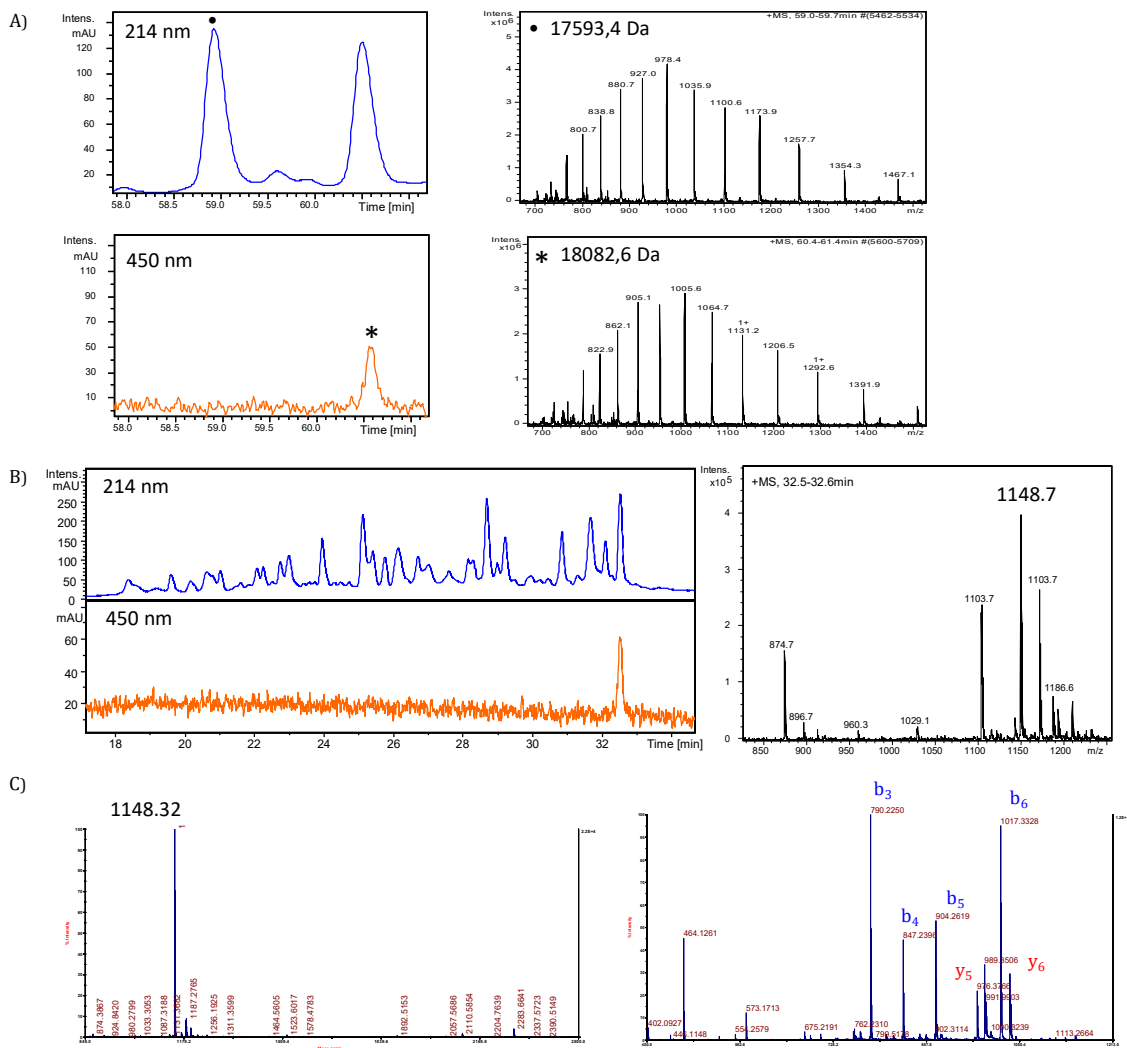


Figure 121: LC and MS data from MMP12 labelling experiments using probe 9 A) LC purification ($\lambda=214$ nm and 450 nm) of labelled MMP12 by probe 9 (*) separated from unlabeled MMP12 (●) and corresponding ESI-MS spectra B) LC profile of labelled MMP12 digest. ESI-MS of fluorescent fragment detected at 450 nm. C) MALDI-MS analysis of fraction corresponding to the fluorescent peak and MS/MS of the peak at 1148.32 Da.

It is worth to mention that the mass 1148.32 Da could be also detected for the direct analysis from digest of labeled MMP12 (Figure 122A). From this peak MS/MS delivered showed the same pattern as previously observed (Figure 122B).

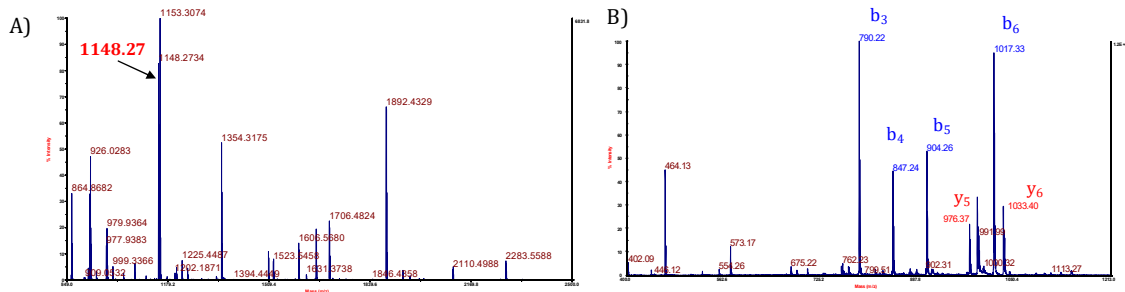


Figure 122 MALDI analysis A) direct analysis of the digest of MMP12 labelled by probe 9 B) MS/MS of peak 1148.27 Da

The same protocol was applied to the MMP12 containing Cy3 TAG. Direct analysis of digest allowed to detect fragment DGKGGIL containing/possessing Cy3 on Lys. $MH^+ = 1402$ Da (Figure 123).

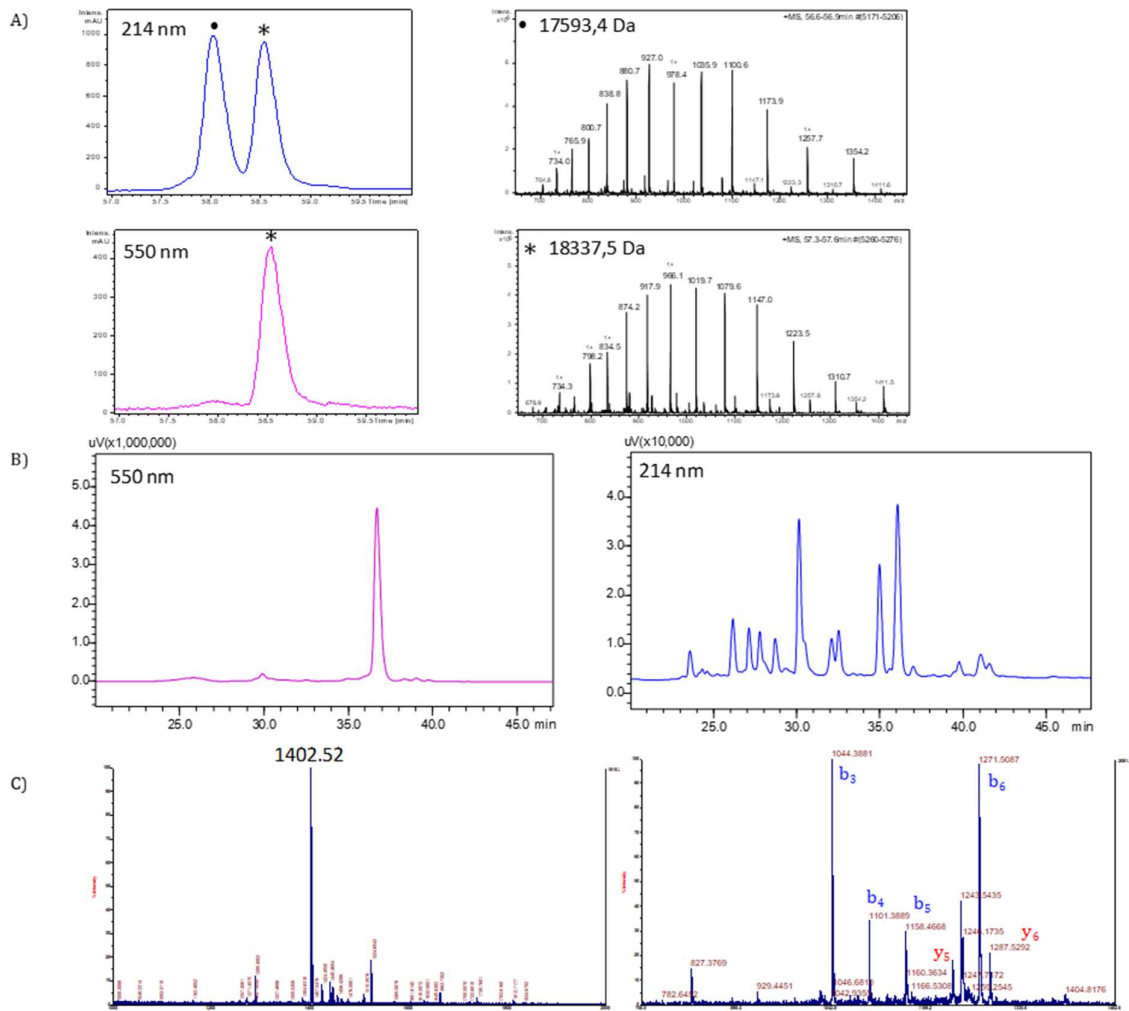


Figure 123: LC and MS data from MMP12 labelling experiments using probe 10 A) LC-MS purification ($\lambda=214$ nm and 550 nm) of labelled MMP12 by probe 10 (*) separated from unlabeled MMP12 (°) and corresponding ESI-MS spectra B) LC profile of labelled MMP12 digest. B) ESI-MS of fluorescent fragment detected at 550 nm. C) MALDI-MS analysis of fraction corresponding to the fluorescent peak and MS/MS of the peak at 1148.32 Da.

Here it was also possible to directly detect peak 1402.62 Da in the digest (Figure 124).

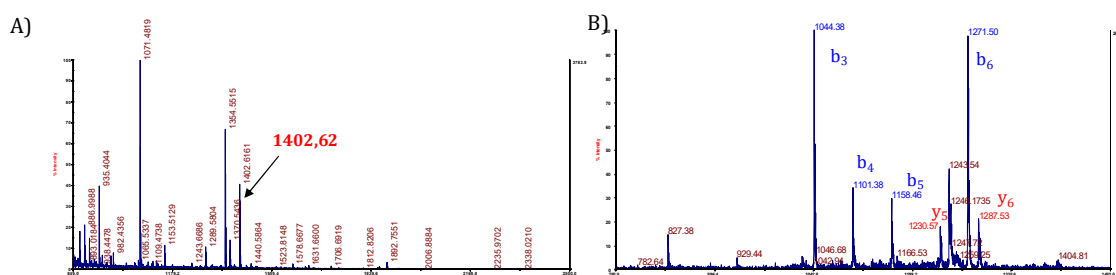


Figure 124 MALDI analysis A) direct analysis of the digest of MMP12 labelled by probe 10 B) MS/MS of peak 1402.62 Da.

17.2. Digestion by chymotrypsin and MALDI analysis

Reagents, equipment and methods

- Reagents**
- Chymotrypsin Sequencing Grade from Roche Diagnostics GmbH was used to provide a mixture a chymotryptic fragment from MMP samples.
 - Digestion samples were shaken and heated using a ThermoMixer C, 800 rpm from Eppendorf and spotted onto MALDI plate with HCCA (C8982 Sigma) solution.

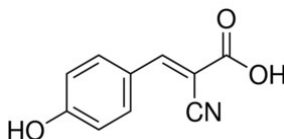


Figure 125. HCCA (Alpha-Cyano-4-hydroxycinnamic acid) structure

- Equipment**
- RP-HPLC Shimadzu apparatus (LC-20AB for pump module, PD-20A for UV detector and RF-20AXS for fluorescent detector, Ex/Em= 550/570 nm, gain x4 and medium sensitivity)
 - X Bridge BEH300 column (21 x 150 mm, 3.5 μ m, Waters, flow rate = 0.2 mL.min⁻¹)
 - 4800 spectrometer MALDI-TOF/TOF Proteomics Analyzer (Applied Biosystems, Foster City, CA).

Methods **Digestion general protocol:** Commercial aliquot of chymotrypsin was dissolved in HCl 1mM solution to reach concentration of the stock solution at 400ng/ μ L. Digestion of labelled MMP12 were performed in TRIS buffer 100mM, CaCl₂ 10mM, pH 7.8

MALDI matrix preparation: HCCA (R-cyano-4-hydroxycinnamic acid) matrix solution was prepared at 10 mg/mL in H₂O/CH₃CN/TFA (50/50/0.1).

Sample deposition for MALDI-TOF analysis: sample (0.5 μ L) was manually spotted on MALDI plate with an equal volume of HCCA matrix solution. MS and MS-MS spectra were recorded from crystallized samples.

Procedure

- Step 1.** For the labeling of MMP12, 5.3 μ M of protein was mixed with 10 μ M of probe 9 (37 $^{\circ}$ C, 24h). Purification was performed as it was described in part 16.3. After the purification of labelled MMP 12 by LCMS, the concentration of proteins was verified by UV measurement.
- Step 2.** Solution was freeze dried and resolved in a buffer for digestion (Tris 100mM, CaCl₂ 10mM, pH 7.8). For LC-MS labelled fragment purification 300 pmol of MMP12 labelled with probe 9 was used for digestion. Labelled MMP12 was dissolved in 25 μ l of Tris buffer and digested during 24 h in 37 $^{\circ}$ with chymotrypsin (1/10).
- Step 3.** 20 μ l of the digest was diluted in A/B solution (80 μ l) and the solution was analyzed by LC-MS. The analytical conditions were the following: Bridge BEH300 column (21 x 150 mm, 3.5 μ m, Waters), flow rate = 0.2 mL.min⁻¹, initial conditions: 5% B, 0 to 5 min: 5% B, 5 to 10 min: 20%, 10 to 55 min: 70%, 55 to 57 min: 100% B with A: H₂O/TFA 0.1% and B: CH₃CN 90%/H₂O 10%/ TFA 0.09%).
- Step 4.** Following the spectrum/chromatogram at 450 nm the fraction corresponding to the peak showing the fluorescence was collected and freeze dried.
- Step 5.** The resulting lyophilisate was dissolved in 10 μ l of water. 0.5 μ l of the solution was loaded on the MALDI plate, immediately mixed with 0.5 μ l of matrix solution (alpha-HCCA) and allowed the solvent to evaporate in the air stream to achieve a homogeneous crystallization of the mixture.
- Step 6.** The sample was analyzed by MALDI TOF in positive mode of ionization.
- Step 7.** MS/MS was performed on the most intensive peak MH⁺ = 1148 Da
- Step 8.** MS/MS spectra was analyzed by identifying **b ions** (extend from the amino terminus/the N-terminus) and **y ions** (extend from the carboxyl terminus/C-terminus). Determination of individual amino acids (y6,y5->DG and b6, b5, b4, b3 -> LIGG) allowed to identify the DGKGGIL fragment. The fragment contains Lys177 which was one of targeted residues. In MSMS spectra the mass of fluorescein tag was also shown (=464.14 Da)

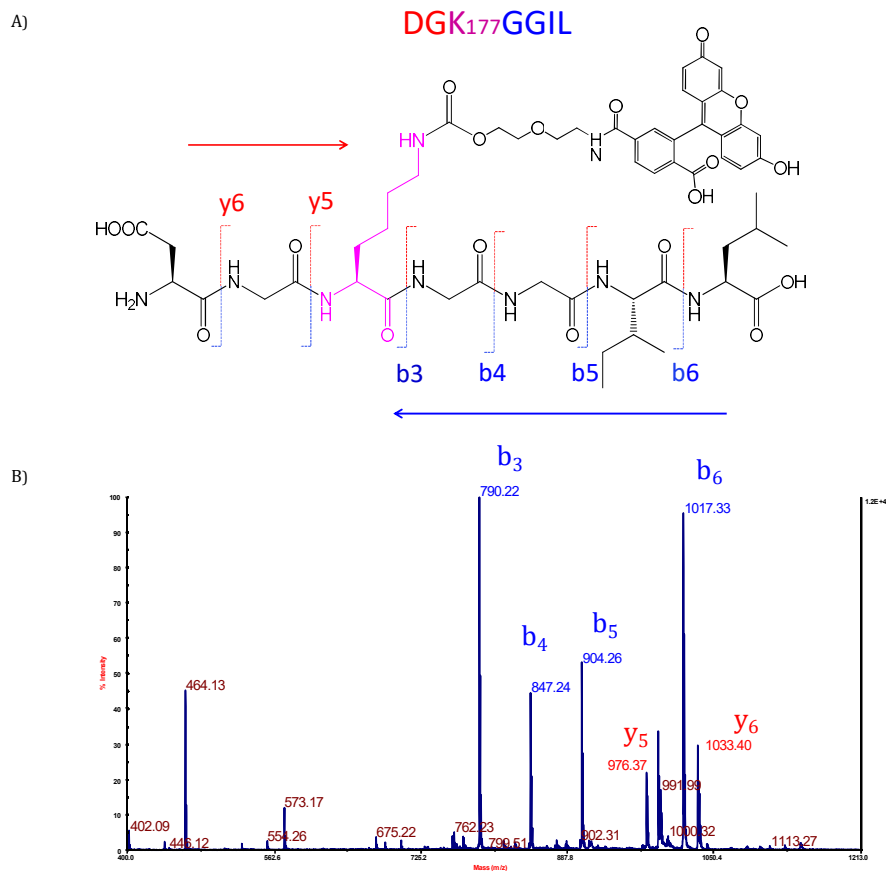


Figure 126. A) DGK₁₇₇GGIL fragment containing fluorescein TAG B) MS/MS of peak 1148.27 Da

Step 9. 1 μ l of the digest was diluted in 50 μ l of water, loaded on the MALDI plate and mixed with matrix. In direct analysis of the digest the peak $MH^+ = 1148$ Da was observed and followed by MS/MS analysis.

The same procedure was applied to analyze MMP12 labelled by probe 10 possessing CY3 tag. In this case only 15 pmol of proteins were digested in 10 μ l of TRIS buffer by chymotrypsin (1/10). 10 pmol in 50 μ l of A/B solution were analyzed by HPLC with sensitive fluorescence detector at wavelength 550 nm to isolate modified MMP12 fragment. The analytical conditions were the following: Bridge BEH300 column (21 x 150 mm, 3.5 μ m, Waters), flow rate = 0.2 mL.min⁻¹, initial conditions: 5% B, 0 to 5 min: 5% B, 5 to 10 min: 20%, 10 to 65 min: 55%, 65 to 67 min: 100% B with A: H₂O/TFA 0.1% and B: CH₃CN 90%/H₂O 10%/ TFA 0.09%). For direct MALDI analysis 1 μ l of the digest was diluted in water and 0.5 μ l of the solution was analyzed mixed to matrix solution. Other steps were followed as it was described above.

The same protocol was used to determine position of labelling on mMMP12.

BIBLIOGRAPHY IV

1. Bordenave, T. *et al.* Synthesis, in vitro and in vivo evaluation of MMP-12 selective optical probes. *Bioconj. Chem.* (2016). doi:10.1021/acs.bioconjchem.6b00377
2. Czarny, B. *et al.* Molecular determinants of a selective matrix metalloproteinase-12 inhibitor: insights from crystallography and thermodynamic studies. *J. Med. Chem.* **56**, 1149–1159 (2013).
3. Wakayama, S. *et al.* Chemical labelling for visualizing native AMPA receptors in live neurons. *Nat Commun* **8**, 14850 (2017).
4. Dabert-Gay, A.-S. *et al.* Molecular Determinants of Matrix Metalloproteinase-12 Covalent Modification by a Photoaffinity Probe. *J Biol Chem* **283**, 31058–31067 (2008).
5. Antoni, C. *et al.* Crystallization of bi-functional ligand protein complexes. *J. Struct. Biol.* **182**, 246–254 (2013).
6. Rouanet-Mehouas, C. *et al.* Zinc-Metalloproteinase Inhibitors: Evaluation of the Complex Role Played by the Zinc-Binding Group on Potency and Selectivity. *J. Med. Chem.* **60**, 403–414 (2017).
7. Morrison, J. F. Kinetics of the reversible inhibition of enzyme-catalysed reactions by tight-binding inhibitors. *Biochim. Biophys. Acta* **185**, 269–286 (1969).
8. Horovitz, A. & Levitzki, A. An accurate method for determination of receptor-ligand and enzyme-inhibitor dissociation constants from displacement curves. *Proc Natl Acad Sci U S A* **84**, 6654–6658 (1987).

I. FIGURES

Figure 1. Proteases standard nomenclature	3
Figure 2. One or two-step mechanism as function to environment in amino acids within protease active site.....	4
Figure 3 Timeline – the number of publications about matrix metalloproteinases over the years.	7
Figure 4. Metzincin superfamily members and structure of Matrixins family	8
Figure 5. Scheme of the zinc-binding motif and the Met-turn showing the common sequence motifs of the metzincins. Variable segments are shown as dotted lines	9
Figure 6. Domain structure of matrix metalloproteinases family.....	10
Figure 7. Regulation of extracellular proteolysis	11
Figure 8. Activation of MMPs, the interaction of cysteine residue from the pro peptide with the catalytic zinc ion of the catalytic domain	12
Figure 9. Schematic representation of two-step ProMMP-2 activation process by the combined action of MT1-MMP (MMP-14) and TIMP-2	14
Figure 10. Crystallographic structure of MMP-3 catalytic domain interacting with TIMP-1	15
Figure 11. In antiviral immunity, MMP12 can adopt a dual localisation associated to opposite functions.....	18
Figure 12. Catalytic domain of hMMP12.....	20
Figure 13. A) Generic structure of the most representative families of MMPs inhibitors sharing a common zinc-binding moiety, a hydrophobic P ₁ ' side chain and a peptide or pseudo peptide backbone to make hydrogen bonds within catalytic site. B) Schematic representation of most standard zinc-chelating moieties found in structure of MMPs inhibitors.	21
Figure 14. RXP470.1 structure and its selectivity profile towards a set of human metalloproteases. .	23
Figure 15. Crystal structure of RXP470.1 in interaction with hMMP12 catalytic domain	24
Figure 16. A) Change in RXP470.1 affinity toward MMP12 as function to pH B) Schematic representation of proton uptake upon phosphinic inhibitor binding, C) Zoom on the catalytic zinc ion region catalytic.	25
Figure 17. Effect of RXP470.1 treatment on atheroma plaque size.....	26
Figure 18. A) A/J mice infected with coxsackievirus type B3 were treated with MMP-12 inhibitor RXP470.1 or saline by continuous minipump infusion for 7 d. ELISA detected plasma IFN- α levels after 96 h of virus infection. Uninfected control animals B) Effect of extracellular MMP-12 inhibition on body weight during coxsackievirus type B3 infection. C) Coxsackievirus replication.	27
Figure 19. Schematic representation of MMPSense agents	28
Figure 20. Structure of SPECT contrast agents targeting MMPs. A) Structure of RP805 composed of a broad-spectrum targeting moiety and a reporter tag B) RXP470.1-derived probes conjugated to a reporter Tag.....	30
Figure 21. Structure of a representative ABPs targeting cysteine proteases	31
Figure 22. A) Schematic representation of a photoaffinity probe B) Two- step process of labelling by a photo affinity probe.	32
Figure 23. Photoreactive crosslinking reactions employing A) a benzophenone B) an aryl azide, and C) trifluoromethylphenyldiazirine group	33

Figure 24. A) HxBO-Rh MMP-directed active probe composed of targeting moiety, a benzophenone photoactivatable group and a Rhodamine (Rh) as reporter tag B) In-gel fluorescence imaging of MMP2 labelled by HxBP-Rh.....	34
Figure 25. A) Chemical structure of photoactivatable probe derived from phosphinic peptide B) In-gel visualisation of MMP12 labelling.	34
Figure 26. A) Chemical structure of phosphinic peptide-derived probe with a diazirine function B) In-gel visualization of recombinant MMP2, MMP-9, MMP-12 and MMP-13 catalytic domain labelled in complex proteome	35
Figure 27. The activity-based labeling mechanism of protease by quinolimine methide probes.	36
Figure 28. Two possible mechanisms of metalloprotease inhibition by a Thiirane derivative.....	36
Figure 29. Binding reaction of a MMPs-directed reactive probes towards A) an engineered MMP and B) a wild type MMP. The reactive probe is composed of a peptide backbone responsible for specific MMPs targeting a reactive warhead and a fluorescent tag	37
Figure 30. A) Mechanism of LDT chemistry B) mechanism of LDAI chemistry C) mechanism of LDSP chemistry.....	39
Figure 31. A) reactive spacer in LDSP, LDT, LDAI chemistry B) different TAGs and LG part of LDSP, LDT and LDAI probes.	40
Figure 32. Analyses of the labelling reactivity of LDSP, LDAI and LDT chemistry in vitro on CA2 A) SDS PAGE and in gel fluorescence analysis of hCA II labelling, B) Time plots of the modification yields by SDS PAGE analysis, Red circle the LDSP chemistry, blue diamond, the LDT chemistry, green square the LDAI chemistry, C) Initial velocity of in vitro CA2 labelling reactions, D) MALDI TOF MS analyses of CA2 labelling	41
Figure 33. Intracellular CA2 labelling by LD chemistry, western blot analyses of the CA2 labelling process in living MCF7 cells.....	42
Figure 34: Schematic representation of MMPs labelling process using a new generation of affinity probes. A) MMP probes composed of ligand part, a chemically sensitive spacer a tag. B) Two steps labelling process of MMPs within a complex proteome.....	55
Figure 35. Crystal structure of hMMP12 in complex with RXP470.1.	56
Figure 36 A) Comparison of affinity/selectivity profile between RXP470.1 and its P3' modified analogues A towards a panel of ten human MMPs identified by the colour code on right of the figure. B) Crystal structure of hMMP12 in complex with compound A.....	57
Figure 37. Chemical structure of probe 9 and 10.....	58
Figure 38: LC/MS profile of 9.....	60
Figure 39. Evaluation of the hydrolysis stability of compound B under different pH conditions.....	61
Figure 40. Change in RXP 470.1 affinity constant towards MMP-12as function of pH.....	62
Figure 41. Evaluation of probe 9 hydrolysis stability	63
Figure 42. hMMP-12 labelling by probe 9 and competitions experiment with RXP470.1	65
Figure 43. LC/MS analysis of the labelled and unlabelled MMP-12 in mixture after 24h of reaction..	66
Figure 44. hMMP-12 labelling by probe 10 in labelling buffer and competitions experiment with RXP470.1, RXP500.1, GM6001 and hTIMP-1.....	67
Figure 45. Amino acids sequence of hMMP-12 and theoretical fragments generated by trypsin digestion and by chymotrypsin digestion	69
Figure 46. Identification of crosslinked residue(s) within fluorescein-labelled hMMP-12.	71
Figure 47. Identification of crosslinked residue(s) within Cy3-labelled hMMP-12.	72
Figure 48. Evaluation of Cy3-labelled hMMP-12 proteolytic activity.....	73

Figure 49. Comparison between the different S ₃ ' regions of MMPs	74
Figure 50. Labelling experiments of MMP-2/3/8/9/10/12 and 13 with probe 10.....	75
Figure 51. Chemical structure of A) RXP500.1 and B) RXP500.1-derived probe 11.....	77
Figure 52. Comparison of hMMPs chemical labelling by probe 10 and 11.....	78
Figure 53. Comparison of hMMP12, 2, 8, 13, 10 and 13 S ₃ ' region considering their labelling by probe 11.	79
Figure 54. Comparison of hMMP12 chemical labelling by probe 10 and 11	80
Figure 55. RP-HPLC analysis of tryptic digest of hMMP13.....	81
Figure 56. hMMP-12 labelling by probe 9, 10 or 11 in presence of Serum Albumin	82
Figure 57. hMMP-12 labelling by probe 10 and 11 in mouse liver extract	84
Figure 58. Human dendritic cells (DCs) labelled by probe 10 and 11.	87
Figure 59. Comparison of hMMP12 and mMMP12 chemical labelling by probe 10 and 11.	90
Figure 60. A) amino acids sequence of mMMP-12 and theoretical fragments generated by chymotrypsin digestion Lys ¹⁸¹ , Thr ²¹⁴ and Tyr ²⁴⁴ are coloured in red, green and blue respectively. ...	91
Figure 61. Identification of crosslinked residue(s) within Cy3-labelled mMMP-12	92
Figure 62. Labelling of murine DCs.....	93
Figure 63. Labelling of murine thioglycolate-stimulated macrophages.....	95
Figure 64. Labelling of murine thioglycolate-stimulated macrophages in the peritoneal cavity.....	96
Figure 65. hMMP-12 labelling capacity comparison between acyl imidazole probe 10 and tosyl probe 19.	98
Figure 66. Detection of native MMPs within various complex proteomes by using a new proteomic approach exploiting both a new generation of probes and a mass signal enhancer.	100
Figure 67. Chemical structure of HCCA probe 14 with a RXP500.1 binding motif.....	101
Figure 68. Labelling of hMMP12 by probe 14	102
Figure 69. hMMP-12 labelling with substrate-derived probes 15, 16, 17 and 18.....	103
Figure 70: RP- HPLC profiles of crude compounds 1 and 2	119
Figure 71: LC/MS profile of purified compound 1.....	120
Figure 72: ¹ H NMR profile of compound 1.	121
Figure 73: LCMS profile of purified compound 2	121
Figure 74: ¹ H NMR profile of compound 2.	122
Figure 75: LC/MS profile of purified compound 3.....	124
Figure 76 ¹ H NMR profile of compound 3.	125
Figure 77: LC/MS profile of purified compound 4.....	125
Figure 78 ¹ H NMR profile of compound 4.	126
Figure 79: RP-HPLC and mass profiles of 5.....	129
Figure 80: RP-HPLC and mass profiles of 6.....	129
Figure 81: LCMS profile of purified compound 7	130
Figure 82: LC/MS profile of purified probe 9.	133
Figure 83: LCMS profile of purified probe 10.....	134
Figure 84: LCMS profile of purified probe 11	135
Figure 85: LCMS profile of purified probe 12	136
Figure 86: LCMS profile of purified probe 13	137
Figure 87: LCMS profile of purified probe 14.....	138
Figure 88: LC/MS profile of 15b in mixture with its amino precursor 15a.....	140
Figure 89: RP-HPLC and mass spectrometry profiles of purified 15a.	141

Figure 90: RP-HPLC and mass spectrometry profiles of purified 16a.	142
Figure 91: RP-HPLC and mass spectrometry profiles of purified 17a.	143
Figure 92: RP-HPLC and mass spectrometry profiles of purified 18a.	144
Figure 93: LCMS profile of purified probe 15.	145
Figure 94: LCMS profile of purified probe 16.	146
Figure 95: LCMS profile of purified probe 17.	147
Figure 96: LCMS profile of purified probe 18.	148
Figure 97: LCMS profile of purified probe 19.	150
Figure 98: A) RP-HPLC profiles of probe 10 at different time points (0, 1h, 2h, 4h and 24h) B) Hydrolysis of probe 10	151
Figure 99 A) Sequence of mMMP12 catalytic domain B) SDS-gel of mMMP12 during different phases of production.....	153
Figure 100. Chemical structure of A) MCA-MAT and B) MCA-MMP.....	155
Figure 101. A graph of MMP12h activity (triplicate).....	157
Figure 102. Titration MMP12 by RXP 500.1 in Tris buffer.....	160
Figure 103. A) SureCast Gel Handcast System B) XCell SureLock electrophoresis system	161
Figure 104. Profile of MMPs on silver stained SDS-PAGE gel.....	164
Figure 105. Example of distribution of the inhibitor for a K_i measurement	165
Figure 106. Sigmoid representing the inhibition constant of mMMP12 against RXP470.1	166
Figure 107. Preparation of liver extract.	168
Figure 108. Coomassie Brilliant Blue G-20 structure.	169
Figure 109. Bradford test – calibration curved of BSA (μg).....	170
Figure 110 Scheme of the protocol of murine macrophages collection.....	172
Figure 111: Representative LC/MS profile of reaction of hMMP-12 labelling by probe 10.....	179
Figure 112: RP-HPLC profile of Cy3-tagged hMMP-12 detected with a fluorescent detector.....	180
Figure 113: Representative RP-HPLC profiles of A) fluorescein-tagged hMMP-12 B) Cy3 -tagged hMMP-12.....	181
Figure 114 Representative ESI profiles of A) hMMP-12 and fluorescein-tagged hMMP-12 B) hMMP- 12 and Cy3 -tagged hMMP-12.....	181
Figure 115: Comparison of detection threshold through in-gel fluorescence imaging	182
Figure 116. Blotting „sandwich”	183
Figure 117 Chemiluminescence detection	184
Figure 118 A) Western Blot and B) in-gel fluorescence of hMMP12 Cy3 and hMMP12.....	185
Figure 119 General work flow to isolate and identify labelled MP fragment.....	185
Figure 120. Probe 9 and 10 structure.....	186
Figure 121: LC and MS datas from MMP12 labelling experiments using probe 9	187
Figure 122 MALDI analysis A) direct analysis of the digest of MMP12 labelled by probe 9 B) MS/MS of peak 1148.27 Da.....	188
Figure 123: LC and MS datas from MMP12 labelling experiments using probe 10	188
Figure 124 MALDI analysis A) direct analysis of the digest of MMP12 labelled by probe 10 B) MS/MS of peak 1402.62 Da.....	189
Figure 125. HCCA (Alpha-Cyano-4-hydroxycinnamic acid) structure.....	189
Figure 126. A) DGKGGIL fragment containg fluorescein TAG B) MS/MS of peak 1148.27 Da	191

II. TABLES

Table 1. Comparison of LDT, LDAI and LDSP chemistry.	41
Table 2. K_i values (nM) for probe 9, 10 and RXP470.1 on a set of MMPs.....	64
Table 3. Theoretical % of probe 9 or 10/hMMP12 complex at equilibrium in labelling buffer.	68
Table 4. (M+H) ⁺ of peptide fragments under chymotrypsin digestion covalently modified by Fluorescein of Cy3 tag.	70
Table 5. Theoretical % of probe 10/hMMP complex at equilibrium in labelling buffer.....	76
Table 6. K_i values (nM) of RXP500.1, probe 11 and probe 10 towards a set of MMPs	77
Table 7. K_i values (nM) of probes 10 and 11 as well as RXP470.1 towards mouse MMP12 (mMMP12) and human MMP12 (hMMP12)	86
Table 8 theoretical ϵ 280 nm and the concentration of mother solutions of used MMPs.....	154
Table 9 K_i (nM) value of RXP 500.1 towards a set of hMMPs.	158
Table 10. ΔF values for each MMP catalytic domain.	160
Table 11 Composition of electrophoresis gels for 2 gels.	161
Table 12 K_i values (nM) for probe 9, 10, 11, RXP470.1, RXP500.1, GM6001 and humanTIMP1 towards a set of metalloproteases.....	167
Table 13. Measurements of Bradford test of mouse liver extract.....	170

III. SCHEMES

Scheme 1. Chemical pathway to access to probe 9 and 10	59
Scheme 2: Synthesis of compound 1 and 2	117
Scheme 3: Synthesis of compounds 3 and 4	123
Scheme 4: Synthesis of precursors 5 , 6 , 7 and 8	127
Scheme 5: Synthesis of acyl imidazole probes 9-14	131
Scheme 6: Synthesis of acyl imidazole probes 15-18	139
Scheme 7: Synthesis of compound 19	149

IV. ANNEXES

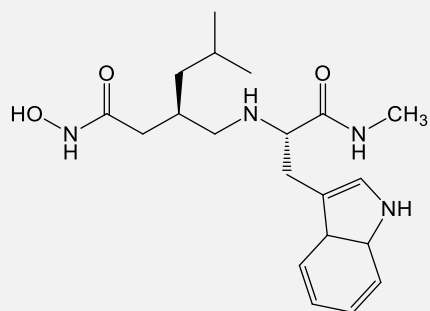
A. LIST OF COMPOUNDS

B. ARTICLE

A. LIST OF COMPOUNDS

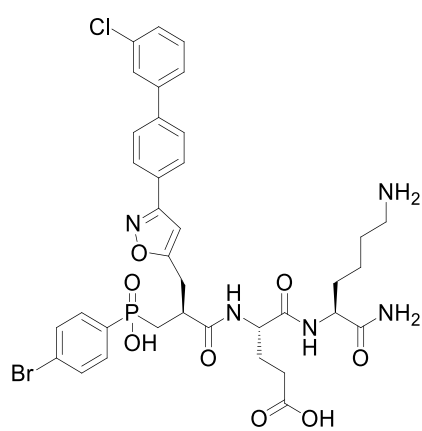
NR

STRUCTURE OF COMPOUNDS



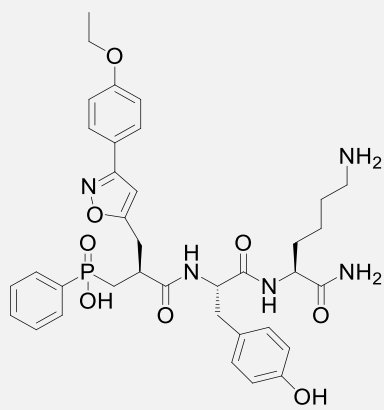
GM6001

1



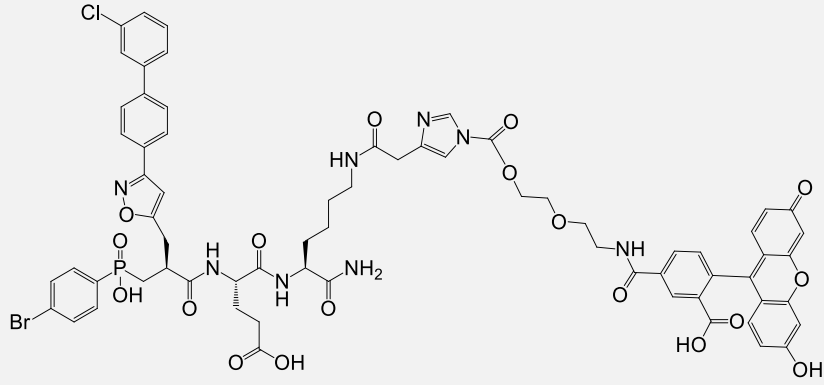
RXP470.1

2

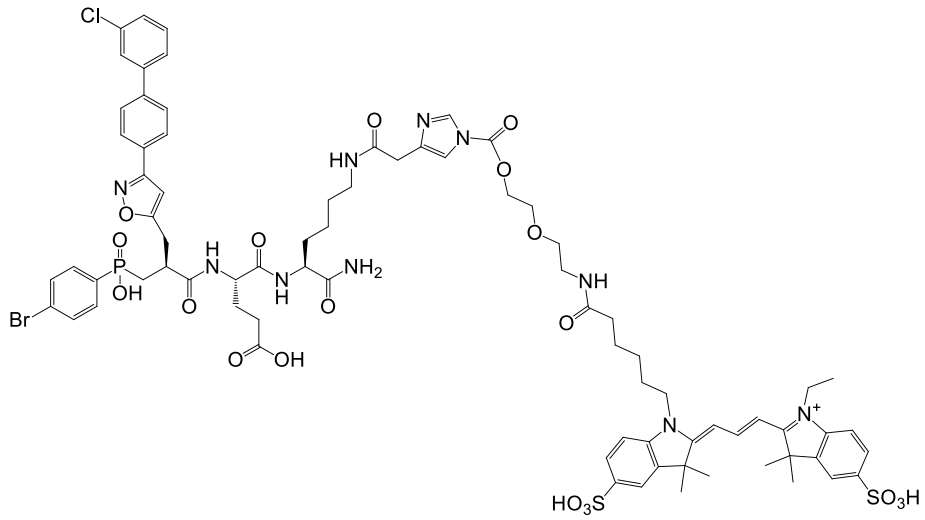


RXP500.1

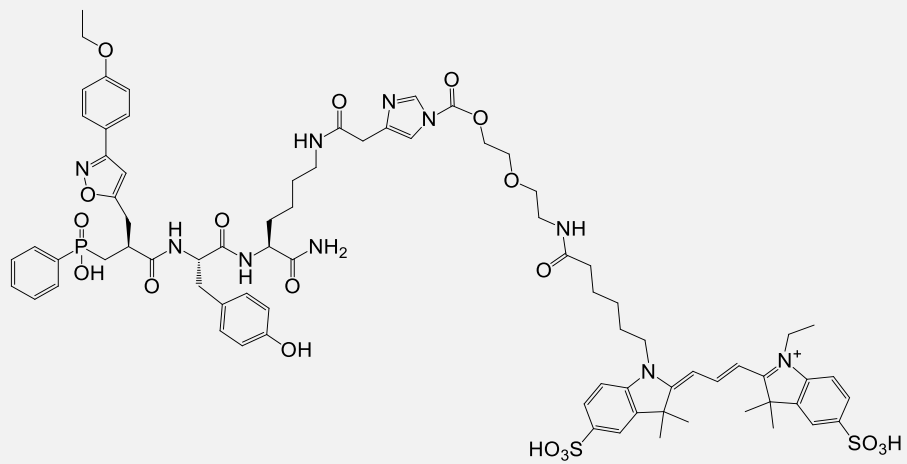
9



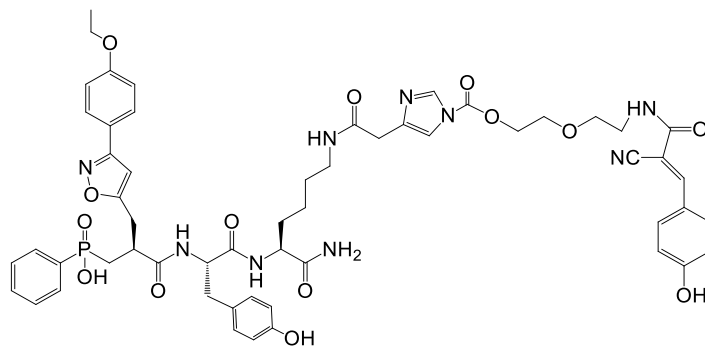
10



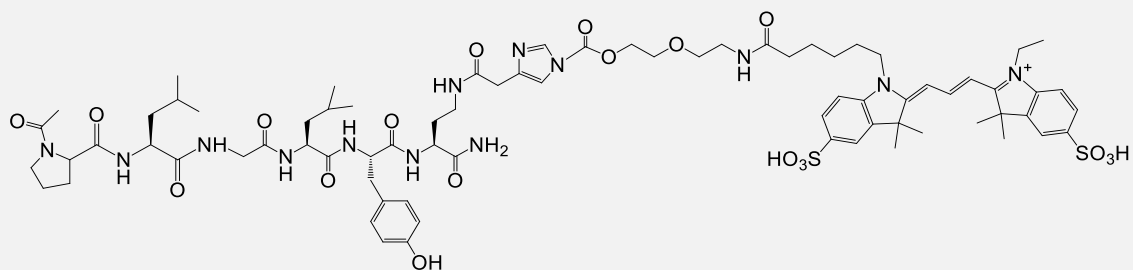
11



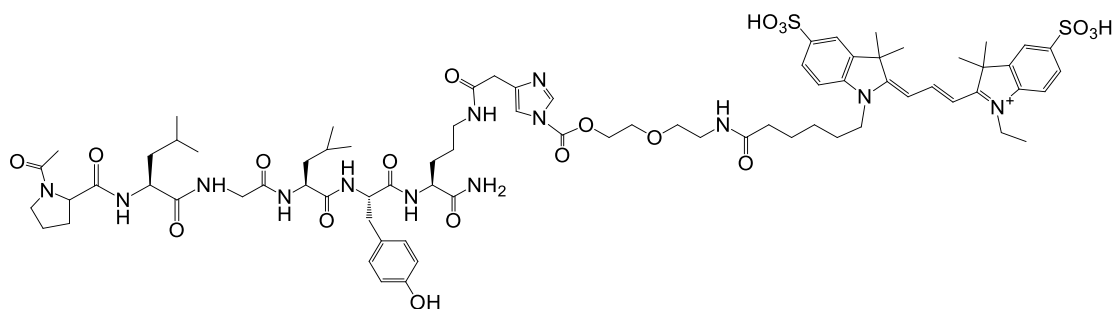
14



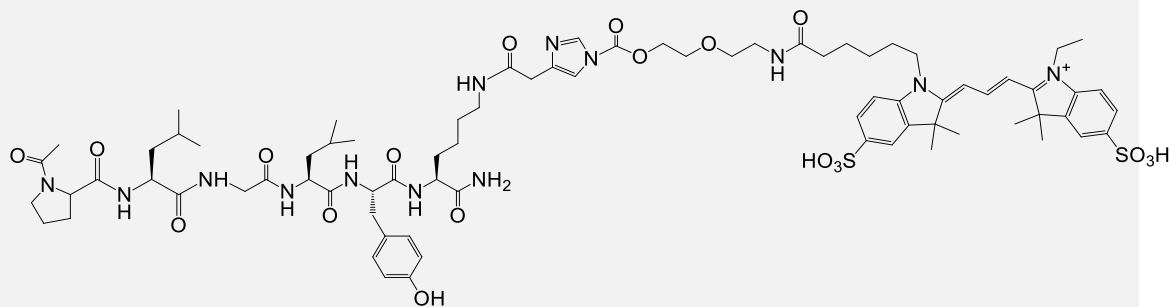
15



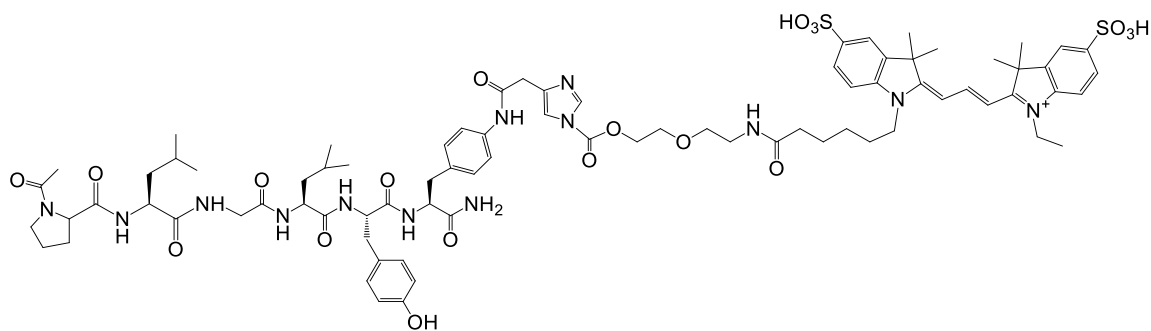
16



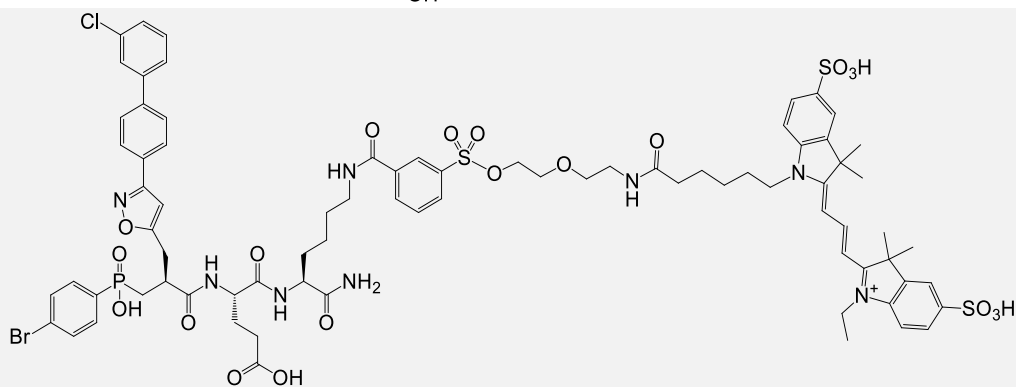
17



18



19



B. ARTICLE

Cite this: DOI: 10.1039/xxxxxxxxxxx

New Activity-Based Probes exploiting the acyl imidazole chemistry for the sensitive detection of Matrix Metallo-Proteinases [†]

 Monika Kaminska,^a Robert Thai,^a Fabrice Beau,^a Sarah Bregant,^a Evelyne Cassar-Lajeunesse,^a Andrzej Galat,^a Dimitris Georgiadis,^b Vincent Dive,^a and Laurent Devel^{**a}

Received Date

Accepted Date

DOI: 10.1039/xxxxxxxxxxx

www.rsc.org/journalname

Activity-based probes bind covalently to their target enzymes in a mechanism-based manner allowing unambiguous discrimination between the active enzyme and its inactive or inhibitor-bound counterparts. Since metalloproteases catalysis is non-covalent, activity-based probes that target them have been developed using reversible inhibitors decorated with photo-crosslinkers, that limit their scope to *ex vivo* use. By relying on a favorable structural context and by exploiting the acyl imidazole chemistry, we identify novel activity-based probes capable of covalently modifying matrix metalloproteases without making use of photo-activation. We have validated the ability of these chemical probes to selectively and efficiently label human macrophage elastase (hMMP-12) both *in vitro* and in complex proteomes. In the latter case, 10 ng of the metalloprotease, corresponding to 0.01% of the proteins content, can be labeled and detected. We have also determined the identity of the sole hMMP-12 residue covalently modified and verified that the modification has little impact on hMMP-12 proteolytic activity. We have extended this affinity-labeling approach to six other matrix metalloproteases and we believe that it may be effectively transferred more widely to other metalloprotease families and further to proteases for which the development of activity-based probes has remained problematic.

1 Introduction

Biological systems often respond to environmental modifications by regulating enzyme activity through a complex array of post translational mechanisms. This results in alterations of their abundance that does not necessarily correlate with changes in activity. Activity-based protein profiling has emerged as an attractive strategy to address this issue¹. In a typical profiling experiment, an activity-based probe (ABP) with an analytical handle reacts with an active site nucleophile forming a covalent complex with the enzyme-active fraction. This adduct can be subsequently distinguished from the unmodified inactive and inhibitor-bound fractions, but also from other proteins, through in-gel fluorescence analysis or affinity purification, followed by mass spectrometry. By targeting specific protein subsets, this chemical-

selection reports directly the enzyme functional status in complex proteomes.

Proteases have a wide range of biological functions, and changes in their activity underlie many disorders, including cancer and inflammatory diseases. These enzymes are subjected to numerous *in vivo* regulatory events, starting with their production as inactive zymogens and the latter inhibition by endogenous proteins². ABPs has been successfully developed for the profiling of serine and cysteine proteases in cells and whole animals³⁻⁶. All these probes contain an electrophilic “warhead” which reacts with the hydroxyl or thiol catalytic group. This approach is however not applicable to zinc-metalloproteinases, a family of 186 members in humans, which lack a targetable nucleophile involved in the catalysis. To target zinc-metalloproteinases, the ABPs must incorporate a photo cross-linking group, which under UV-irradiation, promotes the formation of a covalent bond⁷⁻¹⁸. Such photo-activatable probes have been successful for the detection of metalloproteinases including matrix-metalloproteases (MMPs) under their active forms in fluids and tissue extracts^{9,17}, but not in living animals where the photo-activation step is not feasible.

Among the very few approaches proposed to partly overcome the constraints associated to photoactivatable probes, activatable probes generating a highly reactive quinolimine methide have

^a Service d'Ingénierie Moléculaire des Protéines (SIMOPRO), CEA, Université Paris Saclay, F-91191 Gif/Yvette, France. Fax: +33 16908 9071; Tel: +33 16908 9565; E-mail: Laurent.DEVEL@cea.fr

^b Department of Chemistry, Laboratory of Organic Chemistry, University of Athens, Panepistimiopolis, Zografou, 15771, Athens.

[†] Electronic Supplementary Information (ESI) available: [Supplementary Figure S1 to S7, supplementary table 1, supplementary methods including synthetic protocol, scheme 1 and experimental details, Analytical data including NMR and LC/MS, and supplementary references]. See DOI: 10.1039/b000000x/

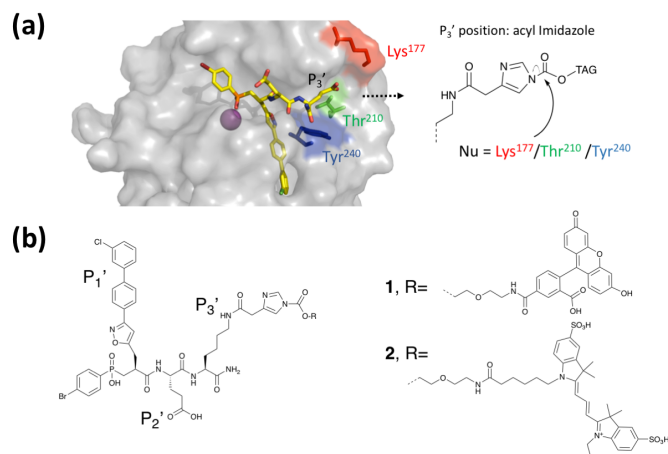


Fig. 1 Design of activity-based probe targeting hMMP-12. (a) Crystal structure of RXP470.1 in interaction with catalytic domain of human MMP-12 (PDB code: 4GQL), hMMP12 is represented as surface and RXP470.1 inhibitor as yellow sticks. The active site Zn^{2+} is shown as a magenta ball. The potential nucleophilic residues facing the P_3' position are shown as red, green and blue sticks for Lys¹⁷⁷, Thr²¹⁰ and Tyr²⁴⁰ respectively. The RXP470.1 P_3' position can be modified into an acyl imidazole moiety, (b) Chemical structure of probe **1** and **2**

been effective in targeting active-site nucleophiles of different protease classes including metalloproteases¹⁹. However, mainly due to their lack of selectivity, their use remained *ex vivo* restricted. Thiirane-based inhibitors were proposed to target the canonical catalytic glutamate in metalloproteases. If successful for metallo carboxypeptidases²⁰, these inhibitors failed to covalently modify MMPs²¹. ABPs possessing an α -chloroacetamide electrophile were used to assess the *in vivo* proteolytic activity of engineered MMPs containing a reactive cysteine²². Although this approach enables monitoring the activity of a single MMP, in cells and in Zebrafish, it depends on genetic manipulations, incompatible with native conditions.

Recently, an elegant affinity-labeling strategy for the covalent modification of native proteins has been reported^{23–25}. Here, a chemically sensitive spacer was introduced as a leaving group (Tosyl or Acyl imidazole reactive moiety) between the targeting ligand and the tag to be conjugated. After a probe binding step, the tag was transferred to the protein through a chemical reaction between a nucleophile close to the self-immolative spacer, resulting in the protein labeling and the concomitant release of the ligand.

Benefiting from a particularly well-defined structural context, with more than 150 crystal structures of MMPs catalytic domains in the protein data-bank, we proposed to assess the reactivity of nucleophiles within the MMPs catalytic cleft, through a proximity-driven reaction. Particularly, our probes design relied on the structure of human MMP-12 catalytic domain in complex with the phosphinic pseudo peptide (RXP470.1), a potent and highly selective competitive inhibitor of this protease^{26,27}. A detailed analysis of this structure revealed that the RXP470.1 P_3' glutamate faces three nucleophiles (Lys¹⁷⁷, Thr²¹⁰ and Tyr²⁴⁰) that could be potential anchoring points for chemical labeling (Fig. 1a). Based on these observations and considering that this P_3' glutamate

was not essential to maintain a favorable affinity-selectivity profile toward hMMP-12^{26,27}, we decided to conserve in the probes structure the P_1' and P_2' side chains and to modify only the P_3' residue. A lysine was chosen for its suitable length and flexibility to direct the self-immolative spacer towards the targeted nucleophile. Conjugated to the lysine ϵ -amino group, a reactive acyl imidazole spacer was selected since it had been described to exhibit faster kinetics and higher labeling efficiency than the tosyl group²⁴, with a preference for amino acids such as lysine, serine or tyrosine^{28–30}. Two fluorescent reporters were envisaged as tags for subsequent in-gel labeled-protein visualization: a fluorescein reporter in probe **1** and a cyanine 3 (Cy3) in probe **2** (Fig. 1b). Since RXP470.1 has been demonstrated to target MMP-12 in four different mouse models^{31–34}, it was also thought to be a good starting point for the development activity-based probes compatible with *in vivo* use.

In this study, we describe the evaluation of RXP470-derived ABPs to target hMMP-12 in media of increasing complexity. In the case of this enzyme, we show that only one nucleophilic residue is covalently modified within the active site S_3' region. We also report that a cyanine 3 moiety installed on a distal residue within this region only slightly impacts the catalytic efficiency of hMMP-12. Finally, we demonstrate that this chemical labeling can be further extended to six other matrix metalloproteases.

2 Results

2.1 hMMP-12 labeling and labeling site determination

After synthesis of the fluorescent probes **1** and **2** (ESI, synthetic procedure and Scheme S1), we first demonstrated that their bindings to hMMP-12 were not affected by the P_3' modification (ESI, Table S1). Their stability over time was examined in aqueous buffer (HEPES buffer, pH=7.5 at 37°C). Interestingly, the probes **1** and **2** displayed similar behavior with a half-life of 11 h and 16 h respectively (ESI, Figure S1 and S2). This hydrolysis rate was in accordance with previous reports for other acyl imidazole probes^{24,28}. This suggested that stability of such reagents was mainly governed by the intrinsic reactivity of the acyl imidazole moiety, with only a minor impact of the tag to which it was conjugated. We then investigated the reactivity of probe **1** (10 μ M) towards the recombinant catalytic domain of hMMP-12 (5 μ M) in HEPES buffer at 37°C. As shown by SDS-PAGE and fluorescence gel imaging, the labeling reaction proceeded in a time dependent manner with a covalent modification of hMMP-12 already detectable after one hour (Fig. 2a). After 24 h, a labeling yield of $47 \pm 2\%$ was determined by comparing the LC peak area of the labeled and unlabeled species at 214 and 280 nm. The yields at intermediate times (1 h, 2 h and 4 h) were then deduced from that at 24 h. The specificity of active site labeling was confirmed through competition experiments in presence of RXP470.1 at two different concentrations (25 μ M and 100 μ M). In these conditions and after 24 h, no significant labeling was observed, demonstrating that the labeling of hMMP-12 by probe **1** was effectively driven by ligand-protein recognition (Fig. 2b). As shown by analysis of the reaction mixture by LC/MS after 24 h (Fig. 2c), the labeled hMMP-12 displayed a multiple-charge ions

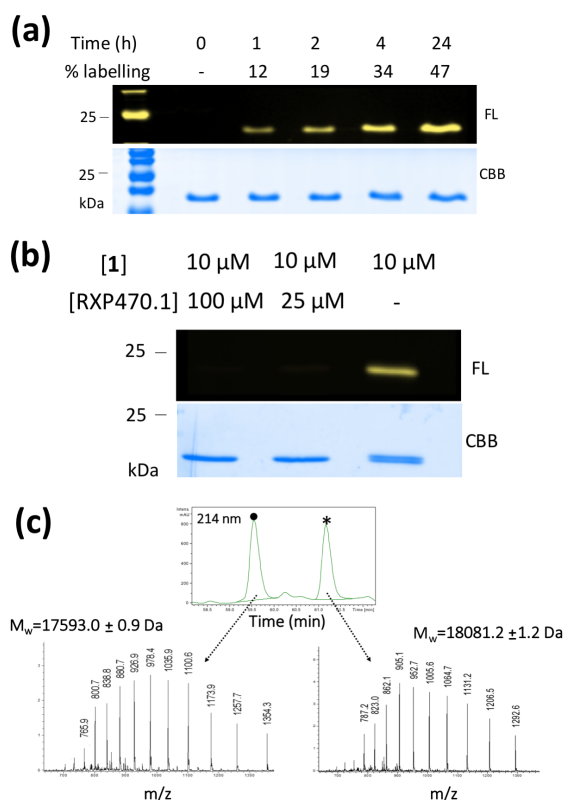


Fig. 2 hMMP-12 labelling by probe **1**. (a) In test tubes, hMMP-12 (5 μ M) was incubated with probe **1** (10 μ M) at 37°C in 20 mM HEPES buffer, pH=7.5, 5 mM CaCl₂, 200 mM NaCl, 0.1 mM ZnCl₂ and 0.1% Brij-35. Labeling efficiency was assayed at different time points (1 h, 2 h, 4 h and 24 h). Samples were subjected to 12% SDS-PAGE and analyzed by in-gel fluorescence imaging (FL) and Coomassie brilliant blue (CBB) staining. (b) In-gel fluorescence analysis of the labeling reaction after 24 h in presence of a competitive ligand RXP470.1 (25 μ M and 100 μ M) in the same conditions of buffer (pH=7.5), salts and temperature (37°C). (c) LC (214 nm) and MS (electrospray, positive mode of ionization) analysis of the labeled and unlabeled hMMP-12 in mixture after 24 h of reaction in the same conditions of buffer (pH=7.5), salts and temperature (37°C). The mass spectra are not deconvoluted *unlabeled hMMP-12 (M_w =17593.0 Da), *singly labeled hMMP-12 (M_w =18081.2 Da).

mass profile associated to a molecular weight of 18081.2 Da corresponding to 488.2 Da mass increment of unlabeled hMMP12 (17593.0 Da). This indicated that a single labeling of hMMP-12 has occurred in these conditions.

We next identified which amino acid residue had been covalently modified by probe **1**. After chymotryptic digestion of the labeled hMMP-12, the resulting digest was analyzed by LC/MS (Fig. 3a). Among the peptide fragments detected at 214 nm, only one absorbed at a wavelength specific of fluorescein (450 nm), suggesting that a single fragment within the S₃' region had been labeled. The MALDI-TOF MS/MS sequencing of this fragment allowed the identification of Lys¹⁷⁷ as covalently modified residue (Fig. 3b). This highly selective labeling was in accordance with those previously reported for an acyl imidazole motif displaying a lysine preference^{24,29,35}. The absence of labeling on Thr²¹⁰ and Tyr²⁴⁰ might be due to the nature of the P₃' side chain of the probe **1**

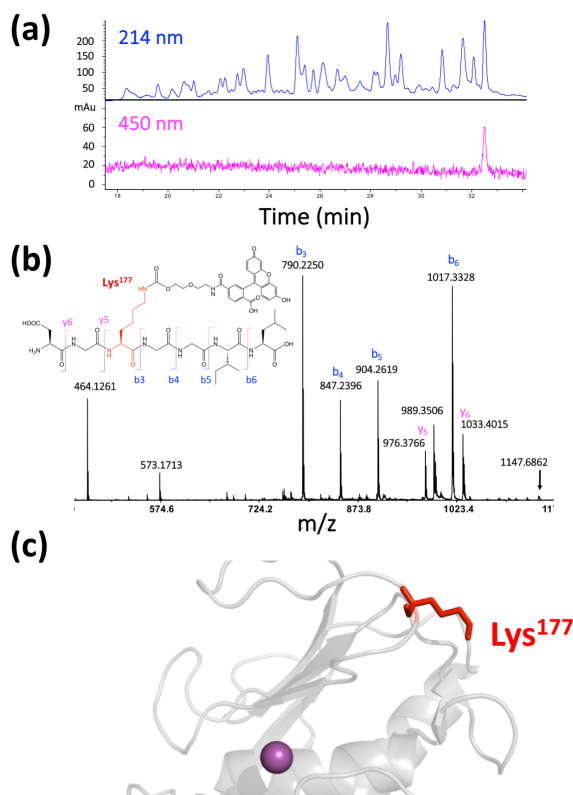


Fig. 3 Identification of the labeling site by LC/MS and MS/MS sequencing. (a) Chromatogram of the chymotrypsin digest of hMMP-12 labeled with probe **1** (24 h of labeling). The UV detection was performed at 214 nm and at 450 nm. (b) MS/MS analysis by MALDI-ToF of the fragment modified by the fluorescein tag. (c) Lys¹⁷⁷ was highlighted in red within the hMMP-12 catalytic domain in cartoon representation (PDB code: 4GQL)

that induced a favorable orientation of the reactive acyl imidazole towards the Lys¹⁷⁷. Overall, these results validate our probe design with an exclusive labeling in the S₃' region.

2.2 hMMP-12 labeling in complex proteomes

The hMMP-12 labeling capacity of probe **1** was first investigated with increasing concentrations of human serum albumin (ESI, Figure S3). Remarkably, although partly consumed through a reaction with serum albumin, this probe conserved its labeling efficiency towards hMMP-12, even when the protease concentration was as low as 5 μ M and that of serum albumin was 500 μ M. In this case, the unspecific labeling component can be partly explained by a significant propensity of the RXP470-targeting moiety to bind serum albumin³⁶. To further explore the probes selectivity in systems of higher proteins complexity, we then focused on probe **2** that allowed detecting labeled hMMP-12 with a better sensitivity than probe **1** through in-gel fluorescent visualization (ESI, Figure S4). We first demonstrated that probe **2** (10 μ M) reacted with hMMP-12 catalytic domain (5 μ M) in a time dependent manner, with a labeling efficiency of 48±1% after 24h, comparable to that of probe **1** (ESI, Figure S5a). Importantly, in shorter time (4 h) when hMMP-12 concentration was decreased

to 100 nM, the labeling efficiency of probe **2** (1 μ M and 100 nM) was maintained and the labeling yields were not substantially impacted (ESI, Figure S5b).

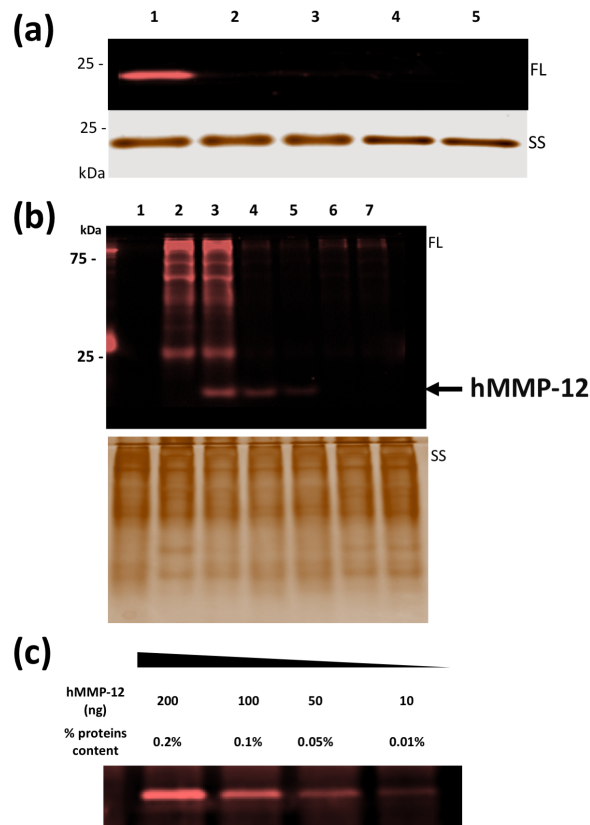


Fig. 4 hMMP-12 labeling by probe **2** in test tube and in mouse liver extract. (a) In-gel fluorescence analysis of the labeling reaction of hMMP-12 (100 nM) with probe **2** (100 nM) in reaction buffer after 4h at 37°C (Lane 1). The reaction specificity was assessed by pre-incubating hMMP-12 (100 nM) with competitive inhibitors at 1 μ M; hMMP-12 selective inhibitor (RXP470.1, lane 2), broad-spectrum phosphinic pseudo peptide (RXP500.1, lane 3), a hydroxamate derivative (GM6001, lane 4) and hTIMP-1 (lane 5). The samples were subjected to 12% SDS-PAGE and analyzed by in-gel fluorescence imaging (FL) and silver staining (SS). (b) In-gel fluorescence analysis of the labeling reaction of hMMP-12 (200 ng) by probe **2** in mouse liver extract (100 μ g) after 4 h at 37°C, the samples were subjected to 12% SDS-PAGE and analyzed by in-gel fluorescence imaging (FL) and silver staining (SS): lane 1 DMSO, lane 2 no hMMP-12 and 1 μ M of probe **2**, lane 3 probe **2** at 1 μ M, lane 4 probe **2** at 100 nM, lane 5 probe **2** at 50 nM, lane 6 pre-incubation with RXP470.1 (1 μ M) followed by probe **2** at 100 nM, lane 7 pre-incubation with GM6001 (1 μ M) followed by probe **2** at 100 nM. (c) In-gel fluorescence analysis of the labeling reaction of hMMP-12 (200, 100, 50 and 10 ng) by probe **2** in mouse liver extract (100 μ g) after 4 h at 37°C in reaction buffer.

As in the case of probe **1**, the Lys¹⁷⁷ was the sole residues targeted within the S₃' region (ESI, Figure S5c). In these conditions of hMMP-12 concentration (100 nM), we first showed that probe **2** (100 nM) only targeted the active forms of MMP-12 and no labeling was observed when the active site was occluded by either a MMP-12 selective (RXP470.1, lane 2) and broad spectrum (RXP500.1 and GM6001, lane 3 and 4 respectively) synthetic inhibitors or by a natural inhibitor hTIMP-1 (Tissue inhibitor of ma-

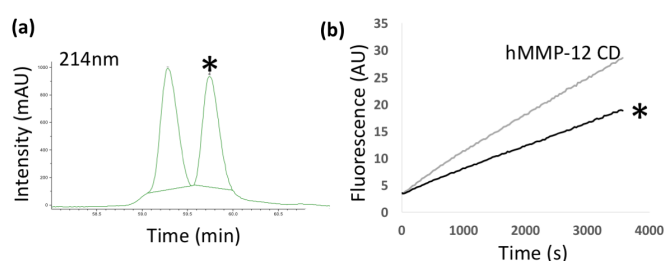


Fig. 5 Evaluation of the proteolytic activity of Cy3-labeled hMMP-12 (a) After 24 h, unlabeled and Cy3-labeled hMMP-12 (*) were separated in the following conditions: X Bridge BEH300 column (21 \times 150 mm, 3.5 μ m, Waters), flow rate = 0.2 mL.min⁻¹, initial conditions: 5% B, 0 to 5 min: 5% B, 5 to 10 min: 20%, 10 to 65 min: 55%, 65 to 67 min: 100% B with A: H₂O/TFA 0.1% and B: CH₃CN 90%/H₂O 10%/ TFA 0.09%, UV detection was performed at 214 nm. (b) The proteolytic activity was assessed through a continuous kinetic assay by recording the fluorescence increase induced by the cleavage of Mca-Pro-Leu-Gly-Leu-Dpa-Ala-Arg-NH₂ substrate (9 μ M) for 60 min in 50 mM Tris-HCl buffer, pH = 6.8, 10 mM CaCl₂ at 25°C

trix metalloproteases, lane 5) at 1 μ M (Fig. 4a). We next examined whether probe **2** could detect active hMMP-12 (100 nM, 0.2 μ g) spiked in a mouse liver extract (100 μ g). The probe was used at different concentrations (1 μ M, 100 nM and 50 nM) with hMMP-12 corresponding to 0.2% of the whole proteome in this case. Although a non-specific labeling of abundant proteins was observed, hMMP-12 was also labeled by probe **2** (Fig. 4b, lane 2 and 3). More importantly, the unspecific component reduced while probe **2** concentration decreased, with a highly selective labeling observed when the probe was used at 50 nM (Fig. 4b, lane 5). In addition, pre-incubation of samples with inhibitors prevented the hMMP-12 labeling (Fig. 4b, lane 6 and 7), thus confirming that a free protease active site is required for installing a covalent tag. Finally, the sensitivity of probe **2** was examined by incubating this reagent at 100 nM with a serial dilution of hMMP-12 (200, 100, 20 and 10 ng) added to 100 μ g of liver extract. As shown in Fig. 4c, probe **2** was able to label and detect active MMP-12 at level as low as 10 ng. This quantity of active MMP, corresponds to 0.01% of proteins content (5 nM) matching the fluorescent detection limit achieved with photo labile probes⁷.

2.3 Proteolytic activity of labeled hMMP-12

The impact of the chemical modification of hMMP-12 on its proteolytic efficiency was evaluated. The Cy3-labeled hMMP-12 was first separated from the unlabeled one under acidic LC conditions (Fig. 5a). Once isolated, the concentration of Cy3-hMMP-12 was measured by UV using the extinction coefficient of Cy3 (150 000 M⁻¹ cm⁻¹) and diluted to 1 nM in activity buffer. After 1 h incubation at 4°C, its proteolytic activity was assessed at 25°C using a synthetic substrate. As shown in Fig. 5b, the Cy3-labeled hMMP-12 cleaved the fluorogenic substrate Mca-Pro-Leu-Gly-Leu-Dpa-Ala-Arg-NH₂ with a slightly lower catalytic efficiency compared to hMMP-12. We also verified that this protocol of acidic purification followed by incubation in activity buffer, did not impact the proteolytic activity of unlabeled hMMP-12 (data not shown). Any loss of activity observed for Cy3-labeled hMMP-12 could be

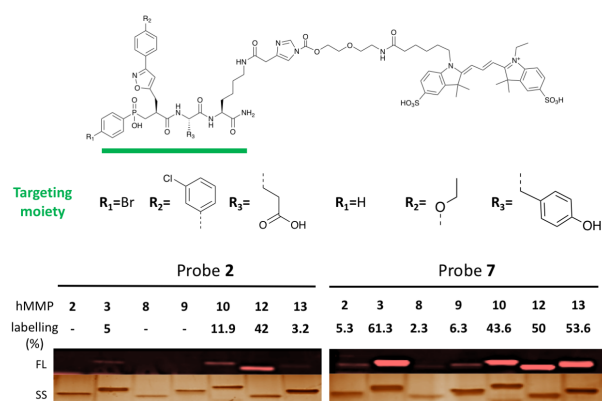


Fig. 6 Evaluation of hMMPs chemical labeling by probe **2** and **7**. The probes share a common scaffold and only the targeting moiety underlined in green is modified (a) In test tubes, hMMP-2/3/8/9/10/12 or 13 (100 nM) were incubated with probe **2** (100 nM) in HEPES buffer, pH=7.5, 5 mM CaCl₂, 200 mM NaCl, 0.1 mM ZnCl₂ and 0.1% Brij-35. After 4h at 25°C, the samples were subjected to 12% SDS-PAGE and analyzed by in gel fluorescence imaging (FL) and silver staining (SS). (b) hMMP-2/3/8/9/10/12 or 13 (100 nM) were incubated with probe **7** (100 nM) in the same conditions of buffer (pH=7,5) and temperature (25°C) and analyzed after 4h in the conditions described above. For each MMP, the yield of labeling was determined relatively to that of MMP-12.

thus assigned to bulky hydrophobic cyanine 3 grafted on the distal Lys¹⁷⁷ that may affect both the substrate binding and the protease turnover. Overall, the labeled hMMP-12 remained 60% active compared to the unlabeled one.

2.4 Chemical labeling of other hMMPs

With the exception of their S₁' subsite, MMPs are structurally highly homologous in their catalytic domains³⁷. In this respect, a detailed analysis of the hMMP-2/3/8/9/10 and 13 S₃' region showed that these proteases displayed potential nucleophiles in positions comparable to those found in hMMP-12 (ESI, Figure S6). Based on these observations, we first assessed the capacity of probe **2** to react with six other hMMPs in the conditions used for hMMP-12. As shown in Fig. 6, after 4 h, probe **2** modified hMMP-12 in a privileged manner but also reacted with hMMP-3, 10 and 13. When probe **2** was used in higher concentrations (1 μM), a labeling of these three proteases was detected within 1 h and the labeling yield significantly increased when the reaction time was prolonged to 4 h (ESI, Figure S7). This first confirmed that probe **2** at low concentration was selective for hMMP-12, an observation in accordance with the affinity constants determined for this probe towards a set of MMPs (ESI, Table S1) but also suggested that nucleophilic residues were accessible for covalent modifications within S₃' region of other hMMPs.

This led us to envisage second generation probes that would enable the efficient labeling of a larger set of MMPs. Particularly, since the labeling efficiency is in part governed by the residence time of the ligand within the active site, we improved the probe binding constant towards MMP-2/3/8/9/10 and 13 by changing the targeting moiety. We previously demonstrated in phosphinic pseudo peptide series that a 3-(4-ethoxyphenyl) isoxazole

P1' side chain yielded a potent and pan-inhibitor of MMPs¹⁴. By relying on this scaffold, probe **7** was synthesized (ESI for synthetic details, Scheme S1) and its affinity and selectivity profile determined on a set of seven hMMPs. First, we showed that, by comparison with probe **2**, its potency was improved for all tested hMMPs with an affinity gain ranging from a factor 2 in the case of hMMP-10 to 710-fold for hMMP-9 (ESI, Table S1). As illustrated in (Fig. 6), after 4 h, probe **7** (100 nM) was able to covalently modified the seven tested hMMPs with substantial labeling of hMMP-3/10/12/13 and a faint but detectable labeling of hMMP-2/8 and 9. The modest labeling observed on hMMP-2 and 9 was rather unexpected since probe **7** affinity constant towards these two proteases was substantially improved compared to that of probe **2** (ESI, Table S1). This was even more surprising considering the presence within the hMMP-2 and 9 S₃' region of a lysine in a comparable position to that of Lys¹⁷⁷ in hMMP-12 (ESI, Figure S6a). Overall, by only changing the phosphinic peptide moiety, the probe selectivity profile was significantly modified and probe **7** proved effective for the labeling of seven hMMPs. This constitutes to our knowledge the first example of ligand-directed acyl imidazole chemistry validated in the context of selectivity within a family whose members are structurally very close.

3 Discussion

By relying on the acyl imidazole chemistry²⁴ and by exploiting the crystal structure of a phosphinic inhibitor (RXP470.1) in interaction with its target (hMMP-12), we demonstrated that it was possible to design activity-based probes able to label MMPs covalently without need for photo activation. Our RXP470-derived probes harboring a reactive acyl imidazole in their P₃' position were validated, with a single and unambiguous labeling on Lys¹⁷⁷ within the MMP-12 S₃' region. The two active-site-directed probes only target functional states of hMMP-12 and spare forms whose active site is occluded either by synthetic inhibitors or natural hTIMP-1. Importantly, the capacity of probe **2** to target active forms of hMMP-12 was demonstrated in complex proteomes such as mouse liver extract. In this case, down to 10 ng of active hMMP-12 catalytic domain corresponding to 0.01 % of total proteins content, can be efficiently detected by in-gel fluorescence analysis. In addition to a sensitivity limit compatible with the profiling of low abundance proteins in complex proteomes, probe **2** turns out highly selective for its privileged target.

We demonstrated that this affinity-labeling method can be extended to further MMPs. As illustrated by the change in the labeling profile between probe **2** and **7**, by increasing the ligand binding capacity to its targets, the labeling efficacy can be significantly improved. Nevertheless, prolonging the probes residence time within the active-site does not ensure an efficient labeling for all MMPs members and other parameters have to be taken into account. This is first illustrated by the modest reactivity of probe **7** with high affinity towards hMMP-2 and 9 (ESI, Table S1). Here, despite a lysine in a comparable position to hMMP-12 Lys¹⁷⁷ (ESI, Figure S6b), the lack of reactivity may be explained by the presence of an adjacent acid aspartic with a negative charge stabilizing the lysine under its protonated state thus decreasing its intrinsic reactivity at pH=7.5. Regarding the differential reactiv-

ity of nucleophiles within the S₃' sub-site, the results obtained on hMMP-3 and 8 are particularly informative. Indeed, these MMPs possess two potential nucleophiles in this region, two tyrosine in the case of hMMP-8 and a threonine and a tyrosine for MMP-3 both in comparable positions (ESI, Figure 6a), and only hMMP-3 displays a significant reactivity towards probe 2 and 7. This suggests on the one hand that the hMMP-3 threonine is more reactive than the tyrosine in the same position in MMP-8. On the other hand, the canonical tyrosine found in almost all MMPs (ESI, Figure 6b) is not accessible for chemical modification with the probe that we designed. Thus, in addition to intrinsic nucleophile reactivity that may vary in function of local environment, other parameters are at play including distance and orientation between the two reactive partners as well as their relative dynamics. Although the dynamics are rather difficult to anticipate, a favorable orientation of the acyl imidazole moiety towards its target nucleophiles can be achieved by optimizing the length and flexibility of the linker. Such an impact of linkers on labeling efficiency was previously documented by Hamachi and collaborators²⁸. In this respect, considering the subtle differences existing within the MMPs S₃' region, finely tuning the linker nature may allow for either selective or pan-reactive probes. This latter ones should be accessible by targeting the canonical tyrosine equivalent to Tyr²⁴⁰ found in hMMP-12 S₃' region (ESI, Figure 6b).

By developing the first “photo activation-free” strategy to covalently modify active forms of MMPs, the unresolved proteomic profiling of native MMPs should be now accessible both in complex proteomes and *in vivo*. Particularly, we believe that RXP470-derived ABPs might be useful to study the complex cell compartmentalization of active MMP-12 which can either localize at the surface³⁸ or translocate to the nucleus^{31,39}. Thus, such probes with a negative net charge would target favorably the extra cellular portion of MMP12, a capacity validated for RXP470-derived tracers with comparable targeting pattern³⁶. Furthermore, as the labeling moderately impacts the MMP-12 proteolytic activity, by replacing the cyanine 3 tag by a fluorophore sensitive to environment variations, both the internalization and trafficking of native MMP-12 might be subsequently monitored³⁹. Our study also enables envisaging the development of novel quenched probes for monitoring MMPs activity *in vivo*, similar to those previously reported for cysteine and serine proteases. By employing appropriate targeting moieties and using the acyl imidazole chemistry, we believe that the scope of this method can be expanded to other metalloproteases but also to proteases without any canonical nucleophiles within their active site such as aspartic proteases.

References

- 1 M. J. Evans and B. F. Cravatt, *Chemical reviews*, 2006, **106**, 3279–3301.
- 2 B. Turk, D. Turk and V. Turk, *The EMBO journal*, 2012, **31**, 1630–1643.
- 3 E. Deu, M. Verdoes and M. Bogyo, *Nature structural & molecular biology*, 2012, **19**, 9–16.
- 4 S. Serim, U. Haedke and S. H. Verhelst, *ChemMedChem*, 2012, **7**, 1146–1159.
- 5 L. I. Willems, H. S. Overkleeft and S. I. van Kasteren, *Bioconjugate chemistry*, 2014, **25**, 1181–1191.
- 6 M. Verdoes and S. H. Verhelst, *Biochimica et Biophysica Acta (BBA)-Proteins and Proteomics*, 2016, **1864**, 130–142.
- 7 A. Saghatelian, N. Jessani, A. Joseph, M. Humphrey and B. F. Cravatt, *Proceedings of the National Academy of Sciences of the United States of America*, 2004, **101**, 10000–10005.
- 8 E. W. Chan, S. Chattopadhyaya, R. C. Panicker, X. Huang and S. Q. Yao, *Journal of the American Chemical Society*, 2004, **126**, 14435–14446.
- 9 S. A. Sieber, S. Niessen, H. S. Hoover and B. F. Cravatt, *Nature chemical biology*, 2006, **2**, 274–281.
- 10 A. David, D. Steer, S. Bregant, L. Devel, A. Makaritis, F. Beau, A. Yiotakis and V. Dive, *Angewandte Chemie International Edition*, 2007, **46**, 3275–3277.
- 11 P. Geurink, T. Klein, M. Leeuwenburgh, G. van der Marel, H. Kauffman, R. Bischoff and H. Overkleeft, *Organic & biomolecular chemistry*, 2008, **6**, 1244–1250.
- 12 A.-S. Dabert-Gay, B. Czarny, L. Devel, F. Beau, E. Lajeunesse, S. Bregant, R. Thai, A. Yiotakis and V. Dive, *Journal of Biological Chemistry*, 2008, **283**, 31058–31067.
- 13 A.-S. Dabert-Gay, B. Czarny, E. Lajeunesse, R. Thai, H. Nagase and V. Dive, *Bioconjugate chemistry*, 2009, **20**, 367–375.
- 14 S. Bregant, C. Huillet, L. Devel, A.-S. Dabert-Gay, F. Beau, R. Thai, B. Czarny, A. Yiotakis and V. Dive, *Journal of proteome research*, 2009, **8**, 2484–2494.
- 15 J. Lenger, F. Kaschani, T. Lenz, C. Dalhoff, J. G. Villamor, H. Köster, N. Sewald and R. A. van der Hoorn, *Bioorganic & medicinal chemistry*, 2012, **20**, 592–596.
- 16 C. Nury, B. Czarny, E. Cassar-Lajeunesse, D. Georgiadis, S. Bregant and V. Dive, *Chembiochem*, 2013, **14**, 107–114.
- 17 C. Nury, S. Bregant, B. Czarny, F. Berthon, E. Cassar-Lajeunesse and V. Dive, *Journal of Biological Chemistry*, 2013, **288**, 5636–5644.
- 18 L. Prely, T. Klein, P. P. Geurink, K. Paal, H. S. Overkleeft and R. Bischoff, *Activity-Based Proteomics: Methods and Protocols*, 2017, 103–111.
- 19 Q. Zhu, A. Girish, S. Chattopadhyaya and S. Q. Yao, *Chemical Communications*, 2004, 1512–1513.
- 20 S. A. Testero, C. Granados, D. Fernaldez, P. Gallego, G. Covalada, D. Reverter, J. Vendrell, F. X. AvileÀs, I. PallareÀs and S. Mobashery, *ACS Medicinal Chemistry Letters*, 2017, **8**, 1122–1127.
- 21 C. Forbes, Q. Shi, J. F. Fisher, M. Lee, D. Heseck, L. I. Llarrull, M. Toth, M. Gossing, R. Fridman and S. Mobashery, *Chemical biology & drug design*, 2009, **74**, 527–534.
- 22 M. Morell, T. Nguyen Duc, A. L. Willis, S. Syed, J. Lee, E. Deu, Y. Deng, J. Xiao, B. E. Turk, J. R. Jessen *et al.*, *Journal of the American Chemical Society*, 2013, **135**, 9139–9148.
- 23 S. Tsukiji, M. Miyagawa, Y. Takaoka, T. Tamura and I. Hamachi, *Nature chemical biology*, 2009, **5**, 341–343.
- 24 S.-h. Fujishima, R. Yasui, T. Miki, A. Ojida and I. Hamachi, *Journal of the American Chemical Society*, 2012, **134**, 3961–3964.

- 25 Y. Takaoka, A. Ojida and I. Hamachi, *Angewandte Chemie International Edition*, 2013, **52**, 4088–4106.
- 26 L. Devel, V. Rogakos, A. David, A. Makaritis, F. Beau, P. Cuni-asse, A. Yiotakis and V. Dive, *Journal of Biological Chemistry*, 2006, **281**, 11152–11160.
- 27 B. Czarny, E. A. Stura, L. Devel, L. Vera, E. Cassar-Lajeunesse, F. Beau, V. Calderone, M. Fragai, C. Luchinat and V. Dive, *Journal of medicinal chemistry*, 2013, **56**, 1149–1159.
- 28 K. Matsuo, Y. Kioi, R. Yasui, Y. Takaoka, T. Miki, S.-h. Fujishima and I. Hamachi, *Chemical Science*, 2013, **4**, 2573–2580.
- 29 T. Miki, S.-h. Fujishima, K. Komatsu, K. Kuwata, S. Kiyonaka and I. Hamachi, *Chemistry & biology*, 2014, **21**, 1013–1022.
- 30 S. Wakayama, S. Kiyonaka, I. Arai, W. Kakegawa, S. Matsuda, K. Ibata, Y. L. Nemoto, A. Kusumi, M. Yuzaki and I. Hamachi, *Nature Communications*, 2017, **8**, year.
- 31 D. J. Marchant, C. L. Bellac, T. J. Moraes, S. J. Wadsworth, A. Dufour, G. S. Butler, L. M. Bilawchuk, R. G. Hendry, A. G. Robertson, C. T. Cheung *et al.*, *Nature medicine*, 2014, **20**, 493–502.
- 32 J. L. Johnson, L. Devel, B. Czarny, S. J. George, C. L. Jackson, V. Rogakos, F. Beau, A. Yiotakis, A. C. Newby and V. Dive, *Arteriosclerosis, thrombosis, and vascular biology*, 2011, **31**, 528–535.
- 33 N. H. Lim, E. Meinjohanns, G. Bou-Gharios, L. L. Gompels, E. Nuti, A. Rossello, L. Devel, V. Dive, M. Meldal and H. Nagase, *Arthritis & Rheumatology*, 2014, **66**, 589–598.
- 34 R. P. Iyer, N. L. Patterson, F. A. Zouein, Y. Ma, V. Dive, L. E. de Castro Brás and M. L. Lindsey, *International journal of cardiology*, 2015, **185**, 198–208.
- 35 K. Yamaura, S. Kiyonaka, T. Numata, R. Inoue and I. Hamachi, *Nature Chemical Biology*, 2016.
- 36 T. Bordenave, M. Helle, F. Beau, D. Georgiadis, L. Tepshi, M. Bernes, Y. Ye, L. Levenez, E. Poquet, H. Nozach *et al.*, *Bioconjugate chemistry*, 2016, **27**, 2407–2417.
- 37 L. Devel, B. Czarny, F. Beau, D. Georgiadis, E. Stura and V. Dive, *Biochimie*, 2010, **92**, 1501–1508.
- 38 A. Cobos-Correa, J. B. Trojanek, S. Diemer, M. A. Mall and C. Schultz, *Nature chemical biology*, 2009, **5**, 628–630.
- 39 R. K. Koppiseti, Y. G. Fulcher, A. Jurkevich, S. H. Prior, J. Xu, M. Lenoir, M. Overduin and S. R. Van Doren, *Nature communications*, 2014, **5**, 5552.

Résumé

Les Métallo Protéases Matricielles (MMP) en tant qu'endopeptidases à zinc ont une large gamme de fonctions biologiques allant du remodelage tissulaire à la modulation de la réponse cellulaire. Une modification de leur activité protéolytique est souvent associée à de nombreux désordres biologiques. In vivo, ces protéases sont soumises à de nombreuses modifications post-traductionnelles afin d'éviter des activités protéolytiques anarchiques pouvant conduire à la destruction des tissus. Ainsi, Elles sont sécrétées sous formes latentes à l'extérieur des cellules pour être ensuite transformées en leur forme fonctionnelles. Ces dernières sont ensuite inhibées par des inhibiteurs endogènes. En raison de leur sécrétion dans l'espace extra cellulaire, les MMP sous formes actives ont longtemps été considérées comme de simples ciseaux moléculaires capable de dégrader uniquement les composants de la matrice extracellulaire. Cependant, le remodelage tissulaire ne constitue pas la fonction unique et encore moins la fonction principale de ces enzymes. Elles peuvent en effet cliver une grande variété de substrats non matriciels et à ce titre sont impliquées dans la régulation de multiples aspects de la progression tumorale, de l'immunité et de l'inflammation. Pour ajouter une complexité supplémentaire à la biologie des MMP, il a été récemment rapporté que certains membres de la famille avaient une localisation intracellulaire associée à des fonctions non protéolytiques. Ces observations, mais aussi celles montrant que certaines MMP participent à la progression de la maladie alors que d'autres ont une fonction protectrice, soulignent la nécessité de mieux documenter leur activation spatiale et temporelle dans divers contextes biologiques.

Le profilage protéique basé sur l'activité vise à analyser l'état fonctionnel des protéines dans des échantillons biologiques complexes. À cette fin, des sondes basées sur l'activité (ABP), qui réagissent avec les enzymes en s'appuyant sur leur mécanisme catalytique, ont été développées avec succès pour la détection d'enzymes sous formes actives, notamment dans le cas des protéases à sérine et à cystéine. Une sonde basée sur l'activité (ABP) est classiquement composée : I) d'un groupement réactif conduisant à la modification covalente de résidus au sein du site actif de l'enzyme, II) d'un motif de liaison imposant la sélectivité au groupement réactif et III) d'un groupement rapporteur permettant la détection des enzymes modifiées. Cette approche ne s'applique toutefois pas aux MMP, pour lesquelles il n'existe pas de résidus nucléophiles conservé au sein du site actif. À cet égard, tous les ABP ciblant les MMP comportent un groupement photo activable qui, sous irradiation UV, favorise la formation du complexe covalent. De telles sondes photo sensibles ont permis de détecter les MMP sous leurs formes actives dans les extraits de tissus et de fluides, mais pas chez les animaux vivants au sein desquels l'étape de photo-activation ne peut être réalisé.

Dans ce contexte, en nous appuyant sur un contexte structural favorable et en exploitant la chimie de l'acyl imidazole (LDAI) dirigée par un ligand, nous avons identifié une nouvelle série de sondes basées sur l'activité capables de modifier de manière covalente les MMP sans recourir à la photo-activation. Nous avons ainsi validé la capacité de ces sondes à marquer de manière sélective et efficace la MMP12 humaine *in vitro* et dans des protéomes complexes. Dans ce dernier cas, jusqu'à 50ng de hMMP12 correspondant à 0,05% du protéome total peuvent être efficacement marqués et détectés. Nous avons également déterminé l'identité de l'unique résidu modifié de façon covalente au sein du site actif de la hMMP-12 et vérifié que cette modification avait peu d'impact sur l'activité protéolytique de cette dernière. Nous avons démontré que cette approche permettait de détecter des MMP endogènes sécrétées par les macrophages stimulés. Enfin, nous avons étendu cette stratégie de marquage à un panel plus large de MMP.

En développant la première stratégie de marquage des formes actives de MMP «sans photo-activation», il semble maintenant possible d'envisager la détection de ces enzymes à la fois dans les protéomes complexes et dans des modèles précliniques dans lesquels les MMP peuvent constituer des cibles thérapeutiques pertinentes.

Abstract

Matrix MetalloProteases (MMPs) as zinc endopeptidases have a wide range of biological functions, and changes in their proteolytic activity underlie many biological disorders. Since their proteolytic activity has to be tightly controlled to prevent tissue destruction, these proteases are subjected to numerous posttranslational modifications *in vivo*. Thus, they are secreted under latent forms outside of the cells, and are subsequently processed into their functional form that can be further inhibited by endogenous inhibitors. Due to their delineated area of activation, MMP active forms have long been considered for their unique ability to degrade extracellular substrates. However, turnover and breakdown of the extracellular matrix are neither the sole nor the main function of MMPs. These enzymes can indeed process a wide variety of non-matrix substrates and are involved in the regulation of multiple aspects of tumor progression, immunity and inflammation. To add further complexity to MMPs biology, some members within the family were recently reported to have intracellular localization associated to non-proteolytic functions. These observations but also those evidencing that some MMPs participate in disease progression while others have a protective function, stress the need to better document their spatial and temporal activation in various biological contexts.

Activity-based protein profiling (ABPP) aims to analyze the functional state of proteins within complex biological samples. To this purpose, activity-based probes (ABPs) that react with enzymes in a mechanism-based manner have been successfully developed for the profiling of several enzymes including serine and cysteine proteases. A typical Activity-Based probe (ABP) is composed of I) a reactive warhead, which reacts in a covalent manner with enzyme active site residues, II) a targeting moiety that imposes selectivity upon the reactive group and III) a detectable group for subsequent analyses. This approach is however not applicable to MMPs, which lack a targetable nucleophile involved in the catalysis. In this respect, all ABPs directed to MMPs are affinity-based probes (AfBPs) containing within their structure a photo cross-linking group that promotes the formation of a covalent complex upon UV-irradiation. Such photoactivatable probes have been successfully developed for the detection of MMPs under their active forms in fluids and tissue extracts, but not in living animals where the photo-activation step is not feasible.

By relying on a favorable structural context and by exploiting the ligand-directed acyl imidazole (LDAI) chemistry, we have identified a novel series of AfBPs capable of covalently modifying matrix metalloproteases without making use of photo-activation. These active-site-directed probes whose structure was derived from that of a MMP12 selective inhibitor harbored a reactive acyl imidazole in their P3' position. Thus, they demonstrated their labelling specificity *in vitro* by covalently modifying a

single Lysine residue within the MMP-12 S₃' region. We also showed that these probes only targeted functional states of hMMP-12 and spared forms whose active site was occluded either by a synthetic or a natural inhibitor. We have validated the ability of these chemical probes to efficiently label human MMP12 in complex proteomes. In this case, down to 50 ng of hMMP12 corresponding to 0.05% of the whole proteome can be labelled and detected by in-gel fluorescence analysis. Importantly, we demonstrated that this approach also allowed detecting endogenous MMPs secreted by stimulated-macrophages. In addition, by modifying the nature of the targeting moiety, we have extended this affinity-labeling approach to six other MMPs.

By developing the first “photo activation-free” strategy to covalently modify active forms of MMPs, the unresolved proteomic profiling of native MMPs should be now accessible both in complex proteomes and in preclinical model in which MMPs are potential relevant targets.

Titre : Nouvelles sondes d'affinité pour la détection de metallo proteases de la matrice.

Mots clés : metallo protéase, sonde d'affinité, marquage covalent.

Résumé : Les sondes d'activité sont des petites molécules chimiques se liant de manière covalente au sein du site actif de leur cible enzymatique, permettant ainsi de différencier l'enzyme sous forme active de ses homologues inactifs ou en interaction avec des inhibiteurs. Dans le cas des métalloprotéases qui ne possèdent pas de résidus nucléophiles réactifs au sein de leur site actif, l'ensemble des sondes d'activité développées à ce jour contiennent des groupements photoactivables, limitant leur portée à une utilisation ex vivo.

En s'appuyant sur un contexte structural favorable et en exploitant la chimie acylimidazole, nous avons développé de nouvelles sondes capables de modifier de manière covalente les métalloprotéases matricielles sans utiliser la photo-activation.

Cette approche s'appuie sur une réaction chimique entre la sonde et sa cible et plus

particulièrement entre un nucléophile à la surface de l'enzyme et le motif acylimidazole à proximité.

Nous avons validé la capacité de ces sondes chimiques à marquer sélectivement et efficacement la macrophage élastase humaine (hMMP-12) à la fois in vitro et dans des protéomes complexes. Nous avons également montré que cette stratégie permettait de détecter des formes endogènes. Enfin, nous avons étendu cette approche de marquage par affinité à six autres MMP en modifiant la nature du motif de ciblage.

L'accès à de telles sondes «sans photo-activation» capables de modifier de manière covalente les formes actives de MMP ouvre une nouvelle voie pour étudier et mieux comprendre la régulation de l'activité des MMP dans différentes conditions physiopathologiques

Title: New activity-based probes to detect matrix metalloproteases.

Keywords : matrix metallo proteinases, affinity probes, covalent labelling.

Abstract : Activity-based probes bind covalently to their target enzymes in a mechanism-based manner allowing unambiguous discrimination between the active enzyme and its inactive or inhibitor-bound counterparts. Since metalloproteases catalysis is non-covalent, activity-based probes that target them have been developed using reversible inhibitors decorated with photo-crosslinkers, that limit their scope to ex vivo use.

By relying on a favorable structural context and by exploiting the acyl imidazole chemistry, we identify novel activity-based probes capable of covalently modifying matrix metalloproteases without using photo-activation.

Characteristics of this approach are a one-step specific labelling process driven by molecular proximity between a target and its ligand, sufficient stability of the resulting covalent linkage in biological conditions, minor

perturbation of the protein function and high selectivity toward the target protein in complex proteome.

We have validated the ability of these chemical probes to selectively and efficiently label human macrophage elastase (hMMP-12) both in vitro and in complex proteomes. We also showed that this strategy allowed detecting endogenous MMPs secreted by stimulated-macrophages and we have extended this affinity-labelling approach to six other MMPs by modifying the nature of the targeting moiety.

Availability of the first "photo activation-free" probes able to covalently modify active forms of MMPs open new avenue to investigate and reveal the complex regulation of MMP activity under different physio-pathological conditions.

